Oxidative Medicine and Cellular Longevity

Mechanisms and Therapies of Oxidative Stress-Mediated Cell Death in Ischemia Reperfusion Injury 2021

Lead Guest Editor: Margaret H Hastings
Guest Editors: Haitao Xiao and Haobo Li

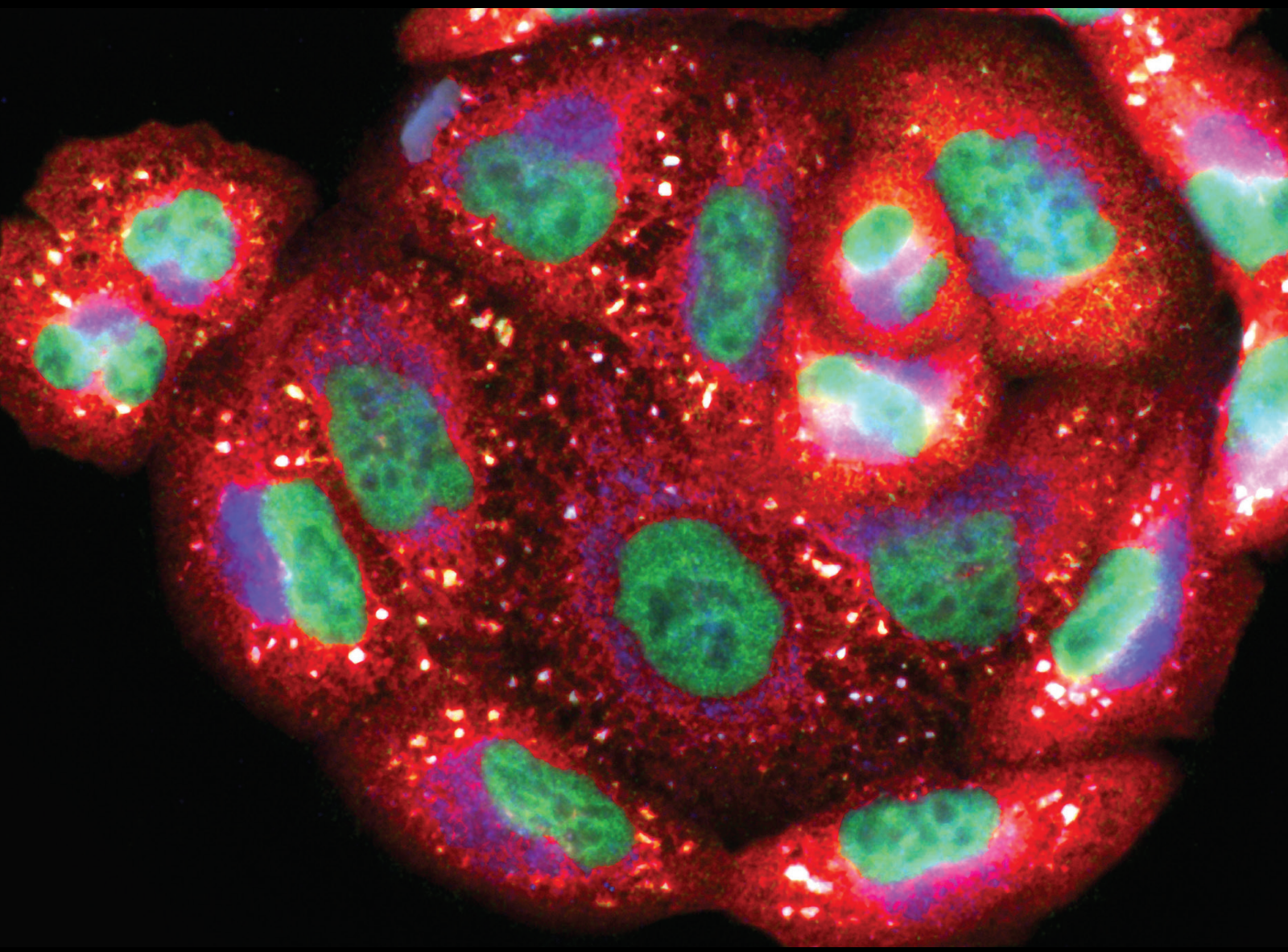

Mechanisms and Therapies of Oxidative Stress-Mediated Cell Death in Ischemia Reperfusion Injury 2021

Oxidative Medicine and Cellular Longevity

Mechanisms and Therapies of Oxidative Stress-Mediated Cell Death in Ischemia Reperfusion Injury 2021

Lead Guest Editor: Margaret H Hastings
Guest Editors: Haitao Xiao and Haobo Li

Contents

Hindawi
Oxidative Medicine and Cellular Longevity
Volume 2021, Article ID 9929687, 12 pages
https://doi.org/10.1155/2021/9929687

Review Article

Ferroptosis: Opportunities and Challenges in Myocardial Ischemia-Reperfusion Injury

Wei-kun Zhao[1], **Yao Zhou**[2,3], **Tong-tong Xu**[1] and **Qi Wu**[4]

[1]*Department of Health Care Ward, First Affiliated Hospital of Guilin Medical University, Guilin, Guangxi Zhuang Autonomous Region 541001, China*
[2]*Department of Pathophysiology, Xuzhou Medical University, Xuzhou, Jiangsu province 221009, China*
[3]*Laboratory of Clinical and Experimental Pathology, Xuzhou Medical University, Xuzhou, Jiangsu province 221009, China*
[4]*Department of Physiology, Xuzhou Medical University, Xuzhou, Jiangsu province 221009, China*

Correspondence should be addressed to Tong-tong Xu; xutongtongguilin@glmc.edu.cn and Qi Wu; wqak123@126.com

Received 18 March 2021; Revised 20 September 2021; Accepted 6 October 2021; Published 23 October 2021

Academic Editor: HAOBO LI

Ferroptosis is a newly discovered form of regulated cell death dependent on iron and reactive oxygen species (ROS). It directly or indirectly affects the activity of glutathione peroxidases (GPXs) under the induction of small molecules, causing membrane lipid peroxidation due to redox imbalances and excessive ROS accumulation, damaging the integrity of cell membranes. Ferroptosis is mainly characterized by mitochondrial shrinkage, increased density of bilayer membranes, and the accumulation of lipid peroxidation. Myocardial ischemia-reperfusion injury (MIRI) is an unavoidable risk event for acute myocardial infarction. Ferroptosis is closely associated with MIRI, and this relationship is discussed in detail here. This review systematically summarizes the process of ferroptosis and the latest research progress on the role of ferroptosis in MIRI to provide new ideas for the prevention and treatment of MIRI.

1. Introduction

Cell death is the natural endpoint of typical cells, occurring in growth and development, division and differentiation, and homeostatic metabolism, ultimately resulting in the irreversible end of the cellular function. The mode of cell death in the process of myocardial ischemia-reperfusion injury (MIRI) has been garnering substantial attention. Although cell death primarily constitutes apoptosis and necrosis, ferroptosis, a new form of programmed cell death that is iron-dependent and distinct from apoptosis and necrosis, has been discovered in recent years [1–3]. In recent years, ferroptosis has received extensive attention because it participates in the pathophysiological processes of tumor formation, kidney-related diseases, neurodegenerative diseases, stroke, and other diseases [4]. The occurrence and development of ferroptosis are closely related to the pathological process of myocardial cells, with ferroptosis participating in the pathogenic mechanisms of MIRI [5]. Ferritin was found to accumulate at the myocardial scar area of the left anterior descending coronary artery of mice in the ischemia-reperfusion injury(IRI) model after 30 min of ligation [6]. In addition, an in vitro study with perfused hearts showed that ferroptosis is crucial for the pathogenic mechanism of IRI; deferoxamine, a chelating agent, can prevent isolated hearts from IRI [7]. Erastin, an agonist of ferroptosis, can inhibit cystine ingestion and the downstream synthesis of glutathione, leading to an imbalance in cellular redox and, thus, cell death. In contrast, ferroptosis inhibitors can effectively alleviate organ injury induced by ischemic

reperfusion [8]. Ferroptosis is a type of cell death in the pathogenic process of MIRI, and its obstruction can lead to substantial protection of myocardial cells. In this paper, we focus on the recent research progress between ferroptosis and MIRI and discuss the important role of ferroptosis in the regulation of MIRI.

2. Ferroptosis

Early studies demonstrated that erastin and RAS-selective lethal compound 3 (RSL3) could cause cell death in a manner that is different from apoptosis, which can be inhibited by iron chelators and antioxidants [9–11]. In 2012, after continuous exploration and discussion of nonapoptosis cell death processes, Dixion and coworkers proposed an iron-dependent nonapoptosis cell death process, now known as ferroptosis [8]. This process involves the iron-dependent accumulation of reactive oxygen species (ROS) that exceeds the cell's ability to maintain redox homeostasis, leading to lipid peroxidation and eventually causing cell death. Glutathione peroxidase-4 (GPX-4) is a key regulatory protein in ferroptosis [1]. The main morphological manifestations of ferroptosis are mitochondrial abnormalities, including reduced mitochondrial volume, mitochondrial cristae dissolution, and increased mitochondrial membrane density and rupture. However, whether mitochondrial damage can be reversed during the process of ferroptosis remains controversial [12]. The biochemical characteristics of ferroptosis mainly include the accumulation of iron and ROS, glutathione (GSH) depletion, the release of arachidonic acid, and inhibition of the cystine/glutamate antiporter system (System Xc-) pathway [13]. Due to continuous research, a preliminary understanding of the process of ferroptosis began to take shape, and it has now been shown that ferroptosis is mainly regulated by multiple intracellular signaling pathways, such as iron homeostasis regulation, lipid peroxidation, System Xc-, and the voltage-dependent anion channel (VDAC) pathway [14–17] (Figure 1).

3. Ferroptosis Process

3.1. Regulatory Pathways of Iron Homeostasis. The maintenance and regulation of iron homeostasis are extremely complex processes. Iron is one of the most important essential trace elements in the human body and is involved in a series of important biological processes. Iron ions exist as Fe^{2+} and Fe^{3+} in the body and can be considered a "double-edged sword." The element is also the primary raw material for the synthesis of hemoglobin and myoglobin and is crucial for important processes, such as electron transport, cellular respiration, DNA synthesis, cell proliferation and differentiation, and gene regulation. However, the excessive accumulation of iron ions can increase ROS production through the Fenton reaction, which affects iron stability and promotes iron deposition in vital organs, thereby leading to severe organ damage.

In the process of iron metabolism, divalent metal transporter-1 (DMT-1) is a key protein in the intracellular transport of iron. Fe^{3+} bound to transferrin enters the cell via the membrane protein, transferrin receptor-1 (TFR-1), to form endosomes. Free Fe^{3+} is reduced to Fe^{2+} in the endosomes by the metal reductase, six-transmembrane epithelial antigen of the prostate-3 (STEAP-3). Fe^{2+} is then transported from the endosomes to the labile iron pool in the cytoplasm under the mediation of DMT-1. This is the process of iron recycling [18]. Ferritin is involved in this process as a complex of iron storage proteins consisting of ferritin light chain (FTL) and ferritin heavy chain-1 (FTH-1) and participates in the regulation of iron ions as a multimer. FTH-1 has iron oxidase activity, which catalyzes the conversion of Fe^{2+} to Fe^{3+} and stores it in ferritin molecules, thereby reducing free iron levels, while FTL is directly involved in iron storage. In addition, heme oxygenase-1 (HO-1) was found to lead to ferroptosis by increasing intracellular iron and mediating lipid peroxidation reactions [19]. When intracellular iron homeostasis is disrupted, excess iron converts hydrogen peroxide and lipid peroxides to ROS via the Fenton reaction, which in turn causes ferroptosis [4, 20].

Various iron regulatory proteins are also involved in the process of iron metabolism. Iron-responsive element-binding protein-2 (IREB-2) also has an important function, which involves the enhanced expression of FTL and FTH-1, leading to decreased levels of intracellular iron and the inhibition of erastin-induced ferroptosis. This implies that the IREB-2 expression can indirectly interfere with iron adsorption and inhibit ferroptosis [1, 21]. In addition to IREB-2, recent studies have revealed that heat shock protein B-1 (HSPB-1) may also play a key role as an iron regulatory protein in iron metabolism. HSPB-1 can inhibit TFR-1, which results in lower iron ion concentration, thereby further suppressing the occurrence of ferroptosis [22]. Therefore, the regulation of iron homeostasis plays an important role in the process of ferroptosis.

3.2. Lipid ROS Production. The formation of lipid ROS is a key component in the onset and development of ferroptosis. ROS production depends on the action of polyunsaturated fatty acid-phosphatidyl ethanolamine (PUFA-PE). PUFA can be acylated under the catalysis of acyl-CoA synthetase long-chain family member-4 (ACSL-4) to produce PUFA acyl-CoA (PUFA-CoA), which then reacts with PE under the action of lysophosphatidylcholine acyltransferase-3 (LPCAT-3) to produce PUFA-PE [16, 23, 24]. Under the enzymatic catalysis of lipoxygenase (LOX), PUFA-PE is essential for the formation of ROS [14, 17].

In this pathway, the action of PUFA-PE depends on two key regulatory points, ACSL-4 and LOX. Therefore, decreasing ACSL-4 and LOX can effectively inhibit the action of PUFA-PE and suppress the onset of ferroptosis [25]. The knockdown of the ACSL-4 gene in breast cancer cells can lead to a significant reduction in PUFA-PE production and suppress ferroptosis [26]. Furthermore, thiazolidinediones specifically inhibit ACSL-4, thereby suppressing ferroptosis [23, 27]. Zileuton (a 5-LOX inhibitor) can also inhibit erastin and ferroptosis in HT22 neuronal cells [28]. In addition, ROS formation is jointly achieved by a combination of iron-mediated Fenton reaction, the System Xc^- pathway, and the VDAC pathway, which ultimately leads to ferroptosis.

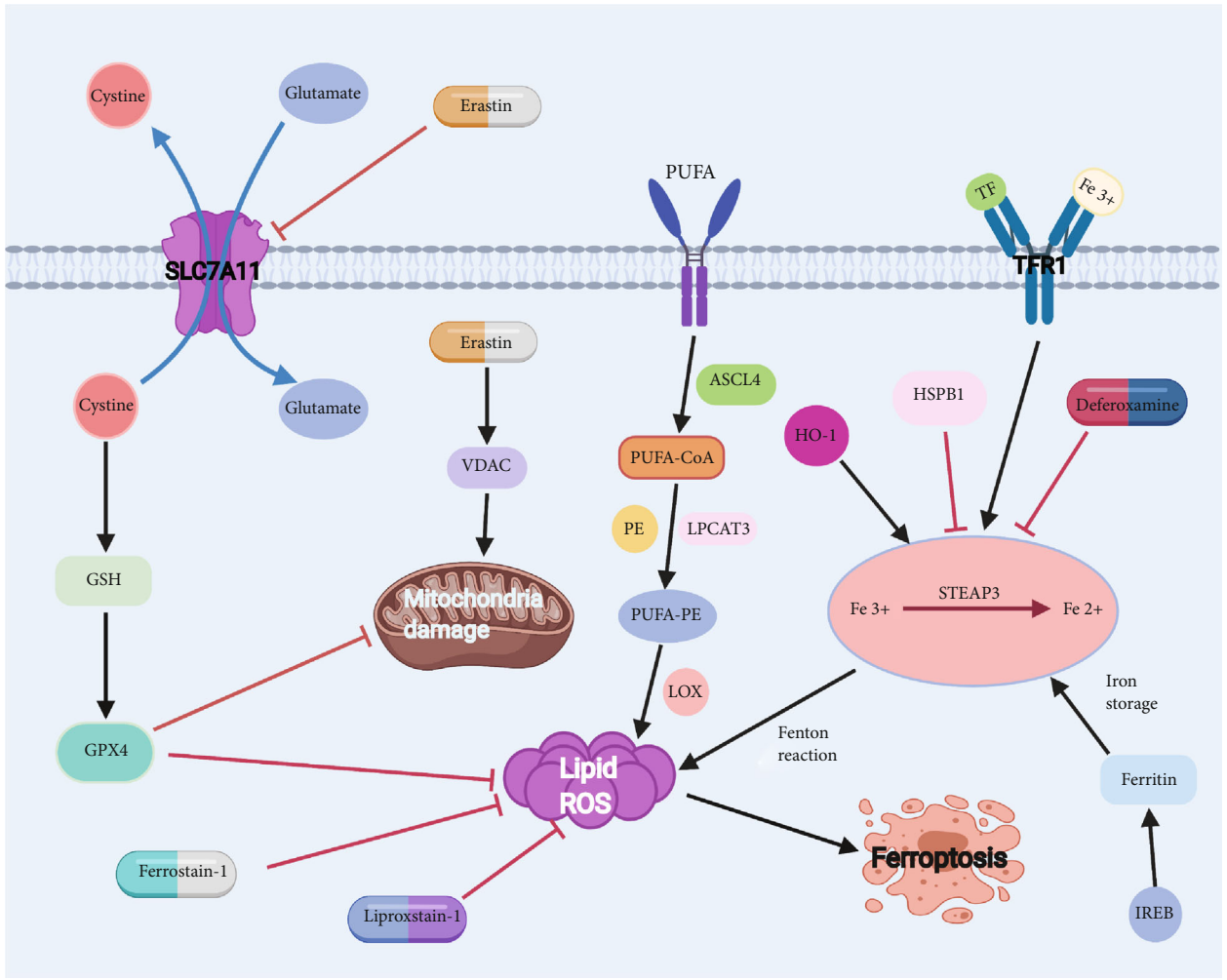

Figure 1: Cartoon depicting the possible mechanism and regulation of ferroptosis. Ferroptosis is mainly regulated by Fe homeostasis, lipid oxidation, System Xc^-, and VDAC. The most important in the ferroptosis signaling pathway is the production of iron ions and ROS. GPX-4 is a key regulator of ferroptosis. Inhibition of GPX-4 causes a large amount of lipid peroxides to aggregate, becoming a sign of ferroptosis.

3.3. System Xc^- Pathway. System Xc^- is an amino acid transporter expressed in the plasma membrane of mammalian cells. It is a heterodimer composed of SLC7A11 and SLC3A2, acting primarily through SLC7A11 (the primary active site of erastin). System Xc- exchanges extracellular cystine (Cys) for intracellular glutamate (Glu) at a 1 : 1 ratio, thus providing the raw material for intracellular GSH synthesis. Cellular uptake of cysteine is an important step in GSH production [29, 30]. GPX-4 is a GSH-dependent enzyme that converts GSH into oxidized glutathione (GSSG), which in turn can scavenge excess peroxides and hydroxyl radicals produced during cellular respiration and metabolism. Thus, GPX-4 plays an indispensable role in preventing lipid peroxidation [31]. When GPX-4 function is restricted, this is often accompanied by a decrease in GSSG and a significant increase in ROS [32]. Furthermore, the inhibition of GPX-4 activity will promote ROS formation and lipid peroxidation, thereby leading to ferroptosis. SLC7A11 gene silencing with siRNA interference substantially increased the sensitivity of HT-1080 cells to erastin-induced ferroptosis, while the overexpression of SLC7A11 in HT-1080 cells significantly enhanced cellular resistance to ferroptosis [33]. Another study found that the tumor suppressor P53 downregulated SLC7A11, inhibited System Xc- uptake of Cys, decreased GPX, increased ROS, and ultimately induced ferroptosis [34]. In addition, nicotinamide adenine dinucleotide phosphate (NADPH) was shown to maintain GSH in a reduced state, which further regulates ferroptosis [35]. Therefore, the inhibition of the System Xc- pathway will reduce intracellular GSH levels, resulting in decreased GPX-4 activity, which will ultimately lead to ferroptosis [30].

3.4. VDAC Pathway. VDAC is a channel protein for transporting ions and metabolites located on the outer mitochondrial membrane and consists of VDAC-1, VDAC-2, and VDAC-3. It controls the exchange of metabolites in the mitochondria and with other organelles [36]. In addition to regulating mitochondrial metabolism and energy production functions, VDAC can also potentially regulate cell survival and death signals by interacting with different ligands and proteins. Erastin, a typical inducer of ferroptosis, can

activate VDAC in the presence of tubulin and cause mitochondrial hyperpolarization, thus leading to ROS production, mitochondrial dysfunction, and cell death [37]. When the VDAC-2 or VDAC-3 expression was inhibited by siRNA interference, cells were tolerant to erastin-induced ferroptosis. However, the overexpression of VDAC-2 or VDAC-3 did not increase cellular sensitivity to erastin. Therefore, VDAC may participate in cellular ferroptosis. In addition, mitochondria are key targets of the MIRI mechanism. The opening of the mitochondrial permeability transition pore (mPTP) can lead to elevated mitochondrial ROS production, membrane potential loss, and ATP depletion, thereby inducing cell death through mechanisms of programmed or nonprogrammed death. Meanwhile, erastin action on VDAC alters the permeability of the outer mitochondrial membrane, thus causing mitochondrial dysfunction, increased ROS production, and ultimately cellular ferroptosis [38–40]. Therefore, the VDAC pathway and mPTP may be involved in the mechanism of MIRI.

3.5. Other Related Signaling Pathways. At present, further indepth investigations have led to the gradual recognition of the roles of NADPH oxidase-4 (NOX-4), HSPB-1, and other related proteins and signaling pathways in the regulation of ferroptosis [22, 41]. The mechanisms of ferroptosis are shown in Figure 1.

4. The Role of Ferroptosis in MIRI

4.1. Ferroptosis and MIRI. Myocardial ischemia caused by coronary artery obstruction is clinically manifested as persistent severe retrosternal pain and can lead to myocardial infarction, shock, arrhythmia, or heart failure. The most common treatment strategy is the early restoration of blood flow to the ischemic area using techniques, such as coronary angioplasty, percutaneous coronary intervention, and coronary artery bypass grafting (CABG), which can restore myocardial oxygen and nutrient supply, salvage the ischemic myocardium, and save the patient's life.

MIRI is a phenomenon wherein cardiac function does not improve but worsens immediately after perfusion is restored to the ischemic myocardium. The pathogenic mechanism of MIRI is not fully understood. At present, it is known to primarily be involved in processes such as oxidative stress, calcium overload, and in inflammatory reactions [42]. Oxidative stress can lead to cell membrane rupture, swelling, or death through intracellular homeostasis, mitosis, cellular differentiation, and intracellular signaling [43]. As research progresses, ferroptosis has been identified as a form of cell death in MIRI pathogenesis that is closely related to oxidative stress. At present, peroxidized phosphatidylethanolamine (PEox) has been identified as a predictive biomarker of ferroptosis, and Sparvero's group was the first to apply gas cluster ion beam secondary ion mass spectrometry (GCIB-SIMS) as a technique to increase PEox in cardiomyocytes, which provided direct evidence for the occurrence of ferroptosis in cardiomyocytes [44]. Iron chelating agents can bind to iron ions in the plasma or tissues and promote their elimination via urea or bile, thereby reducing the iron content in the body. Deferoxamine is a frequently used iron-chelating agent. Furthermore, in a study of patients with coronary artery disease (CAD), when performing CABG, the intravenous infusion of deferoxamine 8 h after anesthesia was effective in ameliorating oxygen radical production and protecting the myocardium from reperfusion injury, with more pronounced benefits in patients with reduced left ventricular ejection fraction (LVEF) [45]. A previous study also showed that using nuclear magnetic resonance spectroscopy in perfusion experiments on isolated rabbit hearts and adding a certain concentration of deferoxamine at the early stage of perfusion could effectively attenuate reperfusion-induced free radical generation, thus achieving cardioprotective effects [46]. Most current studies investigating the role of ferroptosis in MIRI have mainly focused on endoplasmic reticulum stress (ERS) and ROS production, GPX-4, and the autophagy-dependent ferroptotic pathway.

4.1.1. ERS. Ferroptosis occurs with the production of ERS, and ERS-induced unfolded protein response plays an important role in the ferroptotic process. When changes in the calcium level and redox status of the endoplasmic reticulum (ER) lumen induce a decline in chaperone protein function, cells can activate the unfolded protein response and cause ERS. ERS disrupts Ca^{2+} homeostasis in the ER, leading to mitochondrial calcium overload and elevated ROS production, while the accumulation of ROS will activate downstream caspase family proteins through cascade amplification, thereby initiating the process of cellular damage. In addition, the ERS process is induced by upstream signaling proteins, including inositol-requiring enzyme-1, activating transcription factor-6 (ATF-6), and PKR-like ER kinase (PERK) [47]. The ERS response elicited by ferroptosis inducers plays a tandem role between ferroptosis and other types of cell death [48], mainly in the form of ERS-mediated activation of the PERK-eukaryotic initiation factor 2α (eIF2α)-ATF 4-CHOP pathway. The dissociation of PERK from binding immunoglobulin protein BiP will trigger the phosphorylation and subsequent activation of PERK. Furthermore, eIF2α is activated, leading to ATF 4 mRNA translation and the induction of downstream CHOP molecules. The CHOP-mediated apoptosis in ERS plays an important role in the MIRI process in rats [49].

Ferroptosis induces ERS-triggered apoptosis. Studies have found that ferroptosis can induce ERS activation by inhibiting the System Xc–mediated exchange of extracellular cystine for intracellular glutamate [50, 51]. The activation of the PERK- eIF2α-ATF 4 pathway accompanying the ESR response regulates the target gene of the unfolded protein response, CHOP, while the binding of CHOP to the corresponding promoter inducesthe expressions of PUMA, endoplasmic reticulum redox protein-1α, and B-cell lymphoma-2 (Bcl-2) [52, 53]. Furthermore, ferroptosis agonists can induce the PUMA expression but not the Bcl-2 expression, suggesting that the ferroptosis-induced PUMA gene expression was unable to induce apoptosis [54]. In addition, tumor necrosis factor- (TNF-) related apoptosis-inducing ligand (TRAIL) binds to the corresponding death receptors to form a death-inducing signaling complex, which in turn induces apoptosis. With the help of the death-inducing signaling complex, caspase-8 is activated, which can lead to the further

activation of caspase-3, caspase-6, and caspase-7, eventually resulting in apoptosis. Ferroptosis agonists also modulate the cellular activity induced by TRAIL [54]. The interaction between ferroptosis and the apoptotic molecule TRAIL can be mediated by the ERS-induced expression of PUMA molecules. This suggests that ferroptosis-induced ERS can act as a bridge between ferroptosis and apoptosis. MIRI has also been found to be closely associated with ERS [55].

Apoptosis results from ferroptosis-induced ERS and its correlation with MIRI. In a rat MIRI model, it was found that erastin probably increases ERS, which further increases ferroptosis. Inhibition of ferroptosis can reduce myocardial cell injury, and the inhibition of ERS can alleviate ferroptosis and reduce MIRI. These findings suggest that ferroptosis is involved in ERS-associated MIRI. Furthermore, based on a MIRI model established by ligating the left anterior descending branch of the coronary artery in diabetic rats, the tail vein injection of the ferroptosis inhibitor, ferrostatin-1, could attenuate ERS-induced ferroptosis in cardiomyocytes, while the ERS inhibitor, salubrinal, could also attenuate ferroptosis in cardiomyocytes. This suggests that the activation of ERS may exacerbate the process of ferroptosis in cardiomyocytes, while the occurrence of ferroptosis can further exacerbate ERS in cardiomyocytes, which can form a vicious circle [56]. Therefore, ferroptosis-induced ERS and the activation of ERS play crucial roles in apoptosis and are important apoptotic mechanisms in MIRI.

4.1.2. GPX-4. GPX-4 participates in the regulation of ferroptosis. GPX-4 is an endogenous antioxidant for selenium-dependent enzymes that serves as a core regulator in the ferroptotic signaling pathway. Under physiological conditions, GPX-4 can confer cellular protection by scavenging lipid peroxides, thus preventing iron-mediated lipid peroxidation and elevated lipid ROS, whereas GPX inactivation induces ROS lipid peroxidation and ferroptosis [57]. System Xc- mediates cystine uptake and glutamate release to promote GSH synthesis, while GSH acts as a synergistic molecule of GPX-4 to assist in scavenging lipid peroxides for cellular protection. Erastin inhibits System Xc- and indirectly inactivates GPX-4, thus leading to the accumulation of lipid peroxides to promote the onset of ferroptosis [58]. The indirect or direct inactivation of GPX-4 is the classic induction mechanism of ferroptosis. ML162 and RSL3 induce ferroptosis by depleting GPX-4 [59]. In addition, GSH participates as a coenzyme in the breakdown of hydrogen peroxide by GPX-4; therefore, by inhibiting the intracellular activity, GSH and GPX-4 increase intracellular ROS levels and ultimately mediate ferroptosis.

GPX-4 mediates ferroptosis to regulate MIRI. A previous study demonstrated that the levels of iron and malondialdehyde (MDA) in reperfused rat hearts gradually increased with increasing reperfusion time, accompanied by a decrease in GPX-4 levels [60]. Notably, there is evidence showing that the specific overexpression of GPX-4 in mitochondria attenuates cardiac dysfunction in MIRI [61]. Furthermore, GPX-4 is involved in the pathogenesis of MIRI. GPX-4 is an important antioxidant enzyme upstream of the mitochondria that regulate ferroptosis and oxidative stress by catalyzing the conversion of reduced glutathione (GSH) to oxidized glutathione (GSSG). Moreover, the knockdown of GPX-4 in a glutathione-independent manner leads to the destruction of mitochondrial morphology and increased mitochondrial ROS production [62]. In turn, the large production of ROS and ferroptosis are important mechanisms leading to MIRI [63, 64]. Another study found that liproxstatin-1 inhibited ferroptosis by increasing GPX-4 levels, which decreased ROS levels and thus alleviated MIRI [65]. Therefore, in MIRI, increasing GPX-4 expression can inhibit ferroptosis and attenuate the negative effects of MIRI.

4.1.3. ROS. Pathogenic mechanism of ROS participation in MIRI. Oxidative stress, attributed to the enhanced production of ROS during MIRI, is the main cause of MIRI. Excessive ROS accumulation causes membrane lipid peroxidation and disrupts the barrier function of the cell membrane. Excessive oxidation of lipids, DNA, and proteins causes increased cardiomyocyte damage and ultimately cell death. The antioxidant system regulates redox homeostasis by controlling intracellular ROS levels and the interactions between normal cellular metabolism and pathophysiology. Increased expression of antioxidant enzymes protects tissues from oxidative stress and produces cardioprotection after myocardial reperfusion [66]. During reperfusion, myocardial tissue is reoxygenated as blood flow is restored with a sudden increase in ROS production during the first few minutes, which is one of the underlying pathogenic mechanisms causing MIRI.

Increasing ROS levels lead to ferroptosis. Ferroptosis occurs due to increased intracellular iron concentration and the depletion of the antioxidant GSH, which leads to increased levels of ROS and in turn causes lipid peroxidation and eventually cell death. It was found that lipid peroxidation may occur in the lysosomal membrane due to ROS accumulation and iron overload, while the permeabilization of the lysosomal membrane can lead to oxygen radical production, cell membrane degeneration, and increased GSH depletion [67]. Moreover, lysosomes can regulate iron homeostasis and cause a dramatic increase in ROS expression. In addition, under the participation of iron ions, ROS are produced in a nonenzymatic pathway. For example, free iron ions present in the unstable iron pool form Fe^{3+} and hydroxyl radicals in the presence of Fe^{2+} and H_2O_2 through the Fenton reaction. Alternatively, Fe catalyzes the production of -OH through the Haber-Weiss reaction. The inhibition of GPX-4 causes an increase in ROS, whereas the overexpression of GPX-4 reduces ROS and thus cellular ferroptosis [62, 68]. The increase in ROS leads to lipid peroxidation and ferroptosis, which can be inhibited by the iron chelator deferoxamine [69]. On the other hand, higher levels of iron transporters will increase iron-mediated ROS, which subsequently leads to ferroptosis. Liproxstatin-1 has been shown to significantly inhibit ferroptosis and attenuate MIRI by reducing the accumulation of ROS from lipid peroxidation, protecting the structural integrity of mitochondria, increasing the levels of the GPX-4 protein, and reducing ROS levels [70].

ROS play a role in MIRI-mediated ferroptosis. Ferroptosis is highly correlated with cardiomyocyte death. During

MIRI, iron accumulates in cardiomyocytes around the myocardial scar, and excess iron leads to cardiomyocyte death, while the inhibition of ROS production attenuates cardiomyocyte death [6]. Based on in vivo and in vitro models of MIRI, ROS levels were significantly elevated in MIRI myocardial tissues, while sirtuin-1 (SIRT-1) and SLC7A11 expression were downregulated, and p53 was highly expressed. Following the overexpression of SIRT-1, the cardiomyocytes showed a significant improvement in the extent of ferroptosis, reduction in ROS levels, upregulation of the SLC7A11 protein expression, and downregulation of the p53 protein expression. This suggests that ROS plays an important role in MIRI ferroptosis, and that the regulation of ROS may be related to the SIRT-1/p53/SLC7A11 signaling pathway [71].

4.1.4. Cellular Autophagy. Autophagy is an important mechanism of MIRI. Autophagy is a precisely regulated, dynamically developing process that cleans up damaged organelles and proteins via lysosomes, and is a monitoring mechanism that is relatively conserved. It recycles the basic nutrients produced and plays an important role in maintaining the normal structure and function of the heart. This involves not only cell survival but also cell death [72, 73]. In MIRI, the molecular mechanism of autophagy consists mainly of mammalian target of rapamycin (mTOR) and beclin 1, which play indispensable roles at different phases of MIRI. mTOR exerts its effects in the myocardial ischemic phase by mediating AMPK/mTOR and PI3K/Akt/mTOR signaling pathway [74] and further in the reperfusion phase via the upregulation of the beclin 1 pathway [72, 75, 76]. The possible mechanisms of beclin 1 activation in MIRI mainly include the following: (1) the association of beclin 1 with the Bcl-2 protein. (2) ROS can act as an inducer to mediate beclin 1 autophagy during reperfusion injury. (3) ROS can decrease the activity of autophagy-associated proteins through oxidation, thus causing LC 3 lipidation and autophagy. Therefore, autophagy is involved in MIRI [77].

Ferroptosis is closely related to autophagy. To a certain degree, ferroptosis is dependent on autophagy and involves the embryonic lethal abnormal vision-like protein-1 (ELAVL-1) and forkhead box C-1 (FOXC-1) [78]. ELAVL-1 is a protein-coding gene that regulates the gene expression by stabilizing RNA (TNF-α or VEGF-A) and is implicated in the processes of apoptosis and oxidative stress [79]. ELAVL-1 inhibits the inflammatory response in AMI and plays a role in MIRI, where the significant increase in ELAV-1 is accompanied by the excessive production of ROS and inflammatory cytokines [63, 80]. FOXC-1 plays a significant role as a transcription factor in cell growth and survival, as well as in cardiac disease [81]. FOXC-1 transcription activates ELAVL-1, and the ELAVL-1-mediated enhancement of the autophagic ferroptosis pathway has a significant impact on MIRI. During MIRI, decreased GSH and GPX-4 levels can lead to elevated ELAVL-1, which further inhibits enzyme function and cellular antioxidant capacity. ELAVL-1 also inhibits ferroptosis and MIRI, restores GPX-4 expression level, restores cardiomyocyte viability, and attenuates cardiomyocyte injury. Low levels of ELAVL-1 can inhibit MIRI-induced autophagy, suppress ferroptosis, and attenuate myocardial infarct size and MIRI. In addition, a decrease in the FOXC-1 expression was followed by a decrease in ELAVL-1 level, suggesting that FOXC regulates the ELAVL-1 expression during MIRI. Thus, autophagy-dependent ferroptosis counteracts the effects of reduced ELAVL-1 and contributes to the onset of MIRI and the overproduction of lipid signaling. Therefore, the relationship between FOXC-1 and ELAVL-1, as well as its association with ferroptosis, could serve as useful targets against MIRI.

Autophagy regulates ferroptosis to participate in the pathogenic mechanism of MIRI. Previous studies showed that ferroptosis is different from cellular autophagy and other modes of cell death, whether in terms of cell morphology, biochemical characteristics, or the regulatory factors involved. However, recent studies have revealed an interconnection between autophagy and ferroptosis in cardiomyocytes during the course of MIRI, wherein the activation of ferroptosis depends on the induction of autophagy, and the regulatory proteins of autophagy may also be involved in the regulation of ferroptosis. In another study, iron ion levels and ROS were significantly enhanced in the cardiomyocytes of MIRI rats, whereas GPX-4 and GSH protein expressions were significantly reduced, thus suggesting that ferroptosis may be involved in the pathogenesis of MIRI. Further studies revealed that myocardial ferroptosis may be regulated by autophagy-related signaling pathways during the progression of MIRI, and the ELAVL-1 protein is able to bind specifically with the autophagy-related protein beclin 1 to promote the decrease in the P62 protein expression and increase in LC 3 levels. This will induce an increase in the autophagy levels of cardiomyocytes and thus activate the ferroptotic pathway [80]. At present, indepth studies have been conducted on the role of autophagy in ferroptosis in fields, such as cancer. However, in MIRI, most studies have only superficially concluded that ferroptosis in cardiomyocytes may be regulated by autophagy, while its underlying mechanisms of action remain poorly understood. Therefore, we hope that more indepth studies will be conducted in this area in the future, so as to achieve new breakthroughs in the treatment of MIRI.

4.2. Treatment. There is currently no effective treatment for MIRI. With the advancement of research, researchers began identifying the inhibition of ferroptosis cardiomyocytes as a potentially important target for the treatment of MIRI [12]. Pretreatment of MIRI mice with ferrostatin-1 (Fer-1, an inhibitor of ferroptosis) or dexrazoxane (an iron chelating agent) significantly increased the expression level of Ptgs2 mRNA, which further led to a reduction in the myocardial enzyme spectrum and the scar area of myocardial infarction [64]. In contrast, liproxstatin-1 (Lip-1) treatment maintained the structure and function of mitochondria after MIRI by reducing VDAC-1 levels and restoring GPX4 protein levels [70]. Overexpression of USP22 and inhibition of glutaminase can alleviate MIRI by inhibiting ferroptosis [7, 71]. In a MIRI rat model and oxygen–glucose deprivation/-reoxygenation (OGD/R) H9c2 cells, it was found that ACSL4-mediated ferroptosis was a promising target for MIRI treatment, and baicalin can prevent MIRI by inhibiting ACSL-4-mediated ferroptosis [82].

Table 1: Small molecules, drugs, and ferroptosis.

Small molecules or drugs	Intervention target	Molecular weight	Molecular formula	Function	Experimental cells/ animals	References
Erastin	VDAC 2/3 or system Xc^-	547.04	C30H31ClN4O4	Prevents cystine import, causes GSH exhaustion,cause ferroptosis	BJeLR HT1080 143B p° and p^+ cell U2OS DU-145	[1, 9, 10, 51, 88]
RSL3	GPX-4	440.9	C23H21ClN2O5	Covalent inhibitor of GPX-4 that causes accumulation of lipid hydroperoxides and ferroptosis	KBM7 MIA PaCa-2 A549, Calu-1, HCT116, HT1080 BJeLR	[10, 89]
Buthionine sulfoximine	GSH exhaustion	222.305	C8H18N2O3S	Cause ferroptosis	BJeLR HCT116/A549	[51]
Acetaminophen	GSH exhaustion	151.163	C8H9NO2	Cause ferroptosis	HepG2/primary mouse	[90]
Sulfasalazine	System Xc^-	398.394	C18H14N4O5S	Low potency inhibitor that prevents cystine import, causes GSH depletion and ferroptosis	BJeLR/HT1080 HT1080/Calu-1	[1, 51]
Sorafenib	System Xc^-	464.825	C21H16ClF3N4O3	Cause ferroptosis	HT1080/Calu-1DU-145 nude mice	[51, 91–93]
Artesunate	—	384.421	C19H28O8	Cause ferroptosis	PDAC cell lines	[94]
Piperazine erastin	VDACs or system Xc^-	645.19	C35H41ClN6O4	Cause ferroptosis	BJeLR nude mice	[88]
Trolox	Lipophilic antioxidants	250.29	C14H18O4	Blocks propagation of lipid peroxidation, may inhibit lipoxygenases, inhibiting ferroptosis	HT1080/PUFA oxidation-induced death model on S. cerevisiae	[1, 95]
Ebselen	Oxidative pathway	274.17666	C13H9NOSe	Inhibiting ferroptosis	HT1080, Calu-1	[1]
SSRS 11-92	ROS from lipid peroxidation	—	—	Inhibiting ferroptosis	HD model	[95]
α-Tocopherol (vitamin E)	Oxidative pathway	430.71	C29H50O2	Blocks propagation of lipid peroxidation, may inhibit lipoxygenases, inhibitting ferroptosis	BReLR GPX4-deficient T-cell mice	[10, 96]
Deferoxamine	Fenton reaction	560.68	C25H48N6O8	Depletes iron and prevents iron-dependent lipid peroxidation, inhibiting ferroptosis	Wild-type and Bax/ Bak	[1]
Deferoxamine mesylate (DFO)	Intracellular iron	656.8	C25H48N6O8•CH4O3S	Inhibiting ferroptosis	BJeLR	[10]
SRS 16-86	ROS from lipid peroxidation	432.2525	C16H24N2O2	Inhibiting ferroptosis	HT1080/NIH 3T3 IRI mice model	[97]
Ferrostatin-1 (Fer-1)	ROS from lipid peroxidation	262.35	C15H22N2O2	Blocks lipid peroxidation, inhibiting ferroptosis	HT1080	[1, 95]
Liproxstatin-1 (Lip-1)	ROS from lipid peroxidation	340.85	C19H21ClN4	Blocks lipid peroxidation, inhibiting ferroptosis	HRPTEpiCs $GPX4^{-/-}$ cells $GPX4^{-/-}$ mice	[98]

A recent study found that dexrazoxane or ponatinib inhibited ferroptosis during MIRI, and a combined treatment with both drugs markedly reduced the scar area of myocardial infarction. However, for myocardial infarction patients with an elevated ST section, percutaneous coronary intervention before myocardial reperfusion could not significantly reduce the scar area of myocardial infarction [83]. Based on these findings, a combined treatment targeting different types of cell death is proposed as an effective treatment strategy for MIRI.

Recently, it was proven that phosphatidylcholine oxide content increased dramatically during MIRI, leading to reduced GPX-4 activity and ferroptosis. However, it is noteworthy that Fer-1 can inhibit OxPC-triggered ferroptosis [84]. Another study showed that the expression level of ELAVL-1 was upregulated. ELAVL-1 can also be activated by the autophagy-regulated ferroptosis process, which is related to FOXC-1 transcription, and ELAVL-1 knockout can reduce ferroptosis and alleviate MIRI [80]. Cyanidin-3-glucoside (C3G) treatment can effectively alleviate the expression of proteins related to apoptosis, reduce Fe^{2+} content, and improve MIRI. Therefore, C3G is a potential medicine to prevent myocardial cells from being affected by MIRI [85].

Ferroptosis has been shown to be related to diabetic MIRI. Fer-1 alleviates ERS, reduces cellular injury in H9c2 cells, and mitigates myocardial cell injury during diabetic MIRI. In addition, diabetes patients can induce MIRI by activating NOX-2-related oxidative stress and apoptosis, and inhibition of nicotinamide adenine dinucleotide phosphate oxidase-2 (NOX-2) can alleviate MIRI in diabetic rats [56, 86]. Fer-1 can also mitigate myocardial cell injury in H9c2 cells under hyperglycemic conditions and reduce H9c2 cell injury during anoxia/aeration. These results have provided beneficial treatment for patients with diabetic MIRI.

Additionally, further understanding of the association between ferroptosis and MIRI after heart transplantation has been obtained. Fer-1 reduces myocardial cell death and blocks the recruitment of neutrophil granulocytes to damaged myocardial cells by damage-associated molecular patterns (DAMPs) after heart transplantation [87]. Therefore, targeted ferroptosis can potentially provide preventative treatment of MIRI in patients undergoing heart transplantation after coronary artery reperfusion. Other drugs, such as piperlongumine, isothiocyanates, and artemisinin, may exert cardiomyocyte protective effects by inhibiting ferroptosis. However, articles related to the effects of Chinese medicines and other drugs on MIRI are still scarce, which warrants further investigation (see Table 1 for details).

5. Conclusion

Ferroptosis is an iron-dependent, nonapoptotic mode of cell death characterized by ROS accumulation. However, current research on ferroptosis is still in its infancy. Ferroptosis is closely associated with MIRI and regulates MIRI through ERS, ROS production, GPX-4, and the autophagy-dependent ferroptotic pathways. Ferroptosis can serve as an important target in MIRI, which may help in the process of reducing the occurrence of MIRI. Therefore, indepth studies on ferroptotic mechanisms and possible interventions have now become a focus of current research. In addition, the precise stage of MIRI at which ferroptosis mainly occurs have not been located, and some studies have shown that the incidence of ferroptosis is different at different stages of MIRI [99]. Therefore, more indepth investigations will provide new ideas for the prevention and treatment of MIRI.

Abbreviations

ACSL-4: Acyl-CoA synthetase long-chain family member-4
AMI: Acute myocardial infarction
ATF-6: Activating transcription factor 6
Bcl-2: B-cell lymphoma-2
CABG: Coronary artery bypass grafting
CAD: Coronary artery disease
Cys: Cysteine
C3G: Cyanidin-3-glucoside
DAMPs: Damage-associated molecular patterns
DMT-1: Divalent metal transporter 1
eIF2α: Eukaryotic initiation factor
ELAVL-1: Embryonic lethal-abnormal vision like protein 1
ER: Endoplasmic reticulum
ERS: Endoplasmic reticulum stress
Fer-1: Ferrostatin-1
FOXC-1: Forkhead box C-1
FTH-1: Ferritin heavy chain-1
FTL: Ferritin light chain
GCIB-SIMS: Gas cluster ion beam secondary ion mass spectrometry
GPXs: Glutathione peroxidases
GPX-4: Glutathione peroxidase-4
GSH: Glutathione
GSSG: Oxidized glutathione
GSSH: Glutathione hydropersulfides
HO-1: Heme oxygenase-1
HSPB-1: Heat shock protein B-1
IREB-2: Iron responsive element-binding protein-2
IRI: Ischemia-reperfusion injury
LOX: Lipoxygenases
LPCAT-3: Lysophosphatidylcholine acyltransferase-3
Lip-1: Liproxstatin-1
LVEF: Left ventricular ejection fraction
MDA: Malondialdehyde
MIRI: Myocardial ischemia-reperfusion injury
MPO: Myoperoxidase
mTOR: Mammalian target of rapamycin
mPTP: Mitochondrial permeability transition pore
NADPH: Nicotinamide adenine dinucleotide phosphate
NOX-4: NADPH oxidase-4
NOX-2: Nicotinamide adenine dinucleotide phosphate oxidase-2
OGD/R: Oxygen–glucose deprivation/reoxygenation
PERK: PKR-like ER kinase
PUFA-PE: Poly-unsaturated fatty acid-phosphatidyl ethanolamine
PEox: Peroxidized phosphatidylethanolamine
ROS: Reactive oxygen species
RSL3: Ras selective lethal compound 3
SIRT-1: Sirtuin-1
STEAP-3: Six transmembrane epithelial antigen of prostate-3
System Xc^-: Cystine/glutamate antiporter system
TFR-1: Transferrin receptor-1
TLR-4: Toll-like receptor-4

TNF: Tumor necrosis factor
TRAIL: TNF-related apoptosis-inducing ligand
VDAC: Voltage-dependent anion channel.

Data Availability

The data used to support the finding of this study are available from the corresponding author upon request.

Conflicts of Interest

The authors declare that they have no conflicts of interest.

Authors' Contributions

Wei-kun Zhao and Qi Wu drafted and proofed the manuscript. Tong-tong Xu edited the manuscript. All author shave agreed up on the submission and publication of this work. Wei-kun Zhao and Yao Zhou contributed equally to this work and should be considered co-first authors.

Acknowledgments

This study was sponsored by the National Natural Science Foundation of China (Grant No. 81760861 and No. 8210141573) and the Outstanding Talent Research Funding of Xuzhou Medical University (Grant No. D2019005 and No. D2019022).

References

[1] D. Tang, X. Chen, R. Kang, and G. Kroemer, "Ferroptosis: molecular mechanisms and health implications," *Cell Research*, vol. 31, no. 2, pp. 107–125, 2021.

[2] H. T. Yu, P. Y. Guo, X. Z. Xie, Y. Wang, and G. Chen, "Ferroptosis, a new form of cell death, and its relationships with tumourous diseases," *Journal of Cellular & Molecular Medicine*, vol. 21, no. 4, pp. 648–657, 2017.

[3] J. Zeng, Y. Chen, and X. Xu, "Research progress of ferroptosis-related mechanisms, regulation and diseases," *Chinese Pharmaceutical Journal*, vol. 52, no. 4, pp. 253–257, 2017.

[4] J. P. F. Angeli, R. Shah, D. A. Pratt, and M. Conrad, "Ferroptosis inhibition: mechanisms and opportunities," *Trends in Pharmacological Sciences*, vol. 38, no. 5, pp. 489–498, 2017.

[5] J. Lillo-Moya, C. Rojas-Solé, D. Muñoz-Salamanca, E. Panieri, L. Saso, and R. Rodrigo, "Targeting ferroptosis against ischemia/reperfusion cardiac injury," *Antioxidants (Basel)*, vol. 10, no. 5, p. 667, 2021.

[6] Y. Baba, J. K. Higa, B. K. Shimada et al., "Protective effects of the mechanistic target of rapamycin against excess iron and ferroptosis in cardiomyocytes," *American Journal of Physiology. Heart and Circulatory Physiology*, vol. 314, no. 3, pp. H659–H668, 2018.

[7] M. Gao, P. Monian, N. Quadri, R. Ramasamy, and X. Jiang, "Glutaminolysis and transferrin regulate ferroptosis," *Molecular Cell*, vol. 59, no. 2, pp. 298–308, 2015.

[8] S. J. Dixon, K. M. Lemberg, M. R. Lamprecht et al., "Ferroptosis: an iron-dependent form of nonapoptotic cell death," *Cell*, vol. 149, no. 5, pp. 1060–1072, 2012.

[9] S. Dolma, S. L. Lessnick, W. C. Hahn, and B. R. Stockwell, "Identification of genotype-selective antitumor agents using synthetic lethal chemical screening in engineered human tumor cells," *Cancer Cell*, vol. 3, no. 3, pp. 285–296, 2003.

[10] W. S. Yang and B. R. Stockwell, "Synthetic lethal screening identifies compounds activating iron-dependent, nonapoptotic cell death in oncogenic-RAS-harboring cancer cells," *Chemistry & Biology*, vol. 15, no. 3, pp. 234–245, 2008.

[11] N. Yagoda, M. von Rechenberg, E. Zaganjor et al., "RAS-RAF-MEK-dependent oxidative cell death involving voltage-dependent anion channels," *Nature*, vol. 447, no. 7146, pp. 864–868, 2007.

[12] D. Wu and L. X. Chen, "Ferroptosis: a novel cell death form will be a promising therapy target for diseases," *Acta Biochimica et Biophysica Sinica*, vol. 47, no. 10, pp. 857–859, 2015.

[13] C. J. Kang, X. T. Zhang, and W. A. Mei, "Progress in occurrence and development of ferroptosis," *Chinese Journal of Pathophysiology*, vol. 33, no. 3, pp. 567–571, 2017.

[14] H. Z. Feng and B. R. Stockwell, "Unsolved mysteries: how does lipid peroxidation cause ferroptosis?," *PLOS Biology*, vol. 16, no. 5, article e2006203, 2018.

[15] S. H. Hao, B. Liang, Q. Huang et al., "Metabolic networks in ferroptosis," *Oncology Letters*, vol. 15, no. 4, pp. 5405–5411, 2018.

[16] B. R. Stockwell, J. P. Friedmann Angeli, H. Bayir et al., "Ferroptosis: a regulated cell death nexus linking metabolism, redox biology, and disease," *Cell*, vol. 171, no. 2, pp. 273–285, 2017.

[17] Z. Wen-Bo, K. Chen-Fei, Q. Gao-Wei, W. Yuan-Yuan, L. Xin, and W. Xiao-Feng, "Research progresss on mechanism of ferroptosis," *Progress in Biochemistry and Biophysics*, vol. 45, no. 1, pp. 16–22, 2018.

[18] D. J. Lane, A. M. Merlot, M. L. Huang et al., "Cellular iron uptake, trafficking and metabolism: key molecules and mechanisms and their roles in disease," *Biochimica et Biophysica Acta*, vol. 1853, no. 5, pp. 1130–1144, 2015.

[19] M. Y. Kwon, E. Park, S. J. Lee, and S. W. Chung, "Heme oxygenase-1 accelerates erastin-induced ferroptotic cell death," *Oncotarget*, vol. 6, no. 27, pp. 24393–24403, 2015.

[20] H. Gao, Y. S. Bai, Y. Y. Jia et al., "Ferroptosis is a lysosomal cell death process," *Biochemical & Biophysical Research Communications*, vol. 503, no. 3, pp. 1550–1556, 2018.

[21] E. Gammella, S. Recalcati, I. Rybinska, P. Buratti, and G. Cairo, "Iron-induced damage in cardiomyopathy: oxidative-dependent and independent mechanisms," *Oxidative Medicine and Cellular Longevity*, vol. 2015, Article ID 230182, 10 pages, 2015.

[22] X. Sun, Z. Ou, M. Xie et al., "HSPB1 as a novel regulator of ferroptotic cancer cell death," *Oncogene*, vol. 34, no. 45, pp. 5617–5625, 2015.

[23] S. Doll, B. Proneth, Y. Y. Tyurina et al., "ACSL4 dictates ferroptosis sensitivity by shaping cellular lipid composition," *Nature Chemical Biology*, vol. 13, no. 1, pp. 91–98, 2017.

[24] V. E. Kagan, G. Mao, F. Qu et al., "Oxidized arachidonic and adrenic PEs navigate cells to ferroptosis," *Nature Chemical Biology*, vol. 13, no. 1, pp. 81–90, 2017.

[25] J. H. Woo, Y. Shimoni, W. S. Yang et al., "Elucidating Compound Mechanism of Action by Network Perturbation Analysis," *Cell*, vol. 162, no. 2, pp. 441–451, 2015.

[26] H. Yuan, X. M. Li, X. Y. Zhang, R. Kang, and D. Tang, "Identification of ACSL4 as a biomarker and contributor of ferroptosis," *Biochemical & Biophysical Research Communications*, vol. 478, no. 3, pp. 1338–1343, 2016.

[27] K. Shimada, R. Skouta, A. Kaplan et al., "Global survey of cell death mechanisms reveals metabolic regulation of ferroptosis," *Nature Chemical Biology*, vol. 12, no. 7, pp. 497–503, 2016.

[28] Y. Liu, W. Wang, Y. Y. Li, Y. Xiao, J. Cheng, and J. Jia, "The 5-lipoxygenase inhibitor zileuton confers neuroprotection against glutamate oxidative damage by inhibiting ferroptosis," *Biological & Pharmaceutical Bulletin*, vol. 38, no. 8, pp. 1234–1239, 2015.

[29] L. Y. Wang, Y. C. Liu, T. du et al., "ATF3 promotes erastin-induced ferroptosis by suppressing system xc^-," *Cell Death and Differentiation*, vol. 27, no. 2, pp. 662–675, 2020.

[30] M. Conrad and B. Proneth, "Broken hearts: iron overload, ferroptosis and cardiomyopathy," *Cell Reserach*, vol. 29, no. 4, pp. 263-264, 2019.

[31] G. C. Forcina and S. J. Dixon, "GPX4 at the crossroads of lipid homeostasis and ferroptosis," *Proteomics*, vol. 19, no. 18, article e1800311, 2019.

[32] R. Brigelius-Flohé and M. Maiorino, "Glutathione peroxidases," *Biochimica et Biophysica Acta*, vol. 1830, no. 5, pp. 3289–3303, 2013.

[33] L. C. Chang, S. K. Chiang, S. E. Chen, Y. L. Yu, R. H. Chou, and W. C. Chang, "Heme oxygenase-1 mediates BAY 11-7085 induced ferroptosis," *Cancer Letters*, vol. 416, pp. 124–137, 2018.

[34] L. Jiang, N. Kon, T. Y. Li et al., "Ferroptosis as a P53-mediated activity during tumour suppression," *Nature*, vol. 520, no. 7545, pp. 57–62, 2015.

[35] K. Shimada, M. Hayano, N. Pagano, and B. R. Stockwell, "Cell-line selectivity improves the predictive power of pharmacogenomic analyses and helps identify NADPH as biomarker for ferroptosis sensitivity," *Cell Chemical Biology*, vol. 23, no. 2, pp. 225–235, 2016.

[36] M. Skonieczna, A. Cieslar-Pobuda, Y. Saenko et al., "The impact of DIDS-Induced inhibition of voltage-dependent anion channels (VDAC) on cellular response of lymphoblastoid cells to ionizing radiation," *Medicinal Chemistry*, vol. 13, no. 5, pp. 477–483, 2017.

[37] J. J. Lemasters, "Evolution of voltage-dependent anion channel function: from molecular sieve to governator to actuator of ferroptosis," *Frontiers in Oncology*, vol. 7, p. 303, 2017.

[38] D. M. Lin, B. Q. Cui, J. R. Ren, and J. Ma, "Regulation of VDAC1 contributes to the cardioprotective effects of penehyclidine hydrochloride during myocardial ischemia/reperfusion," *Experimental Cell Research*, vol. 367, no. 2, pp. 257–263, 2018.

[39] Y. S. Feng, N. B. Madungwe, C. V. da Cruz Junho, and J. C. Bopassa, "Activation of G protein-coupled oestrogen receptor 1 at the onset of reperfusion protects the myocardium against ischemia/reperfusion injury by reducing mitochondrial dysfunction and mitophagy," *British Journal of Pharmacology*, vol. 174, no. 23, pp. 4329–4344, 2017.

[40] N. B. Madungwe, N. F. Zilberstein, Y. Feng, and J. C. Bopassa, "Critical role of mitochondrial ROS is dependent on their site of production on the electron transport chain in ischemic heart," *American Journal of Cardiovascular Disease*, vol. 6, no. 3, pp. 93–108, 2016.

[41] I. Poursaitidis, X. M. Wang, T. Crighton et al., "Oncogene-Selective Sensitivity to Synchronous Cell Death following Modulation of the Amino Acid Nutrient Cystine," *Cell Reports*, vol. 18, no. 11, pp. 2547–2556, 2017.

[42] H. K. Eltzschig and T. Eckle, "Ischemia and reperfusion–from mechanism to translation," *Nature Medicine*, vol. 17, no. 11, pp. 1391–1401, 2011.

[43] T. Kalogeris, C. P. Baines, M. Krenz, and R. J. Korthuis, "Cell biology of ischemia/reperfusion injury," *International Review of Cell and Molecular Biology*, vol. 298, pp. 229–317, 2012.

[44] L. J. Sparvero, H. Tian, A. A. Amoscato et al., "Direct mapping of phospholipid ferroptotic death signals in cells and tissues by gas cluster ion beam secondary ion mass spectrometry (GCIB-SIMS)," *Angewandte Chemie(International ed. In English)*, vol. 60, no. 21, pp. 11784–11788, 2021.

[45] I. A. Paraskevaidis, E. K. Iliodromitis, D. Vlahakos et al., "Deferoxamine infusion during coronary artery bypass grafting ameliorates lipid peroxidation and protects the myocardium against reperfusion injury: immediate and long-term significance," *European Heart Journal*, vol. 26, no. 3, pp. 263–270, 2005.

[46] R. E. Williams, J. L. Zweier, and J. T. Flaherty, "Treatment with deferoxamine during ischemia improves functional and metabolic recovery and reduces reperfusion-induced oxygen radical generation in rabbit hearts," *Circulation*, vol. 83, no. 3, pp. 1006–1014, 1991.

[47] I. Tabas and D. Ron, "Integrating the mechanisms of apoptosis induced by endoplasmic reticulum stress," *Nature Cell Biology*, vol. 13, no. 3, pp. 184–190, 2011.

[48] Y. S. Lee, D. H. Lee, H. A. Choudry, D. L. Bartlett, and Y. J. Lee, "Ferroptosis-induced endoplasmic reticulum stress: cross-talk between ferroptosis and apoptosis," *Molecular Cancer Research*, vol. 16, no. 7, pp. 1073–1076, 2018.

[49] W. Zhang, Z. Sun, and F. Meng, "*Schisandrin B* ameliorates myocardial ischemia/reperfusion injury through attenuation of endoplasmic reticulum stress-induced apoptosis," *Inflammation*, vol. 40, no. 6, pp. 1903–1911, 2017.

[50] R. J. Bridges, N. R. Natale, and S. A. Patel, "System xc^- cystine/-glutamate antiporter: an update on molecular pharmacology and roles within the CNS," *British Journal of Pharmacology*, vol. 165, no. 1, pp. 20–34, 2012.

[51] S. J. Dixon, D. N. Patel, M. Welsch et al., "Pharmacological inhibition of cystine-glutamate exchange induces endoplasmic reticulum stress and ferroptosis," *eLife Sciences*, vol. 3, article e02523, 2014.

[52] A. P. Ghosh, B. J. Klocke, M. E. Ballestas, and K. A. Roth, "CHOP potentially co-operates with fOXO3a in neuronal cells to regulate PUMA and BIM expression in response to ER stress," *PLoS ONE*, vol. 7, no. 6, article e39586, 2012.

[53] H. Urra, E. Dufey, F. Lisbona, D. Rojas-Rivera, and C. Hetz, "When ER stress reaches a dead end," *Biochimica Biophys et Biophysica Acta*, vol. 1833, no. 12, pp. 3507–3517, 2013.

[54] S. H. Hong, D. H. Lee, Y. S. Lee et al., "Molecular crosstalk between ferroptosis and apoptosis: emerging role of ER stress-induced p53-independent PUMA expression," *Oncotarget*, vol. 8, no. 70, pp. 115164–115178, 2017.

[55] X. Chen, Y. Wang, X. Xie et al., "Heme oxygenase-1 reduces sepsis-induced endoplasmic reticulum stress and acute lung injury," *Mediators of Inflammation*, vol. 2018, no. 4, Article ID 9413876, 10 pages, 2018.

[56] W. Y. Li, W. Li, Y. Leng, Y. Xiong, and Z. Xia, "Ferroptosis is involved in diabetes myocardial ischemia/reperfusion injury through endoplasmic reticulum stress," *DNA and Cell Biology*, vol. 39, no. 2, pp. 210–225, 2020.

[57] V. S. Viswanathan, M. J. Ryan, H. D. Dhruv et al., "Dependency of a therapy-resistant state of cancer cells on a lipid peroxidase pathway," *Nature*, vol. 547, no. 7664, pp. 453–457, 2017.

[58] C. Li, X. B. Deng, W. Zhang et al., "Novel Allosteric activators for ferroptosis regulator glutathione peroxidase 4," *Journal of Medicinal Chemistry*, vol. 62, no. 1, pp. 266–275, 2019.

[59] D. Tang, R. Kang, T. V. Berghe, P. Vandenabeele, and G. Kroemer, "The molecular machinery of regulated cell death," *Cell Research*, vol. 29, no. 5, pp. 347–364, 2019.

[60] L. J. Tang, X. J. Luo, H. Tu et al., "Ferroptosis occurs in phase of reperfusion but not ischemia in rat heart following ischemia or ischemia/reperfusion," *Naunyn-Schmiedeberg's Archives of Pharmacology*, vol. 394, no. 2, pp. 401–410, 2021.

[61] E. R. Dabkowski, C. L. Williamson, and J. M. Hollander, "Mitochondria-specific transgenic overexpression of phospholipid hydroperoxide glutathione peroxidase (GPx4) attenuates ischemia/reperfusion-associated cardiac dysfunction," *Free Radical Biology & Medicine*, vol. 45, no. 6, pp. 855–865, 2008.

[62] A. Jelinek, L. Heyder, M. Daude et al., "Mitochondrial rescue prevents glutathione peroxidase-dependent ferroptosis," *Free Radical Biology & Medicine*, vol. 117, pp. 45–57, 2018.

[63] T. Y. Zhou, C. C. Chen, and Z. Li, "Molecular Characterization of Reactive Oxygen Species in Myocardial Ischemia- Reperfusion Injury," *BioMed research international*, vol. 2015, Article ID 864946, 9 pages, 2015.

[64] X. X. Fang, H. Wang, D. Han et al., "Ferroptosis as a target for protection against cardiomyopathy," *Proceedings of the National Academy of the United States of America*, vol. 116, no. 7, pp. 2672–2680, 2019.

[65] X. Wu, Y. Li, S. Zhang, and X. Zhou, "Ferroptosis as a novel therapeutic target for cardiovascular disease," *Theranostics*, vol. 11, no. 7, pp. 3052–3059, 2021.

[66] R. Rodrigo, J. C. Prieto, and R. Castillo, "Cardioprotection against ischaemia/reperfusion by vitamins C and E plus n-3 fatty acids: molecular mechanisms and potential clinical applications," *Clinical Science (London, England: 1979)*, vol. 124, no. 1, pp. 1–15, 2013.

[67] A. Alu, X. J. Han, X. L. Ma, M. Wu, Y. Wei, and X. Wei, "The role of lysosome in regulated necrosis," *Acta Pharmaceutica Sinica B*, vol. 10, no. 10, pp. 1880–1903, 2020.

[68] Y. Kinowaki, M. Kurata, S. Ishibashi et al., "Glutathione peroxidase 4 overexpression inhibits ROS-induced cell death in diffuse large B-cell lymphoma," *Laboratory Investigation*, vol. 98, no. 5, pp. 609–619, 2018.

[69] S. Doll and M. Conrad, "Iron and ferroptosis: a still ill-defined liaison," *International Union of Biochemistry and Molecular Biology Life*, vol. 69, no. 6, pp. 423–434, 2017.

[70] Y. S. Feng, N. B. Madungwe, A. D. Imam Aliagan, N. Tombo, and J. C. Bopassa, "Liproxstatin-1 protects the mouse myocardium against ischemia/reperfusion injury by decreasing VDAC1 levels and restoring GPX4 levels," *Biochemical and Biophysical Research Communications*, vol. 520, no. 3, pp. 606–611, 2019.

[71] S. Ma, L. Sun, W. Wu, J. Wu, Z. Sun, and J. Ren, "USP22 protects against myocardial Ischemia–Reperfusion injury via the SIRT1-p53/SLC7A11–Dependent inhibition of ferroptosis-induced cardiomyocyte death," *Frontiers in Physiology*, vol. 11, article 551318, 2020.

[72] B. Shi, M. Ma, Y. Zheng, Y. Pan, and X. Lin, "MTOR and beclin1:two key autophagy-related molecules and their roles in myocardial ischemia/reperfusion injury," *Journal of Cellular Physiology*, vol. 234, no. 8, pp. 12562–12568, 2019.

[73] B. Zhou, J. Liu, R. Kang, D. J. Klionsky, G. Kroemer, and D. Tang, "Ferroptosis is a type of autophagy-dependent cell death," *Seminars in Cancer Biology*, vol. 66, pp. 89–100, 2020.

[74] D. W. Zhang, Y. He, X. D. Ye et al., "Activation of autophagy inhibits nucleotide-binding oligomerization domain-like receptor protein 3 inflammasome activation and attenuates myocardial ischemia-reperfusion injury in diabetic rats," *Journal of Diabetes Investigation*, vol. 11, no. 5, pp. 1126–1136, 2020.

[75] M. Aghaei, M. Motallebnezhad, S. Ghorghanlu et al., "Targeting autophagy in cardiac ischemia/reperfusion injury: a novel therapeutic strategy," *Journal of cellular and comparative physiology*, vol. 234, no. 10, pp. 16768–16778, 2019.

[76] S. Wang, C. Wang, F. Yan et al., "N-Acetylcysteine attenuates diabetic myocardial ischemia reperfusion injury through inhibiting excessive autophagy," *Mediators of Inflammation*, vol. 2017, Article ID 9257291, 10 pages, 2017.

[77] D. Wu, K. F. Zhang, and P. F. Hu, "The role of autophagy in acute myocardial infarction," *Frontiers in Pharmacology*, vol. 10, p. 551, 2019.

[78] Y. L. Zhou, Y. Shen, C. Chen et al., "The crosstalk between autophagy and ferroptosis:what can we learn to target drug resistance in cancer?," *Cancer Biology & Medicine*, vol. 16, no. 4, pp. 630–646, 2019.

[79] S. Srikantan and M. Gorospe, "HuR function in disease," *Frontiers in Bioscience*, vol. 17, no. 1, pp. 189–205, 2012.

[80] H. Y. Chen, Z. Z. Xiao, X. Ling, R. N. Xu, P. Zhu, and S. Y. Zheng, "ELAVL1 is transcriptionally activated by FOXC1 and promotes ferroptosis in myocardial ischemia/reperfusion injury by regulating autophagy," *Molecular Medicine*, vol. 27, no. 1, pp. 1–14, 2021.

[81] S. Hannenhalli and K. H. Kaestner, "The evolution of fox genes and their role in development and disease," *Nature Reviews. Genetics*, vol. 10, no. 4, pp. 233–240, 2009.

[82] Z. Fan, L. Cai, S. Wang, J. Wang, and B. Chen, "Baicalin prevents myocardial ischemia/reperfusion injury through inhibiting ACSL4 mediated ferroptosis," *Frontiers in Pharmacology*, vol. 12, article 628988, 2021.

[83] W. Chan, A. J. Taylor, A. H. Ellims et al., "Effect of iron chelation on myocardial infarct size and oxidative stress in ST-elevation-myocardial infarction," *Circulation. Cardiovascular Interventions*, vol. 5, no. 2, pp. 270–278, 2012.

[84] A. Stamenkovic, K. A. O'Hara, D. C. Nelson et al., "Oxidized phosphatidylcholines trigger ferroptosis in cardiomyocytes during ischemia-reperfusion injury," *American Journal of Physiology. Heart and Circulatory Physiology*, vol. 320, no. 3, pp. H1170–H1184, 2021.

[85] X. Shan, Z. Y. Lv, M. J. Yin, J. Chen, J. Wang, and Q. N. Wu, "The Protective Effect of Cyanidin-3-Glucoside on Myocardial Ischemia- Reperfusion Injury through Ferroptosis," *Oxidative Medicine and Cellular Longevity*, vol. 2021, Article ID 8880141, 15 pages, 2021.

[86] C. Y. Wang, L. J. Zhu, W. L. Yuan et al., "Diabetes aggravates myocardial ischaemia reperfusion injury via activating Nox2-related programmed cell death in an AMPK-dependent manner," *Journal of Cellular and Molecular Medicine*, vol. 24, no. 12, pp. 6670–6679, 2020.

[87] W. G. Li, G. S. Feng, J. M. Gauthier et al., "Ferroptotic cell death and TLR4/Trif signaling initiate neutrophil recruitment

after heart transplantation," *The Journal of Clinical Investigation*, vol. 129, no. 6, pp. 2293–2304, 2019.

[88] W. S. Yang, R. SriRamaratnam, M. E. Welsch et al., "Regulation of ferroptotic cancer cell death by GPX4," *Cell*, vol. 156, no. 1-2, pp. 317–331, 2014.

[89] S. J. Dixon, G. E. Winter, L. S. Musavi et al., "Human haploid cell genetics reveals roles for lipid metabolism genes in nonapoptotic cell death," *ACS Chemical Biology*, vol. 10, no. 7, pp. 1604–1609, 2015.

[90] T. Lőrincz, K. Jemnitz, T. Kardon, J. Mandl, and A. Szarka, "Ferroptosis is involved in acetaminophen induced cell death," *Pathology & Oncology Research*, vol. 21, no. 4, pp. 1115–1121, 2015.

[91] C. Louandre, I. Marcq, H. Bouhlal et al., "The retinoblastoma (Rb) protein regulates ferroptosis induced by sorafenib in human hepatocellular carcinoma cells," *Cancer Letters*, vol. 356, no. 2, pp. 971–977, 2015.

[92] C. Louandre, Z. Ezzoukhry, C. Godin et al., "Iron-dependent cell death of hepatocellular carcinoma cells exposed to sorafenib," *International Journal of Cancer*, vol. 133, no. 7, pp. 1732–1742, 2013.

[93] E. Lachaier, C. Louandre, C. Godin et al., "Sorafenib induces ferroptosis in human cancer cell lines originating from different solid tumors," *Anticancer Research*, vol. 34, no. 11, pp. 6417–6422, 2014.

[94] N. Eling, L. Reuter, J. Hazin, A. Hamacher-Brady, and N. R. Brady, "Identification of artesunate as a specific activator of ferroptosis in pancreatic cancer cells," *Oncoscience*, vol. 2, no. 5, pp. 517–532, 2015.

[95] R. Skouta, S. J. Dixon, J. Wang et al., "Ferrostatins inhibit oxidative lipid damage and cell death in diverse disease models," *Journal of the American Chemical Society*, vol. 136, no. 12, pp. 4551–4556, 2014.

[96] M. Matsushita, S. Freigang, C. Schneider, M. Conrad, G. W. Bornkamm, and M. Kopf, "T cell lipid peroxidation induces ferroptosis and prevents immunity to infection," *Journal of Experimental Medicine*, vol. 212, no. 4, pp. 555–568, 2015.

[97] A. Linkermann, R. Skouta, N. Himmerkus et al., "Synchronized renal tubular cell death involves ferroptosis," *Proceedings of the National Academy of Sciences of the United States of America*, vol. 111, no. 47, pp. 16836–16841, 2014.

[98] J. P. Friedmann Angeli, M. Schneider, B. Proneth et al., "Inactivation of the ferroptosis regulator Gpx4 triggers acute renal failure in mice," *Nature Cell Biology*, vol. 16, no. 12, pp. 1180–1191, 2014.

[99] J. Peng and D. O. Pharmacology, "Ferroptosis: a new way of myocardial cell death after ischemia /reperfusion," *Chinese Journal of Arteriosclerosis*, vol. 26, no. 8, pp. 757–760, 2018.

Hindawi
Oxidative Medicine and Cellular Longevity
Volume 2021, Article ID 6256399, 11 pages
https://doi.org/10.1155/2021/6256399

Research Article

PER2 Regulates Reactive Oxygen Species Production in the Circadian Susceptibility to Ischemia/Reperfusion Injury in the Heart

Yaqian Weng, Hui Li, Lin Gao, Wenjing Guo, Shiyuan Xu, and Le Li

Department of Anesthesiology, Zhujiang Hospital, Southern Medical University, Guangzhou, Guangdong 510282, China

Correspondence should be addressed to Shiyuan Xu; xsy998@smu.edu.cn and Le Li; lile11@126.com

Received 30 April 2021; Revised 15 August 2021; Accepted 24 August 2021; Published 8 October 2021

Academic Editor: Haobo Li

The main objective of this study was to investigate the diurnal differences in Period 2 (PER2) expression in myocardial ischemia-reperfusion (I/R) injury. We investigated diurnal variations in oxidative stress and energy metabolism after myocardial I/R in vitro and in vivo. In addition, we also analyzed the effects of H_2O_2 treatment and serum shock in H9c2 cells transfected with silencing RNA against Per2 (siRNA-Per2) in vitro. We used C57BL/6 male mice to construct a model of I/R injury at zeitgeber time (ZT) 2 and ZT14 by synchronizing the circadian rhythms. Our in vivo analysis demonstrated that there were diurnal differences in the severity of injury caused by myocardial infarctions, with more injury occurring in the daytime. PER2 was significantly reduced in heart tissue in the daytime and was higher at night. Our results also showed that more severe injury of mitochondrial function in daytime produced more reactive oxygen species (ROS) and less ATP, which increased myocardial injury. In vitro, our findings presented a similar trend showing that apoptosis of H9c2 cells was increased when PER2 expression was lower. Meanwhile, downregulation of PER2 disrupted the oxidative balance by increasing ROS and mitochondrial injury. The result was a reduction in ATP and failure to provide sufficient energy protection for cardiomyocytes.

1. Introduction

Acute myocardial infarction (AMI) is a major cause of morbidity and mortality worldwide. Emergency treatment for AMI has been revolutionized by timely reperfusion therapy [1]. Reperfusion is "a double-edged sword." It not only provides oxygen and nutrients for ATP production and washes out toxic metabolite accumulation but also induces a burst of reactive oxygen species (ROS) leading to a second injury or dominant injury [2, 3]. However, there is no therapy directly targeting the injury caused by reperfusion.

The frequency of the onset of AMI is not random and has been reported to have a circadian variation, with the peak in the early morning [4]. Also, circadian rhythmicity of the heart has been reported in multiple animal studies [5, 6]. In particular, recent studies using mutant mouse models with cardiomyocyte-specific defects in the core clock machinery suggested that susceptibility of the myocardium itself varies in a time-of-day-specific fashion [7]. However, the molecular mechanism remains poorly understood.

The circadian clock within the heart modulates myocardial metabolism, which in turn facilitates anticipation of diurnal variations in workload, stimuli, and/or the energy supply-to-demand ratio [8]. ROS, as an intrinsic by-product of oxidative phosphorylation, also undergoes circadian rhythms [9]. It may be beneficial for the organism to coordinate catabolism/energy utilization and ROS clearance in a circadian fashion. Nonetheless, a master transcriptional regulator of both processes is not known.

Period 2 (PER2), a molecular component of the mammalian circadian clock, plays a key role in controlling the circadian rhythms in physiology and behavior [10]. Recently, increasing evidence has suggested that PER2 mediates the cardiac protection effect [11, 12]. *Per2*$^{-/-}$ mice have larger infarct sizes with deficient lactate production during myocardial ischemia [13], suggesting that PER2 protects

the heart by regulating catabolism/energy. PER2 was also reported to be involved in regulating the cellular response to oxidative stress in mouse embryonic fibroblasts [14], pancreatic islets [15], and other organs. In the present study, we discovered that the circadian rhythm protein PER2 mediates susceptibility to I/R insult in a time-of-day-dependent fashion by regulating energy utilization and ROS clearance.

2. Methods

2.1. Animals. The use of specific pathogen-free C57BL/6J mice was approved by the Institutional Animal Care Committee at Zhujiang Hospital of Southern Medical University, China. Mice were housed in a temperature- and humidity-controlled specific pathogen-free facility with a 12 h light/-dark cycle and *ad libitum* access to water and standard laboratory rodent chow.

2.2. Ischemia-Reperfusion (I/R) Surgery. I/R studies were performed on 10–12-week-old male mice. Mice were anesthetized with sodium pentobarbital (70 mg/kg intraperitoneally), placed on a temperature-controlled heating pad, and ventilated through endotracheal intubation. A standard 3-lead EKG and a rectal temperature probe were placed for monitoring. A thoracotomy was performed, and the heart was exposed by stripping the pericardium. The left anterior descending coronary artery was encircled by an 8-0 Prolene suture, and ischemia was induced by tightening the suture, which was confirmed visually by blanching of the distal cardiac tissue and ST-elevation on the electrocardiogram [16]. The suture was released after 30 min to allow reperfusion. The mice were maintained on ventilation until recovery from anesthesia. Infarct size was assessed 24 h postreperfusion using 1% Evans blue and 2% triphenyltetrazolium chloride (TTC) staining [17] and was expressed as a percentage of the at-risk area.

2.3. Echocardiographic Assessment. At the end of reperfusion, mice were reanesthetized with isoflurane, fixed on the experimental table, and studied with an echocardiography system (Vevo 2100, a high-resolution ultrasound echocolor Doppler system from VisualSonics, Canada). The following variables were measured and averaged during three consecutive cardiac cycles: left ventricular end-systolic diameter (LVESD), left ventricular end-diastolic diameter (LVEDD), left ventricular end-systolic volume (LVSV), and left ventricular end-diastolic volume (LVDV). The left ventricular ejection fraction (LVEF) and left ventricular fractional shortening (LVFS) values were converted by the Simpson method with the following formula: $\mathrm{LVEF} = (\mathrm{LVDV} - \mathrm{LVSV})/\mathrm{LVDV} \times 100\%$; $\mathrm{LVFS} = (\mathrm{LVDD} - \mathrm{LVSD})/\mathrm{LVDD} \times 100\%$. LVEF and LVFS were used as parameters indicating cardiac function [18]. The experiment was conducted three times, and the mean value was obtained.

2.4. Cell Culture and Serum Shock-Induced Circadian Rhythms. H9c2 cells were purchased from the National Collection of Authenticated Cell Culture (China). H9c2 cells were grown in an incubator in a DMEM-F12 medium (Corning) complemented with 10% fetal bovine serum (FBS; GIBCO) at 37°C in 5% CO_2. Cells were subcultured every 4 days prior to the experiment in 6-well plates; they were confluent after 4 days. The cells were treated with 50% horse serum (50% DMEM-F12 and 50% horse serum, BI) for 2 h and were then washed twice with tepid DMEM-F12 without serum. Samples were taken every 4 h for 24 h following serum shock. Harvested cells were immediately frozen at −80°C until RNA isolation or protein extraction [19, 20].

2.5. H_2O_2 Treatment after Serum Shock in Cells Transfected with siRNA-Per2. For transfection experiments, 1×10^5 H9c2 cells were plated in 6-well plates the day before transfection. Transfections were performed using 1 μg siRNA oligo targeting *Per2* and 5 μl Lipofectamine 3000 (Thermo Fisher, USA) in serum-free media per well, according to the manufacturer's protocol. After 12 h of transfection, the cells were treated with 50% horse serum for 2 h. At the end point or 12 h after serum shock, cells were treated with H_2O_2 for 2 h [21, 22].

2.6. TUNEL Staining. Cardiomyocyte apoptosis was assessed in heart sections by terminal deoxynucleotidyl transferase dUTP nick end labeling (TUNEL). The TUNEL mix (KeyGEN Biotech) contained 50 μl enzyme solution and 450 μl labeling solution. Heart sections were incubated with 50 μl TUNEL mix at 37°C for 1 h. The sections were then washed twice with PBS and stained with DAPI. After washing with PBS for another three times, the sections were observed by fluorescence microscopy with Ex (λ) 450–500 nm, Em (λ) 515–565 nm for TUNEL and Ex (λ) 359 nm, Em (λ) 461 nm for DAPI (NIKON T12-E, Japan). The apoptosis ratio was calculated as apoptotic cell number (green)/total cell number (blue) × 100%.

2.7. Determination of ROS Production. Dihydroethidium (DHE, BestBio, China) staining was used to detect ROS levels in heart tissue. Fresh mouse heart tissue samples were embedded in an OCT compound (Thermo Fisher). Cryopreserved sections were then loaded with 500 μM DHE following the manufacturer's instructions. Oxidized DHE was excited at 543 nm, and emission was collected with a LP 560 nm filter using the NIKON T12-E fluorescence microscope.

Intracellular ROS levels in H9c2 cells were determined by measuring the oxidative conversion of cell-permeable 2′,7′-dichlorofluorescein diacetate (DCFH-DA) to fluorescent dichlorofluorescein (DCF). The cells were washed with D-Hank's balanced salt solution (HBSS) and incubated with DCFH-DA at 37°C for 20 min. Then, fluorescence was detected by flow cytometry at Ex (λ) 488 nm, Em (λ) 525 nm (Beckman Coulter), which would collect and analyze ten thousand cells in each flow cytometric assay.

2.8. Determination of ATP Production. Adenosine 5′-triphosphate (ATP; Nanjing Jiancheng Bioengineering Institute, China) staining was used to detect ATP levels in heart tissue and H9c2 cells according to the manufacturer's instructions, using a microplate reader (Thermo Fisher).

2.9. Mitochondrial Membrane Potential (MMP) Measurement. The MMP of H9c2 cells was measured using the fluorescent probe, JC-1 (KeyGEN Biotech). The cells were rinsed with

HBSS and incubated with JC-1 (10 μM) at 37°C for 30 min. Afterwards, the cells were rinsed with HBSS once again. Fluorescent intensity of the JC-1 monomers and aggregates was detected by flow cytometry with Ex (λ) 490 nm, Em (λ) 530 nm for monomers and Ex (λ) 525 nm, Em (λ) 590 nm for aggregates (Beckman Coulter), and ten thousand cells were collected and analyzed each time.

2.10. Quantitative RT-PCR. Heart samples or H9c2 cells were disrupted/homogenized in a TRIzol reagent (Accurate Biotechnology, China) with a Tissue-lyzer (LUKYM, China), and total RNA was extracted according to the manufacturer's directions. RNA was reverse transcribed using the Accurate Biotechnology reverse transcription kit following the manufacturer's instructions. Quantitative PCR was performed using the SYBR Green Premix Pro Taq HS qPCR Kit (Accurate Biotechnology) using a two-step PCR amplification standard procedure on a Bio-Rad (USA) CFX connect system. Relative expression was calculated using the $\Delta\Delta$Ct method with normalization to *Gapdh*. Specific primer/probe sequences are shown below. Primer sequences are listed in Table 1 of supplementary data.

2.11. Immunoblots and Antibodies. Whole-cell lysates or isolated mitochondrial lysates were prepared by homogenizing the basal regions of the hearts in RIPA buffer (Invitrogen, USA) supplemented with protease 13 inhibitors (Invitrogen). Immunoblots were prepared using the antibodies listed below and were normalized to GAPDH (Sigma, USA). Antibodies used for western blots are listed in Table 2 of supplementary data.

2.12. Statistics. The results are presented as the means ± SEM . Two-tailed Student's *t*-tests were used to compare the difference between two groups. One-way or two-way ANOVA with Bonferroni correction was used for multiple comparisons. Statistical significance was defined as $P < 0.05$.

3. Results

3.1. Diurnal Differences in Myocardial Infarction Injury. The infarct area of cardiac tissue in each group was detected by TTC and Evans blue staining and quantified using ImageJ. The results showed that the area at risk in the left ventricle (AAR/LV) after I/R was not significantly different among the four groups (Figure 1(b), left). However, the infarct area in the area at risk (IR/AAR) after I/R at ZT2 was larger than at ZT14, while no difference was observed at ZT8 or ZT20 (Figure 1(b), right). As shown in Figure 1(c), ischemia followed by reperfusion induced significant myocardial injury as denoted by the white infarct size in mice. In contrast, ZT14 significantly decreased the ratio of infarct area/risk area (MI/AAR) compared with the ZT2 group (Figure 1(c), right).

M-mode ultrasound was used to evaluate changes in cardiac function of 10~12-week-old mice in each group, 24 h after myocardial I/R. Typical M-mode ultrasounds showed that compared with the sham group without I/R at zeitgeber time (ZT) 2 or ZT14, the ejection fraction (EF) of the left ventricle was decreased in mice 24 h after I/R. In addition, the EF in mice after I/R at ZT2 was lower than that in mice after I/R at ZT14 Figure 1(d), left). At the same time, fraction shortening (FS) of the left ventricle in mice after I/R at ZT2 was lower than that in mice with I/R at ZT14 (Figure 1(d), right), which showed that mice receiving I/R at ZT2 had worse cardiac systolic function than at ZT14.

3.2. Diurnal Differences in Oxidative Stress and Energy Metabolism. Histological analysis and immunofluorescence staining were performed to further evaluate myocardial cell activity. Typical results of TUNEL staining showed that cell apoptosis of myocardial tissue after I/R at ZT2 was more extensive than that observed in the ZT14 group (Figure 2(a)). These results suggested that I/R at ZT2 could significantly increase myocardial cell apoptosis (Figure 2(b)).

DHE staining results showed that ROS was increased in myocardial cells after I/R, where the ROS level in the ZT2 group was higher than that in the ZT14 group (Figure 2(c)).

ATP determination assays performed in each group showed that without I/R, sham-ZT14 mice produced more ATP than sham-ZT2 mice, although the difference was not statistically significant. In contrast, 24 h after I/R at ZT2, ATP content was lower than in sham-ZT2 mice. The ATP content 24 h after I/R at ZT14 was higher than that in the sham-ZT14 group, which indicated that mice produced more ATP at ZT14 while producing less ATP at ZT2 (Figure 2(d)).

3.3. Diurnal Differences Affected the Expression of PER2 and CPT1A. mRNA and protein were collected from the mice every 4 h for 24 h. The transcription level of *Per2* showed a distinct rhythmic pattern for nearly 24 h (Figure 3(a)). The transcription level of *Per2* increased from ZT2, reaching a peak value near ZT14, then decreased again to a low value near ZT2 (Figure 3(a)). The change in PER2 protein levels was consistent with the mRNA results. Mice displayed a rhythm in PER2 protein expression with peak values at ZT14 and lowest values at ZT2 as shown by western blotting (Figure 3(b)). The protein expression of PER2, carnitine palmitoyltransferase 1A (CPT1A), and pyruvate dehydrogenase PDH-E1B (PDHB) after I/R was also detected by western blotting (Figure 3(c)). The results showed that the protein expression of PER2 and CPT1A was similar under the same treatment conditions and decreased after I/R at ZT2, while increasing after I/R at ZT14. PDHB showed no difference after I/R.

3.4. Downregulation of PER2 Increased Injury. H9c2 cells that were transfected with siRNA-*Per2* were collected after H_2O_2 treatment and serum shock at 0 h and 12 h. mRNA was collected every 4 h for 24 h. The transcription level of *Per2* showed a distinct rhythmic pattern for nearly 24 h (Figure 4(a)). From 0 h after serum shock, the transcription level of *Per2* decreased until reaching a low value near 12 h (Figure 4(a)). After transfection with siRNA-Per2, there was a significant reduction in PER2, shown in Figure 4(b).

ATP determination assays were also performed for each group. After H_2O_2 treatment, ATP was decreased at 12 h but was increased at 0 h (Figure 4(c)). ATP levels were

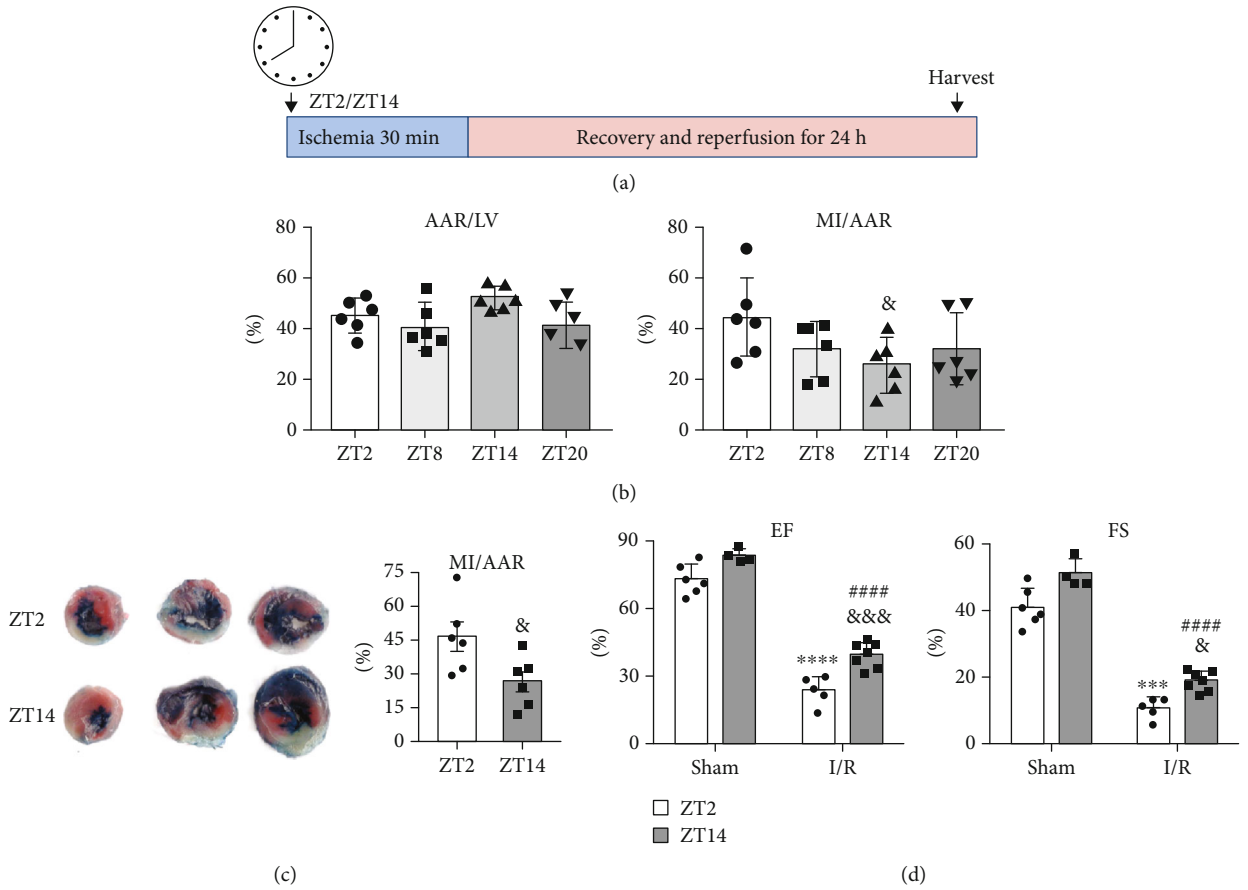

Figure 1: Circadian differences in susceptibility of the heart to I/R injury. (a) Experimental design. Mice were subjected to a protocol of 30 min of ischemia followed by 24 h of reperfusion starting at two time points, ZT2 or ZT14. ZT: zeitgeber time; ZT0: lights on. (b) Percent of area at risk over area of the left ventricle (middle). Percent of infarct over area at risk (right). AAR: area at risk; LV: left ventricle; MI: myocardial infarction ($n = 6$, $^{\&}P < 0.05$ vs. ZT2). (c) Infarct size. Representative Evans blue and TTC staining (left). Percent of infarct over area at risk (right). White: infarct; red: viable; white+red: area at risk; blue: retrograde Evans blue staining, area not at risk ($n = 6$, $^{\&}P < 0.05$ vs. IR-ZT2, two-tailed Student's t-test). (d) Cardiac systolic function of mice with I/R at ZT2 and ZT14. EF of the left ventricle (left), FS of the left ventricle (right). EF: ejection fraction; FS: fraction shortening; sham: sham surgery; I/R: ischemia-reperfusion. ($n = 4$–7, $^{****}P < 0.0001$ and $^{***}P < 0.001$ vs. sham-ZT2; $^{\#\#\#\#}P < 0.0001$ vs. sham-ZT14; $^{\&}P < 0.05$ and $^{\&\&\&}P < 0.001$ vs. IR-ZT2, two-tailed Student's t-tests). Alpha was set as 0.05. Data are presented as the mean ± SEM. The Holm-Sidak method was used to correct for multiple t-tests.

significantly decreased after siRNA-*Per2* transfection (Figure 4(c)), suggesting that downregulation of PER2 decreased ATP.

Histological analysis and immunofluorescence staining were performed to further evaluate H9c2 cell activity. The results of TUNEL staining showed that cellular apoptosis of H9c2 cells after H_2O_2 treatment at 0 h was less than apoptosis at 12 h after serum shock (Figure 4(d)). After siRNA-*Per2* transfection, cell death increased compared with the control group, but there was no significant difference at 0 h or 12 h after serum shock whether the cells were treated with H_2O_2 or not. These results indicated that in H9c2 cells, 12 h of serum shock and siRNA-*Per2* transfection could both increase myocardial cell apoptosis (Figure 4(d)).

ROS detected by flow cytometry showed that in cells treated with H_2O_2, ROS increased significantly (Figure 4(e)). At the same time, ROS increased after siRNA-*Per2* transfection, whether or not the cells were treated with H_2O_2 (Figure 4(e)).

Flow cytometric analysis was performed to identify quantitatively the MMP in H9c2 cells, which is one of the important hallmarks of mitochondrial damage. The contour plots in Figure 4(f) showed that the fluorescence for high MMP in Q2 was shifted to low MMP in Q3. H_2O_2 treatment showed a strong ability to dissipate the MMP, and cells after 12 h of serum shock showed more dissipation of MMP than cells at 0 h (Figure 4(f)). Furthermore, transfection of siRNA-*Per2* resulted in more dissipation of MMP. These results suggested that the mitochondrial membrane was impaired by H_2O_2, siRNA-*Per2* transfection, and 12 h of serum shock (Figure 4(e), lower panel, right figure).

mRNA expression of *Per2*, *Cpt1a*, and *Pdhb* in H9c2 cells was quantified by RT-PCR analysis (Figure 4(g)). The results showed that the expression of *Per2* and *Cpt1a* was similar under the same treatment conditions. Expression of these genes was higher before serum shock compared with 12 h later and decreased after H_2O_2 treatment or siRNA-*Per2* transfection.

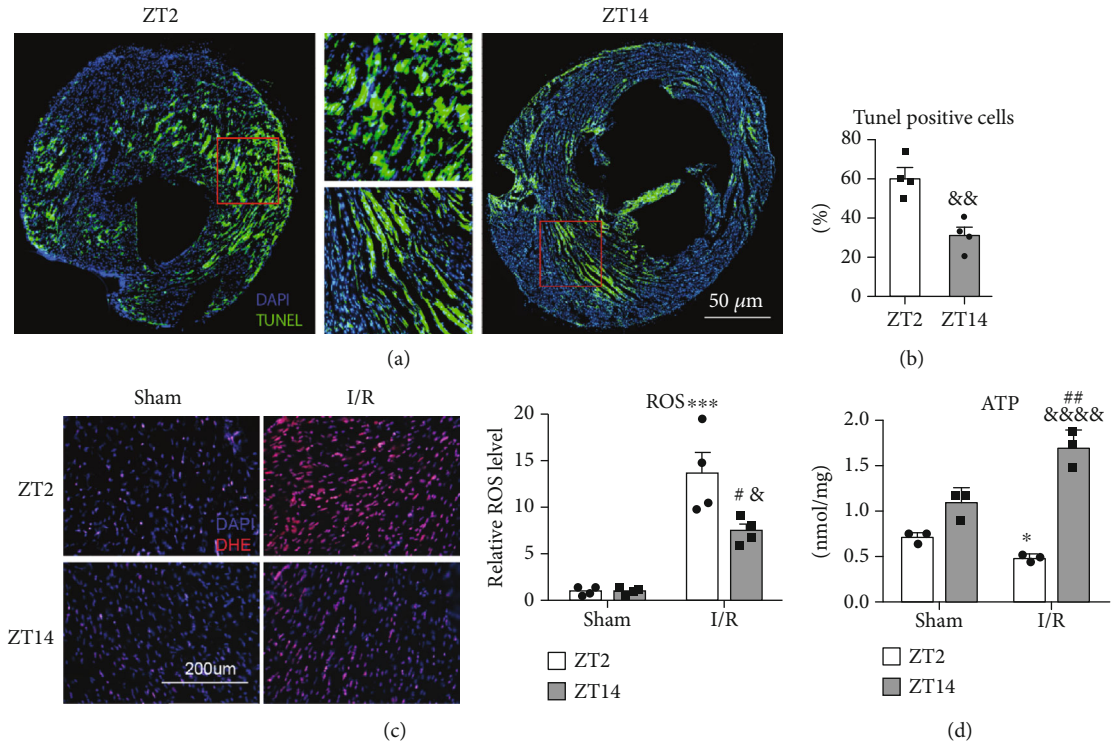

Figure 2: Circadian differences in oxidative stress and energy metabolism. (a) Apoptotic cells were determined by TUNEL staining. Representative apoptotic cells of mouse hearts after I/R injury at ZT2 (left) and ZT14 (right). Magnified area of interest from mouse heart after I/R injury at ZT2 (up middle) and ZT14 (bottom middle). (b) Quantitative analysis of TUNEL cells ($n = 4$, $^{\&\&}P < 0.01$ vs. IR-ZT2, two-tailed Student's t-test). (c) ROS in the hearts of mice. Representative DHE staining of the peri-infarct area of mouse hearts after 24 h IR at ZT2 and ZT14 (left), quantitative analysis of ROS (middle) ($n = 4$, $^{***}P < 0.001$ vs. sham-ZT2; $^{\#}P < 0.05$ vs. sham-ZT14; $^{\&}P < 0.05$ vs. IR-ZT2, two-tailed Student's t-tests). (d) ATP change in mouse hearts with I/R injury ($n = 3$, $^{*}P < 0.05$ vs. sham-ZT2; $^{\#\#}P < 0.01$ vs. sham-ZT14; $^{\&\&\&\&}P < 0.0001$ vs. IR-ZT2, two-tailed Student's t-tests). Alpha was set as 0.05. Data are presented as the means ± SEM. The Holm-Sidak method was used to correct for multiple t-tests.

4. Discussion

Taken as a whole, the current findings suggested that PER2 was the basis of circadian changes in cardiac tolerance to I/R and that knockdown of PER2 expression could increase I/R damage. Furthermore, PER2 likely acted downstream as a mediator underlying the transcriptional clock mechanism in cardiac susceptibility to I/R damage by regulating CPT1A as a key enzyme in fatty acid metabolism and oxidative stress levels. This result is important because it focuses on energy metabolism and reactive oxygen species as potential therapeutic targets, which represent physiological oscillations and metabolic changes in the cardiovascular system itself as the basis for cardiac protection.

Many studies have implicated circadian rhythm in the brain [23], liver [24], lung [25], kidney [26], and heart [27]. Epidemiologic studies have reported circadian rhythmicity in the incidence and the size of myocardial infarctions which were higher during the day and lower at night [28]. In addition to external factors such as neurohormonal regulation, platelet aggregation, and vascular activities, the vulnerability of the myocardium shows a diurnal variation, but the molecular mechanism is not clear.

In this study, we found that mice showed a bigger infarct at ZT2 (Figure 1) and were susceptible to cardiac I/R damage at the end of the light phase. This result was similar to a previous basic research report of Li et al. [7], who suggested that a deficiency of the oscillating transcription factor KLF15 may specifically cause NAD+ deficiency during the sleep-to-active transition and may increase the susceptibility of the heart muscle to I/R injury. Interestingly, other studies have shown opposite results, with ZT14/ZT12 having larger infarcts than ZT2/ZT0 [29]. As Rotter et al. reported, cardiac damage from ischemia/reperfusion was greatest at the transition from sleep to activity, and Rcan1 control of calcineurin activation was necessary for the daily oscillations of the heart against injury [30]. However, Rcan1 KO was equally more susceptible to damage from I/R at the end of the light phase. We hypothesized that these differences in results might be related to the timing of ischemia and reperfusion, reflecting the fundamental difference in the cell injury mechanism between ischemia and reperfusion.

Combined with previous studies, diurnal variations in the onset of myocardial infarction are well established. The influence of the circadian clock cannot be ignored in heart I/R studies. Various proteins compose the circadian clock, including PER2, CRY, CLOCK, and BMAL [31]. PER2 can "buffer" or adjust the antagonism between CLOCK/BMAL1 and CRY, so that CLOCK reaches a self-limiting, rhythmic cycle [32]. Through RT-PCR and western blots, we saw that

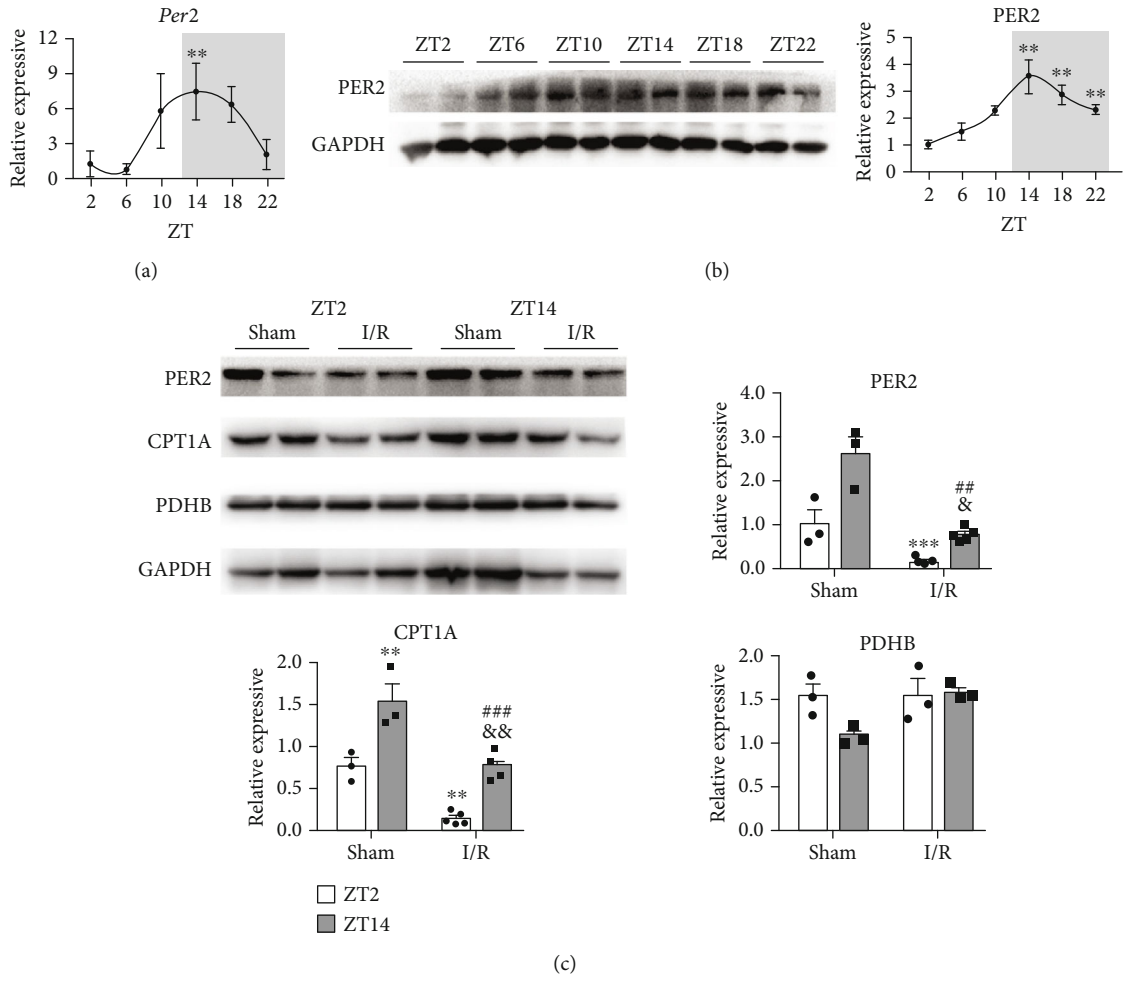

Figure 3: PER2 in circadian I/R susceptibility of the heart. *Per2* mRNA (a) and (b) protein expression in mouse heart during a 24 h day. Quantification was normalized to GAPDH. ZT2 was set to 1 ($n = 3$ per time point, $^{**}P < 0.01$ and $^{***}P < 0.001$ vs. ZT2; one-way ANOVA with Bonferroni correction). (c) PER2 and potential target levels were determined by immunoblots with or without I/R injury at ZT2 and ZT14. Quantification of PER2, CPT1, and PDHB was normalized to GAPDH ($n = 3$–5, $^{**}P < 0.01$ and $^{***}P < 0.001$ vs. sham-ZT2; $^{\#\#}P < 0.01$ and $^{\#\#\#}P < 0.001$ vs. sham-ZT14; $^{\&}P < 0.05$ and $^{\&\&}P < 0.01$ vs. I/R-ZT2, two-tailed Student's *t*-test). Alpha was set as 0.05. Data are presented as the means ± SEM. The Holm-Sidak method was used to correct for multiple *t*-tests.

in C57BL/6 mice, PER2 expression showed a distinct rhythmic pattern for nearly 24 h (Figure 3), and the valley of PER2 expression coincided with the time when the damage resistance of the heart was reduced after the transition from dark to light. Another study has shown that mice with *Per2*-/- had enhanced tissue damage from myocardial ischemia and lacked the capacity to enhance oxygen-efficient glycolysis [33].

Our results suggested that the absence of PER2 was associated with mitochondrial injury, which then led to less ATP and more ROS production, thus increasing cell injury. After cardiac ischemia-reperfusion, the oxidative and antioxidant capacities of myocardial cells are unbalanced, resulting in a state of "oxidative stress," which plays an important role in the injury caused by myocardial infarction. Reactive oxygen species and oxidative stress have been reported to play important roles in the progression after myocardial infarction [34]. Wu et al. demonstrated that acacetin stimulated AMPK, which mediates activation of the Nrf2 signaling pathway in cardiomyocyte protection against hypoxia/reoxygenation injury by increasing the antioxidants heme oxygenase 1 (HO-1), SOD1, and SOD2, reducing ROS production and thereby effectively inhibiting hypoxia/reoxygenation injury [35]. As reported by Ortiz et al., the use of thyroid hormone (TH) as a therapeutic alternative revealed cardioprotective effects after AMI, including decreased oxidative stress, while carvedilol and TH coadministration improved redox balance and cardiac function after AMI [36]. Finding a promising drug which protects cardiomyocytes against hypoxia/reoxygenation may help manage ischemic cardiac disorders.

To pinpoint mitochondrial processes that may be under circadian gene PER2 control, we examined two central mitochondrial metabolic pathways of carbohydrate metabolism and fatty acid uptake. The rate-limiting step in mitochondrial carbohydrate metabolism is carried out by the PDC, a multiprotein complex that catalyzes the oxidative decarboxylation of pyruvate [37]. We found that several components of the PDC, namely, the catalytic pyruvate dehydrogenase PDHB, PDH-E2 (DLAT), and the regulatory subunit PDHX,

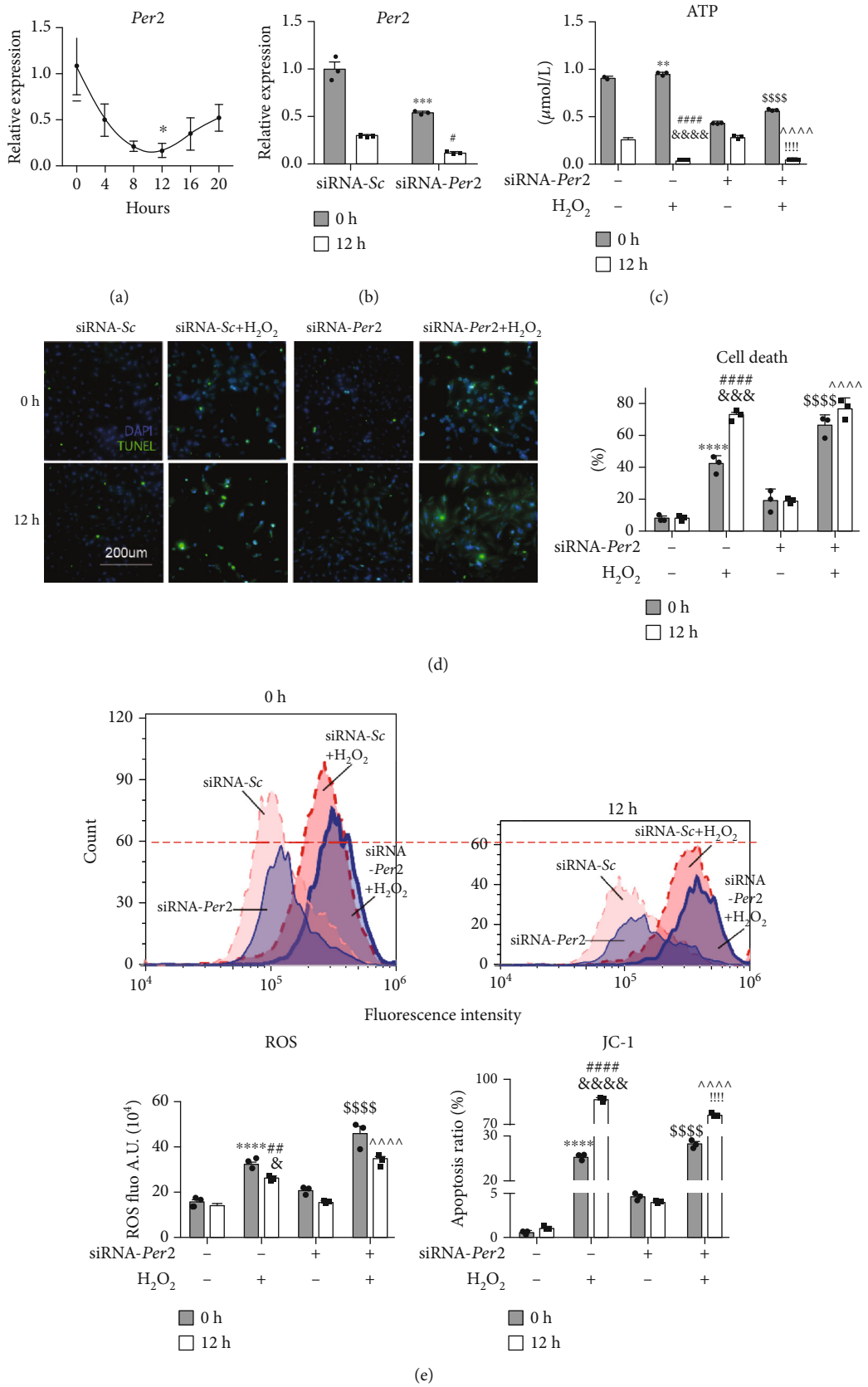

Figure 4: Continued.

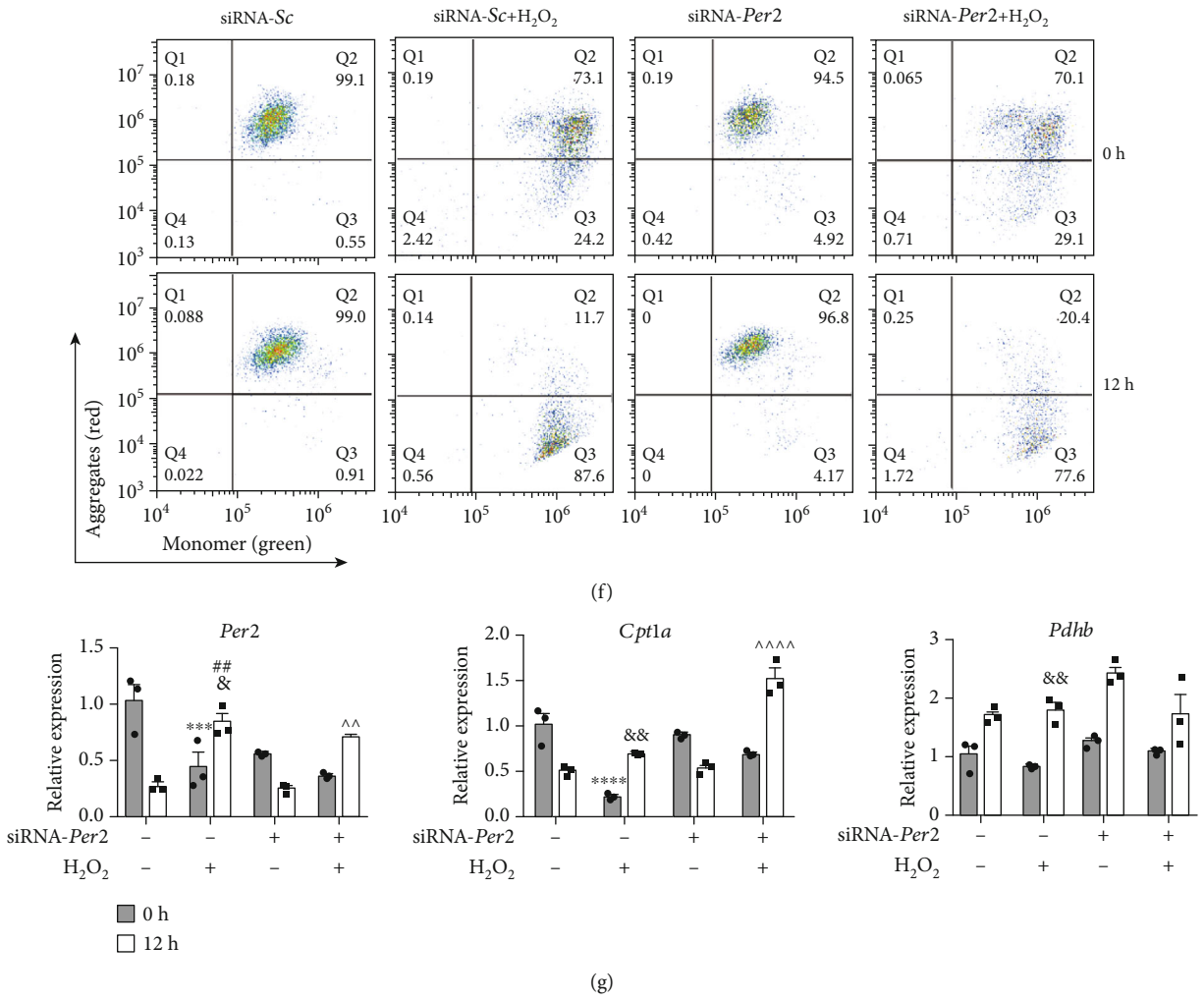

Figure 4: PER2 deficiency in the tolerance of H9c2 cells to H_2O_2 treatment after serum shock. (a) *Per2* mRNA expression during 24 h after serum shock ($n = 3$ per time point, $^{*}P < 0.05$ vs. 0 h after serum shock, one-way ANOVA with Bonferroni correction). (b) *Per2* mRNA expression levels in H9c2 cells after knockdown of *Per2* using siRNA ($n = 3$, $^{***}P < 0.001$ vs. siRNA-Sc-0 hr, $^{\#}P < 0.05$ vs. siRNA-Sc-12 hr). (c–g) H9c2 cells were transfected with siRNA-*Sc* or siRNA-*Per2* 24 h before serum shock. Transfected cells were treated with H_2O_2 for 2 h at the ending point or 12 h after serum shock. (c) ATP change in transfected H9c2 cells treated with H_2O_2 at 0 h and 12 h after serum shock. (d) Cell death determined by TUNEL staining. Representative image (left) and quantification (right). (e) ROS in cells. Flow cytometry images (upper), quantitative analysis of ROS (lower panel, left figure). (f) Flow cytometry of JC-1 in cells. Representative images (f), quantitative analysis of JC-1 ((e), lower panel, right figure). (g) *Per2* and potential target levels in H9c2 cells were determined by RT-PCR at 0 h and 12 h. Quantification of *Per2*, *Cpt1a*, and *Pdhb* was normalized to GAPDH ($n = 3$, $^{**}P < 0.01$, $^{***}P < 0.001$, and $^{****}P < 0.0001$ vs. cells transfected with siRNA-*Sc* at 0 h after serum shock; $^{\#}P < 0.05$, $^{\#\#}P < 0.01$, and $^{\#\#\#\#}P < 0.0001$ vs. cells transfected with siRNA-*Sc* at 12 h after serum shock; $^{\&}P < 0.05$ and $^{\&\&\&\&}P < 0.0001$ vs. cells transfected with siRNA-*Sc* treated with H_2O_2 at 0 h after serum shock; $^{\$\$\$\$}P < 0.0001$ vs. cells transfected with siRNA-*Sc* with H_2O_2 treatment at 0 h after serum shock; $^{\wedge\wedge\wedge\wedge}P < 0.0001$ vs. cells transfected with siRNA-*Sc* with H_2O_2 treatment at 12 h after serum shock; $^{!!!!}P < 0.0001$ vs. cells transfected with siRNA-*Per2* with H_2O_2 treatment at 0 h after serum shock). Alpha was set as 0.05. Data are presented as the means ± SEM. The Holm-Sidak method was used to correct for multiple *t*-tests.

were involved. The rate-limiting step for the entry of long-chain fatty acids into the mitochondrial matrix is the synthesis of acylcarnitine from acyl CoA and carnitine, which is mediated by CPT1A [38]. It has been reported that the mRNA levels of *Pdhb* and *Cpt1a* also cycle for 24 h but reached their peak levels, respectively, at ZT16 and ZT17 [39]. Our results showed that the expression of *Per2* and *Cpt1a* was basically similar, and peak expression of *Per2* and *Cpt1a* coincided with the time when damage resistance of the heart was increased after the transition from light to dark, while that of *Pdhb* was different (Figure 4(g)). This indicated that PER2 damage to cardiomyocytes was mediated by CPT1A, which produced less ATP and provided insufficient energy to cardiomyocytes, thus leading to the aggravation of myocardial injury.

At present, the mechanisms linking circadian rhythm stabilization and myocardial infarction are under investigation and could involve inflammation [40], glycolysis metabolism [41], cyclin-dependent kinase 5 [42], or adenosine [33]. Some of these are known to be associated with PER2 and contribute to the survival of the myocardium after I/R. Sun et al. hypothesized that *Per2* deficiency affected

endothelial progenitor cell function through CXCR4/PI3-k/Akt/FoxO-related mechanisms involving angiogenesis in the ischemic myocardium of mice, thus increasing damage [43]. Kobayashi et al. established the dependence of HIF1A on PER2 as a transcription factor during hypoxia and proposed that PER2 acted as an effector molecule for the recruitment of HIF1A to promoter regions of its downstream genes [44]. On this basis, Oyama et al. also found that specific HIF1A pathways controlled glycolysis, mitochondrial respiration (COX4.2), or endothelial barrier function (ANGPTL-4/claudin-1) after PER2 overexpression [41].

Numerous studies have demonstrated links between myocardial infarction and disruption of circadian homeostasis both in clinical observations and in basic research findings. Therefore, it is important to maintain the homeostasis of circadian rhythms in humans. Interestingly, in addition to the above studies, chronic shift work [45], anesthetics [46], melatonin [47], and intestinal microbiota [48] can also affect circadian rhythms.

In summary, we have shown that the injury caused by myocardial infarctions has circadian rhythmicity. Our study suggests that PER2 deficiency contributed to the susceptibility of the myocardium to I/R injury, with peak susceptibility in the early morning, through reactive oxygen species and CPT1A as a key enzyme in energy metabolism, which may be particularly harmful to patients during a critical time window.

Data Availability

Data are available on request to the authors.

Conflicts of Interest

The authors declare that they have no known competing financial interests or personal relationships that influenced the work reported in this paper.

Authors' Contributions

Yaqian Weng, Hui Li, and Lin Gao contributed equally to this work. Shiyuan Xu and Le Li contributed equally to the article.

Acknowledgments

This research was supported by grants from the National Natural Science Foundation of China (Nos. 81873763 and 81771315).

Supplementary Materials

TABLE 1: primer sequences used in reverse transcription-polymerase chain reactions. TABLE 2: antibodies used for western blots. *(Supplementary Materials)*

References

[1] E. C. Keeley, J. A. Boura, and C. L. Grines, "Primary angioplasty versus intravenous thrombolytic therapy for acute myocardial infarction: a quantitative review of 23 randomised trials," *The Lancet*, vol. 361, no. 9351, pp. 13–20, 2003.

[2] E. Murphy and C. Steenbergen, "Mechanisms underlying acute protection from cardiac ischemia-reperfusion injury," *Physiological Reviews*, vol. 88, no. 2, pp. 581–609, 2008.

[3] E. T. Chouchani, V. R. Pell, A. M. James et al., "A Unifying Mechanism for Mitochondrial Superoxide Production during Ischemia- Reperfusion Injury," *Cell Metabolism*, vol. 23, no. 2, pp. 254–263, 2016.

[4] T. Kono, H. Morita, T. Nishina et al., "Circadian variations of onset of acute myocardial infarction and efficacy of thrombolytic therapy," *Journal of the American College of Cardiology*, vol. 27, no. 4, pp. 774–778, 1996.

[5] M. E. Young, P. Razeghi, A. M. Cedars, P. H. Guthrie, and H. Taegtmeyer, "Intrinsic diurnal variations in cardiac metabolism and contractile function," *Circulation Research*, vol. 89, no. 12, pp. 1199–1208, 2001.

[6] M. E. Young, P. Razeghi, and H. Taegtmeyer, "Clock genes in the heart: characterization and attenuation with hypertrophy," *Circulation Research*, vol. 88, no. 11, pp. 1142–1150, 2001.

[7] L. Li, H. Li, C. L. Tien, M. K. Jain, and L. Zhang, "Kruppel-like factor 15 regulates the circadian susceptibility to ischemia reperfusion injury in the heart," *Circulation*, vol. 141, no. 17, pp. 1427–1429, 2020.

[8] M. E. Young, "The circadian clock within the heart: potential influence on myocardial gene expression, metabolism, and function," *American Journal of Physiology. Heart and Circulatory Physiology*, vol. 290, no. 1, pp. H1–16, 2006.

[9] Y. Xia, Z. Cheng, S. Wang, D. Guan, and F. Liu, "Modeling the crosstalk between the circadian clock and ROS in _Neurospora crassa_," *Journal of Theoretical Biology*, vol. 458, pp. 125–132, 2018.

[10] F. C. Kelleher, A. Rao, and A. Maguire, "Circadian molecular clocks and cancer," *Cancer Letters*, vol. 342, no. 1, pp. 9–18, 2014.

[11] S. Bonney, K. Hughes, P. N. Harter, M. Mittelbronn, L. Walker, and T. Eckle, "Cardiac period 2 in myocardial ischemia: clinical implications of a light dependent protein," *The International Journal of Biochemistry & Cell Biology*, vol. 45, no. 3, pp. 667–671, 2013.

[12] Y. Oyama, C. M. Bartman, J. Gile, D. Sehrt, and T. Eckle, "The circadian PER2 enhancer nobiletin reverses the deleterious effects of midazolam in myocardial ischemia and reperfusion injury," *Current Pharmaceutical Design*, vol. 24, no. 28, pp. 3376–3383, 2018.

[13] C. M. Bartman, Y. Oyama, K. Brodsky et al., "Intense light-elicited upregulation of miR-21 facilitates glycolysis and cardioprotection through Per2-dependent mechanisms," *PLoS One*, vol. 12, no. 4, article e0176243, 2017.

[14] M. C. Magnone, S. Langmesser, A. C. Bezdek, T. Tallone, S. Rusconi, and U. Albrecht, "The mammalian circadian clock gene per2 modulates cell death in response to oxidative stress," *Frontiers in Neurology*, vol. 5, 2015.

[15] P. A. K. Andersen, V. Petrenko, P. H. Rose et al., "Proinflammatory Cytokines Perturb Mouse and Human Pancreatic Islet Circadian Rhythmicity and Induce Uncoordinated β-Cell Clock Gene Expression via Nitric Oxide, Lysine Deacetylases, and Immunoproteasomal Activity," *International Journal of Molecular Sciences*, vol. 22, no. 1, p. 83, 2021.

[16] T. Eckle, M. Koeppen, and H. Eltzschig, "Use of a hanging weight system for coronary artery occlusion in mice," *Journal of Visualized Experiments*, vol. 50, 2011.

[17] T. Eckle, A. Grenz, D. Köhler et al., "Systematic evaluation of a novel model for cardiac ischemic preconditioning in mice,"

American Journal of Physiology. Heart and Circulatory Physiology, vol. 291, no. 5, pp. H2533–H2540, 2006.

[18] X. Liu, Y. Wang, P. Zhang, Q. Wang, Q. Feng, and W. Chen, "Radial motion estimation of myocardium in rats with myocardial infarction: a hybrid method of FNCCGLAM and polar transformation," *Ultrasound in Medicine & Biology*, vol. 46, no. 12, pp. 3413–3425, 2020.

[19] K. Tanaka, N. Ashizawa, H. Kawano et al., "Aldosterone induces circadian gene expression of clock genes in H9c2 cardiomyoblasts," *Heart and Vessels*, vol. 22, no. 4, pp. 254–260, 2007.

[20] A. Balsalobre, F. Damiola, and U. Schibler, "A serum shock induces circadian gene expression in mammalian tissue culture cells," *Cell*, vol. 93, no. 6, pp. 929–937, 1998.

[21] J. X. Wang, X. J. Zhang, Q. Li et al., "MicroRNA-103/107 regulate programmed necrosis and myocardial ischemia/reperfusion injury through targeting FADD," *Circulation Research*, vol. 117, no. 4, pp. 352–363, 2015.

[22] W. Sun, L. Zhao, X. Song et al., "MicroRNA-210 modulates the cellular energy metabolism shift during H_2O_2-induced oxidative stress by repressing ISCU in H9c2 cardiomyocytes," *Cellular Physiology and Biochemistry*, vol. 43, no. 1, pp. 383–394, 2017.

[23] N. Schallner, J. L. Lieberum, D. Gallo et al., "Carbon monoxide preserves circadian rhythm to reduce the severity of subarachnoid hemorrhage in mice," *Stroke*, vol. 48, no. 9, pp. 2565–2573, 2017.

[24] R. R. Almon, E. Yang, W. Lai, I. P. Androulakis, D. C. DuBois, and W. J. Jusko, "Circadian variations in rat liver gene expression: relationships to drug actions," *The Journal of Pharmacology and Experimental Therapeutics*, vol. 326, no. 3, pp. 700–716, 2008.

[25] T. Papagiannakopoulos, M. R. Bauer, S. M. Davidson et al., "Circadian rhythm disruption promotes lung tumorigenesis," *Cell Metabolism*, vol. 24, no. 2, pp. 324–331, 2016.

[26] N. Ohashi, S. Isobe, S. Ishigaki, and H. Yasuda, "Circadian rhythm of blood pressure and the renin-angiotensin system in the kidney," *Hypertension Research*, vol. 40, no. 5, pp. 413–422, 2017.

[27] N. Black, A. D'Souza, Y. Wang et al., "Circadian rhythm of cardiac electrophysiology, arrhythmogenesis, and the underlying mechanisms," *Heart Rhythm*, vol. 16, no. 2, pp. 298–307, 2019.

[28] H. O. Kim, J. M. Kim, J. S. Woo et al., "Circadian distribution of acute myocardial infarction in different age groups," *The American Journal of Cardiology*, vol. 121, no. 11, pp. 1279–1284, 2018.

[29] D. J. Durgan, T. Pulinilkunnil, C. Villegas-Montoya et al., "Short communication: ischemia/reperfusion tolerance is time-of-day-dependent: mediation by the cardiomyocyte circadian clock," *Circulation Research*, vol. 106, no. 3, pp. 546–550, 2010.

[30] D. Rotter, D. B. Grinsfelder, V. Parra et al., "Calcineurin and its regulator, RCAN1, confer time-of-day changes in susceptibility of the heart to ischemia/reperfusion," *Journal of Molecular and Cellular Cardiology*, vol. 74, pp. 103–111, 2014.

[31] B. Grimaldi, M. M. Bellet, S. Katada et al., "PER2 Controls Lipid Metabolism by Direct Regulation of PPARγ," *Cell Metabolism*, vol. 12, no. 5, pp. 509–520, 2010.

[32] S. H. Yoo, S. Kojima, K. Shimomura et al., "Period23'-UTR and microRNA-24 regulate circadian rhythms by repressing PERIOD2 protein accumulation," *Proceedings of the National Academy of Sciences of the United States of America*, vol. 114, no. 42, pp. E8855–E8864, 2017.

[33] T. Eckle, K. Hartmann, S. Bonney et al., "Adora2b-elicited _Per2_ stabilization promotes a HIF-dependent metabolic switch crucial for myocardial adaptation to ischemia," *Nature Medicine*, vol. 18, no. 5, pp. 774–782, 2012.

[34] E. Fuentes, R. Moore-Carrasco, A. M. de Andrade Paes, and A. Trostchansky, "Role of platelet activation and oxidative stress in the evolution of myocardial infarction," *Journal of Cardiovascular Pharmacology and Therapeutics*, vol. 24, no. 6, pp. 509–520, 2019.

[35] W. Y. Wu, Y. D. Li, Y. K. Cui et al., "The natural flavone acacetin confers cardiomyocyte protection against hypoxia/reoxygenation injury via AMPK-mediated activation of Nrf2 signaling pathway," *Frontiers in Pharmacology*, vol. 9, p. 497, 2018.

[36] V. D. Ortiz, P. Türck, R. Teixeira et al., "Carvedilol and thyroid hormones co-administration mitigates oxidative stress and improves cardiac function after acute myocardial infarction," *European Journal of Pharmacology*, vol. 854, pp. 159–166, 2019.

[37] M. S. Patel, N. S. Nemeria, W. Furey, and F. Jordan, "The Pyruvate Dehydrogenase Complexes: Structure-based Function and Regulation∗," *The Journal of Biological Chemistry*, vol. 289, no. 24, pp. 16615–16623, 2014.

[38] M. Schreurs, F. Kuipers, and F. R. van der Leij, "Regulatory enzymes of mitochondrial beta-oxidation as targets for treatment of the metabolic syndrome," *Obesity Reviews*, vol. 11, no. 5, pp. 380–388, 2010.

[39] A. Neufeld-Cohen, M. S. Robles, R. Aviram et al., "Circadian control of oscillations in mitochondrial rate-limiting enzymes and nutrient utilization by PERIOD proteins," *Proceedings of the National Academy of Sciences of the United States of America*, vol. 113, no. 12, pp. E1673–E1682, 2016.

[40] L. K. Fonken, T. A. Bedrosian, N. Zhang, Z. M. Weil, A. C. DeVries, and R. J. Nelson, "Dim light at night impairs recovery from global cerebral ischemia," *Experimental Neurology*, vol. 317, pp. 100–109, 2019.

[41] Y. Oyama, C. M. Bartman, S. Bonney et al., "Intense light-mediated circadian cardioprotection via transcriptional reprogramming of the endothelium," *Cell Reports*, vol. 28, no. 6, pp. 1471–1484.e11, 2019.

[42] A. Brenna, I. Olejniczak, R. Chavan et al., "Cyclin-dependent kinase 5 (CDK5) regulates the circadian clock," *eLife*, vol. 8, 2019.

[43] Y. Y. Sun, W. W. Bai, B. Wang et al., "Period 2 is essential to maintain early endothelial progenitor cell function in vitro and angiogenesis after myocardial infarction in mice," *Journal of Cellular and Molecular Medicine*, vol. 18, no. 5, pp. 907–918, 2014.

[44] M. Kobayashi, A. Morinibu, S. Koyasu, Y. Goto, M. Hiraoka, and H. Harada, "A circadian clock gene,PER2, activatesHIF-1 as an effector molecule for recruitment ofHIF-1α to promoter regions of its downstream genes," *The FEBS Journal*, vol. 284, no. 22, pp. 3804–3816, 2017.

[45] C. J. Morris, T. E. Purvis, J. Mistretta, K. Hu, and F. A. J. L. Scheer, "Circadian misalignment increases C-reactive protein and blood pressure in chronic shift workers," *Journal of Biological Rhythms*, vol. 32, no. 2, pp. 154–164, 2017.

[46] M. A. Wren-Dail, R. T. Dauchy, D. E. Blask et al., "Effect of isoflurane anesthesia on circadian metabolism and physiology in rats," *Comparative Medicine*, vol. 67, no. 2, pp. 138–146, 2017.

[47] T. Y. Feng, Q. Li, F. Ren et al., "Melatonin protects goat spermatogonial stem cells against oxidative damage during cryopreservation by improving antioxidant capacity and inhibiting mitochondrial apoptosis pathway," *Oxidative Medicine and Cellular Longevity*, vol. 2020, Article ID 5954635, 16 pages, 2020.

[48] Z. Kuang, Y. Wang, Y. Li et al., "The intestinal microbiota programs diurnal rhythms in host metabolism through histone deacetylase 3," *Science*, vol. 365, no. 6460, pp. 1428–1434, 2019.

Hindawi
Oxidative Medicine and Cellular Longevity
Volume 2021, Article ID 2514947, 16 pages
https://doi.org/10.1155/2021/2514947

Research Article

miRNA-27a Transcription Activated by c-Fos Regulates Myocardial Ischemia-Reperfusion Injury by Targeting ATAD3a

Yandong Bao,[1] Ying Qiao,[2] Hang Yu,[1] Zeying Zhang,[3] Huimin Yang,[1] Xin Xin,[1] Yuqiong Chen,[1] Yuxuan Guo,[1] Nan Wu,[2] and Dalin Jia[1]

[1]*Department of Cardiology, The First Affiliated Hospital of China Medical University, Liaoning, China*
[2]*The Central Laboratory, The First Affiliated Hospital of China Medical University, Liaoning, China*
[3]*Department of Oromaxillofacial-Head and Neck Surgery, Department of Oral and Maxillofacial Surgery, School of Stomatology, China Medical University, China*

Correspondence should be addressed to Nan Wu; imwunan@163.com

Received 30 April 2021; Accepted 27 July 2021; Published 9 August 2021

Academic Editor: Hai-tao Xiao

MicroRNA-27a (miR-27a) has been implicated in myocardial ischemia-reperfusion injury (MIRI), but the underlying mechanism is not well understood. This study is aimed at determining the role of miR-27a in MIRI and at investigating upstream molecules that regulate miR-27a expression and its downstream target genes. miR-27a expression was significantly upregulated in myocardia exposed to ischemia/reperfusion (I/R) and cardiomyocytes exposed to hypoxia/reoxygenation (H/R). c-Fos could regulate miR-27a expression by binding to its promoter region. Moreover, overexpression of miR-27a led to a decrease in cell viability, an increase in LDH and CK-MB secretion, and an increase in apoptosis rates. In contrast, suppression of miR-27a expression resulted in the opposite effects. ATPase family AAA-domain-containing protein 3A (ATAD3a) was identified as a target of miR-27a. miR-27a regulated the translocation of apoptosis-inducing factor (AIF) from the mitochondria to the nucleus and H/R-induced apoptosis via the regulation of ATAD3a. It was found that inhibiting miR-27a in vivo by injecting a miR-27a sponge could ameliorate MIRI in an isolated rat heart model. In conclusion, our study demonstrated that c-Fos functions as an upstream regulator of miR-27a and that miR-27a regulates the translocation of AIF from the mitochondria to the nucleus by targeting ATAD3a, thereby contributing to MIRI. These findings provide new insight into the role of the c-Fos/miR-27a/ATAD3a axis in MIRI.

1. Introduction

With the dramatic changes in lifestyle and diet that have occurred in modern society, coronary artery disease (CAD) has gradually become one of the major diseases that seriously threaten the lives and health of people worldwide [1]. Severe stenosis or acute occlusion of the coronary arteries can cause myocardial ischemia and even myocardial necrosis. A common approach for treating patients with acute myocardial infarction (AMI) is reconstituting the myocardial blood supply as quickly as possible through the implementation of myocardial reperfusion therapy [2, 3], which includes percutaneous coronary intervention, coronary artery bypass grafting, and thrombolytic therapy. However, during the implementation of myocardial reperfusion therapy, the rapid recovery of the blood supply to the ischemic myocardium does not ameliorate myocardial damage and causes extra-myocardial insult, which is termed myocardial ischemia-reperfusion injury (MIRI) [4]. The occurrence of MIRI is difficult to predict in advance, and once it occurs, it greatly reduces the clinical benefit of myocardial reperfusion therapy [5]. Therefore, it is of great significance to explore the mechanism underlying MIRI and to discover new therapeutic targets for MIRI.

MicroRNAs (miRNAs), short noncoding RNA molecules approximately 21 to 24 nucleotides in length, generally play roles in RNA silencing and regulate gene expression at the posttranscriptional level [6]. miR-27a has been widely reported to play key roles in the initiation and progression of cancer [7, 8], the occurrence of pulmonary and hepatic

fibrosis [9, 10], and the development of arthritis [11]. Notably, miR-27a expression was significantly increased in mouse hearts subjected to ischemia-reperfusion, and downregulation of miR-27a expression mediates the protective effect of high thoracic epidural block against MIRI in mice [12]. However, the upstream molecule that regulates miR-27a expression and its downstream target genes have not been determined.

c-Fos, a member of the Fos family of transcription factors (including c-Fos, FosB, Fra-1, and Fra-2) [13], promotes the formation of the AP-1 transcription factor complex by dimerizing with the c-Jun protein, thereby translating extracellular signals into alterations in gene expression by binding to the promoters of target genes [14]. The level of c-Fos is notably changed under different stress conditions, such as heat stress [15], radiation [16], and ischemia [17]. Accumulating evidence has indicated that c-Fos expression is strongly induced during MIRI [18, 19]. More importantly, c-Fos was reported to increase miRNA expression by binding to miRNA promoters [20, 21]. Moreover, a c-Fos-specific binding site was predicted to exist in the putative promoter region of miR-27a by the PROMO database. Therefore, whether c-Fos regulates miR-27a expression was examined in the present study.

ATPase family AAA-domain-containing protein 3A (ATAD3a), a nuclear DNA-encoded mitochondrial membrane protein [22], has been reported to function in apoptosis [23, 24], mitochondrial dynamics [25], mitophagy [26], mitochondrial DNA replication [27, 28], and cholesterol metabolism [28, 29]. As predicted with TargetScan, miR-27a may specifically bind to the 3′-UTR of ATAD3a. Therefore, whether miR-27a regulates MIRI by targeting ATAD3a was determined in this study.

In the present study, we found that c-Fos activated the transcription of miR-27a and that miR-27a further regulated the ischemia-reperfusion-induced apoptosis of cardiomyocytes by modulating the translocation of apoptosis-inducing factor (AIF) from the mitochondria to the nucleus by targeting ATAD3a. These data suggest that the c-Fos/miR-27a/ATAD3a axis plays a key role in MIRI.

2. Materials and Methods

2.1. miRNA Array Analysis. To explore the differential expression of miRNAs in rats exposed to myocardial ischemia-reperfusion, we searched the GEO database and found the GSE74951 dataset that was contributed by Feng et al. [30]. The miRNA expression profile based on the GPL21136 Multiplex Circulating miRNA Assay was downloaded. We used the "limma R" language package to screen DE-miRNAs between ischemia-reperfusion-treated heart samples and normal heart samples. The cutoff criteria were set to $p < 0.05$ and |log2 multiple change (FC)| >1.

2.2. Animals and Animal Models. Thirty healthy male Wistar rats (body weight 250 ± 20 g) were purchased from Sibefu Biotechnology Co., Ltd. (Sibefu, Beijing, China). All the rats were used and handled in accordance with the Guidelines for Care and Use of Laboratory Animals provided by the National Institute of Health. The use of animals was approved by the Animal Ethics Committee of China Medical University.

The rats were injected with heparin (1500 IU/kg) before surgery to prevent blood clotting in the coronary arteries, and then, the rats were anesthetized by intraperitoneal injection with isopentobarbital (50 mg/kg). The fully anesthetized rats were subjected to thoracotomy. After the aorta was cut, the heart was isolated and immediately immersed in cold heparinized and oxygenated Krebs-Henseleit (KH) solution. The isolated heart was fixed on the Langendorff device and perfused with KH solution at a constant pressure of 75 mmHg and 37°C. MIRI was induced in the isolated rat hearts by interrupting perfusion for 30 min, which was followed by reperfusion for 90 min as previously described [31].

2.3. Cells and Cell Models. H9c2 cells purchased from the National Collection of Authenticated Cell Cultures were cultured in DMEM containing 10% fetal bovine serum, 100 U/ml penicillin, and 100 μg/ml streptomycin. The culture conditions in the incubator were 37°C and 5% CO_2.

An in vitro MIRI model was established as previously described [32]. H9c2 cells were collected in the logarithmic phase of growth, and the normal medium was replaced with Earle's solution without glucose or serum. The cells were placed in a three-gas incubator (94% N_2, 5% CO_2, and 1% O_2; 37°C) and subjected to hypoxia for 8 h. Subsequently, Earle's solution was replaced with normal medium, and the cells were reoxygenated in a standard incubator (5% CO_2, 37°C) for 3 h.

2.4. RT-qPCR. Total RNA was extracted from myocardial tissues and H9c2 cells using TRIzol™ Reagent (Invitrogen, Carlsbad, CA) according to the manufacturer's instructions. The concentration of RNA was measured using a NanoDrop2000 (Thermo Fisher Scientific, Wilmington, DE). The PrimeScript™ RT reagent Kit (Takara, Japan) and Mir-X miRNA First-Strand Synthesis Kit (Clontech, Japan) were used to reverse transcribe miRNA and mRNA, respectively, into cDNA. Real-time quantitative PCR was performed using TB Green® Premix Ex Taq™ II (Takara, Japan) according to the manufacturer's instructions, and the real-time quantitative PCR was carried out with the QuantStudio real-time fluorescent quantitative PCR system (Thermo Fisher Scientific, Wilmington, DE). The primers used were provided by Sangon Biotech (Shanghai, China): miR-27a forward (5′-AGGGCTTAGCTGCTTGTGAGC-3′), miR-27a reverse (5′-CGGCAGAGTCCTTACCCACAA-3′, U6 reverse primer (5′-TGGAACGCTTCACGAATTTGCG-3′), U6 forward primer (5′-GGAACGATACAGAGAAGATTAGC-3′), ATAD3a forward (5′-GATGACGATATGCGGCTGGTACAC-3′), ATAD3a reverse (5′-GATGACGATATGCGGCTGGTACAC-3′), GAPDH forward (5′-CTGGAAAGCTGTGGCGTGAT-3′), and GAPDH reverse (5′-GCGGCATGTCAGATCCACAA-3′).

2.5. Cell Transfection. Short miRNA sequences, small interfering RNAs specific for c-Fos and ATAD3a, c-Fos, and ATAD3a plasmids, and matched negative controls or empty

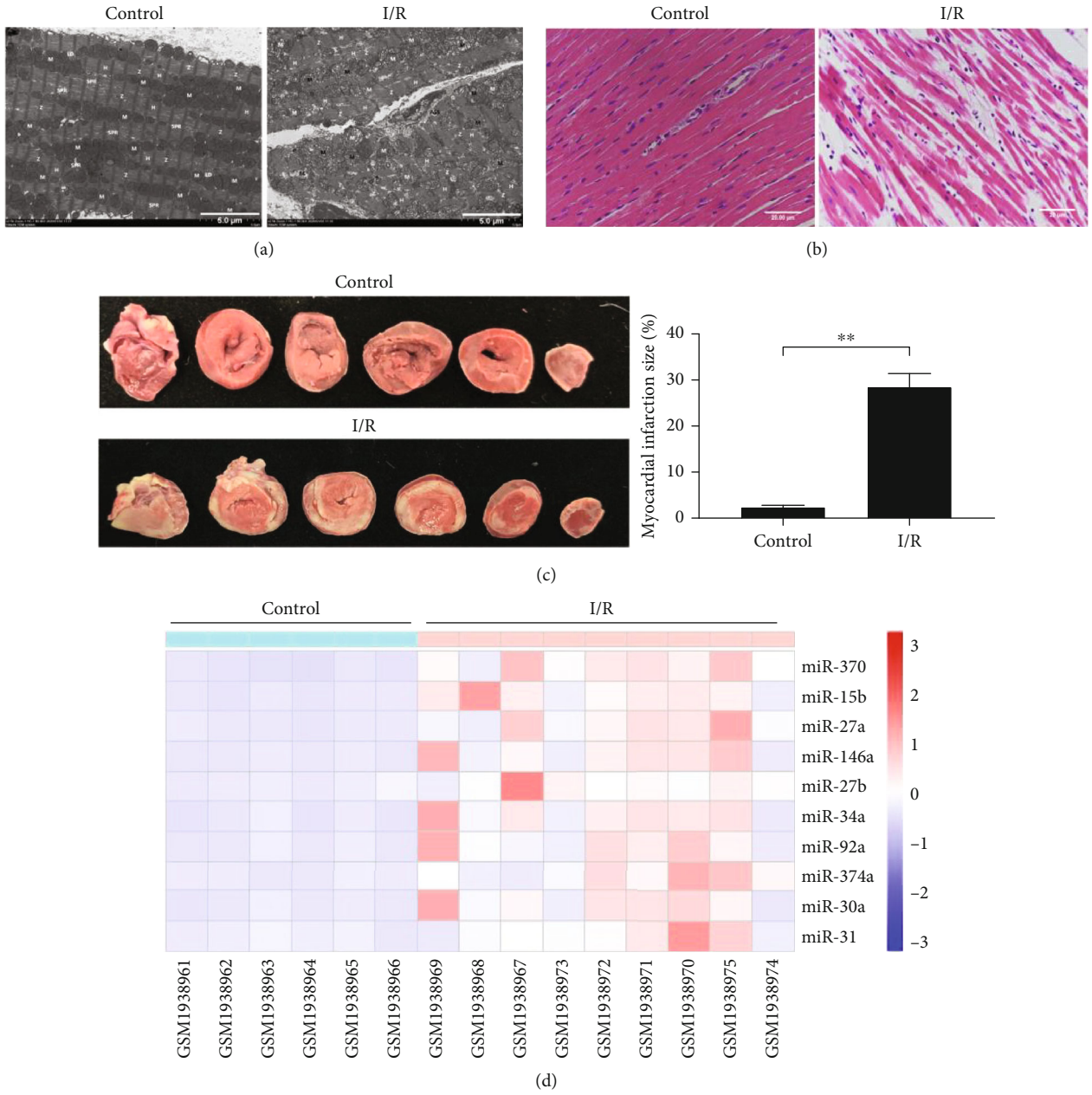

Figure 1: Continued.

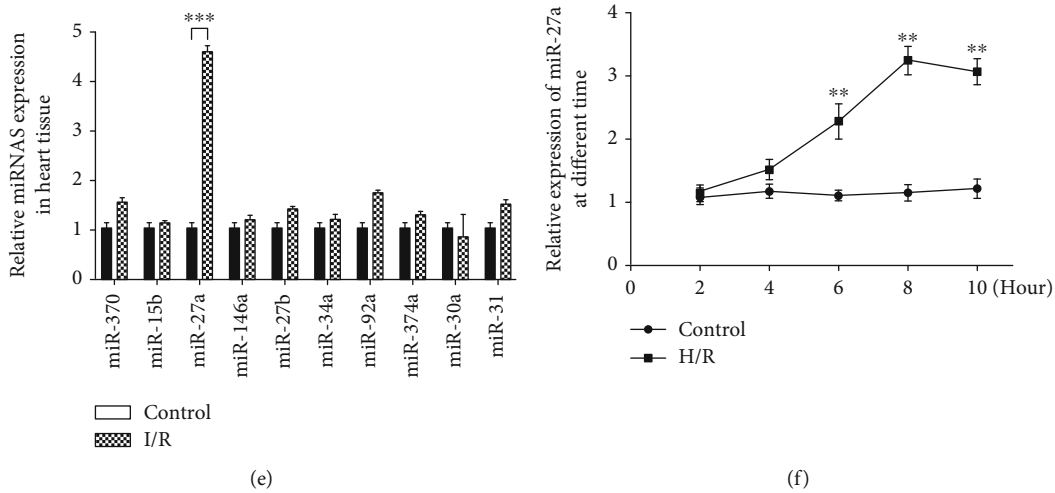

Figure 1: miR-27a expression was induced by myocardial ischemia/reperfusion injury (MIRI). Ischemia-reperfusion was induced by 30 min of ischemia followed by 90 min of reperfusion in an isolated rat heart model. Myocardial structure damage was detected by (a) transmission electron microscopy and (b) HE staining, $n = 3$. (c) Myocardial infarct size was measured by TTC staining, $n = 6$, $^{**}p < 0.01$ vs. the control. (d) Heat maps of the top ten upregulated miRNAs in myocardia subjected to I/R, $n = 6$ in the control group, $n = 9$ in I/R group. (e) MicroRNA expression in myocardia subjected to I/R was confirmed by RT-qPCR, $n = 10$, $^{***}p < 0.001$ vs. the control. (f) miR-27a expression in H9c2 cells subjected to hypoxia for different times was examined by RT-qPCR. The data were obtained from four independent replicate experiments. $^{**}p < 0.01$ vs. the control.

vectors were designed and synthesized by GenePharma (GenePharma Co., Ltd., Shanghai, China). These reagents were transfected into cells using INVI DNA/RNA Transfection Reagent™ (Ivigentech, America) according to the manufacturer's instructions. Subsequent cell experiments were performed 24 h or 48 h after transfection.

2.6. Cell Counting Kit-8 (CCK-8) Assay. H9c2 cells were seeded in 96-well plates (3000 cells per well), and cell viability was assessed using a CCK-8 assay (APExBIO, Houston, USA) according to the manufacturer's protocol.

2.7. Determination of Myocardial Enzyme Levels. The levels of lactate dehydrogenase (LDH) and creatine kinase-MB (CK-MB) in the culture medium were measured using the Lactate Dehydrogenase Release Kit (Jiancheng Bioengineering Institute, Nanjing, China) and the Creatine Kinase-MB Isoenzyme Assay Kit (Jiancheng Bioengineering Institute, Nanjing, China) according to the manufacturer's instructions.

2.8. Flow Cytometry. Cell apoptosis in vitro was detected using the Annexin V FITC Apoptosis Detection Kit (Dojindo, Japan) following the manufacturer's instructions.

2.9. Gene Therapy In Vivo. As adeno-associated virus serotype 9 (AAV9) is superior to other serotypes for global cardiac gene transfer [33], in this study, inhibition of miR-27a in vivo was achieved by injecting AAV9-miR-27a-sponge (HanBio, China) through the rat tail vein, and AAV9-NC was injected as a negative control. miR-27a expression was detected by RT-qPCR three weeks after the injection to assess the suppression rate.

2.10. Transmission Electron Microscopy. The left ventricle was cut into a $1 \times 1 \times 1$ mm cube, fixed with 2.5% glutaraldehyde, and then cut into ultrathin sections. The sections were observed under a transmission electron microscope (JEM-1200EX, JEOL), and alterations in the myocardial submicroscopic structure were observed and photographed.

2.11. HE Staining. The left ventricle was fixed with 4% paraformaldehyde, dehydrated by gradient alcohol, embedded in paraffin, and cut into 4 μm-thick sections. The sections were stained with hematoxylin and eosin (Beyotime Biotechnology, China) according to the manufacturer's recommendations, followed by observation under an optical microscope (Olympus BX51, Olympus).

2.12. 2,3,5-Triphenyltetrazolium Chloride (TTC) Staining. The myocardial infarction area was determined using TTC staining. The perfused heart was harvested at the end of reperfusion and frozen at -20°C. The frozen heart was cut into 1 mm-thick sections, incubated in 1% TTC solution (Solarbio, China) at 37°C for 30 min in the dark and then fixed with 4% paraformaldehyde (Solarbio, China) overnight. The stained sections were photographed using a digital camera.

2.13. Terminal Deoxynucleotidyl Transferase-Mediated dUTP-Biotin Nick End Labeling (TUNEL) Assay. A TUNEL staining kit (Roche Diagnostics, Germany) was used to detect apoptosis in the myocardium, and apoptotic cells were observed under an inverted fluorescence microscope (Nikon Eclipse TE2000-U, Japan).

2.14. Chromatin Immunoprecipitation (ChIP) Assay. ChIP was conducted using a ChIP Assay Kit (cat# 17-295, EMD Millipore, Billerica, MA, USA). After fixation with 1% formaldehyde for 10 min, the cells were subjected to decrosslinking with 0.125 M glycine for 5 min, washed with PBS, and

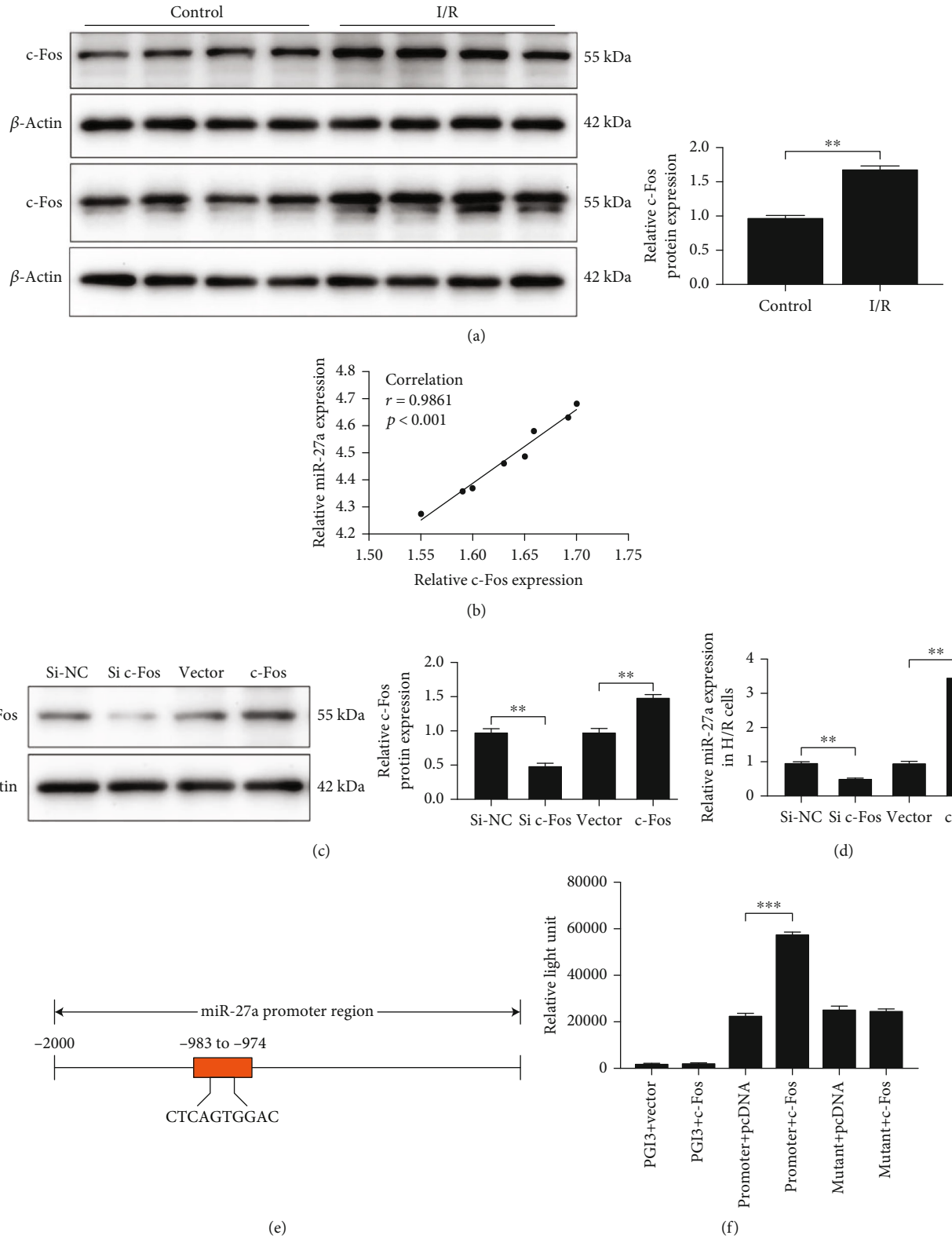

Figure 2: Continued.

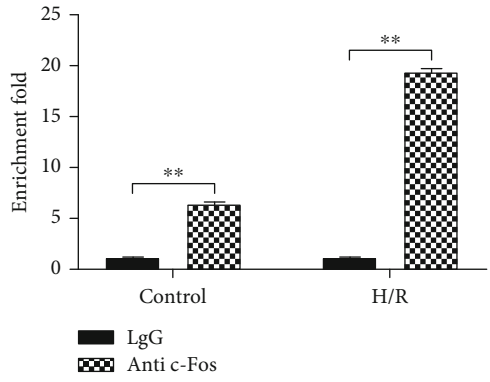

(g)

Figure 2: c-Fos regulated miR-27a expression. (a) c-Fos expression in myocardia subjected to ischemia/reperfusion (I/R) was analyzed by Western blotting, $n = 8$, $^{**}p < 0.01$ vs. the control. (b) c-Fos expression was positively correlated with miR-27a expression in myocardia subjected to I/R. H9c2 cells were transfected with a small interfering RNA (siRNA) specific for c-Fos, c-Fos plasmid, and matched negative controls or empty vectors. (c) c-Fos expression was analyzed by Western blotting. (d) miR-27a expression was detected by RT-qPCR. (e) A c-Fos-specific binding site was predicted in the putative promoter region (-983 to -974 region) of miR-27a. (f) The relative luciferase activity was detected after cotransfecting pGL3 luciferase reporter vectors containing the full-length miR-27a promoter or the corresponding promoter sequence with a mutant binding site with the c-Fos plasmid and empty vector. (g) Hypoxia/reoxygenation (H/R) enhances the enrichment of c-Fos on the miR-27a promoter. H9c2 cells were subjected to H/R. Twenty-four hours after treatment, ChIP-qPCR was performed. All data were obtained from four independent replicate experiments. $^{**}p < 0.01$; $^{***}p < 0.001$.

lysed for 1 h on ice. The cell lysates were sonicated to generate chromatin fragments approximately 500 to 800 bp in length that were assessed by agarose gel electrophoresis. Following preclearing with Protein-A agarose, the samples were incubated with 5 μg of specific antibodies with rotation overnight at 4°C. Then, the immune complexes were precipitated with Protein-A agarose beads and sheared salmon sperm DNA, and the DNA fragments were purified using a QIAquick Spin Kit (Qiagen). The promoter segments containing a c-Fos binding site were amplified using PCR technology.

2.15. Luciferase Reporter Gene Assay. The PROMO database (http://alggen.lsi.upc.es/cgi-bin/promo_v3/promo/promoinit.cgi?dirDB=TF_8.3/) was used to predict the c-Fos-specific binding site in the promoter region of miR-27a. To determine the specific binding of c-Fos to the miR-27a promoter, the wild-type full-length promoter of miR-27a and the corresponding sequence with mutated c-Fos binding sites were cloned into pGL3 luciferase reporter vectors (GenePharma Co., Ltd., Shanghai, China), cotransfected with pcDNA3.1 vector or pcDNA3.1-c-Fos, and detected with the Dual-Glo Luciferase Assay System (Promega) according to the manufacturer's recommendations.

TargetScan version 7.2 (http://www.targetscan.org/) was used to predict the specific binding of miR-27a to the 3′-UTR of ATAD3a. Sequences of the ATAD3a 3′-UTR containing the wild-type or mutant miR-27a binding site were amplified by PCR and cloned into pmirGLO luciferase reporter vectors (GenePharma Co., Ltd., Shanghai, China) and cotransfected with mimic NC or miR-27a mimic. Then, the luciferase activities were measured as described above.

2.16. Western Blotting Analysis. RIPA lysis buffer (Beyotime Biotechnology, China) was used to extract the proteins from myocardial tissues and H9c2 cells, and the protein concentration was determined with the BCA protein concentration determination kit (Beyotime Biotechnology, China). After quantification, the protein samples were separated by SDS-PAGE and transferred to PVDF membranes. The membranes were blocked with 5% BSA for 2 h. After incubation with primary antibodies, including ATAD3a (1 : 2000, ProteinTech, Rosemont, USA), AIF (1 : 8000, ProteinTech, Rosemont, USA), β-actin (1 : 5000, 20536-1-AP, ProteinTech, Rosemont, USA), histone H3 (1 : 6000, 17168-1-AP, ProteinTech, Rosemont, USA), and COXIV (1 : 10000, Proteintech, Rosemont, USA) antibodies, overnight at 4°C, the membranes were incubated with HRP-labeled secondary antibodies for 1 h at room temperature. All the antibodies were purchased from Abcam (UK) and diluted according to the manufacturer's instructions. The Western blots were developed using the Pierce™ ECL Western blotting substrate (Thermo Scientific™, USA).

3. Statistical Analysis

All the data are expressed as the mean ± SD, and statistical analysis was performed with the GraphPad Prism version 8.0 software (San Diego, California, USA). To compare the differences between two groups, Student's t-test was used. When comparing differences among more than two groups, one-way ANOVA was performed, followed by multiple comparison analysis using Fisher's least significant difference test. $p < 0.05$ was considered statistically significant.

4. Results and Discussion

4.1. miR-27a Expression Was Induced by MIRI. As shown in Figures 1(a)–1(c), isolated rat hearts that were subjected to I/R displayed mitochondrial swelling, cristae rupture, myofibrillar vacuolation, interstitial edema, and nuclear

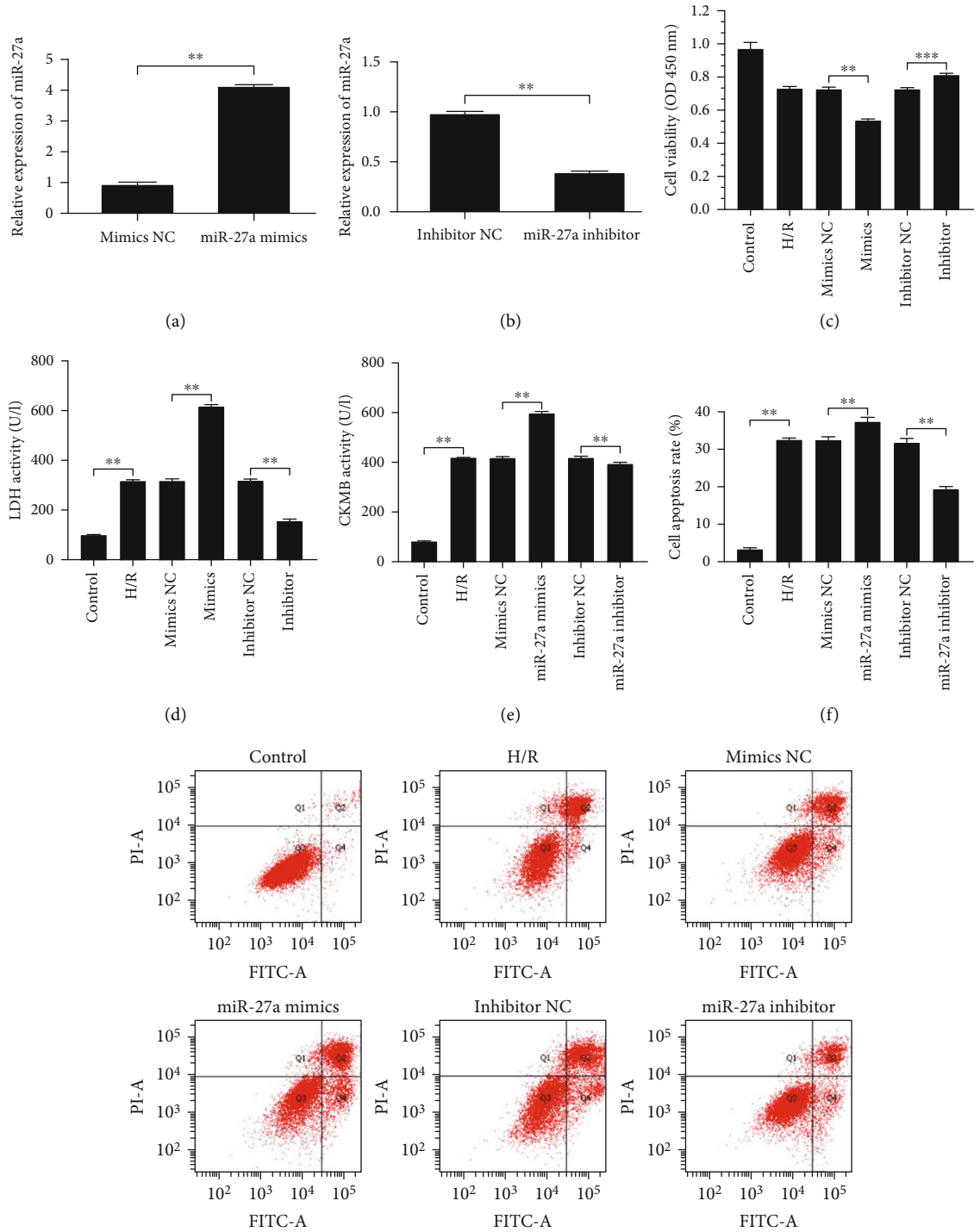

Figure 3: miR-27a regulated hypoxia/reoxygenation- (H/R-) induced myocardial injury in vitro. H9c2 cells were transfected with the miR-27a mimic, miR-27a inhibitor, mimics negative control (NC), and inhibitor NC, followed by 8 h of hypoxia and 3 h of reoxygenation. (a, b) miR-27 expression in H9c2 cells was detected by RT-qPCR after transfection with the miR-27a mimic or miR-27a inhibitor. (c) Analysis of cell viability by CCK-8 assay. (d, e) Measurement of LDH and CK-MB activity in the culture medium. (f) Cell apoptosis was detected by flow cytometry. All data were obtained from four independent replicate experiments. $^{**}p < 0.01$; $^{***}p < 0.001$.

fragmentation, as well as large amounts of inflammatory cell infiltration and large areas of myocardial necrosis, demonstrating that the MIRI model was successfully established. The top 10 upregulated miRNAs in the myocardia subjected to I/R were selected by analysis of GEO data (Figure 1(d)). Verification of the expression of these miRNAs by qRT-PCR revealed that miR-27a expression was significantly upregulated (almost 4.5-fold) in the I/R group compared with the control group (Figure 1(e)). In addition, miR-27a expression in H9c2 cells exposed to sustained hypoxia for

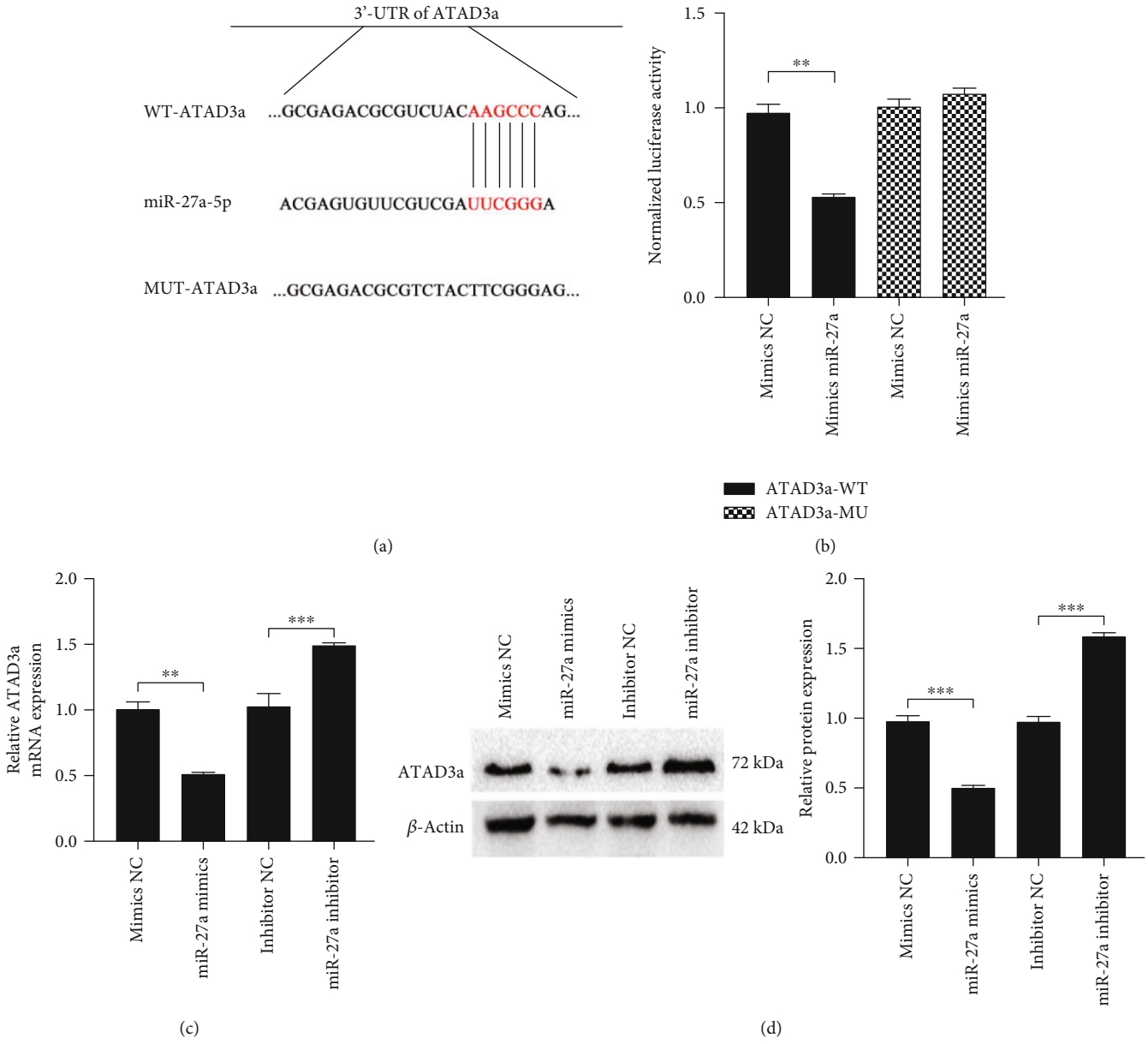

Figure 4: ATAD3a was a target of miR-27a. (a) miR-27a-specific binding on the 3′-UTR of ATAD3a. (b) The relative luciferase activity was analyzed after cotransfecting the pmirGLO luciferase reporter vectors containing wild-type or mutant binding sites with the miR-27a mimic and mimic negative control (NC). (c, d) The mRNA and protein levels of ATAD3a in H9c2 cells transfected with the miR-27a mimics, miR-27a inhibitor, mimics NC, and inhibitor NC were detected by RT-qPCR and Western blotting. All data were obtained from four independent replicate experiments. $^{**}p < 0.01$; $^{***}p < 0.001$.

different times was also examined. The level of miR-27a peaked after 8 h of hypoxia, followed by 3 h of reoxygenation (Figure 1(f)). Altogether, these results suggested that miR-27a was induced by I/R.

4.2. c-Fos Regulated miR-27a Expression. Considering that miRNA expression can be regulated by transcription factors, whether miR-27a is transcriptionally activated by transcription factors was investigated. c-Fos is a key transcription factor that contributes to MIRI. As shown in Figure 2(a), c-Fos protein expression was upregulated in myocardia subjected to I/R, and the c-Fos level was positively correlated with miR-27a expression in these tissues (Figure 2(b)). Furthermore, inhibition of c-Fos expression using siRNA led to reduced miR-27a expression. Moreover, overexpression of c-Fos upregulated miR-27a expression (Figures 2(c) and 2(d)). Therefore, we focused on c-Fos as a putative upstream regulator of miR-27a expression.

As predicted by the PROMO database, a c-Fos-specific binding site existed in the putative promoter region (-983 to -974 region) of miR-27a (Figure 2(e)). The results of luciferase reporter assays indicated that cotransfection of a vector carrying the putative promoter with the pcDNA vector expressing c-Fos led to a remarkable increase in the relative luciferase activity compared with cotransfection of a vector carrying the putative promoter with the pcDNA empty

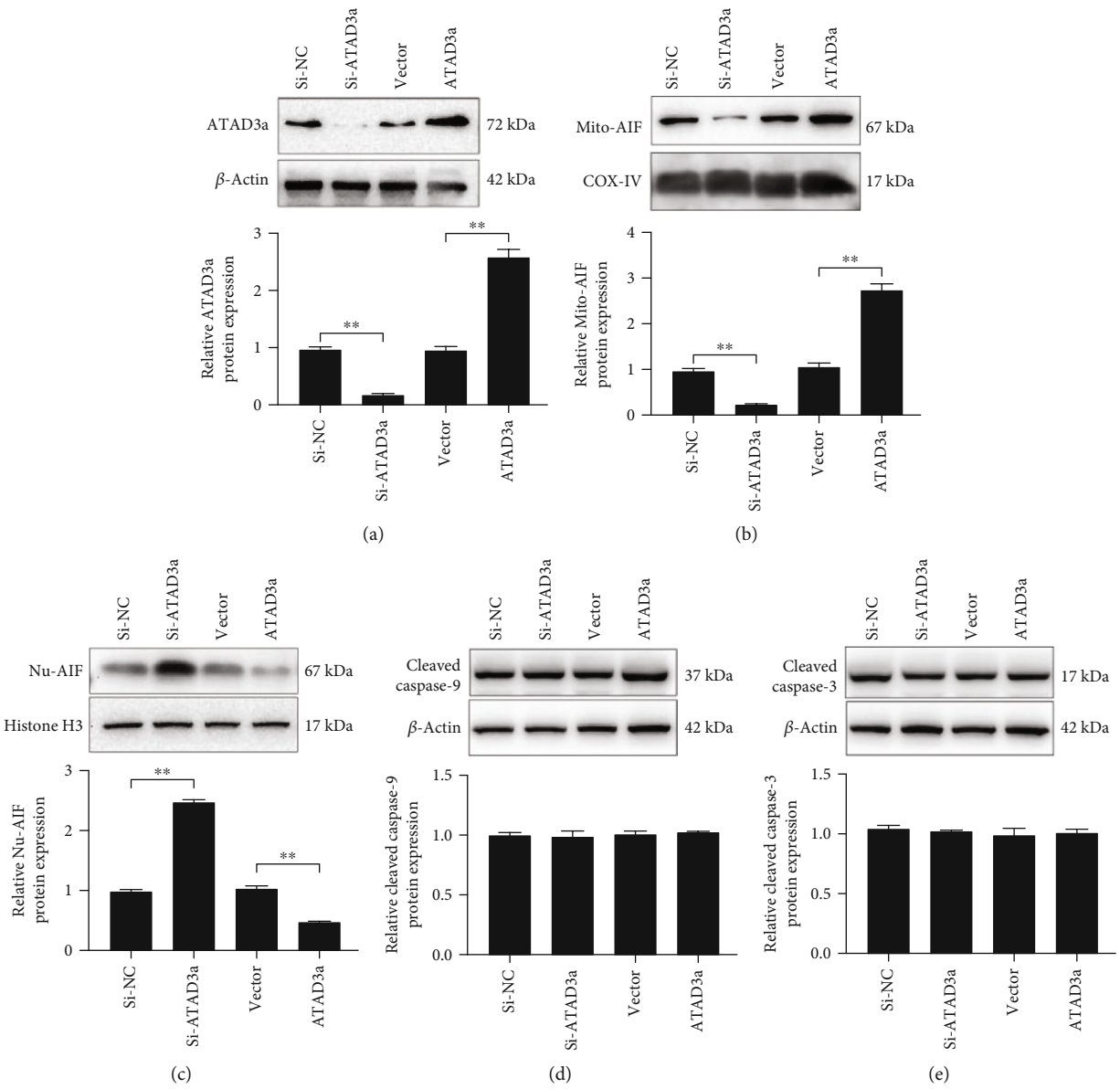

Figure 5: Continued.

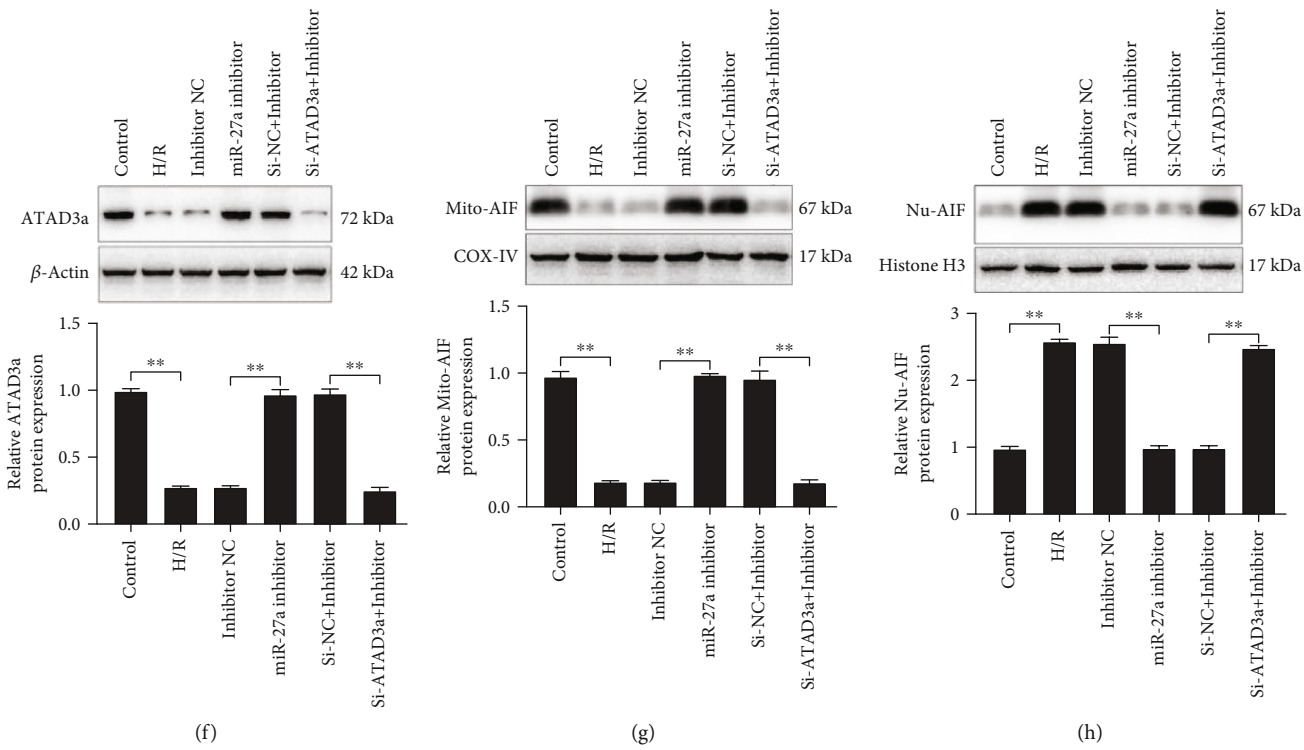

Figure 5: miR-27a regulated the translocation of apoptosis-inducing factor (AIF) from the mitochondria to the nucleus. Small interfering RNA targeting ATAD3a (Si-ATAD3) and matched negative control (Si-NC) ATAD3a plasmid and matched empty vector were transfected into H9c2 cells. The level of ATAD3a (A) and the level of AIF in the mitochondria (b), the nuclei (c), cleaved caspase-9 (d) and cleaved caspase-3 (E) were detected by Western blotting. H9c2 cells were transfected with the miR-27a inhibitor or inhibitor NC, together with the si-ATAD3a or si-NC, and the cells were then exposed to 8 h of hypoxia and 3 h of reoxygenation. Alterations in the levels of ATAD3a (f), AIF in the mitochondria (g), and AIF in the nucleus (h) were detected by Western blotting. All data were obtained from four independent replicate experiments. $^{**}p < 0.01$.

vector. In contrast, there was no significant change in the relative luciferase activity after the cotransfection of a vector carrying the promoter with a mutated c-Fos binding site (Figure 2(f)). In addition, the ChIP-qPCR assay results further demonstrated that c-Fos could bind to the putative promoter region of miR-27a, and H/R treatment enhanced the enrichment of c-Fos on the putative promoter region of miR-27a (Figure 2(g)). Altogether, these results suggested that c-Fos regulates miR-27a expression.

4.3. miR-27a Regulated H/R-Induced Myocardial Injury In Vitro. To determine the role of miR-27a in H/R-induced injury, overexpression and suppression of miR-27a were achieved by transfecting cardiomyocytes with the miR-27a mimic and miR-27a inhibitor (Figures 3(a) and 3(b)), respectively. The results showed that overexpression of miR-27a led to a decrease in cell viability (Figure 3(c)), an increase in LDH (Figure 3(d)) and CK-MB (Figure 3(e)) secretion, and an increase in apoptosis (Figure 3(f)) in the cardiomyocytes subjected to H/R. In contrast, suppression of miR-27a led to the opposite effects. Altogether, these results suggested that miR-27a could regulate MIRI in vitro.

4.4. ATAD3a Was a Target of miR-27a. As predicted with TargetScan, miR-27a may bind to the 3′-UTR of ATAD3a (Figure 4(a)), and a luciferase reporter assay was performed to verify the specific interaction of these two molecules. A decrease in the relative luciferase activity was observed when ATAD3a-WT was cotransfected with the miR-27a mimic compared with when ATAD3a-WT was cotransfected with the mimic NC. In contrast, no significant alteration was observed when ATAD3a-MUT was cotransfected with the miR-27a mimic (Figure 4(b)). Furthermore, overexpression of miR-27a reduced the mRNA and protein levels of ATAD3a, while suppression of miR-27a enhanced the mRNA and protein levels of ATAD3a (Figures 4(c) and 4(d)). Taken together, these results suggested that ATAD3a is a target of miR-27a.

4.5. miR-27a Regulated the Translocation of AIF from the Mitochondria to the Nucleus. AAA-domain-containing 3A (ATAD3a) is recognized as an antiapoptotic factor [24, 25], but the mechanism underlying its antiapoptotic effect is not well understood. It was found that suppression of ATAD3A led to an increase in the AIF levels in the nucleus and a decrease in the AIF levels in the mitochondria, and overexpression of ATAD3A led to the opposite effects (Figures 5(a)–5(c)). However, modulation of ATAD3a expression did not alter the levels of cleaved caspase-9 and cleaved caspase-3 (Figures 5(d) and 5(e)). These results suggested that ATAD3a regulated apoptosis by modulating the translocation of AIF from the mitochondria to the nucleus, and this apoptosis occurred in a caspase-independent

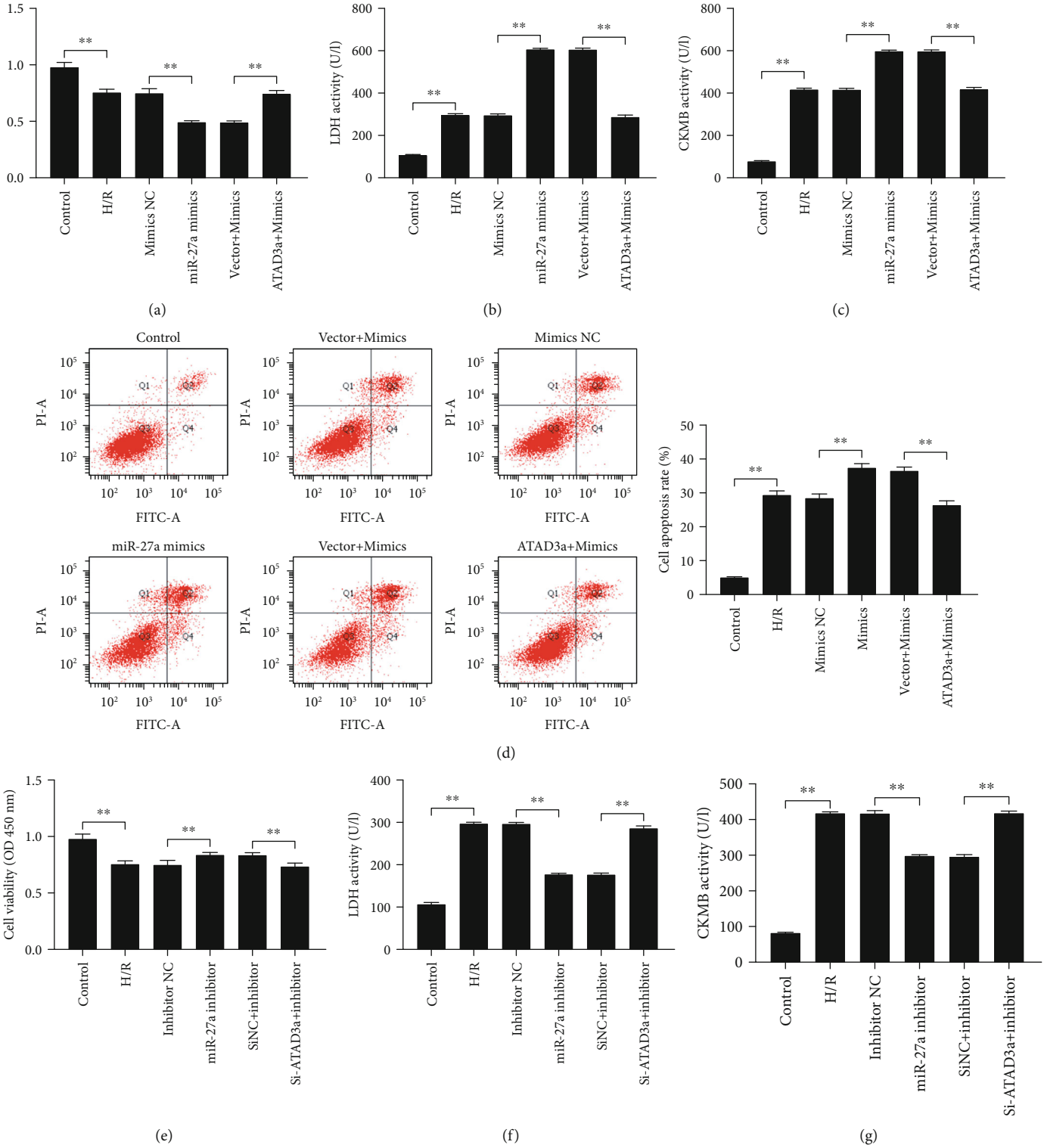

Figure 6: Continued.

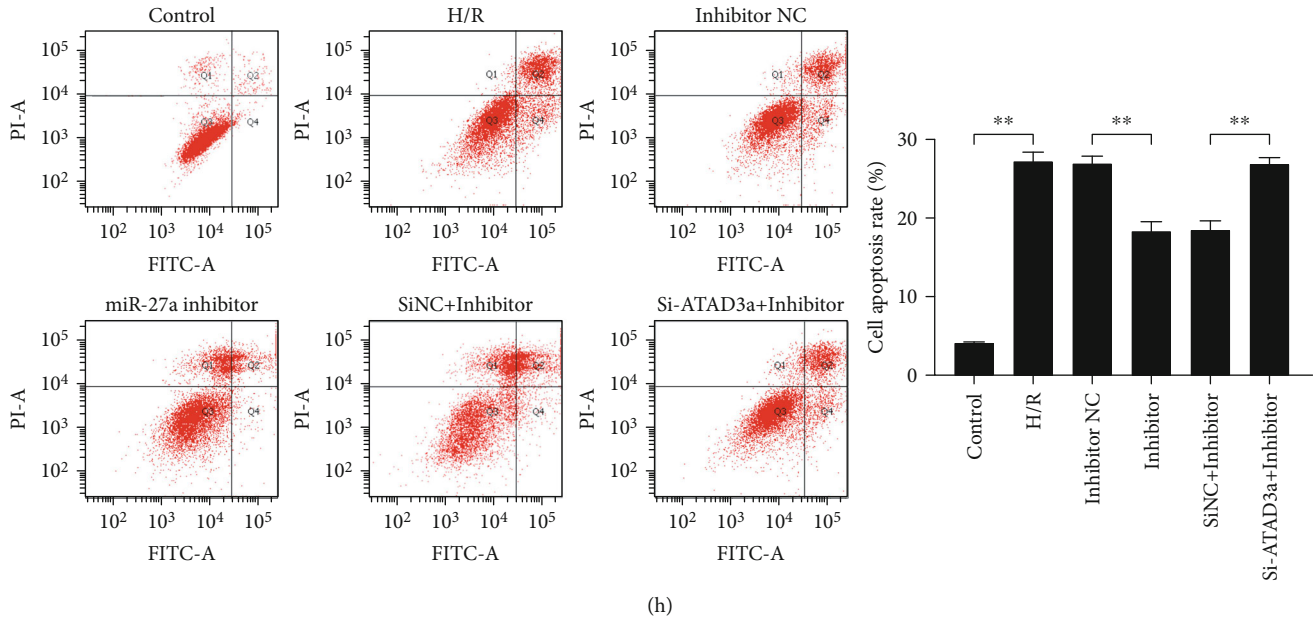

Figure 6: The effect of miR-27a on hypoxia/reoxygenation- (H/R-) induced myocardial injury was mediated by ATAD3a. H9c2 cells were transfected with the miR-27a mimic or mimic negative control (NC), together with the ATAD3a plasmid or empty vector, and then, the cells were subjected to 8 h of hypoxia and 3 h of reoxygenation. (a) Analysis of cell viability by CCK-8 assay. (b, c) Measurement of LDH and CK-MB activity in the culture medium. (d) Cell apoptosis was detected by flow cytometry. H9c2 cells were transfected with the miR-27a inhibitor or inhibitor NC, together with the small interfering RNA targeting ATAD3a (Si-ATAD3) and matched negative control (Si-NC), and the cells were subjected to 8 h of hypoxia and 3 h of reoxygenation. (e) Analysis of cell viability by CCK-8 assay. (f, g) Measurement of LDH and CK-MB activity in the culture medium. (h) Cell apoptosis was detected by flow cytometry. All data were obtained from four independent replicate experiments. $^{**}p < 0.01$.

manner. It was further discovered that inhibition of miR-27a expression suppressed the H/R-induced translocation of AIF from the mitochondria to the nucleus, and this effect was reversed by knockdown of ATAD3a (Figures 5(f)–5(h)), demonstrating that miR-27a regulated the translocation of AIF from the mitochondria to the nucleus via the modulation of ATAD3a.

4.6. The Effect of miR-27a on H/R-Induced Myocardial Injury Was Mediated by ATAD3a. To investigate the regulatory role of ATAD3a in the effect of miR-27a on H/R-induced myocardial injury, we examined whether the effect of miR-27a on MIRI was compromised by downregulation or upregulation of ATAD3a expression in vitro. As shown in Figures 6(a)–6(c), the decrease in cell viability, increase in cardiac enzyme secretion, and increase in apoptosis after treatment with the miR-27a mimic were compromised when the cells were cotransfected with ATAD3a-overexpressing plasmids. In contrast, the beneficial effects of miR-27a inhibitor treatment on the increase in cell viability, decrease in cardiac enzyme secretion, and decrease in apoptosis were abrogated when the cells were cotransfected with si-ATAD3a (Figures 6(d)–6(f)). Altogether, these results demonstrated that the effect of miR-27a on H/R-induced myocardial injury was mediated by ATAD3a.

4.7. Inhibition of miR-27a Using AAV9-Mediated Gene Therapy Mitigated MIRI Ex Vivo. We also examined whether inhibition of miR-27a expression using AAV9-mediated gene therapy could ameliorate MIRI in an isolated rat heart model. After injection of rat hearts with the AAV9-rno-miR-27a sponge, the level of miR-27a in the rat hearts was notably decreased (Figure 7(a)). In addition, the rat hearts treated with the AAV9-miR-27a sponge exhibited less structural damage in the mitochondria and myocardial fibers (Figures 7(b) and 7(c)), decreased myocardial infarct size (Figure 7(d)), and decreased apoptosis rates (Figure 7(e)) compared with those injected with NC. Taken together, these results suggested that inhibition of miR-27a using AAV9-mediated gene therapy mitigated MIRI ex vivo.

5. Discussion

The expression of miR-27a in myocardial ischemic disease remains controversial. Several studies have shown that the level of miR-27a is increased in the peripheral blood mononuclear cells (PBMCs) of CAD patients [34, 35]. However, Xue et al. [36] found that the levels of circulating miR-27a were not significantly different in the peripheral blood of AMI patients compared with control subjects. In the present study, miR-27a expression was markedly induced in myocardia exposed to I/R and cardiomyocytes treated with H/R, which is consistent with the findings of Liu JY et al. in mice [19]. However, miR-27a expression was notably downregulated in a simple model of myocardial hypoxia without reoxygenation [37]. Therefore, we speculated that the discrepancy in the above findings may be ascribed to the differences in the models.

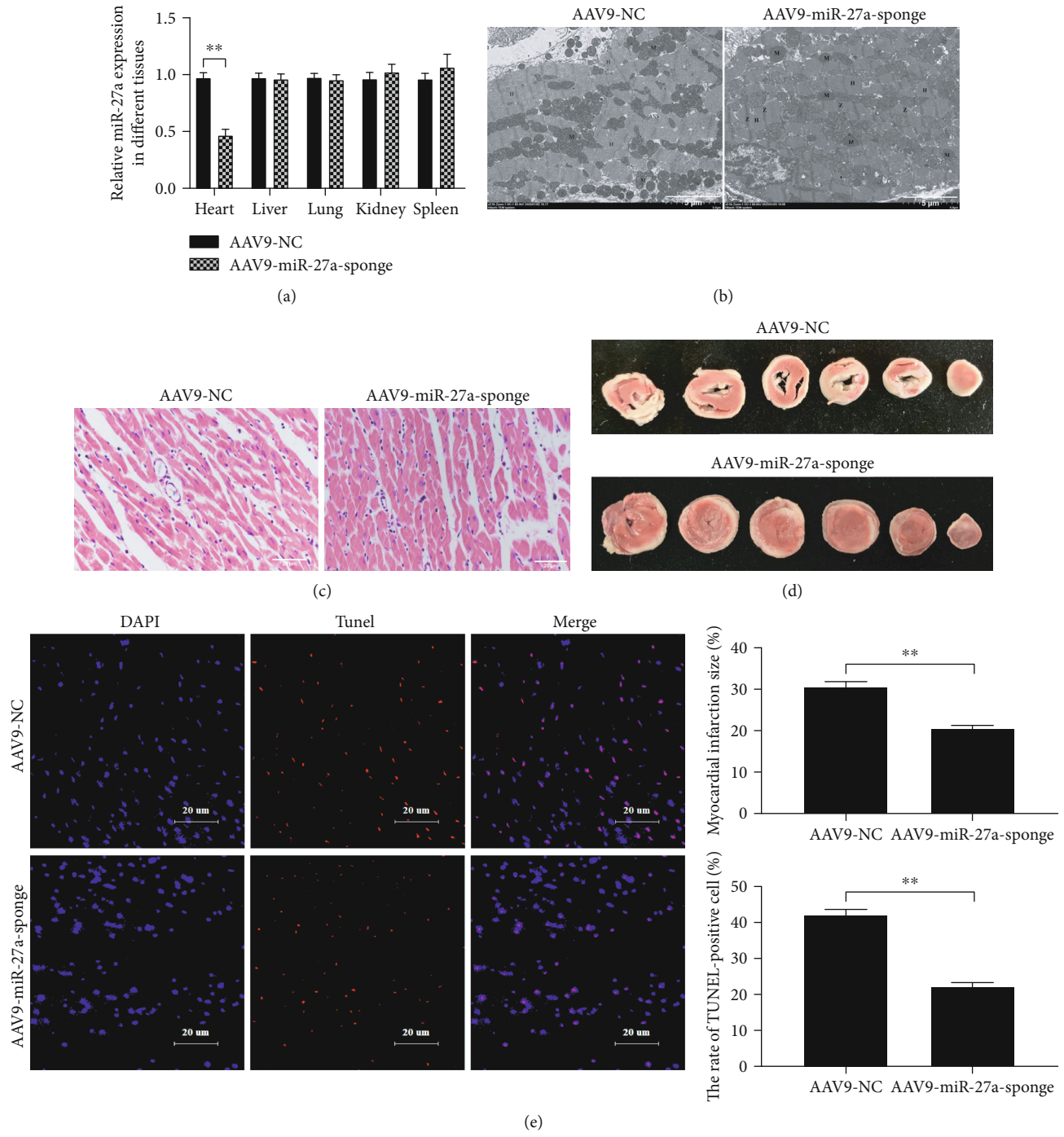

Figure 7: Inhibition of miR-27a using AAV9-mediated gene therapy mitigated MIRI ex vivo. (a) Selective inhibition of miR-27a in the myocardium in vivo was achieved by injecting AAV9-miR-27a-sponge through the rat tail vein. The rat injected with AAV9-miR-27a-negative control (NC) acts as a control. The isolated rat hearts were subjected to 30 min of ischemia, followed by 90 min of reperfusion. Myocardial structure damage was detected by (b) transmission electron microscopy and (c) HE staining, $n = 3$. (d) Myocardial infarct size was measured by TTC staining, $n = 6$. (e) Apoptosis in the myocardium was detected by TUNEL staining, $n = 6$. $^{**}p < 0.01$.

Several studies have demonstrated that transcription factors can regulate miR-27a expression by binding to the miR-27a promoter [38, 39]. For instance, mutant p53 (p53-273H) suppresses miR-27a expression by specifically binding to the miR-27a promoter region (nts -2899 to -2675) and subsequently enhances EGF-mediated ERK1/2 activation in breast and lung cancer cells [38]. Additionally, HIF-1α, a key transcription factor related to the regulation of gene expression under hypoxic conditions, leads to an increase in miR-27a expression by directly binding to the promoter region of miR-27a [39]. In our study, we found that the upregulation of c-Fos expression in myocardia exposed to I/R was positively correlated with the expression of miR-27a. Furthermore, it was found that c-Fos could directly bind to the

promoter region of miR-27a and positively regulate miR-27a expression in vitro. Thus, we suggested that c-Fos, whose expression is induced during MIRI, transcriptionally activated miR-27a, which partly accounted for the upregulation of miR-27a during MIRI.

ATAD3a was verified as a novel target of miR-27a in our study. Although ATAD3a is reported to act as an anti-apoptotic factor in lung adenocarcinoma [24] and prostate cancer [25], the detailed underlying mechanism is not known. In the present study, we found that ATAD3a could regulate the translocation of AIF from the mitochondria to the nucleus, which is consistent with the findings of Chiang et al. [40]. After AIF enters the nucleus, DNA fragmentation is triggered, resulting in the initiation of apoptosis [41]. However, modulation of ATAD3a expression has little effect on the activation of caspases, which demonstrated that the regulation of apoptosis by ATAD3a occurs in a caspase-independent manner. It has been documented that miR-27a plays an important role in the regulation of apoptosis [42–44]. miR-27a can regulate cell apoptosis by targeting Fas-associated protein with death domain (FADD) [42], SMAD5 [43], PPAR gamma [44], etc. In this study, it was demonstrated that the translocation of AIF from the mitochondria to the nucleus and the apoptosis induced by H/R were regulated by miR-27a, and these effects were dependent on ATAD3a, which provided new insight into the mechanism by which miR-27a contributes to the regulation of I/R-induced myocardial apoptosis.

Increasing evidence has shown that miR-27a can be used as a target for gene therapy [45–47]. An antisense oligonucleotide specific for miR-27a (antagomiR-27a) and miR-27a sponges are two common methods used to inhibit the function of miR-27a [48, 49]. Ge et al. [45] suggested that antagomiR-27a inhibits glioblastoma cell growth in vitro and in vivo. Additionally, antagomiR-27a has a good therapeutic effect on the prevention of diabetic nephropathy [46]. In addition, Salah et al. [47] found that miR-27a sponges could inhibit the invasion and metastasis of osteosarcoma. A recent study demonstrated that miR-27a mediates the protective effect of high thoracic epidural block on MIRI [12], but whether inhibition of miR-27a expression decreases the direct protective effect on MIRI was not determined. In the present study, MIRI was alleviated in isolated rat hearts by treatment with an AAV-9 vector expressing miR-27a sponges, which suggested that miR-27a could be used as a target for gene therapy in MIRI in the future.

The MIRI model generated by the Langendorff approach in this study is a robust model for studying ischemia-reperfusion injury [50]. In the present study, Langendorff-perfused rat hearts without I/R that stained by TTC did not indicate any infarct size, while the hearts induced by 30 min ischemia and 90 min reperfusion showed large infarct areas, which provides a direct evidence for MIRI. However, we must acknowledge that there is also a limitation in this model. Because the isolated rat heart is deprived of neurohumoral control, this lack of systemic influence should be further evaluated [51]. Despite of this limitation, the data generated by the Langendorff model still provides useful information in understanding the role of the c-Fos/miR-27a/ATAD3a axis in MIRI.

6. Conclusions

Our study demonstrated that c-Fos functions as an upstream regulator of miR-27a and that miR-27a regulates the translocation of AIF from the mitochondria to the nucleus by targeting ATAD3a, thereby contributing to MIRI. These findings provide new insight into the role of the c-Fos/miR-27a/ATAD3a axis in MIRI and suggest that miR-27a could be used as a target for gene therapy in MIRI.

Data Availability

The data used to support the findings of this study are available from the corresponding author upon request.

Conflicts of Interest

The authors have no conflict of interest.

Authors' Contributions

Yandong Bao and Ying Qiao contributed equally to this work.

Acknowledgments

This study was supported by the National Natural Science Foundation of China (81800232 and 82070267). The authors thank Spandidos Publications English Language Editing Service for language editing of the manuscript.

References

[1] C. J. McAloon, L. M. Boylan, T. Hamborg et al., "The changing face of cardiovascular disease 2000-2012: an analysis of the world health organisation global health estimates data," *International Journal of Cardiology*, vol. 224, pp. 256–264, 2016.

[2] K. P. Rentrop and F. Feit, "Reperfusion therapy for acute myocardial infarction: concepts and controversies from inception to acceptance," *American Heart Journal*, vol. 170, no. 5, pp. 971–980, 2015.

[3] G. Heusch, "Coronary microvascular obstruction: the new frontier in cardioprotection," *Basic Research in Cardiology*, vol. 114, no. 6, 2019.

[4] N.-B. Liu, M. Wu, C. Chen et al., "Novel molecular targets participating in myocardial ischemia-reperfusion injury and cardioprotection," *Cardiology Research and Practice*, vol. 2019, Article ID 6935147, 16 pages, 2019.

[5] A. Araszkiewicz, M. Grygier, M. Lesiak, and S. Grajek, "The impact of ischemia-reperfusion injury on the effectiveness of primary angioplasty in ST-segment elevation myocardial infarction," *Advances in Interventional Cardiology*, vol. 3, no. 3, pp. 275–281, 2013.

[6] C. T. Pager, K. A. Wehner, G. Fuchs, and P. Sarnow, "Chapter 5 MicroRNA-Mediated Gene Silencing," *Progress in Molecular Biology and Translational Science*, vol. 90, pp. 187–210, 2009.

[7] Y. Li, Z. Tian, Y. Tan et al., "Bmi-1-induced miR-27a and miR-155 promote tumor metastasis and chemoresistance by targeting RKIP in gastric cancer," *Molecular Cancer*, vol. 19, no. 1, p. 109, 2020.

[8] X. Yan, H. Yu, Y. Liu, J. Hou, Q. Yang, and Y. Zhao, "miR-27a-3p functions as a tumor suppressor and regulates non-small cell lung cancer cell proliferation via targeting HOXB8," *Technology in Cancer Research & Treatment*, vol. 18, 2019.

[9] J. Zhang, J. Zhang, and Q. Zhang, "The effects of miR-27a-3p-mediated Smurf2 on bleomycin A5-induced pulmonary fibrosis in rats," *Cellular and Molecular Biology*, vol. 66, no. 3, pp. 79–84, 2020.

[10] J. Ji, J. Zhang, G. Huang, J. Qian, X. Wang, and S. Mei, "Over-expressed microRNA-27a and 27b influence fat accumulation and cell proliferation during rat hepatic stellate cell activation," *FEBS Letters*, vol. 583, no. 4, pp. 759–766, 2009.

[11] Y. Xiao, B. Li, and J. Liu, "miRNA-27a regulates arthritis via PPARγ in vivo and in vitro," *Molecular Medicine Reports*, vol. 17, 2018.

[12] J.-Y. Liu, J. Shang, X.-D. Mu, and Z.-Y. Gao, "Protective effect of down-regulated microRNA-27a mediating high thoracic epidural block on myocardial ischemia-reperfusion injury in mice through regulating ABCA1 and NF-κB signaling pathway," *Biomedicine & Pharmacotherapy*, vol. 112, p. 108606, 2019.

[13] K. Milde-Langosch, "The Fos family of transcription factors and their role in tumourigenesis," *European Journal of Cancer*, vol. 41, no. 16, pp. 2449–2461, 2005.

[14] R. Chiu, W. J. Boyle, J. Meek, T. Smeal, T. Hunter, and M. Karin, "The c-fos protein interacts with c-JunAP-1 to stimulate transcription of AP-1 responsive genes," *Cell*, vol. 54, no. 4, pp. 541–552, 1988.

[15] N. Harikai, K. Tomogane, T. Sugawara, and S.-i. Tashiro, "Differences in hypothalamic Fos expressions between two heat stress conditions in conscious mice," *Brain Research Bulletin*, vol. 61, no. 6, pp. 617–626, 2003.

[16] M. Christmann, M. T. Tomicic, and J. Origer, "c-Fos is required for excision repair of UV-light induced DNA lesions by triggering the re-synthesis of XPF," *Nucleic Acids Research*, vol. 34, no. 22, pp. 6530–6539, 2006.

[17] L.-Q. Zhai, X.-J. Guo, Z. Li et al., "Temporal changes in Egr-1 and c-fos expression in rat models of myocardial ischemia," *Annals of Palliative Medicine*, vol. 10, no. 2, pp. 1411–1420, 2021.

[18] T. Brand, H. S. Sharma, K. E. Fleischmann et al., "Proto-oncogene expression in porcine myocardium subjected to ischemia and reperfusion," *Circulation Research*, vol. 71, no. 6, pp. 1351–1360, 1992.

[19] M. Y. Ma and X. Xu, "Experiment study of c-fos expression on myocardial acute ischemia/reperfusion injury in rats," *Fa Yi Xue Za Zhi*, vol. 19, no. 2, pp. 65–67, 2003.

[20] L. A. Anuj, G. Venkatraman, and S. K. Rayala, "increased expression of microRNA 551a by c-Fos reduces focal adhesion kinase levels and blocks tumorigenesis," *Molecular and Cellular Biology*, vol. 39, 2019.

[21] J. Zhou, M. Wang, and D. Deng, "c-Fos/microRNA-18a feedback loop modulates the tumor growth via HMBOX1 in human gliomas," *Biomedicine & Pharmacotherapy*, vol. 107, pp. 1705–1711, 2018.

[22] S. del Mar Díaz-González, E. D. Rodríguez-Aguilar, A. Meneses-Acosta et al., "Transregulation of microRNA miR-21 promoter by AP-1 transcription factor in cervical cancer cells," *Cancer Cell International*, vol. 19, 2019.

[23] Z. Y. Yap, Y. H. Park, S. B. Wortmann et al., "Functional interpretation of ATAD3A variants in neuro-mitochondrial phenotypes," *Genome Medicine*, vol. 13, no. 1, p. 55, 2021.

[24] H.-Y. Fang, C.-L. Chang, S.-H. Hsu et al., "ATPase family AAA domain-containing 3A is a novel anti-apoptotic factor in lung adenocarcinoma cells," *Journal of Cell Science*, vol. 123, no. 7, pp. 1171–1180, 2010.

[25] K.-C. Chow, "ATPase family AAA domain containing 3A is an anti-apoptotic factor and a secretion regulator of PSA in prostate cancer," *International Journal of Molecular Medicine*, vol. 28, no. 1, pp. 9–15, 2011.

[26] H. M. Cooper, Y. Yang, E. Ylikallio et al., "ATPase-deficient mitochondrial inner membrane protein ATAD3A disturbs mitochondrial dynamics in dominant hereditary spastic paraplegia," *Human Molecular Genetics*, vol. 26, no. 8, pp. 1432–1443, 2017.

[27] G. Jin, C. Xu, X. Zhang et al., "Atad3a suppresses Pink1-dependent mitophagy to maintain homeostasis of hematopoietic progenitor cells," *Nature Immunology*, vol. 19, no. 1, pp. 29–40, 2018.

[28] R. Desai, A. E. Frazier, R. Durigon et al., "ATAD3 gene cluster deletions cause cerebellar dysfunction associated with altered mitochondrial DNA and cholesterol metabolism," *Brain*, vol. 140, no. 6, pp. 1595–1610, 2017.

[29] S. Peralta, S. Goffart, S. L. Williams et al., "ATAD3 controls mitochondrial cristae structure in mouse muscle, influencing mtDNA replication and cholesterol levels," *Journal of Cell Science*, vol. 131, 2018.

[30] Y. Feng, L. Zou, D. Yan et al., "Extracellular microRNAs induce potent innate immune responses via TLR7/MyD88-dependent mechanisms," *The Journal of Immunology*, vol. 199, no. 6, pp. 2106–2117, 2017.

[31] B. Qi, X. Zhang, H. Yu, Y. Bao, N. Wu, and D. Jia, "Brazilin prevents against myocardial ischemia-reperfusion injury through the modulation of Nrf2 via the PKC signaling pathway," *Annals of Translational Medicine*, vol. 9, no. 4, p. 312, 2021.

[32] N. Wu, X. Zhang, Y. Bao, H. Yu, D. Jia, and C. Ma, "Down-regulation of GAS5 ameliorates myocardial ischaemia/reperfusion injury via the miR-335/ROCK1/AKT/GSK-3β axis," *Journal of Cellular and Molecular Medicine*, vol. 23, no. 12, pp. 8420–8431, 2019.

[33] L. T. Bish, K. Morine, M. M. Sleeper et al., "Adeno-associated virus (AAV) serotype 9 provides global cardiac gene transfer superior to AAV1, AAV6, AAV7, and AAV8 in the mouse and rat," *Human Gene Therapy*, vol. 19, no. 12, pp. 1359–1368, 2008.

[34] A. Rafiei, G. A. Ferns, R. Ahmadi et al., "Expression levels of miR-27a, miR-329, ABCA1, and ABCG1 genes in peripheral blood mononuclear cells and their correlation with serum levels of oxidative stress and hs-CRP in the patients with coronary artery disease," *IUBMB Life*, vol. 73, no. 1, pp. 223–237, 2021.

[35] M. Babaee, E. Chamani, R. Ahmadi et al., "The expression levels of miRNAs- 27a and 23a in the peripheral blood mononuclear cells (PBMCs) and their correlation with FOXO1 and some inflammatory and anti-inflammatory cytokines in the patients with coronary artery disease (CAD)," *Life Sciences*, vol. 256, p. 117898, 2020.

[36] S. Xue, W. Zhu, D. Liu et al., "Circulating miR-26a-1, miR-146a and miR-199a-1 are potential candidate biomarkers for acute myocardial infarction," *Molecular Medicine*, vol. 25, no. 1, p. 18, 2019.

[37] J. Zhang, W. Qiu, J. Ma et al., "miR-27a-5p attenuates hypoxia-induced rat cardiomyocyte injury by inhibiting Atg7," *International Journal of Molecular Sciences*, vol. 20, 2019.

[38] J. Q. Cheng, "HIF-1α induces multidrug resistance in gastric cancer cells by inducing miR-27a," *PLoS One*, vol. 10, 2015.

[39] W. Wang, B. Cheng, L. Miao, Y. Mei, and M. Wu, "Mutant p53-R273H gains new function in sustained activation of EGFR signaling via suppressing miR-27a expression," *Cell Death & Disease*, vol. 4, 2013.

[40] S.-H. Chiou, "An alternative import pathway of AIF to the mitochondria," *International Journal of Molecular Medicine*, vol. 29, no. 3, pp. 365–372, 2012.

[41] H. Otera, S. Ohsakaya, Z.-I. Nagaura, N. Ishihara, and K. Mihara, "Export of mitochondrial AIF in response to proapoptotic stimuli depends on processing at the intermembrane space," *The EMBO Journal*, vol. 24, no. 7, pp. 1375–1386, 2005.

[42] R. Chhabra, Y. K. Adlakha, M. Hariharan, V. Scaria, and N. Saini, "Upregulation of miR-23a-27a-24-2 cluster induces caspase-dependent and -independent apoptosis in human embryonic kidney cells," *PLoS One*, vol. 4, no. 6, p. e5848, 2009.

[43] M. Nie, S. Yu, S. Peng, Y. Fang, H. Wang, and X. Yang, "miR-23a and miR-27a promote human granulosa cell apoptosis by targeting SMAD5," *Biology of Reproduction*, vol. 93, no. 4, p. 98, 2015.

[44] X. Chi, Y. Jiang, Y. Chen et al., "Suppression of microRNA-27a protects against liver ischemia/reperfusion injury by targeting PPARγ and inhibiting endoplasmic reticulum stress," *Molecular Medicine Reports*, vol. 20, no. 5, pp. 4003–4012, 2019.

[45] Y.-F. Ge, J. Sun, C.-J. Jin, B.-Q. Cao, Z.-F. Jiang, and J.-F. Shao, "AntagomiR-27a targets FOXO3a in glioblastoma and suppresses U87 cell growth in vitro and in vivo," *Asian Pacific Journal of Cancer Prevention*, vol. 14, no. 2, pp. 963–968, 2013.

[46] L. Wu, Q. Wang, F. Guo et al., "MicroRNA-27a induces mesangial cell injury by targeting of PPARγ, and its in vivo knockdown prevents progression of diabetic nephropathy," *Scientific Reports*, vol. 6, 2016.

[47] Z. Salah, R. Arafeh, V. Maximov et al., "miR-27a and miR-27a contribute to metastatic properties of osteosarcoma cells," *Oncotarget*, vol. 6, no. 7, pp. 4920–4935, 2015.

[48] J. F. Lima, L. Cerqueira, C. Figueiredo, C. Oliveira, and N. F. Azevedo, "Anti-miRNA oligonucleotides: a comprehensive guide for design," *RNA Biology*, vol. 15, no. 3, pp. 338–352, 2018.

[49] M. S. Ebert, J. R. Neilson, and P. A. Sharp, "MicroRNA sponges: competitive inhibitors of small RNAs in mammalian cells," *Nature Methods*, vol. 4, no. 9, pp. 721–726, 2007.

[50] R. M. Bell, M. M. Mocanu, and D. M. Yellon, "Retrograde heart perfusion: the Langendorff technique of isolated heart perfusion," *Journal of Molecular and Cellular Cardiology*, vol. 50, no. 6, pp. 940–950, 2011.

[51] D. J. Herr, S. E. Aune, and D. R. Menick, "Induction and assessment of ischemia-reperfusion injury in Langendorff-perfused rat hearts," *Journal of Visualized Experiments*, vol. 101, 2015.

Hindawi
Oxidative Medicine and Cellular Longevity
Volume 2021, Article ID 5543340, 14 pages
https://doi.org/10.1155/2021/5543340

Research Article

Computational and Preclinical Evidence of Anti-ischemic Properties of L-Carnitine-Rich Supplement via Stimulation of Anti-inflammatory and Antioxidant Events in Testicular Torsed Rats

Janet Olayemi Olugbodi,[1,2] **Keren Samaila**,[2] **Bashir Lawal**,[3,4] **Oluchukwu Ogechukwu Anunobi**,[2] **Roua S. Baty**,[5] **Omotayo Babatunde Ilesanmi**,[6] **and Gaber El-Saber Batiha**[7]

[1]*Department of Medicine, Emory University School of Medicine, Atlanta, USA*
[2]*Department of Biochemistry, Bingham University, Abuja-Keffi Expressway Road, Karu, Nigeria*
[3]*PhD Program for Cancer Molecular Biology and Drug Discovery, College of Medical Science and Technology, Taipei Medical University and Academia Sinica, Taipei 11031, Taiwan*
[4]*Graduate Institute for Cancer Biology & Drug Discovery, College of Medical Science and Technology, Taipei Medical University, Taipei 11031, Taiwan*
[5]*Department of Biotechnology, College of Science, Taif University, P.O. Box 11099, Taif 21944, Saudi Arabia*
[6]*Department of Biochemistry, Faculty of Science, Federal University Otuoke, Ogbia, Bayelsa State, Nigeria*
[7]*Department of Pharmacology and Therapeutics, Faculty of Veterinary Medicine, Damanhour University, Damanhour 22511, AlBeheira, Egypt*

Correspondence should be addressed to Janet Olayemi Olugbodi; janetolayemi@binghamuni.edu.ng and Bashir Lawal; bashirlawal12@gmail.com

Received 2 March 2021; Revised 21 May 2021; Accepted 14 June 2021; Published 5 July 2021

Academic Editor: Margaret H Hastings

Ischemia-reperfusion injury is a urological emergency condition that could lead to necrosis, testicular damage subfertility, and infertility. The purpose of this study was to identify changes taking place in the rat testis at short-term (4 hr) as well as long-term (7 days) reperfusion following testicular torsion and to evaluate the effects of Proxeed Plus (PP), L-carnitine-rich antioxidant supplement, on preventing these changes using the biochemical parameters and histopathology. Thirty adult male rats were divided into five groups: in groups, 1-4 testicular ischemia was achieved by rotating the left testis 720° clockwise for 4 h and dividing into the sham, torsion/detorsion (T/D), T/D+1000 mg/kg BW PP, and T/D+5000 mg/kg BW PP groups, respectively. PP was administered intraperitoneally 30 min before detorsion while group 5 served as the normal control. All rats were sacrificed 4 h after detorsion. The same experimental design was set up, and animals were sacrificed after 7 days of detorsion. The testicular levels of human cyclooxygenase-2; tumor necrosis factor; interleukins-1β, 6, and 10; hydrogen peroxide; malonaldehyde; superoxide dismutase; catalase; glutathione transferase; glutathione peroxidase; glutathione reductase; and histopathological damage were evaluated. Our results revealed that rats in the torsion/detorsion group exhibited elevated testicular levels of oxidative markers and proinflammatory cytokines, low levels of antioxidant enzymes, and severe histological alterations relative to the control and sham groups. Treatments with 1000 and 5000 mg/kg BW of PP for 4 hr and 7 days significantly ($p < 0.05$) decreased the levels of the proinflammatory and oxidative markers while increasing the spermatogenesis, testicular levels of antioxidant enzymes, and anti-inflammatory cytokine (IL-10) in a dose-dependent manner. This suggested that PP exhibited anti-inflammatory and antioxidant activities against I/R testes thus serving as an effective supplement to protect against testicular assault.

1. Introduction

Testicular torsion (TT) is a serious medical and surgical crisis, which occurs due to rotation and abnormal twisting of the spermatic cord of the testis or the mesorchium [1]. The degree and length of torsion are vital determinants of testicular damage [1, 2]; thus, prompt diagnosis and early medical intervention are necessary for managing this condition. It is not a frequently encountered condition (1 out of 4000 males) and occurs mostly in males under the age of 25 years [3]. However, it is considered a dangerous pathological condition that causes a decreased flow of blood to the testes causing scrotal pain and finally leading to testicular atrophy [4, 5]. This interrupted blood flow leads to ischemia during which ATP gets depleted while degradation products such as hypoxanthine increase, causing damages to metabolically active tissues [6]. However, following the acute ischemia, the tissues undergo reperfusion during which the tissue blood flow is being attenuated, causing more damaging effects than that induced by ischemia [7].

The reactive oxygen species (ROS) such as superoxide anions, hydrogen peroxide, and hydroxyl radicals have been implicated in the pathogenesis of testicular ischemia/reperfusion (I/R) injury [8, 9], and several antioxidant therapies have been experimentally used to reverse the antioxidant-induced testicular damage [10, 11]. In fact, ROS constitutes the basic pathophysiological processes of the I/R injury in the testis and other tissues such as the brain, myocardium, and kidneys [9, 12]. The restoration of blood flow during ischemia-reperfusion (I/R) injury triggers a chain of reactions that lead to the generation of reactive oxygen species (ROS) by the injured testicular cells and endothelial cells in the ischemic zone, as well as neutrophils that enter the ischemic zone, and become activated on reperfusion [13–15]. This generation of reactive oxygen species (ROS) can cause testicular oxidative cell and tissue damage by the destruction of the integrity of the cell membrane, induction of lipid peroxidation, protein denaturation, and DNA damage [16, 17]. Serum malondialdehyde (MDA) concentration in patients with testis torsion has been identified as a reliable marker of lipid peroxidation and tissue damage [18, 19]. However, time course, short- and long-term testis reperfusion damages, and time course therapeutic strategies have been reported [18, 20].

Furthermore, when a tissue suffers from ischemia-reperfusion, inflammatory mediators like prostaglandin E2 (PGE2) and nitric oxide (NO) are produced through the activations of cyclooxygenase-2 (Cox-2) and inducible NO synthase (iNOS), respectively [14]; also, proinflammatory cytokines like interleukin-6 (IL-6), interleukin-1β (IL-1β), and tumor necrosis factor (TNF-α) are highly produced [21]. These proinflammatory cytokines trigger the productions of ROS, which stimulates neutrophil infiltration and results in ischemic injury [12]. Therefore, inflammatory mediators and proinflammatory markers play important roles in oxidative stress-induced I/R injury [22].

The testes contain some natural antioxidants such as vitamins, thioredoxin, glutathione, and superoxide dismutase [23] that play a vital role in protecting the testes against oxidative damage during assaults. However, relatively low levels of these natural antioxidants in the cytoplasm and high levels of membrane polyunsaturated fatty acids make spermatozoa susceptible to ROS attack from lipid peroxidation [23, 24]. A curative approach that attenuates the production of these inflammatory markers and free radicals could salvage the testis from impairment during I/R injury. Several anti-inflammatory and antioxidant free radical scavengers have been used to prevent I/R injury in tissues.

L-carnitine (LC) plays a pivotal role in cellular energetic metabolism, acting as a shuttle of the activated long-chain fatty acids (acyl-CoA) into the mitochondria, where beta-oxidation takes place [25, 26]. L-carnitine is found at a high level in epididymal fluid due to an active secretory mechanism [27]; in addition, high levels of L-carnitine in epididymal lumen and L-acetylcarnitine (LAC) in sperm cells have been implicated in the initiation of sperm motility [28, 29]. Clinical studies have also indicated that oral administration of L-carnitine improves sperm quality of patients with idiopathic asthenozoospermia [30] and have also been used for the treatment of idiopathic and varicocele-associated oligoasthenospermia [31]. In addition, Lenzi et al. [32] successfully used L-carnitine in idiopathic infertile males while another study demonstrated that a combination of L-carnitine+acetyl-L-carnitine increased sperm count in patients with echographic features of genital inflammation [33]. Decreased total L-carnitine levels may be associated with hyperandrogenism and/or insulin resistance in nonobese women with polycystic ovary syndrome (PCOS) [34].

Proxeed Plus is a lemon flavor carnitine-based supplement specially formulated to support sperm health and boost a man's reproductive ability. It is a composite of L-carnitine, acetyl-L-carnitine, zinc, fumarate, CoQ10, folic acid, fructose, vitamin C, and vitamin B12 [35]. These ingredients are known to play a vital function in spermatozoa by optimizing energy and hormonal metabolism, maintaining sperm health, and exhibiting antioxidant activities [24, 36–38]. A recent randomized clinical study involving over 100 oligoasthenoteratozoospermia men reported a significant increase in progressive sperm motility and total sperm count in groups treated with Proxeed Plus for 6 months compared to the placebo [39]. Another clinical trial with 175 idiopathic oligoasthenozoospermia men who could not impregnate their partners revealed that Proxeed Plus treatments for 3 and 6 months significantly improve the sperm volume and progressive motility compared to the baseline [40]. Other biological activities of Proxeed Plus including neuroprotection [41] have been reported. In the present study, we demonstrated the beneficial effects of Proxeed Plus on attenuating the inflammatory condition and oxidative stress induced by ischemia-reperfusion of the testes in male rats.

2. Materials and Methods

2.1. Test Supplement (Proxeed Plus), Chemicals, and Assay Kits. The test supplement (Proxeed Plus) was obtained from Sigma-Tau Health Science, Utrecht, the Netherlands. Enzyme-linked immunosorbent assay kits are Rat Interleukin-1 ELISA Kit and Rat Tumor Necrosis Factor ELISA Kit, respectively, Shanghai LZ, China. The Glutathione Assay Kit and Lipid

Peroxidation (MDA) Assay Kit were from Sigma-Aldrich, USA. The Cox activity assay kit was from Cayman, Ann Arbor, MI, USA. Ketamine was obtained from Ketalar, Pfizer Pharm GMBH, Germany. All other chemicals were from Sigma-Aldrich Co., St. Louis, MO, USA.

2.2. Experimental Animals. Fifty (50) male albino rats weighing 126.45 ± 3.97 g were procured from the animal farm of Bingham University. The animals were maintained under standard laboratory conditions with access to commercial feed pellets (growers) and water ad libitum. Animal handling and experimentations complied with the principles governing the use of laboratory animals as laid out by the international standard set by the UK Animals (Scientific Procedures) Act, 1986 and associated guidelines, the European Communities' council directive of 24 November 1986 (86/609/EEC), and the National Institutes of Health *Guide for the Care and Use of Laboratory Animals* (NIH Publication No. 8023, revised 1978). All experimental protocols were approved by Bingham University, Committee on Ethics for Medical and Scientific Research (BHU/REC/19/A005), and principles governing the use of laboratory animals as laid out by the Bingham University, Committee on Ethics for Medical and Scientific Research, were duly observed.

2.3. Experimental Design and Animal Grouping. Time course (short- and long-term) testicular reperfusion damages have been reported [18, 20]; for these reasons, two experimental protocols were designed. The first protocol involved 5 experimental groups (5 rats per group) and was designed to identify changes taking place in the rat testis at short-term (4 hr) reperfusion following testicular torsion and to evaluate the effects of Proxeed Plus (PP).

Group 1: control group that received 2 ml/kg BW normal saline

Group 2: sham group

Group 3: torsion/detorsion (T/D)

Group 4: T/D+1000 mg/kg BW PP

Group 5: T/D+5000 mg/kg BW PP

In groups 4 and 5, Proxeed Plus was administered intraperitoneally 30 min before detorsion. 1000 mg/kg BW (low dose) and 5000 mg/kg BW (high dose) of PP were selected based on the recommended therapeutic regime of Proxeed Plus and also based on our previous toxicity study indicating that PP was safe and devoid of adverse effect even at a high dose of 5000 mg/kg BW. All rats were sacrificed 4 h after detorsion. However, in order to identify the changes taking place in the rat testis after long-term (7 days) reperfusion following testicular torsion and to evaluate the effects of Proxeed Plus (PP), the second protocol was designed with 5 experimental groups as described in the first protocol; however, all animals were sacrificed after 7 days of detorsion. The surgical procedure was carried out based on previous experimental studies [42, 43]. In brief, the rats were anesthetized using intraperitoneal injections of 50 mg/kg BW of ketamine hydrochloride and 10 mg/kg BW of xylazine. Through a longitudinal scrotal incision, the left testis of the animals in each group was exposed and dissected. Afterward, the torsion of the left testis was induced by a 720° counterclockwise rotation. One hour later, the testis was counterrotated to the natural position and was inserted into the scrotum. Then, the skin incision was sutured (4–0 nonabsorbable), and animals were kept until harvesting time. In the sham animals, only surgical stress was applied by immediately retracting and replacing the spermatic cord.

2.4. Collection and Preparation of Organ. The testis was carefully harvested and homogenized in 0.25 M in 0.1 M phosphate buffer pH 7.4 using a Teflon homogenizer, and the homogenate was centrifuged at 3,000 r.p.m. for 15 minutes [44, 45], after which the supernatant was transferred into plain sample bottles for analysis.

2.5. Estimation of Testicular Levels of Prooxidative Molecules and Antioxidant Enzymes

2.5.1. Lipid Peroxidation. The testicular concentrations of malonaldehyde (MDA) as an index of lipid peroxidation were estimated spectrophotometrically by the thiobarbituric acid-reactive substance (TBARS) methods as described by Varshney and Kale [46]. Briefly, 0.4 ml of the sample was mixed with 1.6 ml of Tris KCl buffer (0.15 M) to which 30% TCA (0.5 ml) was added. Then, 0.5 ml of 52 mM TBA was added and incubated in a water bath (80°C) for 45 min; this was followed by ice cooling centrifugation (3,000 rpm) at room temperature for 10 min. The supernatant was separated, and the absorbance was measured against the reference blank of distilled water at 531.8 nm.

2.5.2. Proteins and H_2O_2. The testicular proteins and H_2O_2 concentrations were assessed by the spectrophotometric methods of Gornall et al. [47] and Koroliuk et al. [48], respectively. Briefly, 10 μl of the sample was incubated for 10 min with 100 μmol/ml H_2O_2 in 0.05 mmol/l Tris-HCl buffer (pH = 7). The yellow complex of ammonium molybdate ($(NH_4)_2MoO_4$) and H_2O_2 was monitored at 410 nm after terminating the reaction with 50 μl of 4% $(NH_4)_2MoO_4$.

2.5.3. Catalase (CAT). The testicular activities of catalase were evaluated using a spectrophotometer by monitoring H_2O_2 clearance as described by Sinha [49]. The reaction mixture contained 2.9 ml of 10 mM H_2O_2 in 50 μM potassium phosphate buffer (pH 7) followed by 0.1 ml of tissue homogenate. The rate of decrease in the absorbance at 240 nm was recorded for 3 min. The results were expressed as μmol H_2O_2/min/mg of protein.

2.5.4. Superoxide Dismutase (SOD). The superoxide dismutase activity was estimated based on the principle of inhibition of autoxidation of epinephrine at 30°C and pH 10.2 as described by Misra and Fridovich [50]. Briefly, 25 μl of the homogenate was mixed with 0.1 mM epinephrine in carbonate buffer (pH 10.2) in a total volume of 1 ml, and the formation of adrenochrome was measured at 295 nm using a spectrophotometer. The SOD activity (U/mg of protein) was calculated by using the standard plot.

2.5.5. Glutathione Reductase (GSH). The activity of glutathione reductase was determined as described by Smith et al. [51] with small modifications. The reaction mixture in a total

of 3 ml consists of 2.9 ml of 5,5-dithiobis(2-nitrobenzoic acid) prepared in potassium phosphate buffer (0.1 M, pH 7.4), and 0.1 ml of tissue homogenate was incubated for 15 min at 37°C, and the absorbance was measured at 412 nm. The results were expressed as μmol/mg protein.

2.5.6. Glutathione Peroxidase (GPx). Glutathione peroxidase (GPx) activities were estimated using the spectrophotometric methods as described by Hu and Dillard [52]. Glutathione peroxidase (GPX) catalyzed the oxidation of glutathione by cumene hydroperoxide. In the presence of NADPH and glutathione reductase, the oxidized glutathione was immediately converted to the reduced form with concomitant oxidation of NADPH to $NADP^+$ [53]. An aliquot (10 μl) of the tissue homogenate was mixed with 500 μl mixed reagent and 20 μl cumene hydroperoxide. The absorbance was measured at 340 nm.

2.5.7. Glutathione S-Transferase (GST). Glutathione S-transferase (GST) activities were estimated using a spectrophotometer as described by Habig et al. [54]. The reaction mixture in a volume of 3 ml contained 2.4 ml of 0.3 M potassium phosphate buffer (pH 6.9), 0.1 mL of 30 mM 1-chloro-2,4-dinitrobenzene (CDNB), 0.1 ml of 30 mM GSH, and the enzyme source. The reaction was initiated by glutathione. The absorbance was followed for 5 min at 340 nm against a reagent blank.

2.6. Estimation of Testicular Levels of Inflammatory Markers. The testicular levels of tumor necrosis factor-alpha (TNF-α), cyclooxygenase- (Cox-) 2 activity, interleukin-1β (IL-1β), interleukin-6 (IL-6), and interleukin-10 (IL-10) levels were measured in duplicate by ELISA kits as described previously [55] and by following the manufacturer's directives.

2.7. Histopathological Evaluation of Testis. The testes of rats were fixed in 10% formalin and processed for histology using standard procedures. Further histological preparations were carried out as described by Igwebuike and Eze [56] and stained with hematoxylin and eosin for light microscopy.

2.8. Molecular Docking. The chemical structure of our ligand drug (L-carnitine) was retrieved as mol file format from the PubChem database. The ligand was converted into PDB format using Pymol and converted into PDBQT format using AutoDock Tools 1.5.6. All the protein targets (receptors), human cyclooxygenase-2 (PDB = 5kir), tumor necrosis factor (PDB = 1TNF), human interleukin-6 (PDB = 1ALU), and human interleukin-1 beta (PDB = 9ILB) were retrieved as PDB format file from Protein Data Bank and subsequently converted to PDBQT format. The ligands were prepared for docking by deletion of H_2O molecules, adjustment of polar hydrogen, and addition of Kollman charges. The molecular docking was performed using AutoDock Vina with all parameters set as default, and all bonds in the ligand are rotated freely, considering the receptor as rigid [57–59]. A grid box of $40\,\text{Å} \times 40\,\text{Å} \times 40\,\text{Å}$ was generated on defined binding site residues of the ligand. The docked ligand-receptor complex was visualized and analyzed using Pymol.

2.9. Bioinformatics Study. We used the testicular necrosis bioinformatics tools (https://www.novusbio.com/diseases/testicular-necrosis) to explore the genes, diseases, and pathways that are strongly associated with testicular torsion and necrosis.

2.10. Data Analysis. Data were expressed as the mean ± SD of six determinations. The analysis was performed using the SPSS statistical package for Windows (version 21.0; SPSS Inc, Chicago). Results were subjected to ANOVA followed by DMRT. Statistically significant was considered at $p < 0.05$.

3. Results

3.1. CAT/SOD/CASP3/TNF/GPx Is a Regulatory Signature of Testicular Torsion and Is Associated with Testicular Necrosis. Testicular torsion occurs when there is a mechanical twisting of the spermatic cord. Using the testicular necrosis bioinformatics tools (https://www.novusbio.com/diseases/testicular-necrosis), we found that there is a strong association between testicular necrosis and spermatic cord torsion, testicular diseases, testicular pain, atrophy, hernia, and inguinal. In addition, we found that spermatogenesis is an important pathway related to testicular torsion. Furthermore, we identified catalase, superoxide dismutase, caspase 3, TNF, glutathione peroxidase, and MSTD as the most important regulatory genes involved in spermatic cord torsion (Figure 1).

3.2. Proxeed Plus Exhibits Anti-Inflammatory Activities via Downregulation of TNF-α/IL-6/IL-1β/Cox-2 in Testicular Reperfused Rats. The torsion/detorsion rats displayed elevated levels of testicular TNF-α, interleukin-6 (IL-6), interleukin-1β (IL-1β), and Cox-2 but low level of interleukin-10 (IL-10) as compared with the control rats ($p < 0.05$). The sham group also exhibited a slight increase in the levels of inflammatory markers but lower compared with the T/D groups. Treatments of T/D with 1000 and 5000 mg/kg BW of Proxeed Plus for 4 hr and 7 days produce a significant and dose-dependent decrease to the levels of the inflammatory markers. The 7 days' treatment displays higher modulation of the inflammatory markers than the 4 hr treatments. The level of Cox-2 in T/D rats following 7 days' treatments with 1000 and 5000 mg/kg BW of Proxeed Plus was significantly lower than that of the control groups (Figure 2).

3.3. Proxeed Plus Prevents Reperfusion-Induced Oxidative Stress by Decreasing the Generation of H_2O_2 and MDA in Testicular Reperfused Rats. Evaluation of antioxidant markers following testicular torsion/detorsion indicated that rats in the torsion/detorsion groups had significantly ($p < 0.05$) high levels of H_2O_2 and MDA than the control group and other experimental groups. Treatments of T/D rats with 1000 and 5000 mg/kg BW of Proxeed Plus for 4 hr and 7 days produce significant decreases in the levels of H_2O_2 and MDA relative to the untreated (T/D) group. Rats treated with 5000 mg/kg BW restored the normal levels of H_2O_2 and MDA. Furthermore, the reduction in the levels of total proteins observed in T/D groups was significantly reversed by PP treatments (Figure 3).

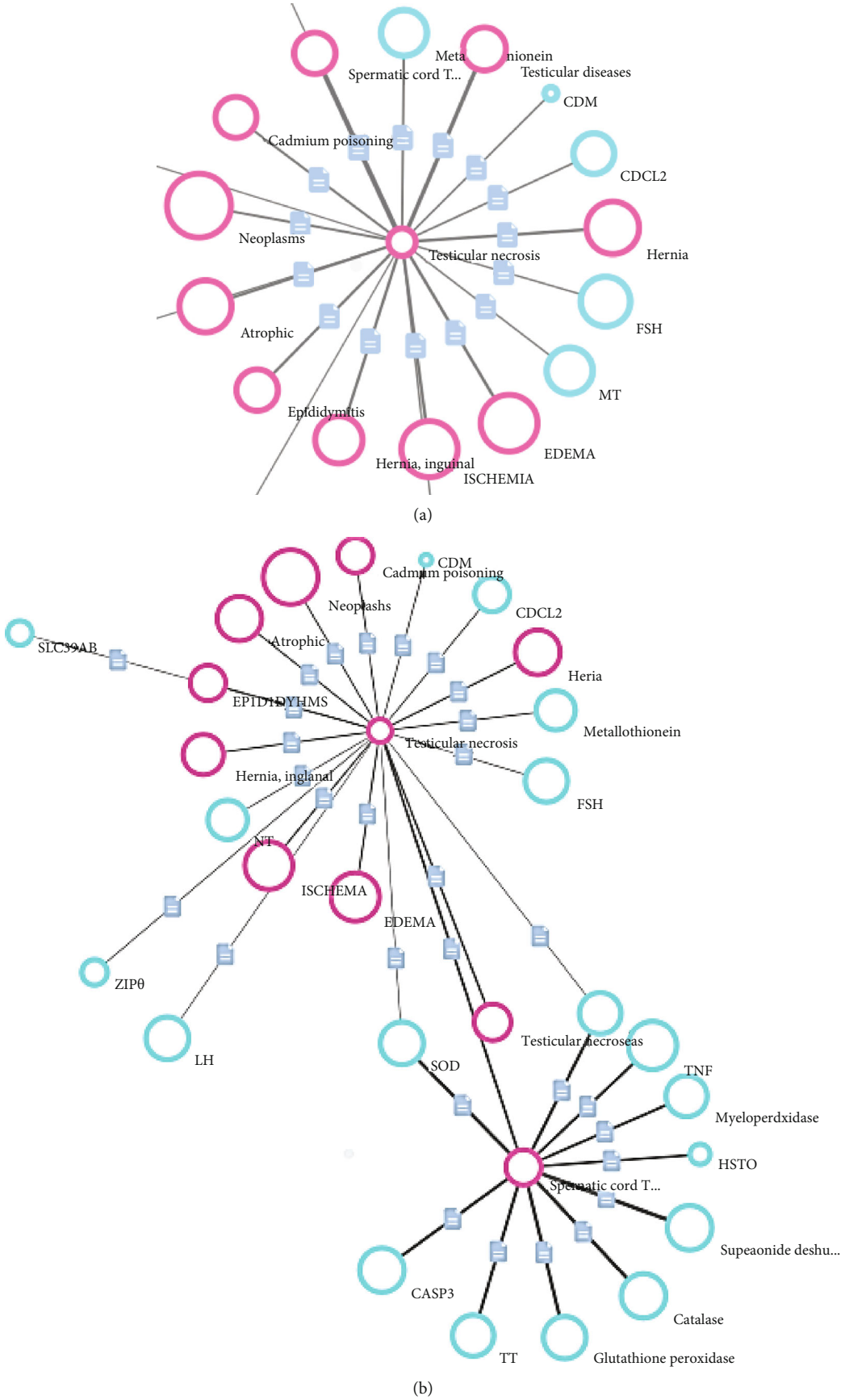

Figure 1: Genes, diseases, and pathways associated with testicular torsion and necrosis.

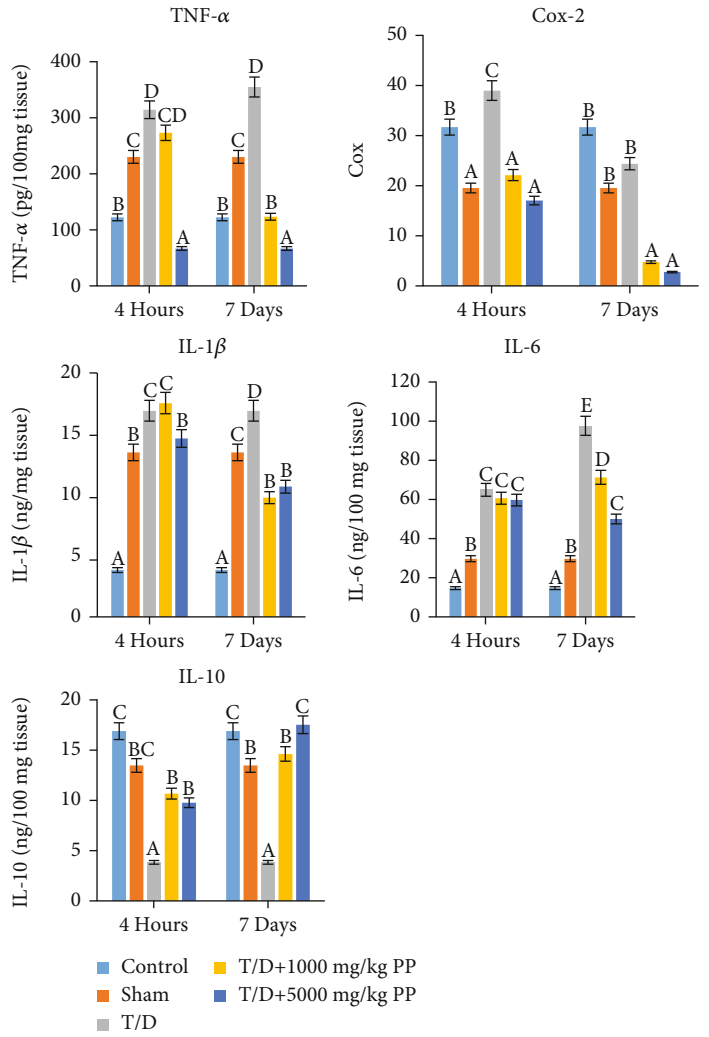

Figure 2: Proxeed Plus elicits anti-inflammatory response in torsion/detorsion rat testis. Tumor necrosis factor-alpha (TNF-α), cyclooxygenase- (Cox-) 2 activity, interleukin-1β (IL-1β), interleukin-6 (IL-6), and interleukin-10 (IL-10) level. Each bar represents the mean ± SD of 6 determinations. Bars with different superscript alphabets are significantly different ($p < 0.05$). The high significant levels of the parameters were in the order of a < b < c. Bars with superscript alphabet "a" are significantly lower than bars with superscript alphabet "b" while bars with superscript "b" are lower than bars with superscript alphabet "c" at $p < 0.05$.

3.4. Proxeed Plus Enhances the Antioxidant Status of Testicular Reperfused Rat via Induction of CAT/GST/SOD/GPx Activities. The antioxidant enzymes evaluated after 4 hr and 7 days of torsion/detorsion indicated that rats in the torsion/detorsion groups had significantly ($p < 0.05$) low levels of antioxidant enzymes, catalase (CAT), glutathione reductase (RG), glutathione S-transferase (GST), superoxide dismutase (SOD), and glutathione peroxidase (GPx) than the control group and other experimental groups. Treatments of T/D rats with 1000 and 5000 mg/kg BW of Proxeed Plus for 4 hr and 7 days produce significant and dose-dependent increases in the levels of the antioxidant's enzymes. Furthermore, Proxeed Plus treatments increase the levels of catalase, superoxide dismutase, glutathione reductase, and glutathione S-transferase than the levels in the control rats (Figure 4).

3.5. Proxeed Plus Ameliorates Reperfusion-Induced Histological Impairments in Rats. Histological examinations of the testes revealed normal testicular architecture with normal germ layer and maturation stages of control rats. Similarly, the sham group shows a normal histological picture of the testes. The torsion/detorsion group shows very poor architecture with several degenerated seminiferous tubules and degenerated germinal epithelial cells. Also, testis of rats treated with PP (1000 mg/kg) at 4 hr had similar histoarchitecture with the T/D rats while that of 5000 mg/kg BW has moderately normal spermatogonia cells and Sertoli cells and few seminiferous tubules. However, 7 days' treatment (1000 mg/kg) exhibited poor architecture, in which seminiferous tubules show tubular vacuolation and cessation of spermatogenesis while testes of rats under 7 days' treatments (5000 mg/kg) have moderately normal testicular architecture with normal Sertoli cells and several seminiferous tubules (Figures 5–8).

3.6. Proxeed Plus Enhances the Spermatogenesis Ability of the Testicular Reperfused Rats. Testicular ischemia-reperfusion

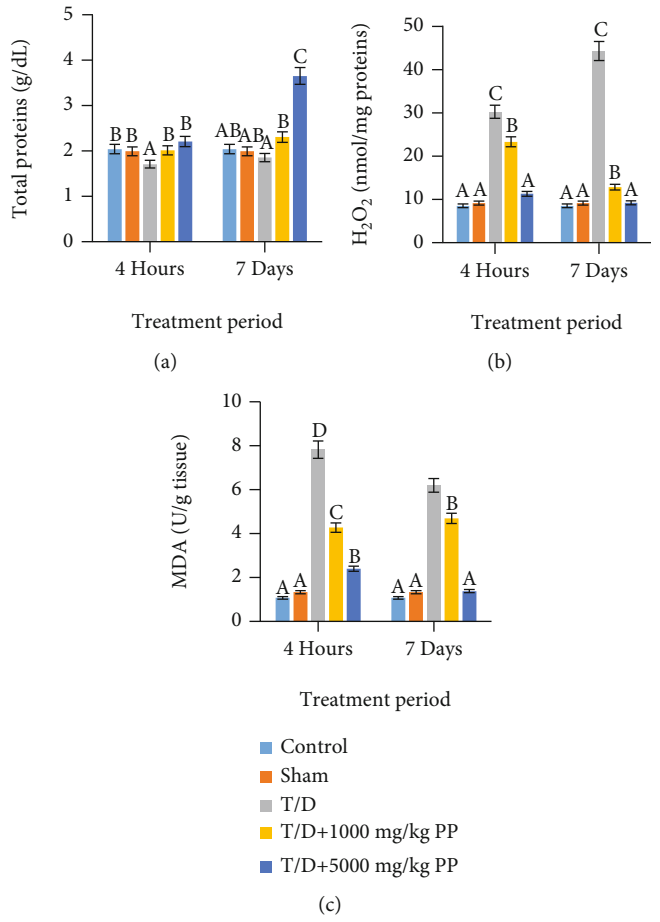

Figure 3: Proxeed Plus prevents torsion/detorsion-induced free radical generation and lipid peroxidation in rat testis: (a) total proteins; (b) hydrogen peroxide (H_2O_2); (c) malonaldehyde (MDA). Each bar represents the mean ± SD of 6 determinations. Bars with different superscript alphabets are significantly different ($p < 0.05$). The high significant levels of the parameters were in the order of a < b < c. Bars with superscript alphabet "a" are significantly lower than bars with superscript alphabet "b" while bars with superscript "b" are lower than bars with superscript alphabet "c" at $p < 0.05$.

of male rats induces spermatogenic impairments in rats as evidenced by significant ($p < 0.05$) decreases in all sperm velocity parameters (ALH, beat cross frequency, linearity, and straightness), sperm kinematics (straight-line velocity, curvilinear velocity, and average path velocity), and sperm motility (total motility, progressive motility, mean move angle degree, and wobble), while the sperm nonprogressive motility and immobility increase in the T/D group (Table 1). Interestingly, treatments with Proxeed Plus (1000 and 5000 mg/kg BW) exhibited significant ($p < 0.05$) and dose-dependent increases in parametric measures of sperm velocity, kinematics, and progressive motilities while decreasing sperm nonprogressive motility and immobility (Table 1).

3.7. Molecular Docking Analysis Revealed That L-Carnitine Component of Proxeed Plus Formed Stable Interaction with the Binding Cavity of IL-6/IL-1β/Cox-2. Docking simulation of L-carnitine with IL-1β, IL-6, and Cox-2 revealed binding affinities of -5.5. -5.9, and -6.8 kcal/mol. The L-carnitine backbone interacts with IL-1β by H-bonding with GLU64 residue of the binding pocket while it interacts with the binding pocket of IL-6 and Cox-2 by hydrogen bonding with ARG 104 and ASN 144 residue, respectively. The binding distance between the ligand and IL-1β, IL-6, and Cox-2 was 4.9, 2.2, and 3.1 Ă, respectively (Figure 9 and Table 2).

4. Discussion

Our study pioneered the report of testicular-protective effects of Proxeed Plus against T/D-induced testis impairments. Ischemia-reperfusion provokes an inflammatory immune response and promotes tissue oxidative stress-induced damages [60]. Overproduction of inflammatory mediators, such as prostaglandin E2 (PGE2) through the activations of cyclooxygenase-2 (Cox-2), and proinflammatory cytokines, including IL-1β, TNF-α, and IL-6, has been implicated in diseases associated with inflammatory response [21, 22]. Furthermore, elevated levels of cytokine in serum and liver, lung, kidney, gut, brain, and heart have been documented during organ T/D [33–37]. Consistently, the present study showed elevated levels of testicular TNF-α, interleukin-6 (IL-6), interleukin-1β (IL-1β), and Cox-2 but decreased interleukin-10 (IL-10) in rats that underwent T/D. The elevation of such proinflammatory mediators in T/D rats may be a

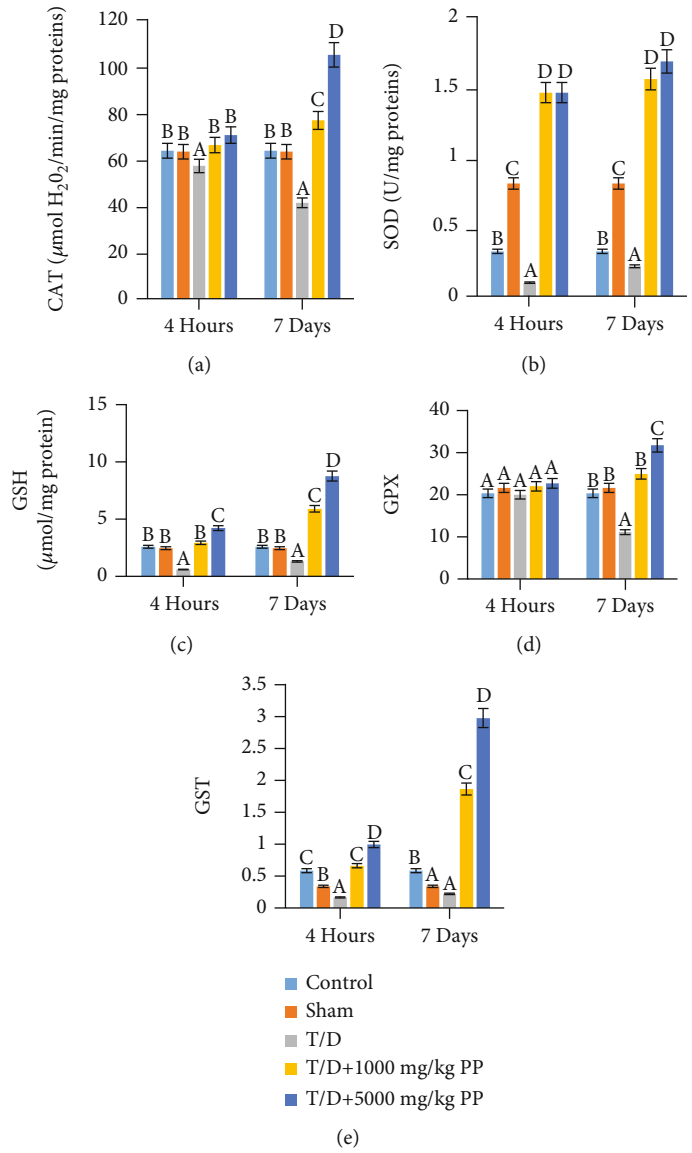

Figure 4: Proxeed Plus enhances antioxidant system and prevents torsion/detorsion-induced oxidative impairment in rat testis: (a) catalase (CAT); (b) superoxide dismutase (SOD); (c) glutathione reductase (GSH); (d) glutathione peroxidase (GPx); (e) glutathione S-transferase (GST). Each bar represents the mean ± SD of 6 determinations. Bars with different superscript alphabets are significantly different ($p < 0.05$). The high significant levels of the parameters were in the order of a < b < c. Bars with superscript alphabet "a" are significantly lower than bars with superscript alphabet "b" while bars with superscript "b" are lower than bars with superscript alphabet "c" at $p < 0.05$.

mechanism by which ischemia-reperfusion accelerates testicular distortion and sterility in man.

Fortunately, treatment of T/D rats with PP exhibited remarkable anti-inflammatory effects by significantly reducing the testicular concentrations of the inflammatory mediators (Cox enzyme) and proinflammatory markers TNF-α, interleukin-6 (IL-6), and interleukin-1β (IL-1β) and increasing the levels of interleukin-10 (IL-10). IL-10 is a T helper 2 type cytokine that inhibits the generations of the proinflammatory cytokines, including IL-1, IL-6, and TNF-α [61]. It exhibited its inhibitory effects by upregulating the generation of soluble TNF-α and IL-1 receptor antagonist [62] thus reducing the levels of proinflammatory cytokines and subsequently attenuating inflammation-induced free radical generations and oxidative stress [62]. Thus, treatments with PP could be considered a good curative approach to salvage the testis from impairment against T/D-induced inflammatory response. Consistent with the results obtained in the present study, previous studies also reported that treatments of rats with vitamin supplements exhibited an anti-inflammatory effect via inhibition of PGE2 production and Cox enzyme [63, 64].

Oxidative stress and an imbalance between the generation of prooxidant and antioxidant systems have been associated with several organ abnormalities [65–67] and implicated in ischemia-reperfusion-induced testicular impairments [44]. The increased ROS generation leads to oxidative stress and activates apoptosis and increased DNA damage. Therefore,

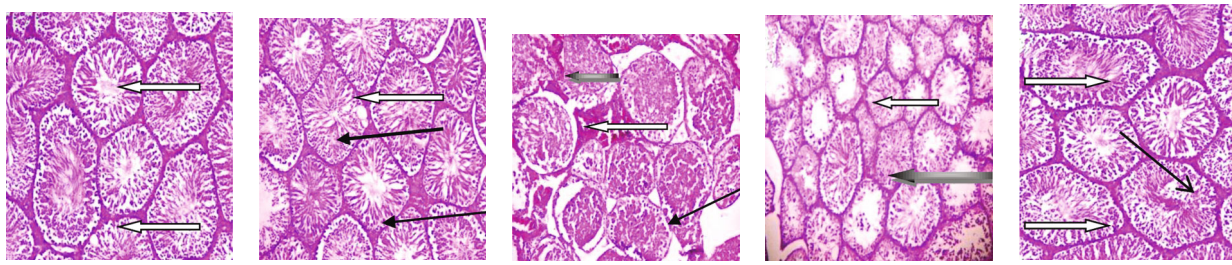

Figure 5: Photomicrographs of testis sections stained with hematoxylin and eosin after administration of Proxeed Plus to rats for 4 hours: (a) control group showing normal testicular architecture, the lumen appears normal with presence of spermatozoa (white arrow); (b) sham group showing normal testicular architecture, the lumen appears normal with presence of spermatozoa (white arrow), the interstitial spaces show normal Leydig cells (slender arrow) and mild vascular congestion (black arrow); (c) T/D group showing very poor architecture, severe degeneration of seminiferous tubules (slender arrow), these tubules are fibrotic and show thickened propria (white arrow), they exhibit degenerated germinal epithelial cells and necrosis (black arrow); (d) posttreatment with 1000 mg/kg Proxeed Plus after TD showing interstitial spaces with normal Leydig cells (black arrow), presence of spermatozoa in the lumen (white arrow); (e) posttreatment with 5000 mg/kg Proxeed Plus after TD showing several normal testicular architecture, interstitial spaces with normal Leydig cells (slender arrow), the lumen appears normal with presence of spermatozoa (white arrow). Magnification ×100.

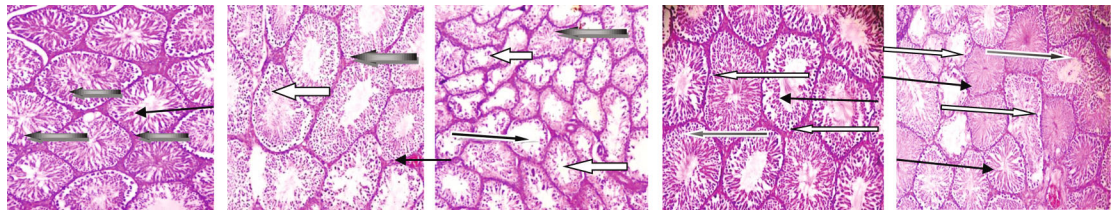

Figure 6: Photomicrographs of testis sections stained with hematoxylin and eosin after administration of Proxeed Plus to rats after 7 days: (a) control group showing normal testicular architecture, the lumen appears normal with presence of spermatozoa (slender arrow), normal seminiferous tubules with normal germ cell layer (black arrow). (b) Sham group showing moderately normal testicular architecture, the lumen appears normal with presence of spermatozoa (white arrow), germ cell layer with marked maturation arrest (slender arrow). The interstitial spaces show normal Leydig cells (black arrow); (c) T/D group showing very poor architecture, degenerated and sloughed germinal epithelial cells and obvious maturation arrest (black arrow), and severe vascular congestion (white arrow), generalized and severe degeneration of seminiferous tubules (slender black arrow); (d) posttreatment with 1000 mg/kg Proxeed Plus after TD showing normal Leydig cells (slender arrow), lumen with presence of spermatozoa (white arrow); (e) 5000 mg/kg Proxeed Plus after TD showing normal testicular architecture, the lumen appears normal with presence of spermatozoa (white arrow), normal seminiferous tubules with normal germ cell layer and maturation stages (slender arrow). Magnification ×100.

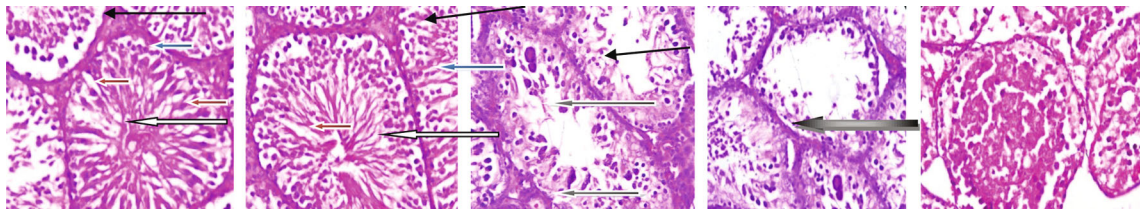

Figure 7: Photomicrographs of testis sections stained with hematoxylin and eosin after administration of Proxeed Plus to rats after 4 hours: (a) control group showing normal testicular architecture with seminiferous tubules having normal germ cell layer (slender arrow) and normal maturation stages, there are normal spermatogonia cell (blue arrow) and normal Sertoli cells (red arrow), the lumen appears normal with presence of spermatozoa (white arrow). The interstitial spaces show normal Leydig cells (slender arrow). (b) Sham group showing normal testicular architecture, with normal germ cell layer (slender arrow) and normal maturation stages, there are normal spermatogonia cell (blue arrow) and normal Sertoli cells (red arrow), the lumen appears normal with presence of spermatozoa (white arrow). The interstitial spaces show normal Leydig cells (slender arrow). (c) T/D group very poor architecture, degenerated and sloughed germinal epithelial cells (black arrow), severe degeneration of seminiferous tubules with fibrotic and thickened propria and necrosis (black arrow). (d) 1000 mg/kg Proxeed Plus after TD. The interstitial spaces show normal Leydig cells (slender arrow) normal lumen with presence of spermatozoa (white arrow). (e) 5000 mg/kg Proxeed Plus after TD showing several normal testicular architecture, seminiferous tubules with germ cells and lumen maturation stages (black arrow). Magnification ×400.

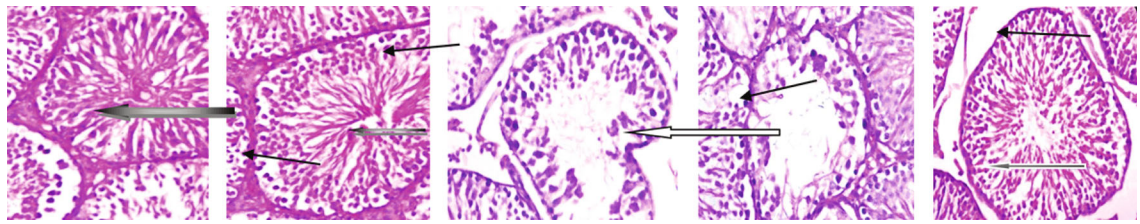

Figure 8: Photomicrographs of testis sections stained by hematoxylin and eosin after administration of Proxeed Plus to rats after 7 days: (a) control group showing normal testicular architecture. Normal germ cell layer (spanned) and normal maturation stages, there are normal spermatogonia cells (blue arrow) and normal Sertoli cells (red arrow), the lumen appears normal with presence of spermatozoa (white arrow). The interstitial spaces show normal Leydig cells (slender arrow). (b) Sham group showing normal testicular architecture. Normal maturation stages, normal spermatogonia cell (blue arrow) and normal Leydig and Sertoli cells (red arrow), the lumen appears normal with presence of spermatozoa (white arrow). The interstitial spaces show normal Leydig cells (slender arrow). (c) T/D group showing very poor architecture, generalized and severe degeneration of seminiferous tubules, fibrotic tubules and thickened propria, and sloughed germinal epithelial cells (slender arrow). (d) 1000 mg/kg Proxeed Plus after TD showing moderately normal testicular architecture, few seminiferous tubules with marked maturation arrest (black arrow). The interstitial spaces show normal Leydig cells (slender arrow). (e) 5000 mg/kg Proxeed Plus after TD showing normal testicular architecture, the lumen appears normal with presence of spermatozoa (white arrow). Normal Leydig and Sertoli cells (slender arrow) several normal seminiferous tubules with germ cells (slender arrow). Magnification ×400.

Table 1: Effect of Proxeed Plus on sperm parameters of the reperfusion-induced testicular impaired rats.

Parameters	Control	Sham	T/D	T/D+PP 1000 mg/kg	T/D+PP 5000 mg/kg
			Four (4) hours of treatments		
VAP	17.92 ± 1.20^{bc}	14.77 ± 0.12^{b}	4.36 ± 0.62^{a}	12.00 ± 0.80^{b}	23.88 ± 2.53^{c}
VCL	19.98 ± 0.67^{c}	12.34 ± 0.72^{b}	5.08 ± 0.43^{a}	22.36 ± 2.31^{c}	29.80 ± 1.70^{d}
VSL	18.95 ± 1.28^{b}	16.78 ± 0.03^{b}	2.74 ± 0.18^{a}	15.01 ± 0.66^{b}	27.51 ± 1.64^{c}
Motility	75.49 ± 5.31^{bc}	63.99 ± 2.87^{b}	39.58 ± 4.50^{a}	82.86 ± 2.31^{c}	90.54 ± 1.15^{d}
IM	25.82 ± 1.36^{b}	22.33 ± 1.69^{b}	73.11 ± 4.84^{c}	17.26 ± 0.62^{b}	13.76 ± 0.41^{a}
STR	68.30 ± 0.35^{cd}	52.07 ± 33.71^{b}	40.39 ± 7.51^{a}	62.74 ± 1.55^{c}	71.39 ± 0.61^{d}
LIN	62.20 ± 0.16^{b}	61.59 ± 0.75^{b}	29.28 ± 4.53^{a}	75.75 ± 2.27^{c}	76.03 ± 4.22^{c}
PR	49.57 ± 6.09^{c}	31.98 ± 1.25^{b}	18.10 ± 1.09^{a}	43.92 ± 2.65^{c}	50.95 ± 0.89^{c}
NP	12.63 ± 0.45^{a}	43.05 ± 3.33^{c}	38.17 ± 0.80^{c}	25.61 ± 2.09^{b}	13.92 ± 1.20^{a}
WOB	71.21 ± 0.82^{b}	84.46 ± 3.45^{bc}	83.18 ± 0.85^{bc}	61.54 ± 2.07^{a}	93.33 ± 1.88^{c}
MAD	2.07 ± 0.08^{b}	1.41 ± 0.20^{b}	0.66 ± 0.16^{a}	3.53 ± 0.27^{c}	5.89 ± 0.23^{d}
ALH	0.21 ± 0.06^{a}	0.29 ± 0.02^{b}	0.17 ± 0.01^{a}	0.32 ± 0.02^{b}	0.71 ± 0.02^{c}
BCF	0.54 ± 0.09^{a}	1.25 ± 0.14^{b}	0.44 ± 0.22^{a}	2.62 ± 0.02^{c}	3.13 ± 0.12^{d}
			Seven (7) days of treatments		
VAP (μm/s)	18.51 ± 1.07^{b}	16.62 ± 3.07^{b}	3.52 ± 0.28^{a}	19.39 ± 0.28^{b}	26.54 ± 4.41^{c}
VCL (μm/s)	27.03 ± 3.90^{c}	26.66 ± 1.24^{c}	2.61 ± 0.56^{a}	16.22 ± 1.94^{b}	29.01 ± 0.41^{c}
VSL (μm/s)	24.04 ± 0.53^{c}	22.17 ± 2.10^{c}	1.16 ± 0.09^{a}	11.33 ± 1.88^{b}	33.09 ± 4.49^{d}
Motility	85.49 ± 1.81^{b}	78.58 ± 0.52^{b}	22.52 ± 1.12^{a}	87.99 ± 3.30^{b}	97.06 ± 2.10^{c}
IM	20.95 ± 1.72^{a}	23.66 ± 0.47^{a}	71.21 ± 3.39^{b}	20.29 ± 4.74^{a}	18.58 ± 0.44^{a}
STR	82.57 ± 5.21^{c}	74.37 ± 2.58^{c}	21.57 ± 1.27^{a}	59.35 ± 4.08^{b}	92.76 ± 4.02^{d}
LIN	81.32 ± 6.17^{b}	77.81 ± 3.99^{b}	22.55 ± 1.60^{a}	73.61 ± 2.66^{b}	83.48 ± 3.44^{b}
PR	62.51 ± 2.62^{c}	56.38 ± 8.62^{bc}	10.38 ± 0.39^{a}	48.84 ± 10.61^{b}	58.27 ± 10.66^{bc}
NP	31.74 ± 4.42^{c}	46.55 ± 2.35^{d}	43.98 ± 9.03^{d}	23.94 ± 3.73^{b}	9.74 ± 0.36^{a}
WOB	80.66 ± 9.84^{b}	64.06 ± 3.27^{a}	62.62 ± 4.07^{a}	58.06 ± 1.23^{a}	48.58 ± 5.40^{a}
MAD	5.80 ± 0.52^{b}	5.72 ± 0.50^{b}	0.25 ± 0.04^{a}	4.28 ± 0.86^{b}	10.29 ± 0.04^{c}
ALH (μm)	1.57 ± 0.35^{b}	2.39 ± 0.05^{c}	0.14 ± 0.03^{a}	1.19 ± 0.20^{b}	3.08 ± 1.58^{d}
BCF (Hz)	4.09 ± 0.94^{c}	2.27 ± 0.49^{b}	0.25 ± 0.13^{a}	2.98 ± 0.94^{b}	5.61 ± 0.13^{d}

VAP: average path velocity; VCL: curvilinear velocity; VSL: straight-line velocity; ALH: amplitude of lateral head; BCF: beat cross frequency; LIN: linearity; STR: straightness; WOB: wobble; MAD: mean move angle degree. Data are the mean ± SD of triplicate determination. Values followed by different superscript alphabets are significantly different.

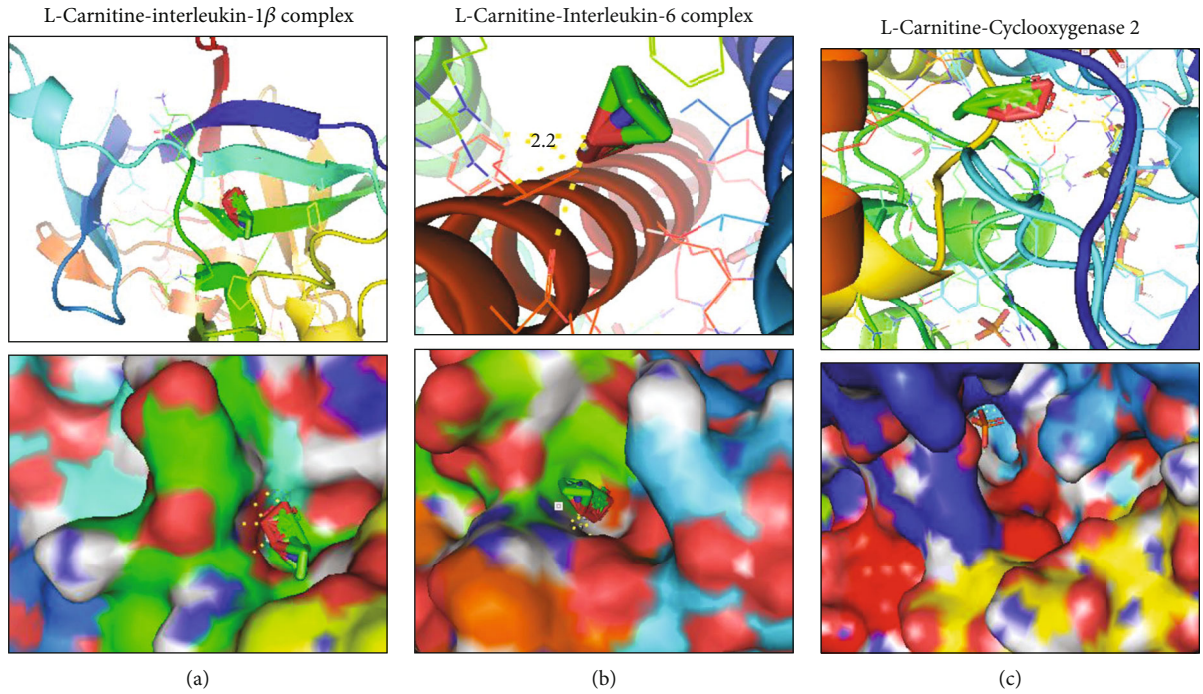

Figure 9: Receptor-ligand interaction of inflammatory markers with the Proxeed Plus backbone (L-carnitine): (a) L-carnitine-interleukin-1β complex; (b) L-carnitine-interleukin-6 complex; (c) L-carnitine-cyclooxygenase 2 complex. The upper panel shows the interacting amino acid residues and the binding distances, while the lower panels show the ligand interaction in the binding pocket of the receptors.

Table 2: Docking profile of inflammatory and antioxidant markers with the Proxeed Plus scaffold (L-carnitine).

Protein targets	Binding affinity (kcal/mol)	Binding distance (Ă)	Interacting atom (protein-ligand)	Interacting amino acid
Interleukin-1β	-5.5	4.9	H-O	GLU 64
Interleukin-6	-5.9	2.2	H-O	ARG 104
Cyclooxygenase 2	-6.8	3.1	H-N	ASN 144

in this study, H_2O_2 and MDA were assessed as indicators of oxidative damage of cellular macromolecules. Consistent with our expectation, T/D considerably raised the testicular levels of H_2O_2 and MDA but depleted protein levels.

The observed decrease in the total protein in T/D could be attributed to the decreased levels of the antioxidant enzymes which are known to constitute the total protein pool. Such a decrease in total protein could be detrimental to cellular homeostasis [68]. This will negatively affect the metabolic activities within the testis and consequently the health of the organ. MDA is a product of lipid peroxidation and a marker of oxidative stress that impairs physiological mechanisms in the human body because of its ability to react with macromolecules such as proteins and DNA [69]. Herein, the testicular-protective potential of PP could be highly linked to its strong antioxidant characteristics as revealed by decreased levels of H_2O_2 and MDA in the treated rats. Similarly, PP induced significant enrichment of the antioxidant capability of the testis as evidenced by dose-dependent elevation of the testicular levels of free radical scavengers including the catalase (CAT), glutathione reductase (GSH), glutathione S-transferase (GST), superoxide dismutase (SOD), and glutathione peroxidase (GPx) relative to the T/D groups thus protecting against ischemia-reperfusion-induced oxidative stress during I/R of rats' testes.

It is well established that PP has a great pool of nutrients with high antioxidant activities like zinc, L-carnitine, acetyl-L-carnitine, fumarate, CoQ10, folic acid, fructose, vitamin C, and vitamin B12 [35]. Accordingly, the antioxidant activities of PP could be attributed to the synergetic effect of its highly rich antioxidant components; zinc is well known to increase the levels of glutathione and antioxidant enzyme activities [38]. Vitamin E scavenges lipid peroxide radicals and limits the peroxidation of polyunsaturated fatty acids in the spermatozoa membrane [24]. L-carnitine and L-acetyl carnitine control the flow of the acetyl group via the cell membrane thus reducing the levels of toxic intracellular acetyl-CoA to protect spermatozoa from oxidative stress and support sperm maturation and male reproductive health [37].

Our results are consistent with previous studies which reported that L-carnitine has antioxidant activities and enhances the reproductive health and functions. In fact, clinical studies have indicated that oral administration of L-carnitine improves sperm quality of patients with idiopathic asthenozoospermia [30] and has also been used for the

treatment of idiopathic and varicocele-associated oligoasthenospermia [31]. In addition, Lenzi et al. [32] successfully used L-carnitine in idiopathic infertile males while another study demonstrated that a combination of L-carnitine+acetyl-L-carnitine increased sperm count in patients with echographic features of genital inflammation [33].

Consistent with the testicular biochemical parameters, histopathological examination of testis of T/D rats presents evidence of testis abnormalities as indicated by a very poor architecture of the testis with several degenerated seminiferous tubules and degenerated germinal epithelial cells. These findings were in accordance with the study of Jahromi et al. [69] which reported that after torsion and 4 h detorsion, degenerated germinal epithelial cells were present in the lumen of the seminiferous tubule in the T/D group. Treatment with the PP, particularly for 7 days, significantly reduced the aforementioned histotesticular abnormalities in a dose-dependent manner, suggesting the testicular-protective effect of the used supplement against ischemic/reperfusion injury.

Previous clinical studies have indicated that treatment with Proxeed Plus significantly increases the progressive sperm motility and total sperm count of oligoasthenoteratozoospermia men compared to the placebo [39]. Another clinical trial with 175 idiopathic oligoasthenozoospermia men who could not impregnate their partners revealed that Proxeed Plus significantly improved the sperm volume and progressive motility compared to baseline [40]. In line with these studies, our study showed that treatment with Proxeed Plus has a protective effect on T/D-induced testicular damage. This is attributed to its ability to modulate anti-inflammatory response and improve the antioxidant system, thus decreasing the levels of free radicals within the testis and prevent oxidative stress-induced damages. This study therefore calls for further preclinical and clinical studies in patients with testicular or reproductive deficiencies.

5. Conclusion

Our results indicated that both short-term and long-term testicular T/D induce an inflammatory response, oxidative stress, and histoarchitectural alteration. Interestingly, conclusively, our study showed that treatment with Proxeed Plus has both short-term and long-term protective effects on T/D-induced testicular damage. This is attributed to its ability to modulate anti-inflammatory response and improve the antioxidant system, thus decreasing the levels of free radicals within the testis and preventing oxidative stress-induced damages.

Data Availability

The datasets generated and/or analyzed in this study are available on reasonable request.

Conflicts of Interest

The authors declare that they have no competing interests.

Acknowledgments

All authors acknowledged the laboratory where the work was done. This work was supported by the Taif University Researchers Supporting Program (project number: TURSP-2020/269), Taif University, Saudi Arabia.

References

[1] G. Vaos and N. Zavras, "Antioxidants in experimental ischemia-reperfusion injury of the testis: where are we heading towards?," *World journal of methodology*, vol. 7, no. 2, pp. 37–45, 2017.

[2] Y. Kumtepe, F. Odabasoglu, M. Karaca et al., "Protective effects of telmisartan on ischemia/reperfusion injury of rat ovary: biochemical and histopathologic evaluation," *Fertility and Sterility*, vol. 93, no. 4, pp. 1299–1307, 2010.

[3] N. Luhtala, A. Aslanian, J. R. Yates 3rd, and T. Hunter, "Secreted Glioblastoma Nanovesicles Contain Intracellular Signaling Proteins and Active Ras Incorporated in a Farnesylation-dependent Manner," *The Journal of Biological Chemistry*, vol. 292, no. 2, pp. 611–628, 2017.

[4] A. Ünsal, E. Devrim, C. Guven et al., "Propofol attenuates reperfusion injury after testicular torsion and detorsion," *World Journal of Urology*, vol. 22, no. 6, pp. 461–465, 2004.

[5] E. N. Ringdahl and L. Teague, "Testicular torsion," *American Family Physician*, vol. 74, no. 10, pp. 1739–1743, 2006.

[6] D. S. Sheriff, F. A. Elshaari, R. I. Elfagih, and I. Barassi, "Oxidative and antioxidative defense system in testicular torsion/detorsion," *Indian Journal of Urology*, vol. 27, no. 4, article 91436, pp. 479–484, 2011.

[7] H. Akbas, M. Ozden, M. Kanko et al., "Protective antioxidant effects of carvedilol in a rat model of ischaemia-reperfusion injury," *Journal of International Medical Research*, vol. 33, no. 5, pp. 528–536, 2005.

[8] D. W. Filho, M. A. Torres, A. L. Bordin, T. B. Crezcynski-Pasa, and A. Boveris, "Spermatic cord torsion, reactive oxygen and nitrogen species and ischemia- reperfusion injury," *Molecular Aspects of Medicine*, vol. 25, no. 1-2, pp. 199–210, 2004.

[9] D. N. Granger and P. R. Kvietys, "Reperfusion injury and reactive oxygen species: the evolution of a concept," *Redox Biology*, vol. 6, pp. 524–551, 2015.

[10] M. Shokoohi, A. Khaki, H. Shoorei, A. Khaki, M. Moghimian, and S. H. Abtahi-Eivary, "Hesperidin attenuated apoptotic-related genes in testicle of a male rat model of varicocoele," *Andrology*, vol. 8, no. 1, pp. 249–258, 2020.

[11] M. Moghimian, S.-H. Abtahi-Evari, M. Shokoohi, M. Amiri, and M. Soltani, "Effect of Syzygium aromaticum (clove) extract on seminiferous tubules and oxidative stress after testicular torsion in adult rats," *Physiology and Pharmacology*, vol. 21, pp. 343–350, 2018.

[12] S. Arena, R. Iacona, P. Antonuccio et al., "Medical perspective in testicular ischemia-reperfusion injury," *Experimental and Therapeutic Medicine*, vol. 13, no. 5, pp. 2115–2122, 2017.

[13] M. Al-Maghrebi and W. M. Renno, "The tACE/Angiotensin (1-7)/Mas Axis Protects Against Testicular Ischemia Reperfusion Injury," *Urology*, vol. 94, pp. 312.e1–312.e8, 2016.

[14] J. MacMicking, Q. W. Xie, and C. Nathan, "Nitric oxide and macrophage function," *Annual Review of Immunology*, vol. 15, no. 1, pp. 323–350, 1997.

[15] C. Welbourn, G. Goldman, I. Paterson, C. Valeri, D. Shepro, and H. Hechtman, "Pathophysiology of ischaemia reperfusion injury: central role of the neutrophil," *British Journal of Surgery*, vol. 78, no. 6, pp. 651–655, 1991.

[16] G. Kadirvel, S. Kumar, and A. Kumaresan, "Lipid peroxidation, mitochondrial membrane potential and DNA integrity of spermatozoa in relation to intracellular reactive oxygen species in liquid and frozen-thawed buffalo semen," *Animal Reproduction Science*, vol. 114, no. 1-3, pp. 125–134, 2009.

[17] S. I. Peris, J. F. Bilodeau, M. Dufour, and J. L. Bailey, "Impact of cryopreservation and reactive oxygen species on DNA integrity, lipid peroxidation, and functional parameters in ram sperm," *Molecular Reproduction and Development*, vol. 74, no. 7, pp. 878–892, 2007.

[18] E. O. Kehinde, O. A. Mojiminiyi, A. H. Mahmoud, K. H. A. L. E. E. L. A. Al-Awadi, A. D. E. L. al-Hunayan, and A. E. Omu, "The significance of measuring the time course of serum malondialdehyde concentration in patients with torsion of the testis," *Journal of Urology*, vol. 169, no. 6, pp. 2177–2180, 2003.

[19] N. Hosseini Ahar, A. Khaki, G. Akbari, and M. Ghafarinovin, "The effect of busulfan on body weight, testis weight and MDA enzymes in male rats," *International Journal of Women's Health and Reproduction Sciences*, vol. 2, no. 5, pp. 316–319, 2014.

[20] E. Yuluğ, S. Türedi, E. Karagüzel, Ö. Kutlu, A. Menteşe, and A. Alver, "The short term effects of resveratrol on ischemia-reperfusion injury in rat testis," *Journal of Pediatric Surgery*, vol. 49, no. 3, pp. 484–489, 2014.

[21] R. Korhonen, A. Lahti, H. Kankaanranta, and E. Moilanen, "Nitric oxide production and signaling in inflammation," *Current Drug Target-Inflammation & Allergy*, vol. 4, no. 4, pp. 471–479, 2005.

[22] Y. M. Ha, S. W. Chung, J. M. Kim et al., "Molecular activation of NF-κB, pro-inflammatory mediators, and signal pathways in γ-irradiated mice," *Biotechnology Letters*, vol. 32, no. 3, pp. 373–378, 2010.

[23] D. Sanocka and M. Kurpisz, "Reactive oxygen species and sperm cells," *Reproductive Biology and Endocrinology*, vol. 2, no. 1, pp. 12–17, 2004.

[24] J. H. Jung and J. T. Seo, "Empirical medical therapy in idiopathic male infertility: promise or panacea?," *Clinical and Experimental Reproductive Medicine*, vol. 41, no. 3, pp. 108–114, 2014.

[25] J. Bremer, "Carnitine–metabolism and functions," *Physiological Reviews*, vol. 63, no. 4, pp. 1420–1480, 1983.

[26] C. Jeulin, J. L. Dacheux, and J. C. Soufir, "Uptake and release of free L-carnitine by boar epididymal spermatozoa in vitro and subsequent acetylation rate," *Reproduction*, vol. 100, no. 1, pp. 263–271, 1994.

[27] A. Enomoto, M. F. Wempe, H. Tsuchida et al., "Molecular identification of a novel carnitine transporter specific to human testis. Insights into the mechanism of carnitine recognition," *Journal of Biological Chemistry*, vol. 277, no. 39, pp. 36262–36271, 2002.

[28] L. Johansen and T. Bøhmer, "Carnitine-binding related supressed oxygen uptake by spermatozoa," *Archives of Andrology*, vol. 1, no. 4, pp. 321–324, 1978.

[29] C. Jeulin and L. M. Lewin, "Role of free L-carnitine and acetyl-L-carnitine in post-gonadal maturation of mammalian spermatozoa," *Human Reproduction Update*, vol. 2, no. 2, pp. 87–102, 1996.

[30] M. Costa, D. Canale, M. Filicori, S. D'lddio, A. Lenzi, and Italian study group on carnitine and male infertility, "L- carnitine in idiopathic asthenozoospermia: a multicenter study," *Andrologia*, vol. 26, no. 3, pp. 155–159, 1994.

[31] G. Cavallini, A. P. Ferraretti, L. Gianaroli, G. Biagiotti, and G. Vitali, "Cinnoxicam and L-carnitine/acetyl-L-carnitine treatment for idiopathic and varicocele-associated oligoasthenospermia," *Journal of Andrology*, vol. 25, no. 5, pp. 761–770, 2004.

[32] A. Lenzi, F. Lombardo, P. Sgrò et al., "Use of carnitine therapy in selected cases of male factor infertility: a double-blind crossover trial," *Fertility and Sterility*, vol. 79, no. 2, pp. 292–300, 2003.

[33] E. Vicari and A. E. Calogero, "Effects of treatment with carnitines in infertile patients with prostato-vesiculo-epididymitis," *Human Reproduction*, vol. 16, no. 11, pp. 2338–2342, 2001.

[34] S. M. Fenkci, V. Fenkci, O. Oztekin, S. Rota, and N. Karagenc, "Serum total L-carnitine levels in non-obese women with polycystic ovary syndrome," *Human Reproduction*, vol. 23, no. 7, pp. 1602–1606, 2008.

[35] S. Micic, N. Lalic, N. Bojanic, D. Djordjevic, A. Virmani, and A. Agarwal, "Oligoastenospermic men treated with Proxeed Plus showed correlation between sperm motility and seminal carnitine," *Fertility and Sterility*, vol. 106, no. 3, pp. e298–e299, 2016.

[36] U. Schagdarsurengin and K. Steger, "Epigenetics in male reproduction: effect of paternal diet on sperm quality and offspring health," *Nature Reviews Urology*, vol. 13, no. 10, pp. 584–595, 2016.

[37] X. Zhou, F. Liu, and S. Zhai, "Effect of L-carnitine and/or L-acetyl-carnitine in nutrition treatment for male infertility: a systematic review," *Asia Pacific Journal of Clinical Nutrition*, vol. 16, Supplement 1, pp. 383–390, 2007.

[38] L. Y. Al-Ayadhi and N. E. Elamin, "Camel milk as a potential therapy as an antioxidant in autism spectrum disorder (ASD)," *Evidence-based Complementary and Alternative Medicine*, vol. 2013, 8 pages, 2013.

[39] G. Busetto, A. Agarwal, A. Virmani et al., "Effect of metabolic and antioxidant supplementation on sperm parameters in oligo-astheno-teratozoospermia, with and without varicocele: a double-blind placebo-controlled study," *Andrologia*, vol. 50, no. 3, article e12927, 2018.

[40] S. Micic, N. Lalic, D. Djordjevic et al., "Double-blind, randomised, placebo-controlled trial on the effect of L-carnitine and L-acetylcarnitine on sperm parameters in men with idiopathic oligoasthenozoospermia," *Andrologia*, vol. 51, no. 6, article e13267, 2019.

[41] M. S. Aydin, R. Kazancioglu, M. Seker et al., "Effects of Proxeed Plus in the prevention and treatment of cisplatin nephrotoxicity: an experimental rat study," in *55th Congress of the European-Renal-Association (ERA) and European-Dialysis-and-Transplantation-Association (EDTA)*, Copenhagen, Danimarka, 2018.

[42] F. Fırat, F. Erdemir, E. Kölükçü, F. Gevrek, İ. Benli, and V. Ünsal, "Oxytocin in The Prevention of injury due to testicular torsion/detorsion in rats," *Ulusal Travma ve Acil Cerrahi Dergisi*, vol. 24, no. 2, pp. 89–96, 2018.

[43] A. Gezici, H. Ozturk, H. Buyukbayram, H. Ozturk, and H. Okur, "Effects of gabexate mesilate on ischemia-reperfusion-induced testicular injury in rats," *Pediatric Surgery International*, vol. 22, no. 5, pp. 435–441, 2006.

[44] J. O. Sangodele, Z. Inuwa, B. Lawal, G. Adebayo-Gege, B. J. Okoli, and F. Mtunzi, "Proxeed plus salvage rat testis from ischemia- reperfused injury by enhancing antioxidant's activities and inhibition of iNOS expression," *Biomedicine & Pharmacotherapy*, vol. 133, article 111086, 2021.

[45] B. Lawal, O. K. Shittu, F. I. Oibiokpa, H. Mohammed, S. I. Umar, and G. M. Haruna, "Antimicrobial evaluation, acute and sub-acute toxicity studies of *Allium sativum*," *Journal of Acute Disease*, vol. 5, no. 4, pp. 296–301, 2016.

[46] R. Varshney and R. Kale, "Effects of calmodulin antagonists on radiation-induced lipid peroxidation in microsomes," *International Journal of Radiation Biology*, vol. 58, no. 5, pp. 733–743, 1990.

[47] A. G. Gornall, C. J. Bardawill, and M. M. David, "Determination of serum proteins by means of the biuret reaction," *Journal of Biological Chemistry*, vol. 177, no. 2, pp. 751–766, 1949.

[48] M. Koroliuk, L. Ivanova, I. Maïorova, and V. Tokarev, "A method of determining catalase activity," *Laboratornoe Delo*, vol. 1, pp. 16–19, 1988.

[49] A. K. Sinha, "Colorimetric assay of catalase," *Analytical Biochemistry*, vol. 47, no. 2, pp. 389–394, 1972.

[50] H. P. Misra and I. Fridovich, "The role of superoxide anion in the autoxidation of epinephrine and a simple assay for superoxide dismutase," *Journal of Biological Chemistry*, vol. 247, no. 10, pp. 3170–3175, 1972.

[51] I. K. Smith, T. L. Vierheller, and C. A. Thorne, "Assay of glutathione reductase in crude tissue homogenates using 5,5′ -dithiobis(2-nitrobenzoic acid)," *Analytical Biochemistry*, vol. 175, no. 2, pp. 408–413, 1988.

[52] M. Hu and C. Dillard, "[41] Measurement of protein thiol groups and glutathione in plasma," *Methods in Enzymology*, vol. 233, no. 3, pp. 380–385, 1994.

[53] R. H. Jaskot, E. G. Charlet, E. C. Grose, M. A. Grady, and J. H. Roycroft, "An automated analysis of glutathione peroxidase, S-transferase, and reductase activity in animal tissue," *Journal of Analytical Toxicology*, vol. 7, no. 2, pp. 86–88, 1983.

[54] W. H. Habig, M. J. Pabst, and W. B. Jakoby, "Glutathione S-transferases: the first enzymatic step in mercapturic acid formation," *Journal of Biological Chemistry*, vol. 249, no. 22, pp. 7130–7139, 1974.

[55] J. O. Olugbodi, O. David, E. N. Oketa, B. Lawal, B. J. Okoli, and F. Mtunzi, "Silver nanoparticles stimulates spermatogenesis impairments and hematological alterations in testis and epididymis of male rats," *Molecules*, vol. 25, no. 5, p. 1063, 2020.

[56] U. Igwebuike and U. U. Eze, "Morphological characteristics of the small intestine of the African pied crow (Corvus albus)," *Animal Research International*, vol. 7, pp. 1116–1120, 2010.

[57] B. Lawal, Y.-L. Liu, N. Mokgautsi et al., "Pharmacoinformatics and preclinical studies of NSC765690 and NSC765599, potential STAT3/CDK2/4/6 inhibitors with antitumor activities against NCI60 human tumor cell lines," *Biomedicines*, vol. 9, no. 1, p. 92, 2021.

[58] J.-C. Lee, A. T. H. Wu, J.-H. Chen et al., "HNC0014, a multitargeted small-molecule, inhibits head and neck squamous cell carcinoma by suppressing c-met/STAT3/CD44/PD-L1 oncoimmune signature and eliciting antitumor immune responses," *Cancers (Basel)*, vol. 12, no. 12, p. 3759, 2020.

[59] B. Lawal, C.-Y. Lee, N. Mokgautsi et al., "mTOR/EGFR/iNOS/MAP2K1/FGFR/TGFB1 are druggable candidates for N-(2,4-difluorophenyl)-2′,4′-difluoro-4-hydroxybiphenyl-3-carboxamide (NSC765598), with consequent anticancer implications," *Frontiers in Oncology*, vol. 11, 2021.

[60] L. Bosca, M. Zeini, P. Traves, and S. Hortelano, "Nitric oxide and cell viability in inflammatory cells: a role for NO in macrophage function and fate," *Toxicology*, vol. 208, no. 2, pp. 249–258, 2005.

[61] M. A. Cassatella, L. Meda, S. Bonora, M. Ceska, and G. Constantin, "Interleukin 10 (IL-10) inhibits the release of proinflammatory cytokines from human polymorphonuclear leukocytes. Evidence for an autocrine role of tumor necrosis factor and IL-1 beta in mediating the production of IL-8 triggered by lipopolysaccharide," *The Journal of Experimental Medicine*, vol. 178, no. 6, pp. 2207–2211, 1993.

[62] H. Ozturk, H. Ozturk, E. H. Terzi, G. Bugdayci, and A. Duran, "Interleukin 10 reduces testicular damage in experimental testicular ischemia/reperfusion injury," *Urology*, vol. 83, no. 2, pp. 508.e1–508.e6, 2014.

[63] A. A. Beharka, D. Wu, M. Serafini, and S. N. Meydani, "Mechanism of vitamin E inhibition of cyclooxygenase activity in macrophages from old mice: role of peroxynitrite," *Free Radical Biology and Medicine*, vol. 32, no. 6, pp. 503–511, 2002.

[64] Q. Jiang, I. Elson-Schwab, C. Courtemanche, and B. N. Ames, "gamma -Tocopherol and its major metabolite, in contrast to alpha -tocopherol, inhibit cyclooxygenase activity in macrophages and epithelial cells," *Proceedings of the National Academy of Sciences*, vol. 97, no. 21, pp. 11494–11499, 2000.

[65] A. Topal, G. Alak, M. Ozkaraca et al., "Neurotoxic responses in brain tissues of rainbow trout exposed to imidacloprid pesticide: assessment of 8-hydroxy-2-deoxyguanosine activity, oxidative stress and acetylcholinesterase activity," *Chemosphere*, vol. 175, pp. 186–191, 2017.

[66] B. Lawal, O. K. Shittu, F. I. Oibiokpa, E. B. Berinyuy, and H. Mohammed, "African natural products with potential antioxidants and hepatoprotectives properties: a review," *Clinical Phytoscience*, vol. 2, no. 1, pp. 1–66, 2017.

[67] J. Ibrahim, A. Y. Kabiru, T. Abdulrasheed-Adeleke, B. Lawal, and A. H. Adewuyi, "Antioxidant and hepatoprotective potentials of curcuminoid isolates from turmeric (Curcuma longa) rhizome on CCl4-induced hepatic damage in Wistar rats," *Journal of Taibah University for Science*, vol. 14, no. 1, pp. 908–915, 2020.

[68] O. K. Shittu, B. Lawal, B. U. Alozieuwa, G. M. Haruna, A. N. Abubakar, and E. B. Berinyuy, "Alteration in biochemical indices following chronic administration of methanolic extract of Nigeria bee propolis in Wistar rats," *Asian Pacific Journal of Tropical Disease*, vol. 5, no. 8, pp. 654–657, 2015.

[69] A. R. Jahromi, R. Rasooli, Y. Kamali, N. Ahmadi, and E. Sattari, "Short-term effects of date palm extract (*Phoenix dactylifera*) on ischemia/reperfusion injury induced by testicular torsion/detorsion in rats," *Pharmacognosy research*, vol. 9, no. 1, pp. 69–73, 2017.

Hindawi
Oxidative Medicine and Cellular Longevity
Volume 2021, Article ID 8377362, 16 pages
https://doi.org/10.1155/2021/8377362

Review Article

Baicalein, Baicalin, and Wogonin: Protective Effects against Ischemia-Induced Neurodegeneration in the Brain and Retina

Li Pan[1,2] **Kin-Sang Cho**[2] **Irvin Yi**[2] **Chi-Ho To**[1,3] **Dong Feng Chen**[2] **and Chi-Wai Do**[1,3]

[1]*School of Optometry, The Hong Kong Polytechnic University, Hong Kong*
[2]*Schepens Eye Research Institute of Massachusetts Eye and Ear, Department of Ophthalmology, Harvard Medical School, Boston, MA, USA*
[3]*Centre for Eye and Vision Research, Hong Kong*

Correspondence should be addressed to Dong Feng Chen; dongfeng_chen@meei.harvard.edu and Chi-Wai Do; chi-wai.do@polyu.edu.hk

Received 30 April 2021; Revised 8 June 2021; Accepted 19 June 2021; Published 30 June 2021

Academic Editor: Juan Gambini

Ischemia is a common pathological condition present in many neurodegenerative diseases, including ischemic stroke, retinal vascular occlusion, diabetic retinopathy, and glaucoma, threatening the sight and lives of millions of people globally. Ischemia can trigger excessive oxidative stress, inflammation, and vascular dysfunction, leading to the disruption of tissue homeostasis and, ultimately, cell death. Current therapies are very limited and have a narrow time window for effective treatment. Thus, there is an urgent need to develop more effective therapeutic options for ischemia-induced neural injuries. With emerging reports on the pharmacological properties of natural flavonoids, these compounds present potent antioxidative, anti-inflammatory, and antiapoptotic agents for the treatment of ischemic insults. Three major active flavonoids, baicalein, baicalin, and wogonin, have been extracted from *Scutellaria baicalensis* Georgi (*S. baicalensis*); all of which are reported to have low cytotoxicity. They have been demonstrated to exert promising pharmacological capabilities in preventing cell and tissue damage. This review focuses on the therapeutic potentials of these flavonoids against ischemia-induced neurotoxicity and damage in the brain and retina. The bioactivity and bioavailability of baicalein, baicalin, and wogonin are also discussed. It is with hope that the therapeutic potential of these flavonoids can be utilized and developed as natural treatments for ischemia-induced injuries of the central nervous system (CNS).

1. Introduction

Ischemia is a common pathological or traumatic condition accompanied by the reduction of blood supply to the major organs, such as the heart, kidney, intestine, brain, and eye [1]. This leads to an insufficient supply of oxygen and nutrients and an accumulation of metabolic wastes, causing organ damage or failure and resulting in death in severe cases [1]. Neurons in the brain are the most sensitive and vulnerable cells to ischemia. Only a short period of ischemia can elicit irreversible damage to brain tissue, leading to paralysis or death [2, 3]. Stroke was defined by the World Health Organization (WHO) in the 1970s as "rapidly developing clinical signs of focal disturbance of cerebral function, lasting more than 24 hours or leading to death with no apparent cause other than that of vascular origin" [4]. Around 87% of stroke cases are ischemic stroke, which is triggered by a lack of blood supply to focal brain areas, leading to subsequent damage and neurodegeneration [5–7]. Stroke is a leading cause of disability and death worldwide [7, 8]. Thrombolytic medication, such as alteplase (t-PA), is the only FDA-approved therapeutic agent for treating acute ischemic stroke within a few hours after its onset [9]. Given the narrow time window of treatment and high risk of complications, such as hemorrhagic transformation, cerebral edema, and other adverse effects [10], the development of novel neuroprotective therapies against ischemia is paramount.

The visual system is comprised of the sensory organ (eyes) and connecting axon fibers to the visual targets of the brain [11]. Light, as a stimulus, is captured by photoreceptors in the retina, initiating a cascade of chemical and electrical events. The signal is then transferred to the visual center of the brain via the ganglion cell axons of the optic nerve [12–14]. The visual centers process and transform these signals into visual images. Retinal ischemia is frequently involved in various forms of retinal neuropathies, such as age-related macular degeneration (AMD), diabetic retinopathy (DR), glaucoma, and central/branch retinal artery/vein occlusion [15–19]. Following ischemic injuries, a series of events are triggered, including oxidative stress, neovascular and apoptotic changes, and, ultimately, the death of retinal neurons and vision loss [5, 20]. The retina is an extension of the brain in terms of anatomical and embryonic development [21, 22]. The retina also displays similarities to the brain regarding its neuronal and immune responses to injury [22]. The latter is possibly contributed by the structural similarity between the blood-retinal barrier (BRB) and blood-brain barrier (BBB), to which the retina sustains an immune privilege site and shares a similar pattern of immune surveillance and immunoregulatory processes [23, 24]. In response to perturbations in the retina and the brain, innate immunity can be rapidly activated through transcriptional and phenotypic alterations of immune glial cells and the release of inflammatory cytokines [25, 26]. However, excessive activation of innate immune reactivity under injury or traumatic stress can promote further activation of adaptive immunity by antigen-presenting cells that attract and guide peripheral immune cells, such as T cells to the injury sites [27–29]. Neuroinflammation has been well documented as a pathological factor in neuronal death in the brain and in retinal disorders. Because of these similarities, the retina has been commonly considered as an easily accessible indicator of brain disorders, such as Alzheimer's disease (AD), Parkinson's disease (PD), and stroke.

Accumulating evidence suggests that natural herbs exhibit therapeutic potential for the treatment of ischemic stroke [30]. Active ingredients extracted from herbs, including salvianolic acid B and tanshinone from *Salvia miltiorrhiza*, scutellarin from *Scutellaria baicalensis* Georgi (*S. baicalensis*), and honokiol and magnolol from the bark of *Magnolia officinalis*, have been found to have therapeutic potential, because of their antioxidative and anti-inflammatory properties, as well as their ability to maintain BBB permeability [30–36]. The neuroprotective capabilities of other natural extracts, including resveratrol, curcumin, vitamins C and E, and *Gingko biloba*, have also been reported in various CNS disorders [37]. Flavonoids, which are easily accessible by daily consumption of fruits and vegetables, have been found to have high therapeutic efficacy and fewer side effects in both in vitro and in vivo studies [38, 39]. Because of their various pharmacological effects, many flavonoids have demonstrated promising protective effects in the prevention or treatment of various diseases [40–46]. This review mainly focuses on three flavonoids: baicalein (5,6,7-trihydroxyflavone; $C_{15}H_{10}O_5$), baicalin (5,6-dihydroxy-7-O-glucuronide), and wogonin (5,7-dihydroxy-8-methoxy-flavone) (Figure 1), all of which are isolated from the roots of *S. baicalensis*, a widely used herbal medicine in Asian countries [47–51]. Previous studies have demonstrated that baicalein, baicalin, and wogonin have a broad spectrum of biological functions, including antioxidation, anti-inflammation, antiapoptosis, and antiexcitotoxicity [51, 52]. Because of these bioactivities, many published reports have suggested the possibility of developing flavonoids for the treatment of various diseases, including hepatitis, breast cancer, virus infection, and neurodegenerative diseases [43–46]. These pharmacological activities also provide a solid basis for their neuroprotective properties in different models of neuropathies and cognitive impairments. Because of their easy accessibility and low toxicity, baicalein, baicalin, and wogonin may be effective alternatives for the treatment of stroke and other neurodegenerative diseases affecting CNS.

2. Bioactivity and Safety of Baicalein, Baicalin, and Wogonin

As the major active flavonoids extracted from *S. baicalensis*, baicalein, baicalin, and wogonin share some common pharmacological properties against inflammation, oxidation, and apoptosis. A comparison of baicalein, baicalin, and wogonin is shown in Table 1, based on the parameters collected from the database of the traditional Chinese medicine lab of systems pharmacology (TCMSP), a database integrating systems biology and pharmacology for drug discovery, development, and understanding of therapeutic mechanisms [53]. The database can be found in the following link (https://old.tcmsp-e.com/tcmsp.php).

Baicalein and wogonin have a lower molecular weight (MW) and a lower value of the topological polar surface area (TPSA) than baicalin, indicating a higher cell membrane permeability of baicalein and wogonin [54]. Furthermore, the permeability of Caco-2 monolayers (intestinal epithelial cells) and the BBB, calculated based on the values of TPSA [55, 56], was found to be higher for baicalein and wogonin, compared to baicalin. In addition, baicalein and wogonin display slower elimination half-time (HL) and higher oral bioavailability (OB) compared to baicalin, suggesting a longer duration of these two flavonoids in systemic circulation. Based on multiparametric guidelines, also known as rules and ligand efficiency (LE) metrics, which determine the extent of druglikeness (DL) [57], all three flavonoids meet the criteria of "drug-like" compounds. This demonstrates the potential of baicalein, baicalin, and wogonin to be easily accessible agents for future clinical use. However, the relatively high hydrophobicity of baicalein and wogonin is reflected by their lipophilicity (AlogP, a logarithm of 1-octanol/water partition coefficient) values [58], compared to that of baicalin. Due to this low water solubility, solvents or carriers may be necessary to enhance the solubility of these flavonoids for therapeutic purposes [50, 59–61].

S. baicalensis is a major ingredient in many prescriptions of traditional Chinese medicine (TCM). Numerous studies have been conducted to evaluate its pharmacokinetic profile and bioavailability for its safety and efficacy in clinical applications. It has been reported that baicalein and its metabolite

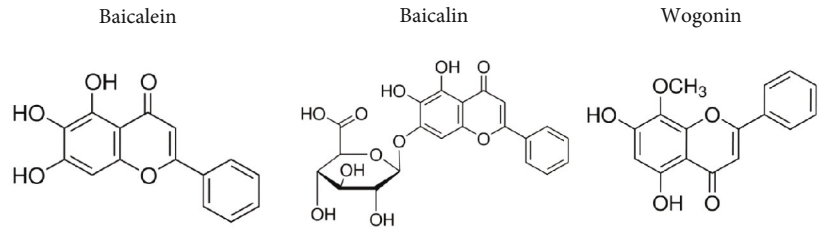

Figure 1: Molecular structures of baicalein, baicalin, and wogonin.

Table 1: Summary of physical parameters of baicalein, baicalin, and wogonin. MW: molecular weight (Dalton (Da)); TPSA: topological polar surface area (angstroms squared (A^2)) indicates the membrane permeability; Caco-2: Caco-2 cell monolayer permeability (10^{-6} cm·s^{-1}); and BBB: blood-brain barrier permeability (10^{-6} cm·s^{-1}) were derived based on TPSA; half-time (HL) (hours (h)), oral bioavailability (OB) (%), the logarithm of 1-octanol/water partition coefficient (AlogP), and drug-likeness (DL) represent the pharmacological properties for each molecule.

Molecule	MW (Da)	TPSA (A^2)	Caco-2 (10^{-6} cm·s^{-1})	BBB (10^{-6} cm·s^{-1})	HL (h)	OB (%)	AlogP	DL
Baicalein	270.25	90.9	0.63	−0.05	16.25	33.52	2.33	0.21
Baicalin	460.42	187.12	−1.1	−1.97	—	29.53	0.84	0.77
Wogonin	284.28	79.9	0.79	0.04	17.75	30.68	2.56	0.23

baicalein 6-O-sulfate exist in blood plasma for up to 36 hours after a single oral administration of Xiaochaihu Tang (Sho-Saiko-To) [62], a popular TCM treatment containing extract of *S. baicalensis*. The bioavailability of wogonin, baicalein, and baicalin has also been evaluated in healthy human urine. After a single administration of *S. baicalensis* decoction (equal to 9 g of crude drug), wogonin, baicalein, and baicalin were still detectable in the urine 36 hours postdosing [63]. A similar time profile has also been demonstrated in monkey plasma after three doses of baicalein [64]. The presence of baicalin has been detected in human plasma after administration [65, 66]. Additionally, the safety profile of single or multiple administrations of chewable baicalein tablets has been assessed in healthy subjects. In addition to detecting sustained levels of baicalein and its metabolite baicalin in vivo, these studies revealed that single or multiple doses of baicalein (100–800 mg) were safe and well tolerated with no sign of toxicity in the kidney or liver [67, 68]. These findings implicate the feasibility of developing baicalein, baicalin, and wogonin as safe and long-lasting agents for clinical application.

3. Neuroprotective Effects of Baicalein, Baicalin, and Wogonin on the Brain and Retina Ischemia

Neurodegeneration often occurs through the progressive loss of the structure or functions of neurons [69]. Neurodegenerative diseases, such as Parkinson's disease (PD), Alzheimer's disease (AD), and stroke, affect millions of people worldwide, especially in aging populations. The pathogenesis of neurodegeneration is complicated and has been associated with genetics, protein misfolding, intracellular mechanisms, and programmed cell death [70–74]. In ischemic stroke patients, typical symptoms are characterized by the sudden loss of mobility, speaking, or vision unilaterally [75]. Ischemia in the brain can be caused by cardioembolic vessel occlusion, artery to artery embolism, or in-situ small-vessel disease [75]. In the retina, ischemia can result from occlusion of the central or branch retinal vessels or DR [76]. Retinal ischemia may lead to visual impairment and blindness [19].

Ischemia induces a cascade of neuropathological activities, including oxygen and energy depletion, disruption of ion homoeostasis, glutamate and free radical release, Ca^{2+} channel dysfunction, BBB or BRB disruption, and changes to the inflammatory microenvironment, ultimately leading to cell death and irreversible functional loss [5, 77, 78]. The cellular changes after ischemic stroke are illustrated in Figure 2. There are three major types of stress. First, oxidative stress is induced by rapidly increased reactive oxygen species (ROS) postischemia [79]. This stress can subsequently lead to the peroxidation of membrane lipid, mitochondrial dysfunction, and DNA damage, eventually causing apoptosis and irreversible neuron loss [80, 81]. Second, neuroinflammatory stress, initiated by the activation of innate and adaptive immunity, is a well-known pathological factor in CNS disorders [82, 83]. The resident immune cells (microglia and astrocytes) can be rapidly activated upon sensing damage-associated molecular patterns (DAMPs) released by apoptotic cells [83, 84]. Subsequently, adaptive immune cells can be recruited even with minimized disturbances or disruptions of BBB or BRB postischemia insults, ultimately causing neuron death [29, 69, 85]. Lastly, stress of energy deprivation triggers cytotoxicity at the lesion site. Apart from the excessive free radicals, the disruption of ion homeostasis post-ischemia/reperfusion injury can lead to overload of Na^+ and Ca^{2+}, which aggravates mitochondrial dysfunction and initiates apoptosis and inflammatory cascades [86]. Furthermore, the release and accumulation of glutamate can cause excitotoxicity of neurons and ultimately leads to cell death [87, 88]. Based on the understanding of neurochemical events under ischemic stress, many neuroprotective therapies are focused on targeting the upstream pathways to reduce

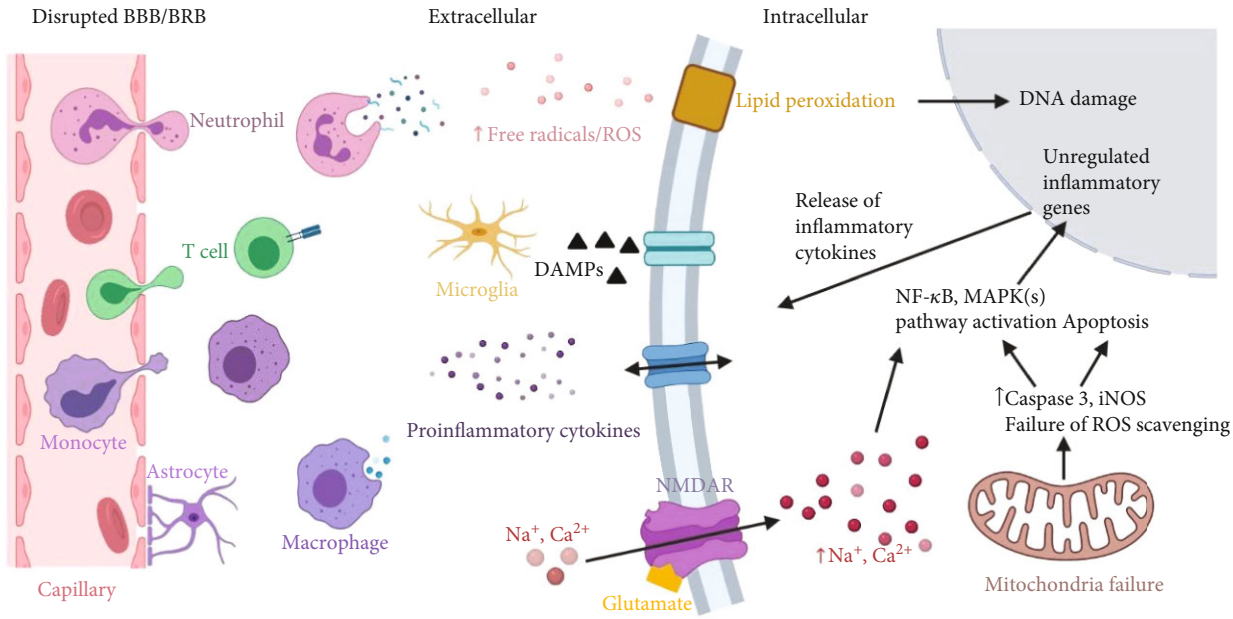

Figure 2: Schematic representation of the main pathological events subsequent to brain ischemia. Created with http://BioRender.com.

damage to the neurons induced by downstream cascades. The protective effects of natural herbs have been demonstrated by many research groups [89]. In the following discussion, the neuroprotective effects of baicalein, baicalin, and wogonin, the major bioactive molecules in *S. baicalensis*, are described based on the sites (i.e., the brain and retina) of postischemic injury.

3.1. Ischemia in the Brain. Following ischemic injury in the brain, a cascade of changes is elicited, including oxygen and energy deprivation, increased expression of free radicals and inflammatory cytokines, ion overload, and activation of immune responses [90, 91]. The upstream triggers of these changes and maintenance of tissue homeostasis are recognized as potential therapeutic targets for ischemic stroke treatment. Multiple pharmacological properties of flavonoids as reported in the literature include antioxidant, anti-inflammation, antiapoptosis, and antiexcitotoxicity characteristics that are neuroprotective [92, 93]. The neuroprotective effects of baicalein, baicalin, and wogonin on both in vitro and in vivo ischemic models are discussed (also see Tables 2 and 3 for details).

3.1.1. In Vitro Studies. Free radicals and ROS are known as inducers of cell death postischemic injury. Baicalein has been shown to exert neuroprotective effects and attenuate apoptosis by acting as a scavenger of ROS and nitric oxide (NO) [94]. These baicalein-induced protective effects have been found to be mediated by upregulating the phosphatase and tensin homolog gene (PTEN) and the phosphoinositide 3-kinase (PI3K/AKT) pathway in primary cultures of cortical neurons after oxygen and glucose deprivation (OGD) treatment [94]. Additionally, it has been reported that baicalein improves the survival of HT22 cells after iodoacetic acid-(IAA-) induced oxidative stress, by inhibiting 12/15-lipoxygenase (12/15-LOX) [93], an enzyme which oxidizes polyunsaturated fatty acids to generate bioactive lipid metabolites [95] and is toxic to neurons in neurological disorders [96].

Neuroprotective abilities of wogonin and baicalin have also been reported. In OGD-induced toxicity to rat hippocampal slice culture, pretreatment and posttreatment of hippocampal slices with 50 μM baicalin could significantly prevent cell death, especially in the pyramidal cell layer [97]. Wogonin has been demonstrated to act as an antioxidant and 12/15-LOX inhibitor to improve the survival of primary cortical neurons after H_2O_2 or xanthine/xanthine oxidase challenge [98].

It is worth noting that not only oxidative stress but also the dysregulated immune microenvironment can lead to the degeneration of brain cells. In OGD-induced ischemia of PC12 cells, which were derived from a pheochromocytoma of the rat adrenal medulla, baicalein, baicalin, and wogonin all exhibited significant neuroprotective effects by inhibiting oxidation and suppressing inflammation [99]. These protective effects were shown to be mediated by the reduced expression of Toll-like receptor 2 (TLR2), tumor necrosis factor alpha (TNF-α), and caspase-3 [99]. Baicalin acts through suppressing OGD-induced phosphorylation of calmodulin- (CaM-) dependent protein kinase II (CaMKII) in primary hippocampal neurons and SH-SY5Y cells [100]. The antiapoptotic effects of baicalin have also been shown to suppress caspase-3 and Bax expression and to promote antiapoptotic factor Bcl-2 expression in hippocampal neurons [100]. The effect of baicalin on rescuing neurons from OGD was comparable with that of CaMKII siRNA knockdown in SH-SY5Y cells, suggesting that baicalin may function as a potent CaMKII inhibitor in neuroprotection [100].

3.1.2. In Vivo Studies. Neuroprotective effects of baicalein, baicalin, and wogonin against ischemic injuries have been

Table 2: In vitro findings of baicalein, baicalin, and wogonin on different brain cell types.

Cell types	Stimulating molecule(s)	Baicalein		Baicalin		Wogonin		Reference(s)
		Conc.	Effects	Conc.	Effects	Conc.	Effects	
Mouse hippocampal HT22 cell line	20 μM IAA	2 μM	Antioxidant 12/15-lipoxygenase inhibitor					[93]
Primary cortical neurons	Glutamate, OGD, H_2O_2, or xanthine/xanthine oxidase	10 μM; 3.5 μM	Promote cell survival through inhibiting 12/15-LOX and removing intracellular ROS and nitrotyrosine reactivities by regulating the PI3/AKT pathway			9.0 μg/ml; 23.7 μg/ml	Improve neuron survival by radical scavenging activity and inhibiting the initiation of LOX-induced apoptosis	[92, 94, 98]
PC-12	OGD	1 μg/ml; 10 μg/ml	Increase survival rate and suppress pro-inflammatory cytokine expression	0.01 mg/ml, 0.1 mg/ml, and 1 mg/ml	Increase survival rate and suppress proinflammatory cytokine expression	0.01 mg/ml, 0.1 mg/ml, and 1 mg/ml	Increase survival rate and suppress proinflammatory cytokine expression	[99]
Primary hippocampal neurons	OGD			1 μM	Protect neurons from apoptosis by suppressing phosphorylation of CaMKII	50 μM	Improve neuron survival on hippocampal slice culture	[97, 100]

Table 3: Baicalein, baicalin, and wogonin performance on different brain ischemia models.

Models	Species	Baicalein		Baicalin		Wogonin		Reference(s)
		Conc.	Effects	Conc.	Effects	Conc.	Effects	
SCEM	Rabbit	100 mg/kg	Improve behavioral performance					[93]
MCAO	Rat/mouse	20 mg/kg; 200 mg/kg	Decrease the infarct volume and neurological score; inhibiting 12/15-LOX-induced oxidative toxicity; regulate M1/M2 transformation of microglia/macrophages and block NF-κB nuclear translocation; suppress PARP-1/AIF pathway-induced neuroinflammation; antioxidant 12/15-LOX inhibitor	5, 100, and 200 mg/kg	Reduced the neurological deficit scores, cerebral infarct volume by inhibiting TLR2/4-mediated NF-κB pathway, and expression of iNOS, COX2, and caspase3	20 mg/kg; 50 μM	Reduce infarct area and improve behavior performance through upregulating TGF-β1	[92, 94, 106–109, 112–116, 118, 119]
GCI/R	Gerbil/rats			100 mg/kg; 200 mg/kg	Improve learning and memory ability post-I/R injury via anti-inflammatory and antiapoptosis; perform neuroprotection by upregulating HSP70 expression and influencing MAPK cascades in the gerbil hippocampus	0.5, 1, and 10 mg/kg	Increase neuron survival in the hippocampus area by suppressing inflammation (iNOS, TNF-α)	[100, 101, 103, 117, 118]

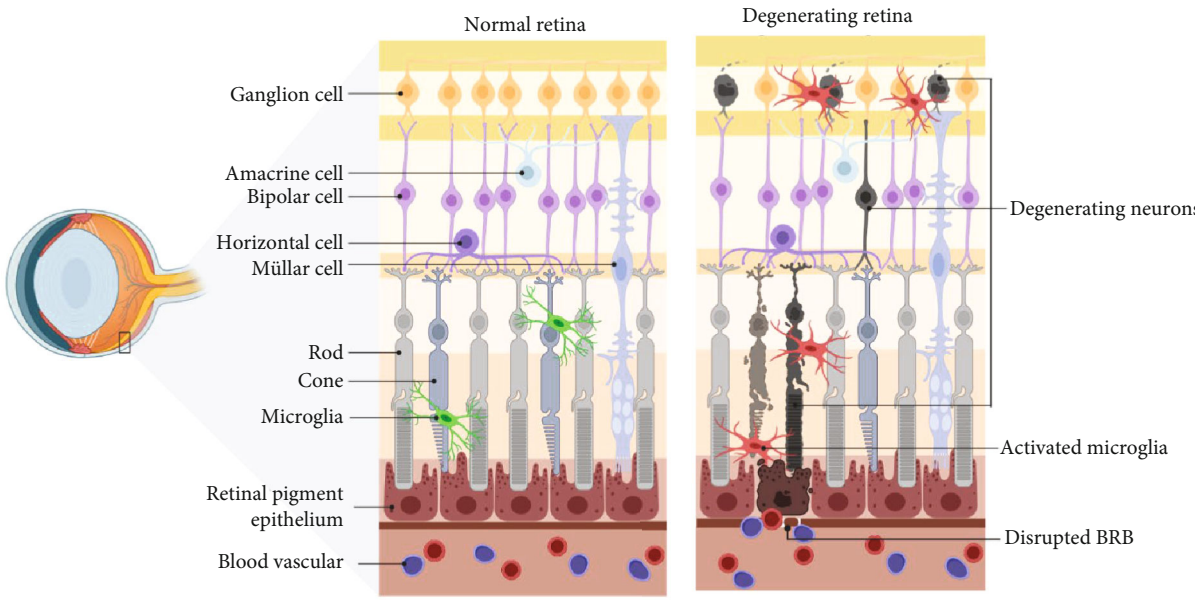

Figure 3: Schematic diagram showing the normal retina and degenerating retina resulting from ischemia. Created with http://BioRender.com.

reported in various animal models. In the global cerebral ischemia/reperfusion (GCI/R) rat model, Cheng et al. reported that oral administration of 100 mg/kg baicalin for 7 d consecutively can rescue the spatial learning and memory abilities of gerbil significantly, as assessed by the water maze test [101]. Subsequently, Wang et al. showed that baicalin, given at the same dose by intraperitoneal injection for one week immediately after GCI/R injury, can improve the learning and memory abilities in gerbil [100]. These neuroprotective effects exerted by baicalin have been found to be related to the inhibition of CaMKII-mediated downstream biochemical events [100]. CaMKII is an important protein involved in Ca^{2+}/glutamate-mediated excitotoxicity under the stress of ischemia [87, 102]. These findings imply that neuroprotective effects arising from baicalin are possibly related to its antiexcitotoxicity capacity. In addition to the CaMKII pathway, Dai et al. found that neuroprotective effects of baicalin can be achieved by its mediation of heat shock protein 70 (HSP70) and mitogen-activated protein kinase (MAPKs) cascades [103]. HSP70 is a critical cytoprotective factor, which is responsible for proper protein folding [104]. And MAPKs are important pathways regulating cell survival and death, including the subgroups of phosphorylated extracellular signal-regulated kinase (pho-ERK), phosphorylated c-Jun N-terminal kinase (pho-JNK), and phosphorylated p38 (pho-p38) [105]. Upregulation of HSP70 and mediation of MAPK subgroups by intraperitoneal administration of baicalin could effectively rescue neurons in the hippocampus after GCI/R injuries [103]. In addition, other studies have shown that baicalin can inhibit the activation of TLR signaling and the relevant downstream inflammatory pathway (i.e., nuclear factor kappa-light-chain-enhancer of activated B cells (NF-κB) pathway) [106, 107]. Following middle cerebral artery occlusion (MCAO), intravenous or intraperitoneal administration of baicalin has been shown to effectively attenuate cerebral infarction by regulating inflammation, including the expression of proinflammatory cytokines TNF-α and interleukin-1β (IL-1β), via TLR2/4 and NF-κB pathway signaling cascades [106, 107]. Baicalin's antioxidative and anti-inflammatory properties are also indicated by decreased levels of both mRNA and iNOS and COX2 protein levels [106, 108].

Similar neuroprotective and antineuroinflammatory effects have been reported with baicalein. For instance, baicalein was found to ameliorate the neurobehavioral deficits and infarct volume caused by small clot embolic stokes (SCEM) or MCAO [93, 94]. Modulating microglia/macrophage M1/M2 polarization and suppressing the NF-κB signaling are suggested to be responsible for the antineuroinflammation and neuroprotection [109]. As a potent antioxidant inhibitor of 12/15-LOX, baicalein was shown to effectively reduce infarct size, edema formation, and 12/15-LOX-induced neuron death in various brain ischemia animal models [92, 110–112]. The inhibitory effect of baicalein is comparable to the protective effects observed in 12/15-LOX knockout mice ALOX15$^{-/-}$ [92]. Pallast et al. found that the protective effects of baicalein are mediated by the suppression of apoptosis-inducing factor (AIF) nuclear translocation in an MCAO model [113]. Later, in addition to confirming the antiapoptotic effect through AIF regulation, Li et al. reported the involvement of the poly (ADP-ribose) polymerase-1 (PARP-1)/AIF pathway in baicalein-induced neuroprotection [114]. Furthermore, inflammation-related factors, such as cytosolic phospholipase A2 (cPLA2) and p38 MAPK, have been reported to be downregulated after baicalein administration in the MCAO rat model [112, 115]. The alteration of peroxisome proliferator-activated receptor γ (PPARγ) and nuclear translocation induced by brain ischemia/reperfusion injury have also been reported to be returned to the balanced stage by baicalein pretreatment [116].

Wogonin is also found to exert neuroprotective effects on both GCI/R and MCAO rat models. In the GCI/R rat model, wogonin was shown to effectively attenuate neuron loss and

Table 4: In vitro findings of baicalein, baicalin, and wogonin on different brain cell types.

Cell types	Baicalein			Baicalin			Wogonin			Reference(s)
	Stimulator	Conc.	Effects	Stimulator	Conc.	Effects	Stimulator	Conc.	Effects	
Primary rat retinal cells	Ascorbate/$FeSO_4$	100 μM	Attenuate oxidative stress-induced ROS							[123]
ARPE-19 cells	H_2O_2; IL-1b	50 μM; 40 μM	Antioxidation by scavenging ROS; inhibit the expression of MMP-9 and VEGF; suppress IL-6 and IL-8 proinflammatory cytokines	High glucose	50 μM	Protect ARPE-19 cells from apoptosis through upregulating the release of microRNA-145; anti-inflammation by initiating the regulation of NF-κB and p38MAPK signaling pathways	LPS; IL-1 β	10 μM or 50 μM; 1–10 μM	Suppress LPS-induced inflammatory responses via the TLR4/NF-κB pathway and protect the tight junctions; inhibit IL-6 and IL-8 via NF-κB pathway suppression; upregulated claudin-1 and ZO-1	[122, 124, 125, 127]
HRMEC	High glucose			High glucose	50 μM	Protect ARPE-19 cells from apoptosis through upregulating the release of microRNA-145; anti-inflammation by initiating the regulation of NF-κB and p38MAPK signaling pathways				[127]

Table 5: In vivo findings of baicalein, baicalin, and wogonin on different animal models.

Models	Species	Baicalein		Baicalin		Wogonin		References
		Conc.	Effects	Conc.	Effects	Conc.	Effects	
I/R	Rat	0.5 nmol	Effectively protect retinal cells and electrical functions from oxidation and apoptosis; upregulation of HO-1 and downregulation of HIF-1α, VEGF, and MMP-1	12.5 mg/kg	Protect RGCs from retinal ischemia injury and suppress glial cell activity			[123, 128]
DR	Rat; mice	150 mg/kg in rat; 75 mg/kg in mice	Significantly suppressed the inflammatory processes of retinal microglia and Muller cells; enhanced vascular permeability and blood-retina barrier; protect BRB permeability as antioxidant 12/15-LOX inhibitor, anti-inflammation, and antiangiogenesis	150 mg/ml in rat	Protect retinal cells from apoptosis by promoting Bcl-2; perform as an inhibitor of ARA and delay the progression of diabetic retinopathy			[130, 131]

histological changes in the hippocampal CA1 region [117]. The expression of inflammatory mediators (e.g., iNOS and TNF-α) at the injury site was significantly suppressed by intraperitoneal administration of wogonin in rats after ischemia injury [117]. In the MCAO rat model, wogonin pre- and posttreatment was shown to both alleviate the infarct volume and behavioral deficits and promote angiogenesis in the peri-ischemia area [118, 119]. Upregulation of transforming growth factor beta (TGF-β1) expression in the ischemic brain tissue was observed in wogonin-treated rats 2 weeks after ischemic injury [119]. TGF-β1 has previously been reported as an important regulator of angiogenesis in hypoxic tissue [120]. This finding indicates that wogonin protects neurons by promoting microvascular formation and subsequently restoring blood supply via the TGF-β1 pathway. The vasodilatory effect of wogonin mediated by inhibition of both intracellular Ca^{2+} release and extracellular Ca^{2+} influx could be a potential treatment paradigm for ischemia [121]. This evidence strongly supports the feasibility of developing baicalein, baicalein, and wogonin as candidates for neuroprotection following ischemic stroke.

3.2. In Retina Ischemia. Injuries caused by retinal ischemia are common in many ocular disorders, such as central/-branch retinal artery/vein occlusion, DR, glaucoma, and AMD [15–19]. Similar to ischemic brain injuries, retinal ischemia triggers oxidative stress, inflammation, neovascularization, and, ultimately, the death of retinal neurons [5, 20]. Figure 3 illustrates the morphological changes to the retina and neuron death after ischemia-induced stress. In the following, the antioxidative, anti-inflammatory, antiapoptotic effects of baicalein, baicalin, and wogonin after retinal ischemia for in vitro and in vivo studies are summarized (Tables 4 and 5).

3.2.1. In Vitro Studies. The antioxidative properties of baicalein against retinal ischemia were first reported by Liu et al. [122]. Baicalein was shown to significantly increase cell viability of human retinal pigment epithelium cells (hRPEs) against H_2O_2-induced oxidative stress by scavenging ROS and suppressing the production of matrix metalloproteinase-9 (MMP-9) and vascular endothelial growth factor (VEGF) [122]. Subsequently, the antioxidative effects of baicalein on dissociated primary rat retinal cells were demonstrated to be subjected to ascorbate- and $FeSO_4$-induced oxidative stress [123]. Baicalein pretreatment not only suppresses the expression of hypoxia-inducible factor-1α (HIF-1α), VEGF, and MMP-9 but also increases the level of heme oxygenase-1 (HO-1) in ascorbate- and $FeSO_4$-stimulated retinal cells [123]. These findings indicate that baicalein has strong antioxidative capabilities in retinal cells, which are comparable to the antioxidative effects exerted by Trolox (6-hydroxy-2,5,7,8-tetramethylchroman-2-carboxylic acid) [123]. In addition, baicalein and wogonin have been found to demonstrate anti-inflammatory effects by suppressing *IL-6* and *IL-8* expression in IL-1β-challenged ARPE-19 cells, while NF-κB binding activity is suppressed by wogonin [124]. Similar anti-inflammatory effects have been reported by other recent studies. Chen et al. found that wogonin effectively suppressed LPS-induced activation of the TLR4/NF-κB pathway and subsequently increased expression of inflammatory cytokines IL-1β, IL-6, IL-8, cyclooxygenase-2 (COX-2), TNF-α, and iNOS in ARPE-19 cells [125]. It was also reported that administration of wogonin to endoplasmic reticulum- (ER-) challenged ARPE-19 cells increased the expression of tight junction proteins claudin-1 and ZO-1 [126]. In another study which mimicked DR in vitro by treating ARPE-19 cells and human retinal microvascular endothelial cells (HRMECs) with high glucose, baicalin was shown to exert antiapoptotic effects by inhibiting the release of proinflammatory cytokines and ROS [127]. These protective effects of baicalin are likely mediated by the suppression of NF-κB and p38 MAPK pathways by upregulating miRNA-145 expression [127].

3.2.2. In Vivo Studies. In the rat retinal ischemia/reperfusion model, baicalein pretreatment effectively regulated the expression of apoptotic factors, including Bax and Bcl-2, subsequently reducing retinal cell apoptosis [123]. In addition, baicalein pretreatment significantly improved the inner

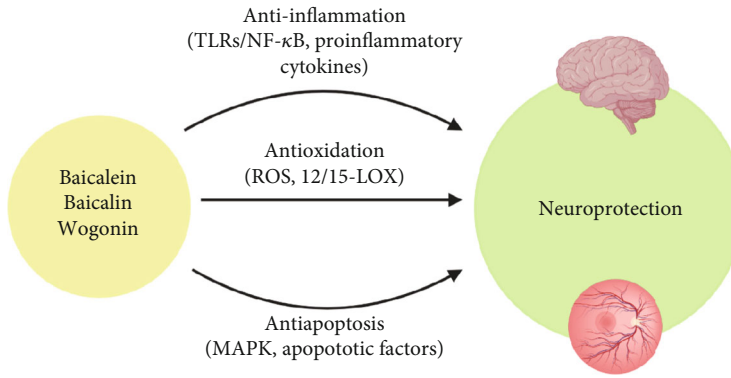

Figure 4: Targeted pathways initiated by baicalein, baicalin, and wogonin demonstrating the neuroprotective effects in the brain and retina. Created with http://BioRender.com.

retinal functions in electroretinogram (ERG) assessments [123]. Similar neuroprotective effects were also observed in baicalin-treated rats with ischemia/reperfusion injury. A reduced loss of Thy-1^+ neuron cells and reduced expression of apoptosis markers, including caspase-3 and 8 and poly (ADP-ribose) polymerase-1 (PARP-1), have been found in the retina after ischemic insults [128]. In addition, the downregulated expression of GFAP after baicalin treatment indicates the involvement of baicalin in regulating glial responses and neuroinflammation [128], in addition to its antioxidant and antiapoptosis properties.

The anti-inflammatory effects of baicalein and baicalin have been demonstrated in rats with DR. The excessive activation of resident retinal immune cells is widely known as a pathogenic factor of neurodegeneration in retinal disorders [84, 129]. Yang et al. reported the occurrence of vascular abnormality and RGC loss in the DR rat retina in combination with activation of microglia and Müller cell dysfunction [130]. Oral administration of baicalein has been shown to significantly protect retinal vessels and neurons from DR-induced dysfunction and apoptosis through suppressing the activation of retinal inflammatory processes modulated by microglia and Müller cells and by reducing the release of pro-inflammatory cytokines, including IL-18, TNF-α, and IL-1β [130]. The protective effects of baicalin are believed to function through inhibiting the expression of apoptosis regulators, including Bax and Bcl-2, on the RGC layer [131]. Intraperitoneal application of baicalin was found to inhibit the otherwise-elevated aldose reductase activity (ARA) in diabetes. This suggests that baicalin acts as an aldose reductase inhibitor, potentially retarding the progression of apoptosis induced by diabetes [131].

In addition to oxidative stress and inflammation, vascular hyperpermeability of retinal blood vessels has been suggested to be a pathogenic factor in retinal ischemia, DR, and AMD. Othman et al. reported that 12/15-LOX activation leads to vascular hyperpermeability in DR by inhibiting protein tyrosine phosphatase and activating VEGF-R2 signaling pathways [132]. As a potent inhibitor of 12/15-LOX, baicalein significantly reduces the lipid metabolites of 12- and 15-hydroxyeicosatetreanoic acids (HETE) expressed during 12/15-LOX activation in DR [132]. The HETE-induced upregulation of NOX2 and ROS is also reported to be downregulated by baicalein treatment in *Ins2*^{Akita} diabetic mouse retina. Likewise, baicalein has been shown to protect against HETE-induced vascular hyperpermeability by acting as a VEGF-R2 inhibitor, restoring phosphoserine phosphatase-1 (pSHP1) levels in DR [132]. The inflammatory cytokine IL-6 and intracellular adhesion molecules (ICAMs) ICAM-1 and vascular cell adhesion molecule-1 (VCAM-1) were remarkably inhibited in the diabetic retina [132]. Taken together, baicalein functions as a 12/15-LOX inhibitor, mediating its effects primarily on vascular and retinal barriers.

4. Pathways Targeted by Baicalein, Baicalin, and Wogonin during Neuroprotective Processes

As described above, the neuroprotective effects triggered by baicalein, baicalin, and wogonin are possibly related to their anti-inflammatory, antioxidative, and antiapoptotic capabilities (Figure 4).

Firstly, the antioxidative effects of baicalein, baicalin, and wogonin are recognized by their ROS scavenging properties. Under normal circumstance, ROS play a pivotal role in many biological processes, such as redox balance in cells. However, a dramatic increase of ROS production may disturb this homeostatic balance under oxidative stress conditions (e.g., ischemia), eventually leading to cell death. Typically, scavenging excessive ROS is a neuroprotective target in neurodegenerative disorders [133]. Baicalein and baicalin serve as potent 12/15-LOX inhibitors with high antioxidative efficiencies. 12/15-LOX is found to be upregulated after stroke, resulting in neuronal death and leakage of BBB and BRB [134]. Inhibition of 12/15-LOX was also shown to reduce infarct volume and edema in the stroke area, suggesting its potential role as an effective and viable therapeutic option for ischemia [92, 135, 136]. Furthermore, the protection of BBB and BRB help preserves the microenvironment at the injured site from disruption by systemic immunity and secondary inflammatory responses caused by degeneration.

Secondly, the anti-inflammatory effect initiated by these flavonoids after ischemia is revealed by the suppression of proinflammatory cytokine release. Excessive activation of microglia has been emergingly reported as a pathogenesis for the development of neurodegenerative diseases [137]. In addition, baicalein and baicalin exhibit the capability in

regulating microglia homeostasis after ischemic stress [109]. These properties have been demonstrated to be mediated through interactions with TLR/NF-κB and PARP-1/AIF pathways [99, 106, 107, 124, 125, 127].

Lastly, the antiapoptotic capacity of baicalein, baicalin, and wogonin has been reported in ischemia-injured brain and retina. Through modulating the MAPK pathway and the production of apoptotic factors, these flavonoids effectively rescue neurons in the brain and retina [100, 112, 113, 115, 123, 127, 128, 131]. In addition, the blockage of ion channel dysfunction after ischemic stress remarkably ameliorates the excitotoxicity caused by ion overload and subsequently decreases neuronal death [86, 121]. Taken together, all the evidence strongly supports the feasibility of developing these flavonoids as natural neuroprotectants.

5. Conclusion and Future Directions

Ischemia often results in physical disabilities, including paralysis and blindness. This is particularly common in the aging population. Currently, effective clinical intervention for ischemia-induced damage is limited. Ample evidence has demonstrated the potent neuroprotective properties of baicalein, baicalin, and wogonin in both in vitro and in vivo models of ischemia. Flavonoids exert their anti-inflammatory, antioxidative, and antiapoptotic effects on CNS postischemia insults by initiating various potential signaling pathways. Flavonoids are herb extracts, suggesting their potential to be developed as natural neuroprotective agents.

Additional studies are required to elucidate and characterize the pharmacological properties and bioactivities of these flavonoids in combating neuropathies, in order to facilitate the future development of neuroprotectants that are safe and effective. As an extension of the brain, the retina may serve as an easily accessible model and potential therapeutic target site for various neuropathies and other neurodegenerative diseases. Additionally, pharmacodynamic and pharmacokinetic studies, including time- and dose-dependent responses, cytotoxicity, and drug metabolism after systemic and topical administration of these three flavonoids, need to be established. One recent study has reported that the metabolic abilities of flavonoids in the liver and intestines are markedly different among different species, including mice, rats, dogs, monkeys, and humans [138]. In addition, potential targets or receptors through which baicalein, baicalin, and wogonin act on may need to be further characterized and studied. Studies on the combined effects of baicalein, baicalin, and wogonin are limited, raising the possibility that combined flavonoids can achieve longer and stronger protective effects. Lastly, due to the limited water solubility and liposolubility of baicalein, baicalin, and wogonin, formulations and optimizations of these flavonoids, possibly including nanoparticles or other newly developed carriers, may be needed to achieve higher bioactivity and clinical efficacy. It is envisaged that these natural flavonoids can eventually offer new therapeutic therapies for patients with ischemia-induced neural disorders.

Data Availability

All data mentioned in this review article are published findings. They have been properly cited in the article.

Conflicts of Interest

D.F.C. is a consultant for Boston Pharma and Pri-Med. Other authors have no conflicts of interest.

Acknowledgments

This work was supported by grants from the National Institutes of Health (NIH)/National Eye Institute (NEI) (Grants EY025913 and EY025259 to D.F.C.), Bright Focus Foundation grant and The Glaucoma Foundation grant to K.C., the Core Grant for Vision Research from NIH/NEI to the Schepens Eye Research Institute (P30EY03790), Health Medical Research Fund (16172571 to C.W.D), PolyU Postgraduate Studentship (L.P.), Henry G. Leong Endowed Professorship in Elderly Vision Health and Dean Reserve (8-8475 and 1-ZVN2 to C.H.T), and PolyU internal grants (UAGF and UAHG to C.W.D).

References

[1] H. K. Eltzschig and T. Eckle, "Ischemia and reperfusion-from mechanism to translation," *Nature Medicine*, vol. 17, no. 11, pp. 1391–1401, 2011.

[2] H. Amani, E. Mostafavi, M. R. Alebouyeh et al., "Would colloidal gold nanocarriers present an effective diagnosis or treatment for ischemic stroke?," *International Journal of Nanomedicine*, vol. 14, pp. 8013–8031, 2019.

[3] H. Amani, R. Habibey, F. Shokri et al., "Selenium nanoparticles for targeted stroke therapy through modulation of inflammatory and metabolic signaling," *Scientific Reports*, vol. 9, no. 1, article 6044, 2019.

[4] R. Capildeo, S. Haberman, and F. C. Rose, "The definition and classification of stroke: a new approach," *The Quarterly Journal of Medicine*, vol. 47, no. 2, pp. 177–196, 1978.

[5] P. Deb, S. Sharma, and K. M. Hassan, "Pathophysiologic mechanisms of acute ischemic stroke: an overview with emphasis on therapeutic significance beyond thrombolysis," *Pathophysiology*, vol. 17, no. 3, pp. 197–218, 2010.

[6] Writing Group Members, T. Thom, N. Haase et al., "Heart disease and stroke statistics—2006 Update," *Circulation*, vol. 113, no. 6, pp. e85–e151, 2006.

[7] B. Boling and K. Keinath, "*Acute ischemic stroke*," *AACN Advanced Critical Care*, vol. 29, no. 2, pp. 152–162, 2018.

[8] Q. Yang, X. Tong, L. Schieb et al., "Vital signs: recent trends in stroke death rates - United States, 2000-2015," *MMWR Morbidity and Mortality Weekly Report*, vol. 66, no. 35, pp. 933–939, 2017.

[9] J. S. Kim, "tPA helpers in the treatment of acute ischemic stroke: are they ready for clinical use?," *Journal of Stroke*, vol. 21, no. 2, pp. 160–174, 2019.

[10] V. K. Sharma, H. L. Teoh, L. Y. H. Wong, J. Su, B. K. C. Ong, and B. P. L. Chan, "Recanalization therapies in acute ischemic stroke: pharmacological agents, devices, and combinations," *Stroke Research and Treatment*, vol. 2010, Article ID 672064, 8 pages, 2010.

[11] J. K. Mai and G. Paxinos, *The Human Nervous System*, Academic Press, Cambridge, MA, USA, 2011.

[12] J. J. Pang, F. Gao, and S. M. Wu, "Light-evoked excitatory and inhibitory synaptic inputs to ON and OFF α ganglion cells in the mouse retina," *The Journal of Neuroscience*, vol. 23, no. 14, pp. 6063–6073, 2003.

[13] M. Tessier-Lavigne, "Visual processing by the retina," in *Principles of Neural Science*, pp. 507–522, Elsevier, 2000.

[14] S. Prasad and S. L. Galetta, "Chapter 1 - Anatomy and physiology of the afferent visual system," in *Handbook of Clinical Neurology*, C. Kennard and R. J. Leigh, Eds., pp. 3–19, Elsevier, 2011.

[15] Y. Q. Chen, W. H. T. Pan, J. H. Liu et al., "The effects and underlying mechanisms ofS-Allyll-Cysteine treatment of the retina after ischemia/reperfusion," *Journal of Ocular Pharmacology and Therapeutics*, vol. 28, no. 2, pp. 110–117, 2012.

[16] P. H. Peng, H. M. Chao, S. H. Juan, C. F. Chen, J. H. Liu, and M. L. Ko, "Pharmacological preconditioning by low dose cobalt protoporphyrin induces heme oxygenase-1 overexpression and alleviates retinal ischemia-reperfusion injury in rats," *Current Eye Research*, vol. 36, no. 3, pp. 238–246, 2011.

[17] M. M. Wessel, N. Nair, G. D. Aaker, J. R. Ehrlich, D. J. D'Amico, and S. Kiss, "Peripheral retinal ischaemia, as evaluated by ultra-widefield fluorescein angiography, is associated with diabetic macular oedema," *The British Journal of Ophthalmology*, vol. 96, no. 5, pp. 694–698, 2012.

[18] N. N. Osborne, M. Ugarte, M. Chao et al., "Neuroprotection in relation to retinal ischemia and relevance to glaucoma," *Survey of Ophthalmology*, vol. 43, pp. S102–S128, 1999.

[19] N. N. Osborne, R. J. Casson, J. P. M. Wood, G. Chidlow, M. Graham, and J. Melena, "Retinal ischemia: mechanisms of damage and potential therapeutic strategies," *Progress in Retinal and Eye Research*, vol. 23, no. 1, pp. 91–147, 2004.

[20] T. T. Lam, A. S. Abler, and M. Tso, "Apoptosis and caspases after ischemia-reperfusion injury in rat retina," *Investigative Ophthalmology & Visual Science*, vol. 40, no. 5, pp. 967–975, 1999.

[21] I. J. MacCormick, G. Czanner, and B. Faragher, "Developing retinal biomarkers of neurological disease: an analytical perspective," *Biomarkers in Medicine*, vol. 9, no. 7, pp. 691–701, 2015.

[22] A. London, I. Benhar, and M. Schwartz, "The retina as a window to the brain–from eye research to CNS disorders," *Nature Reviews Neurology*, vol. 9, no. 1, pp. 44–53, 2013.

[23] M. H. Madeira, A. F. Ambrósio, and A. R. Santiago, "Glia-mediated retinal neuroinflammation as a biomarker in Alzheimer's disease," *Ophthalmic Research*, vol. 54, no. 4, pp. 204–211, 2015.

[24] J. A. Fernández-Albarral, E. Salobrar-García, R. Martínez-Páramo et al., "Cambios de las celulas gliales de la retina en la enfermedad de Alzheimer - Revision bibliografica," *Journal of Optometry*, vol. 12, no. 3, pp. 198–207, 2019.

[25] J. Y. Niederkorn, "See no evil, hear no evil, do no evil: the lessons of immune privilege," *Nature Immunology*, vol. 7, no. 4, pp. 354–359, 2006.

[26] C. Arcuri, C. Mecca, R. Bianchi, I. Giambanco, and R. Donato, "The pathophysiological role of microglia in dynamic surveillance, phagocytosis and structural remodeling of the developing CNS," *Frontiers in Molecular Neuroscience*, vol. 10, no. 191, 2017.

[27] T. H. Khanh Vu, H. Chen, L. Pan et al., "$CD4^+$ T-Cell Responses Mediate Progressive Neurodegeneration in Experimental Ischemic Retinopathy," *The American Journal of Pathology*, vol. 190, no. 8, pp. 1723–1734, 2020.

[28] A. Murshid, J. Gong, and S. K. Calderwood, "The role of heat shock proteins in antigen cross presentation," *Frontiers in Immunology*, vol. 3, p. 63, 2012.

[29] S. Jiang, M. Kametani, and D. F. Chen, "Adaptive immunity: new aspects of pathogenesis underlying neurodegeneration in glaucoma and optic neuropathy," *Frontiers in Immunology*, vol. 11, p. 65, 2020.

[30] T. Peng, Y. Jiang, M. Farhan, P. Lazarovici, L. Chen, and W. Zheng, "Anti-inflammatory effects of traditional chinese medicines on preclinical in vivo models of brain ischemia-reperfusion-injury: prospects for neuroprotective drug discovery and therapy," *Frontiers in Pharmacology*, vol. 10, no. 204, 2019.

[31] J. H. Park, O. . Park, J. H. Cho et al., "Anti-inflammatory effect of tanshinone I in neuroprotection against cerebral ischemia–reperfusion injury in the gerbil hippocampus," *Neurochemical Research*, vol. 39, no. 7, pp. 1300–1312, 2014.

[32] K. Dong, W. Xu, J. Yang, H. Qiao, and L. Wu, "Neuroprotective effects of Tanshinone IIA on permanent focal cerebral ischemia in mice," *Phytotherapy Research*, vol. 23, no. 5, pp. 608–613, 2009.

[33] C. Ling, J. Liang, C. Zhang et al., "Synergistic effects of salvianolic acid B and puerarin on cerebral ischemia reperfusion injury," *Molecules*, vol. 23, no. 3, p. 564, 2018.

[34] X. Fang, Y. Li, J. Qiao, Y. Guo, and M. Miao, "Neuroprotective effect of total flavonoids from Ilex pubescens against focal cerebral ischemia/reperfusion injury in rats," *Molecular Medicine Reports*, vol. 16, no. 5, pp. 7439–7449, 2017.

[35] Y. Yuan, M. Fang, C. Y. Wu, and E. A. Ling, "Scutellarin as a potential therapeutic agent for microglia-mediated neuroinflammation in cerebral ischemia," *Neuromolecular Medicine*, vol. 18, no. 3, pp. 264–273, 2016.

[36] C. Y. Wu, M. Fang, A. Karthikeyan, Y. Yuan, and E. A. Ling, "Scutellarin attenuates microglia-mediated neuroinflammation and promotes astrogliosis in cerebral ischemia-a therapeutic consideration," *Current Medicinal Chemistry*, vol. 24, no. 7, pp. 718–727, 2017.

[37] A. Wąsik and L. Antkiewicz-Michaluk, "The mechanism of neuroprotective action of natural compounds," *Pharmacological Reports*, vol. 69, no. 5, pp. 851–860, 2017.

[38] M. Daglia, A. Lorenzo, S. Nabavi, Z. Talas, and S. Nabavi, "Polyphenols: well beyond the antioxidant capacity: gallic acid and related compounds as neuroprotective agents: you are what you eat!," *Current Pharmaceutical Biotechnology*, vol. 15, no. 4, pp. 362–372, 2014.

[39] I. E. Orhan, M. Daglia, S. F. Nabavi, M. R. Loizzo, E. Sobarzo-Sanchez, and S. M. Nabavi, "Flavonoids and dementia: an update," *Current Medicinal Chemistry*, vol. 22, no. 8, pp. 1004–1015, 2015.

[40] A. Y. Chen and Y. C. Chen, "A review of the dietary flavonoid, kaempferol on human health and cancer chemoprevention," *Food Chemistry*, vol. 138, no. 4, pp. 2099–2107, 2013.

[41] N. S. Alrawaiq and A. Abdullah, "A review of flavonoid quercetin: metabolism, bioactivity and antioxidant properties," *International Journal of PharmTech Research*, vol. 6, no. 3, pp. 933–941, 2014.

[42] H. Hosseinzadeh and M. Nassiri-Asl, "Review of the protective effects of rutin on the metabolic function as an important dietary flavonoid," *Journal of Endocrinological Investigation*, vol. 37, no. 9, pp. 783–788, 2014.

[43] A. Liu, W. Wang, H. Fang et al., "Baicalein protects against polymicrobial sepsis-induced liver injury via inhibition of inflammation and apoptosis in mice," *European Journal of Pharmacology*, vol. 748, pp. 45–53, 2015.

[44] X. Ma, W. Yan, Z. Dai et al., "Baicalein suppresses metastasis of breast cancer cells by inhibiting EMT via downregulation of SATB1 and Wnt/β-catenin pathway," *Drug Design, Development and Therapy*, vol. 10, article 1419, 2016.

[45] Z. Huang, X. Pan, J. Zhou, W. T. Leung, C. Li, and L. Wang, "Chinese herbal medicine for acute upper respiratory tract infections and reproductive safety: a systematic review," *Bioscience Trends*, vol. 13, no. 2, pp. 117–129, 2019.

[46] M. J. Bae, H. S. Shin, H. J. See, S. Y. Jung, D. A. Kwon, and D. H. Shon, "Baicalein induces $CD4^{+}Foxp3^{+}$ T cells and enhances intestinal barrier function in a mouse model of food allergy," *Scientific Reports*, vol. 6, no. 1, pp. 1–11, 2016.

[47] Y. Amakura, A. Yoshimura, M. Yoshimura, and T. Yoshida, "Isolation and characterization of phenolic antioxidants from Plantago herb," *Molecules*, vol. 17, no. 5, pp. 5459–5466, 2012.

[48] Q. Cong, M. Shang, Q. Dong, W. Liao, F. Xiao, and K. Ding, "Structure and activities of a novel heteroxylan from *Cassia obtusifolia* seeds and its sulfated derivative," *Carbohydrate Research*, vol. 393, pp. 43–50, 2014.

[49] J. Ming, L. Zhuoneng, and Z. Guangxun, "Protective role of flavonoid baicalin from *Scutellaria baicalensis* in periodontal disease pathogenesis: A literature review," *Complementary Therapies in Medicine*, vol. 38, pp. 11–18, 2018.

[50] W. Y. Gong, Z. X. Zhao, B. J. Liu, L. W. Lu, and J. C. Dong, "Exploring the chemopreventive properties and perspectives of baicalin and its aglycone baicalein in solid tumors," *European Journal of Medicinal Chemistry*, vol. 126, pp. 844–852, 2017.

[51] J. R. Xiao, C. W. Do, and C. H. To, "Potential therapeutic effects of baicalein, baicalin, and wogonin in ocular disorders," *Journal of Ocular Pharmacology and Therapeutics*, vol. 30, no. 8, pp. 605–614, 2014.

[52] B. Dinda, S. Dinda, S. DasSharma, R. Banik, A. Chakraborty, and M. Dinda, "Therapeutic potentials of baicalin and its aglycone, baicalein against inflammatory disorders," *European Journal of Medicinal Chemistry*, vol. 131, pp. 68–80, 2017.

[53] J. Ru, P. Li, J. Wang et al., "TCMSP: a database of systems pharmacology for drug discovery from herbal medicines," *Journal of Cheminformatics*, vol. 6, no. 1, pp. 1–6, 2014.

[54] P. Matsson and J. Kihlberg, "How big is too big for cell permeability?," *Journal of Medicinal Chemistry*, vol. 60, no. 5, pp. 1662–1664, 2017.

[55] P. Ertl, B. Rohde, and P. Selzer, "Fast calculation of molecular polar surface area as a sum of fragment-based contributions and its application to the prediction of drug transport properties," *Journal of Medicinal Chemistry*, vol. 43, no. 20, pp. 3714–3717, 2000.

[56] M. H. N. Tattersall, J. E. Sodergren, S. K. Sengupta, D. H. Trites, E. J. Modest, and E. Frei III, "Pharmacokinetics of actinomycin 0 in patients with malignant melanoma," *Clinical Pharmacology and Therapeutics*, vol. 17, no. 6, pp. 701–708, 1975.

[57] W. Tao, X. Xu, X. Wang et al., "Network pharmacology-based prediction of the active ingredients and potential targets of Chinese herbal *Radix Curcumae* formula for application to cardiovascular disease," *Journal of Ethnopharmacology*, vol. 145, no. 1, pp. 1–10, 2013.

[58] V. N. Viswanadhan, A. K. Ghose, G. R. Revankar, and R. K. Robins, "Atomic physicochemical parameters for three dimensional structure directed quantitative structure-activity relationships. 4. Additional parameters for hydrophobic and dispersive interactions and their application for an automated superposition of certain naturally occurring nucleoside antibiotics," *Journal of Chemical Information and Modeling*, vol. 29, no. 3, pp. 163–172, 1989.

[59] J. Luo, H. Kong, M. Zhang et al., "Novel carbon dots-derived fromRadix PuerariaeCarbonisata significantly improve the solubility and bioavailability of baicalin," *Journal of Biomedical Nanotechnology*, vol. 15, no. 1, pp. 151–161, 2019.

[60] G. Zahra, B. Khadijeh, K. Mortaza, and S. Ali, "Potential therapeutic effects and bioavailability of wogonin, the flavone of Baikal skullcap," *Journal of Nutritional Medicine and Diet Care*, vol. 5, no. 2, p. 39, 2019.

[61] Y. Gao, S. A. Snyder, J. N. Smith, and Y. C. Chen, "Anticancer properties of baicalein: a review," *Medicinal Chemistry Research*, vol. 25, no. 8, pp. 1515–1523, 2016.

[62] R. Muto, T. Motozuka, M. Nakano, Y. Tatsumi, F. Sakamoto, and N. Kosaka, "The chemical structure of new substance as the metabolite of baicalin and time profiles for the plasma concentration after oral administration of sho-saiko-to in human," *Yakugaku Zasshi*, vol. 118, no. 3, pp. 79–87, 1998.

[63] M. Y. Lai, Y. C. Hou, S. L. Hsiu, C. C. Chen, and P. D. L. Chao, "Relative flavone bioavailability of Scutellariae Radix between traditional decoction and commercial powder preparation in humans," *Journal of Food and Drug Analysis*, vol. 10, no. 2, 2002.

[64] S. Tian, G. He, J. Song et al., "Pharmacokinetic study of baicalein after oral administration in monkeys," *Fitoterapia*, vol. 83, no. 3, pp. 532–540, 2012.

[65] T. Huang, Y. Liu, and C. Zhang, "Pharmacokinetics and bioavailability enhancement of baicalin: a review," *European Journal of Drug Metabolism and Pharmacokinetics*, vol. 44, no. 2, pp. 159–168, 2019.

[66] Y. Tang, H. Zhu, Y. Zhang, and C. Huang, "Determination of human plasma protein binding of baicalin by ultrafiltration and high-performance liquid chromatography," *Biomedical Chromatography*, vol. 20, no. 10, pp. 1116–1119, 2006.

[67] H. Pang, W. Xue, A. Shi et al., "Multiple-ascending-dose pharmacokinetics and safety evaluation of baicalein chewable tablets in healthy Chinese volunteers," *Clinical Drug Investigation*, vol. 36, no. 9, pp. 713–724, 2016.

[68] M. Li, A. Shi, H. Pang et al., "Safety, tolerability, and pharmacokinetics of a single ascending dose of baicalein chewable tablets in healthy subjects," *Journal of Ethnopharmacology*, vol. 156, pp. 210–215, 2014.

[69] W. W. Chen, X. Zhang, and W. J. Huang, "Role of neuroinflammation in neurodegenerative diseases (Review)," *Molecular Medicine Reports*, vol. 13, no. 4, pp. 3391–3396, 2016.

[70] S. DiMauro and E. A. Schon, "Mitochondrial disorders in the nervous system," *Annual Review of Neuroscience*, vol. 31, no. 1, pp. 91–123, 2008.

[71] R. Lardenoije, A. Iatrou, G. Kenis et al., "The epigenetics of aging and neurodegeneration," *Progress in Neurobiology*, vol. 131, pp. 21–64, 2015.

[72] A. Ciechanover and Y. T. Kwon, "Degradation of misfolded proteins in neurodegenerative diseases: therapeutic targets and strategies," *Experimental & Molecular Medicine*, vol. 47, no. 3, article e147, 2015.

[73] Z. Liu, T. Zhou, A. C. Ziegler, P. Dimitrion, and L. Zuo, "Oxidative stress in neurodegenerative diseases: from molecular mechanisms to clinical applications," *Oxidative Medicine and Cellular Longevity*, vol. 2017, Article ID 2525967, 11 pages, 2017.

[74] M. Vila and S. Przedborski, "Targeting programmed cell death in neurodegenerative diseases," *Nature Reviews Neuroscience*, vol. 4, no. 5, pp. 365–375, 2003.

[75] G. A. Donnan, M. Fisher, M. Macleod, and S. M. Davis, "Stroke," *Lancet*, vol. 371, no. 9624, pp. 1612–1623, 2008.

[76] H. Z. Xu and Y. Z. Le, "Significance of outer blood–retina barrier breakdown in diabetes and ischemia," *Investigative Ophthalmology & Visual Science*, vol. 52, no. 5, pp. 2160–2164, 2011.

[77] U. Dirnagl, C. Iadecola, and M. A. Moskowitz, "Pathobiology of ischaemic stroke: an integrated view," *Trends in Neurosciences*, vol. 22, no. 9, pp. 391–397, 1999.

[78] B. P. Gaire, "Herbal medicine in ischemic stroke: challenges and prospective," *Chinese Journal of Integrative Medicine*, vol. 24, no. 4, pp. 243–246, 2018.

[79] H. Chen, H. Yoshioka, G. S. Kim et al., "Oxidative stress in ischemic brain damage: mechanisms of cell death and potential molecular targets for neuroprotection," *Antioxidants & Redox Signaling*, vol. 14, no. 8, pp. 1505–1517, 2011.

[80] H. M. Honda, P. Korge, and J. N. Weiss, "Mitochondria and ischemia/reperfusion injury," *Annals of the New York Academy of Sciences*, vol. 1047, no. 1, pp. 248–258, 2005.

[81] T. M. Woodruff, J. Thundyil, S.-C. Tang, C. G. Sobey, S. M. Taylor, and T. V. Arumugam, "Pathophysiology, treatment, and animal and cellular models of human ischemic stroke," *Molecular Neurodegeneration*, vol. 6, no. 1, p. 11, 2011.

[82] L. Guzman-Martinez, R. B. Maccioni, V. Andrade, L. P. Navarrete, M. G. Pastor, and N. Ramos-Escobar, "Neuroinflammation as a common feature of neurodegenerative disorders," *Frontiers in Pharmacology*, vol. 10, article 1008, 2019.

[83] R. L. Jayaraj, S. Azimullah, R. Beiram, F. Y. Jalal, and G. A. Rosenberg, "Neuroinflammation: friend and foe for ischemic stroke," *Journal of Neuroinflammation*, vol. 16, no. 1, p. 142, 2019.

[84] H. S. Kwon and S. H. Koh, "Neuroinflammation in neurodegenerative disorders: the roles of microglia and astrocytes," *Translational Neurodegeneration*, vol. 9, no. 1, p. 42, 2020.

[85] H. Zhang, X. Xiong, L. Gu, W. Xie, and H. Zhao, "CD4 T cell deficiency attenuates ischemic stroke, inhibits oxidative stress, and enhances Akt/mTOR survival signaling pathways in mice," *Chinese Neurosurgical Journal*, vol. 4, no. 1, p. 32, 2018.

[86] A. Khanna, K. T. Kahle, B. P. Walcott, V. Gerzanich, and J. M. Simard, "Disruption of ion homeostasis in the neurogliovascular unit underlies the pathogenesis of ischemic cerebral edema," *Translational Stroke Research*, vol. 5, no. 1, pp. 3–16, 2014.

[87] S. J. Coultrap, R. S. Vest, N. M. Ashpole, A. Hudmon, and K. U. Bayer, "CaMKII in cerebral ischemia," *Acta Pharmacologica Sinica*, vol. 32, no. 7, pp. 861–872, 2011.

[88] A. W. Siu, M. K. Lau, J. S. Cheng et al., "Glutamate-induced retinal lipid and protein damage: the protective effects of catechin," *Neuroscience Letters*, vol. 432, no. 3, pp. 193–197, 2008.

[89] T. Tao, M. Liu, M. Chen et al., "Natural medicine in neuroprotection for ischemic stroke: challenges and prospective," *Pharmacology & Therapeutics*, vol. 216, article 107695, 2020.

[90] D. Radak, N. Katsiki, I. Resanovic et al., "Apoptosis and acute brain ischemia in ischemic stroke," *Current Vascular Pharmacology*, vol. 15, no. 2, pp. 115–122, 2017.

[91] M. Yousufuddin and N. Young, "Aging and ischemic stroke," *Aging*, vol. 11, no. 9, pp. 2542–2544, 2019.

[92] K. van Leyen, H. Y. Kim, S. R. Lee, G. Jin, K. Arai, and E. H. Lo, "Baicalein and 12/15-lipoxygenase in the ischemic brain," *Stroke*, vol. 37, no. 12, pp. 3014–3018, 2006.

[93] P. A. Lapchak, P. Maher, D. Schubert, and J. A. Zivin, "Baicalein, an antioxidant 12/15-lipoxygenase inhibitor improves clinical rating scores following multiple infarct embolic strokes," *Neuroscience*, vol. 150, no. 3, pp. 585–591, 2007.

[94] C. Liu, J. Wu, K. Xu et al., "Neuroprotection by baicalein in ischemic brain injury involves PTEN/AKT pathway," *Journal of Neurochemistry*, vol. 112, no. 6, pp. 1500–1512, 2010.

[95] H. Kuhn, S. Banthiya, and K. van Leyen, "Mammalian lipoxygenases and their biological relevance," *Biochimica et Biophysica Acta (BBA) - Molecular and Cell Biology of Lipids*, vol. 1851, no. 4, pp. 308–330, 2015.

[96] N. K. Singh and G. N. Rao, "Emerging role of 12/15-lipoxygenase (ALOX15) in human pathologies," *Progress in Lipid Research*, vol. 73, pp. 28–45, 2019.

[97] D. Son, P. Lee, J. Lee, H. Kim, and S. Y. Kim, "Neuroprotective effect of wogonin in hippocampal slice culture exposed to oxygen and glucose deprivation," *European Journal of Pharmacology*, vol. 493, no. 1-3, pp. 99–102, 2004.

[98] J. Cho and H. K. Lee, "Wogonin inhibits excitotoxic and oxidative neuronal damage in primary cultured rat cortical cells," *European Journal of Pharmacology*, vol. 485, no. 1-3, pp. 105–110, 2004.

[99] H. Y. Li, J. Hu, S. Zhao et al., "Comparative Study of the Effect of Baicalin and Its Natural Analogs on Neurons with Oxygen and Glucose Deprivation Involving Innate Immune Reaction of TLR2/TNFα," *Journal of Biomedicine and Biotechnology*, vol. 2012, Article ID 267890, 9 pages, 2012.

[100] P. Wang, Y. Cao, J. Yu et al., "Baicalin alleviates ischemia-induced memory impairment by inhibiting the phosphorylation of CaMKII in hippocampus," *Brain Research*, vol. 1642, pp. 95–103, 2016.

[101] O. Cheng, Z. Li, Y. Han, Q. Jiang, Y. Yan, and K. Cheng, "Baicalin improved the spatial learning ability of global ischemia/reperfusion rats by reducing hippocampal apoptosis," *Brain Research*, vol. 1470, pp. 111–118, 2012.

[102] H. T. Lu, R. Q. Feng, J. K. Tang, J. J. Zhou, F. Gao, and J. Ren, "CaMKII/calpain interaction mediates ischemia/reperfusion injury in isolated rat hearts," *Cell Death & Disease*, vol. 11, no. 5, p. 388, 2020.

[103] J. Dai, L. Chen, Y. M. Qiu et al., "Activations of GABAergic signaling, HSP70 and MAPK cascades are involved in baicalin's neuroprotection against gerbil global ischemia/reperfusion injury," *Brain Research Bulletin*, vol. 90, pp. 1–9, 2013.

[104] S. Demyanenko, V. Nikul, S. Rodkin, A. Davletshin, M. B. Evgen'ev, and D. G. Garbuz, "Exogenous recombinant Hsp70 mediates neuroprotection after photothrombotic stroke," *Cell Stress & Chaperones*, vol. 26, no. 1, pp. 103–114, 2021.

[105] K. Nozaki, M. Nishimura, and N. Hashimoto, "Mitogen-activated protein kinases and cerebral ischemia," *Molecular Neurobiology*, vol. 23, no. 1, pp. 01–20, 2001.

[106] X. K. Tu, W. Z. Yang, S. S. Shi et al., "Baicalin inhibits TLR2/4 signaling pathway in rat brain following permanent cerebral ischemia," *Inflammation*, vol. 34, no. 5, pp. 463–470, 2011.

[107] X. Xue, X. J. Qu, Y. Yang et al., "Baicalin attenuates focal cerebral ischemic reperfusion injury through inhibition of nuclear factor κB p65 activation," *Biochemical and Biophysical Research Communications*, vol. 403, no. 3-4, pp. 398–404, 2010.

[108] X. K. Tu, W. Z. Yang, S. S. Shi, C. H. Wang, and C. M. Chen, "Neuroprotective effect of baicalin in a rat model of permanent focal cerebral ischemia," *Neurochemical Research*, vol. 34, no. 9, pp. 1626–1634, 2009.

[109] S. Yang, H. Wang, Y. Yang et al., "Baicalein administered in the subacute phase ameliorates ischemia-reperfusion-induced brain injury by reducing neuroinflammation and neuronal damage," *Biomedicine & Pharmacotherapy*, vol. 117, article 109102, 2019.

[110] K. Yigitkanli, A. Pekcec, H. Karatas et al., "Inhibition of 12/15-lipoxygenase as therapeutic strategy to treat stroke," *Annals of Neurology*, vol. 73, no. 1, pp. 129–135, 2013.

[111] G. Jin, K. Arai, Y. Murata et al., "Protecting against cerebrovascular injury: contributions of 12/15-lipoxygenase to edema formation after transient focal ischemia," *Stroke*, vol. 39, no. 9, pp. 2538–2543, 2008.

[112] L. Cui, X. Zhang, R. Yang et al., "Baicalein is neuroprotective in rat MCAO model: role of 12/15-lipoxygenase, mitogen-activated protein kinase and cytosolic phospholipase A2," *Pharmacology, Biochemistry, and Behavior*, vol. 96, no. 4, pp. 469–475, 2010.

[113] S. Pallast, K. Arai, A. Pekcec et al., "Increased nuclear apoptosis-inducing factor after transient focal ischemia: a 12/15-lipoxygenase-dependent organelle damage pathway," *Journal of Cerebral Blood Flow and Metabolism*, vol. 30, no. 6, pp. 1157–1167, 2010.

[114] W. H. Li, Y. L. Yang, X. Cheng et al., "Baicalein attenuates caspase-independent cells death via inhibiting PARP-1 activation and AIF nuclear translocation in cerebral ischemia/reperfusion rats," *Apoptosis*, vol. 25, no. 5-6, pp. 354–369, 2020.

[115] D. Stephenson, K. Rash, B. Smalstig et al., "Cytosolic phospholipase A2 is induced in reactive glia following different forms of neurodegeneration," *Glia*, vol. 27, no. 2, pp. 110–128, 1999.

[116] Y. W. Xu, L. Sun, H. Liang, G. M. Sun, and Y. Cheng, "12/15-Lipoxygenase inhibitor baicalein suppresses PPARγ expression and nuclear translocation induced by cerebral ischemia/reperfusion," *Brain Research*, vol. 1307, pp. 149–157, 2010.

[117] H. Lee, Y. O. Kim, H. Kim et al., "Flavonoid wogonin from medicinal herb is neuroprotective by inhibiting inflammatory activation of microglia," *The FASEB Journal*, vol. 17, no. 13, pp. 1–21, 2003.

[118] J. Cho and H. K. Lee, "Wogonin inhibits ischemic brain injury in a rat model of permanent middle cerebral artery occlusion," *Biological & Pharmaceutical Bulletin*, vol. 27, no. 10, pp. 1561–1564, 2004.

[119] Z. Kong, Q. Shen, J. Jiang, M. Deng, Z. Zhang, and G. Wang, "Wogonin improves functional neuroprotection for acute cerebral ischemia in rats by promoting angiogenesis via TGF-β1," *Annals of Translational Medicine*, vol. 7, no. 22, pp. 639–639, 2019.

[120] P. A. Guerrero and J. H. McCarty, *TGF-β Activation and Signaling in Angiogenesis*, IntechOpen, 2017.

[121] J. T. Qu, D. X. Zhang, F. Liu et al., "Vasodilatory effect of wogonin on the rat aorta and its mechanism study," *Biological & Pharmaceutical Bulletin*, vol. 38, no. 12, pp. 1873–1878, 2015.

[122] J. H. Liu, H. Wann, M. M. Chen et al., "Baicalein significantly protects human retinal pigment epithelium cells against H_2O_2-Induced oxidative stress by scavenging reactive oxygen species and downregulating the expression of matrix metalloproteinase-9 and vascular endothelial growth factor," *Journal of Ocular Pharmacology and Therapeutics*, vol. 26, no. 5, pp. 421–429, 2010.

[123] H. M. Chao, M. J. Chuang, J. H. Liu et al., "Baicalein protects against retinal ischemia by antioxidation, antiapoptosis, downregulation of HIF-1α, VEGF, and MMP-9 and upregulation of HO-1," *Journal of Ocular Pharmacology and Therapeutics*, vol. 29, no. 6, pp. 539–549, 2013.

[124] N. Nakamura, S. Hayasaka, X. Y. Zhang et al., "Effects of baicalin, baicalein, and wogonin on interleukin-6 and interleukin-8 expression, and nuclear factor-κb binding activities induced by interleukin-1β in human retinal pigment epithelial cell line," *Experimental Eye Research*, vol. 77, no. 2, pp. 195–202, 2003.

[125] C. Chen, D. Guo, and G. Lu, "Wogonin protects human retinal pigment epithelium cells from LPS-induced barrier dysfunction and inflammatory responses by regulating the TLR4/NF-κB signaling pathway," *Molecular Medicine Reports*, vol. 15, no. 4, pp. 2289–2295, 2017.

[126] T. Yoshikawa, N. Ogata, H. Izuta, M. Shimazawa, H. Hara, and K. Takahashi, "Increased expression of tight junctions in ARPE-19 cells under endoplasmic reticulum stress," *Current Eye Research*, vol. 36, no. 12, pp. 1153–1163, 2011.

[127] C. Dai, S. Jiang, C. Chu, M. Xin, X. Song, and B. Zhao, "Baicalin protects human retinal pigment epithelial cell lines against high glucose-induced cell injury by up-regulation of microRNA-145," *Experimental and Molecular Pathology*, vol. 106, pp. 123–130, 2019.

[128] S. H. Jung, K. D. Kang, D. Ji et al., "The flavonoid baicalin counteracts ischemic and oxidative insults to retinal cells and lipid peroxidation to brain membranes," *Neurochemistry International*, vol. 53, no. 6-8, pp. 325–337, 2008.

[129] D. Kaur, V. Sharma, and R. Deshmukh, "Activation of microglia and astrocytes: a roadway to neuroinflammation and Alzheimer's disease," *Inflammopharmacology*, vol. 27, no. 4, pp. 663–677, 2019.

[130] L. P. Yang, H. L. Sun, L. M. Wu et al., "Baicalein reduces inflammatory process in a rodent model of diabetic retinopathy," *Investigative Ophthalmology & Visual Science*, vol. 50, no. 5, pp. 2319–2327, 2009.

[131] X. J. Wang, C. S. Liu, and Z. X. Li, "The effect of baicalin on tissue aldose reductase activity and retinal apoptosis in diabetic rats," *Chinese Journal of Diabetes*, vol. 16, no. 8, p. 26, 2008.

[132] A. Othman, S. Ahmad, S. Megyerdi et al., "12/15-Lipoxygenase-derived lipid metabolites induce retinal endothelial cell barrier dysfunction: contribution of NADPH oxidase," *PLoS One*, vol. 8, no. 2, article e57254, 2013.

[133] B. Uttara, A. Singh, P. Zamboni, and R. Mahajan, "Oxidative stress and neurodegenerative diseases: a review of upstream and downstream antioxidant therapeutic options," *Current Neuropharmacology*, vol. 7, no. 1, pp. 65–74, 2009.

[134] K. van Leyen, T. R. Holman, and D. J. Maloney, "The potential of 12/15-lipoxygenase inhibitors in stroke therapy," *Future Medicinal Chemistry*, vol. 6, no. 17, pp. 1853–1855, 2014.

[135] Y. Liu, Y. Zheng, H. Karatas et al., "12/15-lipoxygenase inhibition or knockout reduces warfarin-associated hemorrhagic transformation after experimental stroke," *Stroke*, vol. 48, no. 2, pp. 445–451, 2017.

[136] H. Karatas and C. Cakir-Aktas, "12/15 lipoxygenase as a therapeutic target in brain disorders," *Noro Psikiyatri Arsivi*, vol. 56, no. 4, pp. 288–291, 2019.

[137] Y. Tang, Z. Xiao, L. Pan et al., "Therapeutic targeting of retinal immune microenvironment with CSF-1 receptor antibody promotes visual function recovery after ischemic optic neuropathy," *Frontiers in Immunology*, vol. 11, article 585918, 2020.

[138] N. Hanioka, T. Isobe, T. Tanaka-Kagawa, and S. Ohkawara, "Wogonin glucuronidation in liver and intestinal microsomes of humans, monkeys, dogs, rats, and mice," *Xenobiotica*, vol. 50, no. 8, pp. 906–912, 2020.

Hindawi
Oxidative Medicine and Cellular Longevity
Volume 2021, Article ID 5524705, 13 pages
https://doi.org/10.1155/2021/5524705

Research Article

Supplemental N-3 Polyunsaturated Fatty Acids Limit A1-Specific Astrocyte Polarization via Attenuating Mitochondrial Dysfunction in Ischemic Stroke in Mice

Jun Cao,[1,2] **Lijun Dong**,[3,4] **Jialiang Luo**,[4] **Fanning Zeng**,[5] **Zexuan Hong**,[5] **Yunzhi Liu**,[4] **YiBo Zhao**,[4] **Zhengyuan Xia**,[6] **Daming Zuo**,[4,7] **Li Xu**,[7] **and Tao Tao**[1]

[1]*Department of Anesthesiology, Central People's Hospital of Zhanjiang, Zhanjiang, Guangdong 524045, China*
[2]*Department of Anesthesiology, Affiliated Shenzhen Maternity and Child Healthcare Hospital, Southern Medical University, Shenzhen, Guangdong 518000, China*
[3]*The Fifth Affiliated Hospital, Southern Medical University, Guangzhou, Guangdong 510900, China*
[4]*Department of Medical Laboratory, School of Laboratory Medicine and Biotechnology, Southern Medical University, Guangzhou, Guangdong 510515, China*
[5]*Department of Anesthesiology, Nanfang Hospital, Southern Medical University, Guangzhou 510515, China*
[6]*State Key Laboratory of Pharmaceutical Biotechnology, The University of Hong Kong, Hong Kong, China*
[7]*Department of Neurosurgery II, Central People's Hospital of Zhanjiang, Zhanjiang, Guangdong 524045, China*

Correspondence should be addressed to Li Xu; xuliniu@126.com and Tao Tao; taotaomzk@smu.edu.cn

Received 9 January 2021; Revised 17 April 2021; Accepted 12 May 2021; Published 10 June 2021

Academic Editor: Hai-tao Xiao

Ischemic stroke is one of the leading causes of death and disability for adults, which lacks effective treatments. Dietary intake of n-3 polyunsaturated fatty acids (n-3 PUFAs) exerts beneficial effects on ischemic stroke by attenuating neuron death and inflammation induced by microglial activation. However, the impact and mechanism of n-3 PUFAs on astrocyte function during stroke have not yet been well investigated. Our current study found that dietary n-3 PUFAs decreased the infarction volume and improved the neurofunction in the mice model of transient middle cerebral artery occlusion (tMCAO). Notably, n-3 PUFAs reduced the stroke-induced A1 astrocyte polarization both in vivo and in vitro. We have demonstrated that exogenous n-3 PUFAs attenuated mitochondrial oxidative stress and increased the mitophagy of astrocytes in the condition of hypoxia. Furthermore, we provided evidence that treatment with the mitochondrial-derived antioxidant, mito-TEMPO, abrogated the n-3 PUFA-mediated regulation of A1 astrocyte polarization upon hypoxia treatment. Together, this study highlighted that n-3 PUFAs prevent mitochondrial dysfunction, thereby limiting A1-specific astrocyte polarization and subsequently improving the neurological outcomes of mice with ischemic stroke.

1. Introduction

Ischemic stroke is caused by interruption of the blood supply to a part of the brain leading to the sudden loss of function, which now is one of the leading causes of death and disability worldwide [1]. As the most abundant and diverse glial cells in the brain, astrocytes are believed to play a crucial role in neuroinflammation and the pathogenesis of ischemic neuronal death. In the condition of an acute ischemic stroke, the proliferated reactive astrocytes in the peri-infarct areas are favourable for maintaining neuronal homeostasis. An increasing number of studies indicate that in the acute phase of ischemic stroke, astrocytes limit brain damage by activation and glial scar formation [2], modulate neuroinflammation by releasing cytokines [3], reconstruct the blood-brain barrier by reestablishment of the astrocytic water channels [4], and affect the neuron survival by metabolic substrates [5, 6] and signalling molecule transfer [7]. In addition to such functional diversity, the transcripts of reactive astrocytes are also different. According to the transcripts, the reactive

astrocytes are further classified into A1 astrocytes and A2 astrocytes, which exhibit temporal and functional specificity in ischemic stroke [8]. After nerve injury, A1 astrocytes can release inflammatory cytokines and neurotoxins that induce cellular and neuronal apoptosis in the brain, while A2 astrocytes promote neuronal survival and tissue repair by secreting several trophic factors. Therefore, it is important to investigate the proliferation and function of these two reactive astrocyte subtypes in the acute phase of cerebral ischemia.

N-3 polyunsaturated fatty acids (n-3 PUFAs), mainly including docosahexaenoic acid (DHA) and eicosapentaenoic acid (EPA), are essential to human health [9]. The brain is highly enriched with the essential n-3 PUFAs, especially DHA, which plays a fundamental role in the normal development and function of the central nervus system [10]. DHA, a major form of n-3 PUFAs in the brain, cannot be generated in vivo, being supplied instead from a constant of food such as fish oil [11]. Diet supplementation of n-3 PUFAs is well documented to elevate brain levels of DHA. In the past decades, a series of epidemiological studies and clinical trials have suggested that increasing dietary intake or nutritional supplementation of n-3 PUFAs is closely associated with a reduced risk to or therapeutic effects in various neurological disorders [12, 13]. Diet supplementation of n-3 PUFAs exerts beneficial effects on ischemic stroke as well [14]. Poststroke n-3 PUFA therapeutic regimen protects against neuronal loss in the grey matter and promotes white matter integrity. N-3 PUFAs reduce the infarction volume by attenuating reactive oxygen species (ROS) activation in neurons [15]. Moreover, n-3 PUFAs exhibit neuroprotection by anti-inflammation relied on its modification of microglia/macrophage plasticity in cerebral ischemia injury [16]. DHA enhances macrophage phenotypic shift toward an anti-inflammatory phenotype to reduced central and peripheral inflammation after stroke. Begum et al. reported that DHA has protective effects in cultural astrocytes in vitro ischemia by suppressing calcium dysregulation and ER stress [17]. However, the effects and mechanism of n-3 PUFAs on astrocytes and its potential function in stroke have not yet been well reported.

Our present study evaluated the efficiency of n-3 PUFA supplement in the transient cerebral ischemia model and investigated the impact of n-3 PUFAs on astrocytes. Our results showed that n-3 PUFA feeding improved stroke outcomes during the acute phase of cerebral ischemia associated with astrocyte plasticity. Dietary n-3 PUFA supplement upregulated the transcripts of A1-specific astrocytes, which is related to mitochondrial damage-related oxidative stress.

2. Materials and Methods

2.1. Animals. Male C57/BL6 mice (22 ± 2 g, Specific Pathogen Free, 8 weeks old) were obtained from the central animal facility of Southern Medical University (Guangzhou, China). The animals were housed under standard conditions of light and dark cycles (12 h : 12 h, temperature 25°C) with free access to food and water. In addition, the cages were regularly cleaned. All the animal studies were carried out according to the approved protocols and guidelines of the Institutional Animal Ethical Care Committee of Southern Medical University Experimental Animal Centre.

2.2. Transient Middle Cerebral Artery Occlusion Model Establishment. Establishment of the transient middle cerebral artery occlusion (tMCAO) model has been described in our previous article [18]. Briefly, mice were anesthetized with continuous inhalation of sevoflurane (2%-5%); the inner and outer muscles of the sternocleidomastoid muscle were separated to expose and isolate the right common, external, and internal carotid arteries. Subsequently, the superior thyroid and occipital arteries were separated and cauterized using a preheated electrocautery to prevent bleeding. The model was established by inserting a monofilament (approximately 2 cm) from the external carotid artery to the middle cerebral artery, avoiding the pterygopalatine artery. After the monofilament was inserted for 1.5 hours of ischemia, the monofilament was gently pulled out to form reperfusion. The wound was disinfected with iodine and sutured. To test the beneficent effect of n-3 PUFAs in the mice model of tMCAO, the mice were fed with an n-3 PUFA-enriched diet (concentration of DHA reaching 39.6%) 7 days before tMCAO procedure, as previously described [19].

2.3. Cell Treatment. Primary cultural astrocytes were subjected to oxygen and glucose deprivation (OGD) followed by reoxygenation, to mimic the ischemic/reperfusion-like condition in vitro. To induce OGD, the primary astrocytes were incubated with glucose-free DMEM and placed within a hypoxic chamber which was continuously maintained with 95% N_2 and 5% CO_2 at 37°C to obtain 1% O_2 for 5 h. OGD was terminated by replacing the medium to DMEM/F12 with 10% FBS for 12 hours. Cells incubated in DMEM/F12 with 10% FBS under a normoxic atmosphere were used as the normoxic control. The cells were pretreated with 20 μM docosahexaenoic acid (DHA) (Sigma, USA) for 6 hours before OGD. Subsequently, the A1/A2-associated genes were assessed. In some cases, cells were pretreated with 2 μM mitochondria-targeted antioxidant (Mito-TEMPO) (Merck, USA) for 24 hours.

2.4. Infarct Volume Analysis. TTC (2,3,5-Triphenyltetrazolium chloride) staining was used to reflect cerebral infarction as a percentage of brain volume. The mice were anesthetized and the integral brains were quickly obtained and cut into 2 mm tissue slices, then stained with 2% TTC for 5 minutes and soaked in 4% formaldehyde for 6 hours. The brain slices were arranged in order and photographed. The area of cerebral infarction was calculated using the Image J 1.52a (the red area indicated no infarction; the white area indicated infarction). The infarct area was calculated as the area of the nonischemic hemisphere minus the noninfarcted area of the ischemic hemisphere. Infarct volume = infarct area × thickness (2 mm). The percent of cerebral infarction was calculated using the following formula: The percentage of cerebral infarction = infarct volume/the volume of the nonischemic hemisphere × 100%.

2.5. Rotarod Test. Sensorimotor functions were accessed by rotarod test after stroke. All mice were trained for 2 days

before the model establishment (each mouse was tested twice and the speed of rotation was 5 rpm for 10 minutes). During rotarod testing, the speed of rotation was accelerated from 5 to 15 rpm over 60 seconds with a testing period cut-off of 300 seconds for each trial and 2 total trials performed. The fall latency of each mouse was recorded and averaged. The experimenter was blinded to the treatments given to each mouse.

2.6. Neurological Scoring. The neurological evaluation was conducted based on the Garcia scale as illustrated in Supplementary Table 1. The Garcia scale was divided into 6 subjects, including spontaneous activity, symmetry in movement of 4 limbs, forepaw outstretching, climbing, body proprioception, and vibrissae touch. The mice demonstrated normal neurological functions were assigned as the highest score (18 scores), and the severe functional impaired rats were assigned as the lowest score (0 score).

2.7. Primary Astrocyte Culture. Astrocytes were harvested from both the cortices of C57/BL6 on postnatal day (P1 to P3). Briefly, the brain tissue was collected and digested with 0.25% trypsin and Dnase I (ROCHE, USA) in 37°C for 10 minutes. Then, cells were suspended in single cells and cultured in Dulbecco's Modified Eagle's medium (DMEM)/F12 with 10% fetal bovine serum which was heat inactivation in 56°C for 30 minutes beforehand, then incubated at 37°C and 5% CO_2. The culture medium was then replaced twice a day.

2.8. Immunofluorescence Staining and Quantification. At 1 day after tMCAO, animals were euthanized and perfused with saline followed with phosphate-buffered saline (PBS) containing 4% paraformaldehyde (PFA, Sigma-Aldrich). Brains were removed and cut into 20 μm frozen cryosections using a microtome. Brain sections were fixed for 10 minutes in 4% paraformaldehyde (Solarbio, China) at room temperature, then permeabilized and blocked with 0.5% TritonX-100 (Sigma-Aldrich) and 3% bovine serum albumin (BSA, Solarbio, China) for 1 h at room temperature. Next, the brain sections were incubated with primary antibodies against S100β (1 : 200 dilution, Proteintech, China) and C3 (complement 3) (1 : 250 dilution, Abcam, USA) at 4°C overnight. The brain slices were washed three times with PBS-Tween-20 (0.1% *v*/*v*) and were incubated for 1 hour at room temperature with fluorescently labelled secondary antibodies including FITC-conjugated goat anti-mouse IgG (1 : 100 dilution, Bioss, China), Cy3-conjugated goat anti-mouse IgG (1 : 100 dilution, Bioss, China), and Cy3-conjugated goat anti-rabbit IgG (1 : 100 dilution, Bioss, China). After washing, cells were counterstained with DAPI (Solarbio, China) and analyzed using laser-scanning confocal microscopy (LSM900, Japan). Immunopositive cell quantifications were performed with the software of Image J software 1.52a by an investigator who was blinded to the experimental design.

Primary cultural astrocytes were washed once with PBS, fixed for 30 minutes in 4% paraformaldehyde (Solarbio, China) at 37°C and permeabilized with 0.5% Triton X-100 (Sigma-Aldrich) for 10 minutes. After 5 min wash with PBS three times, the cells were blocked with 1% bovine serum albumin (BSA, Solarbio, China) for 1 hour at room temperature. Cells were incubated overnight at 4°C with primary antibodies against S100β (1 : 300 dilution, Proteintech, China) or C3 (1 : 300 dilution, Gentex, Switzerland). The cells were washed three times with PBS-Tween-20 (0.1% *v*/*v*) and were incubated for 1 hour at room temperature with fluorescently labelled secondary antibodies the same as brain section immunofluorescence mentioned above.

2.9. RNA Extraction and Quantitative Real-Time PCR (qRT-PCR). Total RNA was isolated from primary astrocytes using TRIzol reagent (Thermo Fisher Scientific, United States) according to the manufacturer's instructions. Total RNA (1 mg) was used to synthesize cDNA using a PrimeScript RT reagent Kit with gDNA Eraser (TaKaRa, China). Expression of mRNA was determined by quantitative real-time PCR (qRT-PCR) using the TB Green Premix Ex Taq II (TaKaRa, China). QRT-PCR was performed on the ABI QuantStudio 6 flex (Applied Biosystems, United States). β-Actin expression was quantified as internal control for mRNA analysis. The primer sequences used in these analyses can be found in the Supplementary Table 2. The results of the analyses were calculated and expressed according to an equation ($2^{-\Delta\Delta Ct}$) which provides the amount of the targets, normalized to an internal reference. Ct is a threshold cycle for target amplification. Each biological sample was tested in triplicate.

2.10. Western Blot. Astrocytes or brain tissues were digested in RIPA extraction buffer (Beyotime, China). Protein samples were separated by 8% SDS-PAGE and transferred onto PVDF (polyvinylidene difluoride) membranes (Millipore, United States) in tank transfer system (Bio-Rad, United States). Membranes were blocked with 5% nonfat milk in Tris-buffered saline containing 0.1% Tween-20 (TBST) for 1 hour, washed three times in TBST, and incubated overnight at 4°C with primary antibodies against C3 (1 : 1000 dilution, Abcam, USA) or β-actin (1 : 1000 dilution, Abcam, USA). After incubation with the HRP-conjugated goat anti-rabbit IgG secondary antibody (1 : 10000 dilution, Da-UN, China), immunoreactive bands were detected by enhanced chemiluminescence (Millipore, United States). The protein bands were quantitatively analysed using ImageJ software 1.52a.

2.11. JC-1 Analysis. Briefly, cells were washed with PBS and suspended in 1 ml fresh medium containing 1 μM JC-1 for 20 minutes at 37°C in the dark. After washing with PBS twice, the fluorescence intensity was captured with an inverted fluorescence microscopy (Nikon, Japan). For red fluorescence, the fluorescence intensity was measured at Ex/Em: 525/590 nm. The green fluorescence intensity was measured at Ex/Em: 490/530 nm.

2.12. Mito-Tracker Staining. The cells were washed twice with PBS and labelled at 37°C for 30 minutes with 400 nM MitoTracker Green (Ex 490 nm/Em 516 nm). Cells were then washed with PBS and incubated with Hoechst 33342 (1 μg/ml) for 10 minutes at room temperature. Fluorescence was detected on a Nikon A1R scanning laser confocal microscope (Nikon, Tokyo, Japan). Fluorescence was detected on a

Nikon A1R scanning laser confocal microscope (Nikon Corporation, Tokyo, Japan). The images were analysed using an image analysis system (Image-Pro Plus, version 6.0) with the Mitochondrial Network Analysis (MiNA) toolset according to a previously article [20].

2.13. Mito-SOX Staining. For Mito-SOX staining, astrocytes were harvested and stained with 5 μM dye for 10 minutes at 37°C. The stained cells were excited at 510 nm, and the emitted fluorescence was detected at 580 nm by flow cytometry or confocal microscope.

2.14. Statistical Analysis. Data are expressed as mean ± SD. Differences were evaluated by one-way analysis of variance (ANOVA; three or more groups). $p < 0.05$ was considered statistical significance. Statistical analyses were performed using SPSS 22.0 Statistics (IBM SPSS Statistics for Version 22.0, IBM Corp, North Castle, NY, USA).

3. Results

3.1. Dietary n-3 PUFA Supplement Improved Infarction and Functional Outcomes after tMCAO. The experimental schedule was shown in Figure 1(a). In order to estimate whether dietary n-3 PUFAs reduce infarction and improve neurofunctional recovery after tMCAO, we used TTC staining, neurobehavioral test, and neurological scores to assess brain injury in mice. As shown in Figure 1(b), n-3 PUFA feeding significantly decreased the infarct volume in the mice model of tMCAO. The rotation duration of the sham group (194.8 ± 13.4 s and 185.2 ± 12.1 s) was longer than that of the tMCAO group (55.4 ± 10.1 s and 59.8 ± 11.2 s) on day 1 and day 3 after surgery (Figure 1(c)). Additionally, the neurological functions of n-3 PUFA-treated tMCAO mice improved significantly compared with the tMCAO mice (Figure 1(d)). Together, these results indicate a protective effect of dietary n-3 PUFAs in mice with cerebral ischemia/reperfusion injury.

3.2. N-3 PUFA Treatment Reduces A1-Specific Astrocytes Activation Both In Vivo and In Vitro. A great number of evidences pointed out that astrocytes play critical roles in the regulation of neurotransmission and neuron homeostasis and involved in the progression of acute CNS injury [21]. Recent studies reported that reactive astrocytes were distinguished into two types, A1 and A2 astrocytes [8]. We, therefore, raised a question whether n-3 PUFA affects the astrocytes polarization during cerebral ischemia/reperfusion injury. Immunofluorescence staining was employed to identify the level of complement 3 (C3), a particular A1 marker [8], on the S100β-positive astrocytes in hippocampus. The brain regions of hippocampus were displayed in Figure 2(a). As shown in Figures 2(b) and 2(c), the expression of C3 was increased significantly in the brain tissue from tMCAO mice compared to that from sham mice. Of note, n-3 PUFA treatment markedly suppressed the level of C3 in the mice model of tMCAO. To confirm the impact of n-3 PUFAs on astrocyte activation in vitro, primary cortex astrocytes were isolated and stimulation with or without DHA in the condition of low oxygen supply. The result displayed that DHA treatment limited the C3 expression induced by hypoxia in astrocytes (Figures 2(d) and 2(e)). Furthermore, our data showed that hypoxia treatment increased the mRNA expression of A1-specific markers (i.e., Amigo2, H2-D1, H2-T23, Serping1, and Ugt1a) in the primary astrocytes, and DHA treatment inhibited the upregulated levels of these A1 markers in the astrocytes under hypoxia (Figure 2(f)). By contrast, the mRNA expression of A2-specific markers (i.e., B3gmt5, CD14, Emp1, and Slc10a6) was not changed after DHA stimulation in the condition of low oxygen (Figure 2(g)). Together, these results suggest that n-3 PUFA administration reduces the A1 astrocyte polarization in mice with cerebral ischemia/reperfusion injury.

3.3. N-3 PUFAs Protect against Hypoxia-Induced Mitochondrial Dysfunction of Astrocytes. In astrocytes, mitochondria play an essential role in determining the cell fate. It has been reported that hypoxia induces impaired mitochondrial function and oxidative damage. We, therefore, investigated whether n-3 PUFAs influence the hypoxia-induced mitochondrial dysfunction in astrocytes. The result showed that DHA markedly reduced the hypoxia-induced mitochondrial dysfunction as indicated by increased mitochondrial membrane potential (Figures 3(a) and 3(b)) and reduced levels of mitochondrial oxidants (Figures 3(c) and 3(d)). Additionally, DHA treatment restored mitochondrial morphology under hypoxia conditions, as indicated by the mito-tracker fluorescence intensity, the number of networks, and the number of fragmented mitochondria (Figures 3(e) and 3(f)). These data indicate that n-3 PUFA treatment attenuates mitochondrial dysfunction and increase mitochondrial membrane potential in the astrocytes in the condition of hypoxia.

3.4. DHA Increases Mitophagy of Astrocytes under Hypoxia Condition. Mitochondrial fusion and mitophagy are recognized as two critical processes underlying mitochondrial homeostasis. We investigated whether n-3 PUFAs affect mitochondrial fusion and mitophagy in astrocytes. DHA stimulation significantly decreased the expression of cytoplasmic parkin (cyto-parkin), but the total Parkin level was maintained, indicating that Parkin might translocate from the cytoplasm to the mitochondria (Figure 4(a)). Besides, the expressions of mitochondrial Parkin (mito-parkin) and pink1 (mito-pink1) were increased dramatically in the DHA treatment group compared with the control group in the condition of hypoxia (Figure 4(d)). Additionally, DHA treatment remarkably decreased p62 and increased LC3 under hypoxic condition both in brain tissue (Figure 4(b)) and primary astrocytes (Figures 4(a) and 4(c)). DHA significantly enhanced the expression level of mfn1 and mfn2 protein in the hypoxia-treated cells (Figure 4(e)). These results indicate that n-3 PUFAs promote mitophagy and mitochondrial fusion in astrocytes under hypoxia condition.

3.5. N-3 PUFAs Reduce the Astrocytes Polarization by Mitochondria-Targeted Antioxidation. To explore whether n-3 PUFAs reduced A1 polarization through modulating the mitochondria dysfunction, we treated the astrocytes with

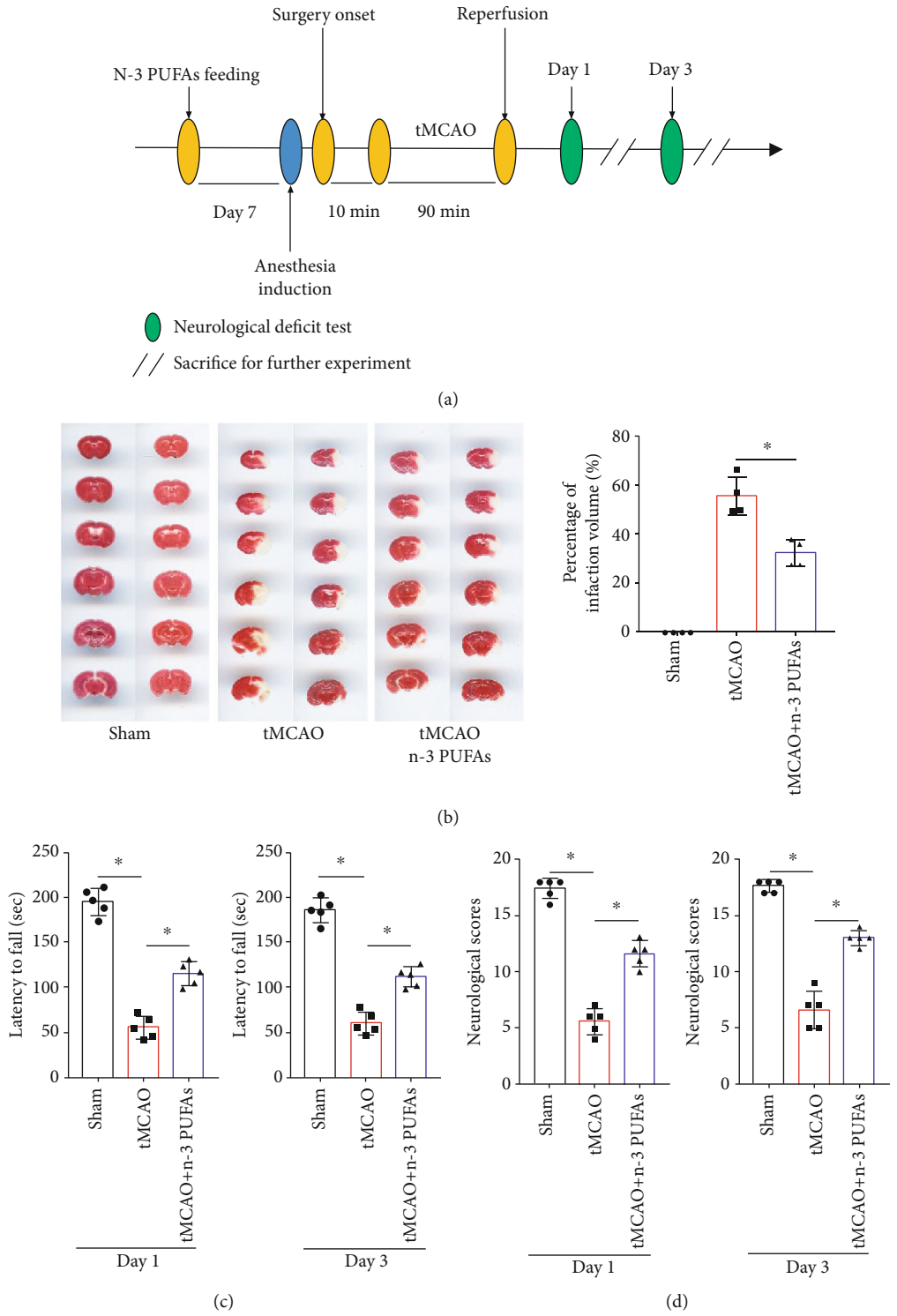

Figure 1: Effects of dietary n-3 PUFA supplementation on functional outcomes after tMCAO. (a) The schematic of experiments on male C57/BL6 mice in vivo. (b) 2,3,5-Triphenyltetrazolium chloride- (TTC-) stained brain slices from each group. (c) Sensorimotor functions were accessed by rotarod test after stroke. (d) Estimation of GARCIA neurological scores at day 1 and day 3 after tMCAO procedure. $^{*}p < 0.05$.

a mitochondria-targeted antioxidant, Mito-TEMPO, along with DHA in the condition of hypoxia. Compared to DHA stimulation alone, the combination of Mito-TEMPO and DHA administration downregulated the mRNA level of A1 markers in the astrocytes with OGD/R treatment (Figure 5(a)). Moreover, DHA complexed with Mito-TEMPO significantly reduced the expression of C3 in astrocytes compared with DHA, as determined by Western blotting (Figure 5(b)) and immunofluorescence staining (Figure 5(c)). Upon Mito-TEMPO treatment, expressions

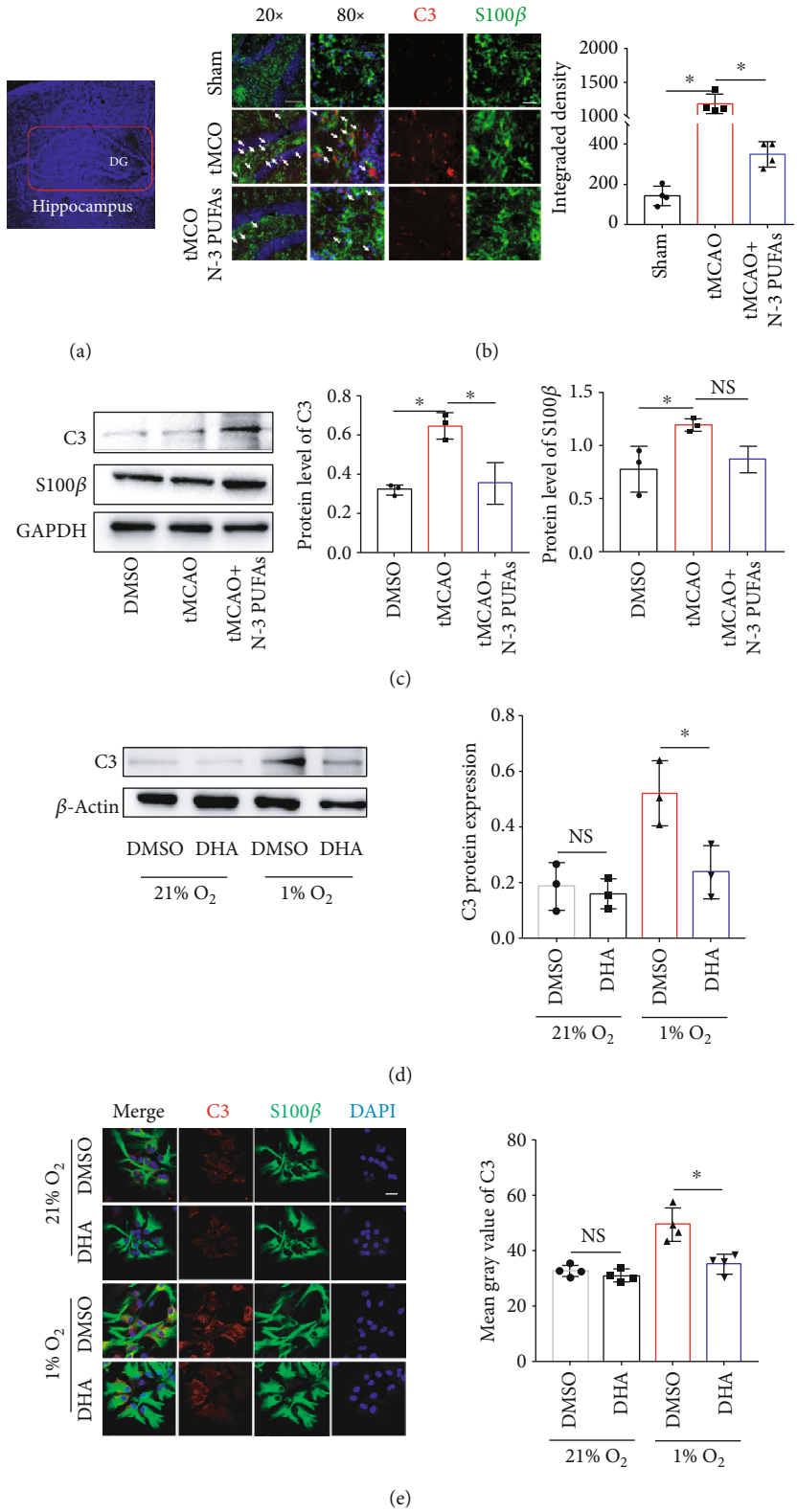

Figure 2: Continued.

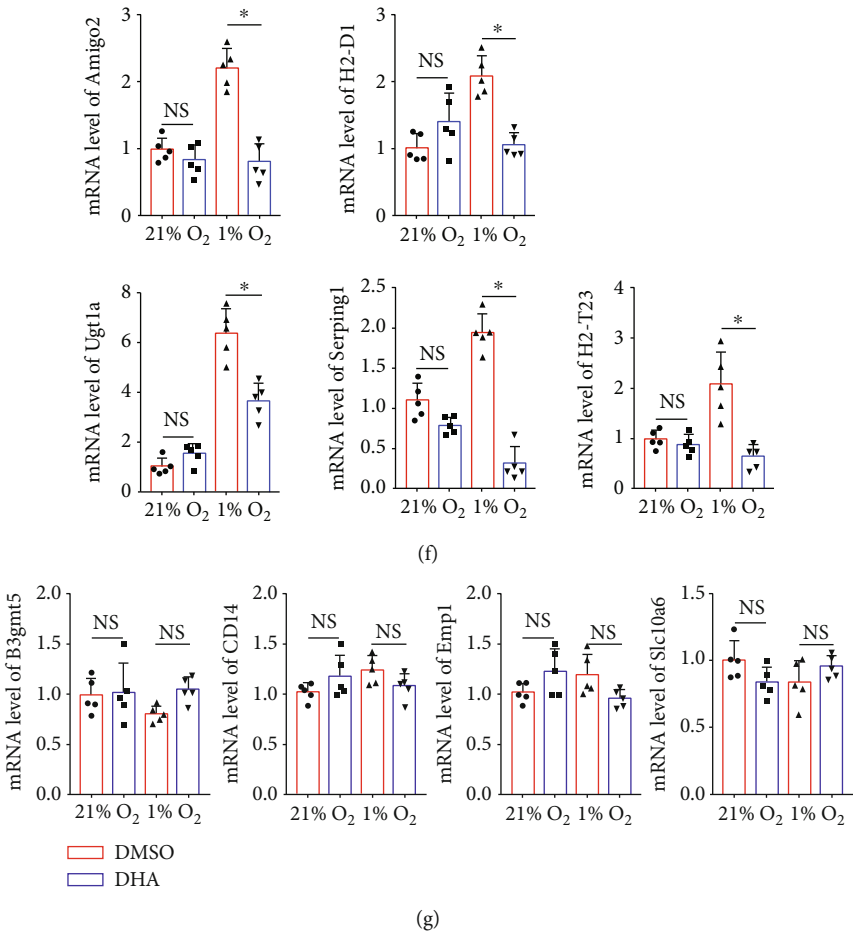

Figure 2: N-3 PUFAs influence the astrocyte polarization both in vivo and in vitro. (a) The brain regions of hippocampus were shown. (b) N-3 PUFA-fed mice and control mice underwent tMCAO procedure. The brain frozen cryosections were conducted with immunofluorescence staining for C3 and S100β. (c) The levels of C3 and S100β in brain tissue were evaluated using Western blot. (d–g) Primary astrocytes were cultured under 1% or 21% oxygen, respectively, followed by reoxygenation. The protein level of C3 in the astrocytes were determined by Western blotting (d) and immunostaining analysis (e) of C3 and S100β in primary cultural astrocytes. Additionally, the mRNA levels of A1 markers (f) and A2 markers (g) were evaluated by quantitative RT-PCR. $^*p < 0.05$. One of the three independent experiments is shown. NS: not significant. Scale bar in 20x magnification = 100 μm and scale bars in 80x magnification = 20 μm (a). Scale bar in (e) is 20 μm.

of C3 and A1-specific transcript markers were comparable between DHA-treated and control cells (Figures 5(a)–5(c)). These results implied a possibility of DHA reducing A1-specific astrocytes polarization through the mitochondrial-derived oxidative stress.

4. Discussion

N-3 PUFAs play a critical role in the development and function of the CNS. In the current study, we determined that n-3 PUFA supplementation significantly decreased the infarction volume and improved the neurofunction after cerebral ischemia. Our data showed that n-3 PUFAs reduce stroke-induced A1 astrocyte polarization, probably via regulating the mitochondrial dysfunction, and exert anti-inflammatory and neuroprotective effects following ischemic stroke. Moreover, the n-3 PUFA-mediated modulation of mitophagy activity might be partially involved in the induction of A1 astrocytes.

Astrocytes undergo a transformation called "reactive astrocytosis" after cerebral ischemia stroke, whereby the transcription level of many genes upregulated [22, 23]. Functions of reactive astrocytes remain subjects of debate in ischemic brain injury, with previous studies showing that they can both hinder and support neurofunction recovery [22]. According to the different transcript expression profiles, astrocytes are classified into two major groups, A1-specific or A2-specific astrocytes [8]. Immediately after ischemic stroke, A1 astrocytes produce and secrete several proinflammatory mediators, such as IL-6, TNF-α, IL-1α, IL-1β, and IFN-γ [24, 25]. Additionally, A1 astrocytes can release neurotoxins that induce rapid death of neurons [3]. While in the later stage of stroke (after 72 hours), proliferation and glial scar formation of A2 astrocytes restrict the diffusion of neuroinflammation and produce neurotrophic factors [26]. The A2 astrocytes facilitate the generation of new blood vessels, protect neurons from excitotoxicity injury, and promote the formation of synapses [27]. Therefore, attenuation of the

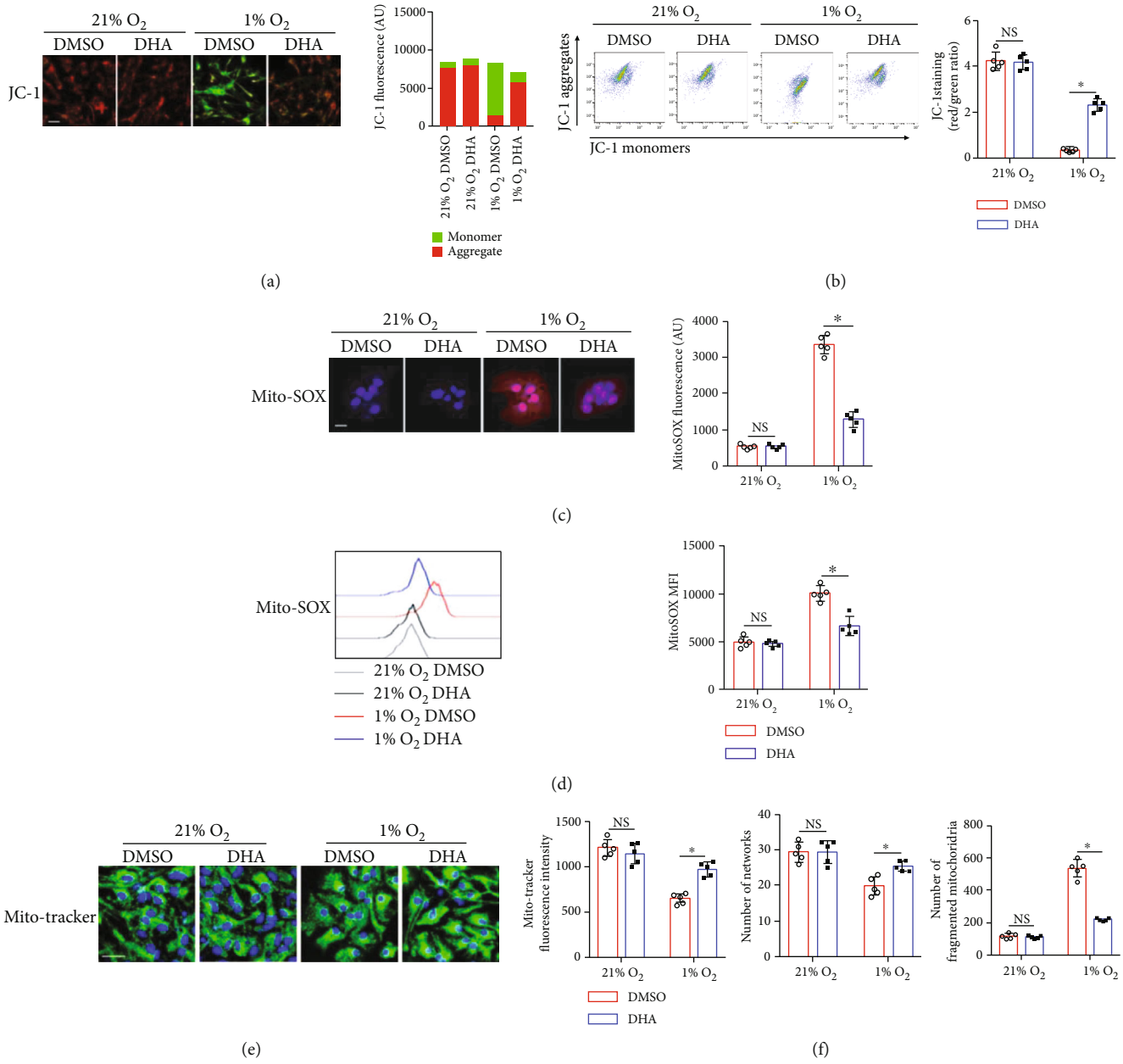

FIGURE 3: DHA protects against mitochondrial dysfunction in the astrocytes under hypoxia condition. Primary astrocytes were treated with DHA for indicated time periods under hypoxia condition. (a, b) The mitochondrial membrane potential in astrocytes was measured by the membrane-permeant JC-1 staining for confocal scanning (a) and flow cytometry analysis (b). (c, d) Mitochondrial ROS was measured by MitoSOX probes (c), and the MFI of MitoSOX (d) was calculated by Image J software. (e, f) MitoTracker was employed to mark mitochondria (e). Statistical analysis was performed on 200 cells in each group to obtain five data sets; quantification of mito-tracker fluorescence intensity, number of individuals, number of networks, and number of fragmented mitochondria were analyzed using the Image-Pro Plus with MiNA on mitochondrion-labelled images (f). Scale bar = 20 μm. $^*p < 0.05$. One of the three independent experiments is shown.

A1 astrocytes' polarization is supposed to reduce neuronal death and improve recovery from ischemic stroke. The current study shows that n-3 PUFA treatment markedly reverses the induction of A1 astrocytes caused by brain ischemia injury. Studies about astrocyte subtypes indicate that A1 astrocytes can be induced by IL-1α, TNF-α, and C1q secreted by LPS-stimuli microglia or other inflammatory signal pathways [8]. Joffre et al. reported that n-3 PUFAs have a suppressive effect on the production of proinflammatory cytokines in microglial cells, thereby resolving the brain inflammation and contributing to neuroprotective functions [28]. Therefore, it is possible that modulation of brain inflammation following ischemic stroke partially owing to the effect of n-3 PUFAs on microglia. However, DHA transported to brain tissues accumulates as a component of phosphatidylcholine or phosphatidylethanolamine in the cell membrane of astrocytes [29]. On the other hand, astrocytes have been shown to supply DHA to neurons and contribute to

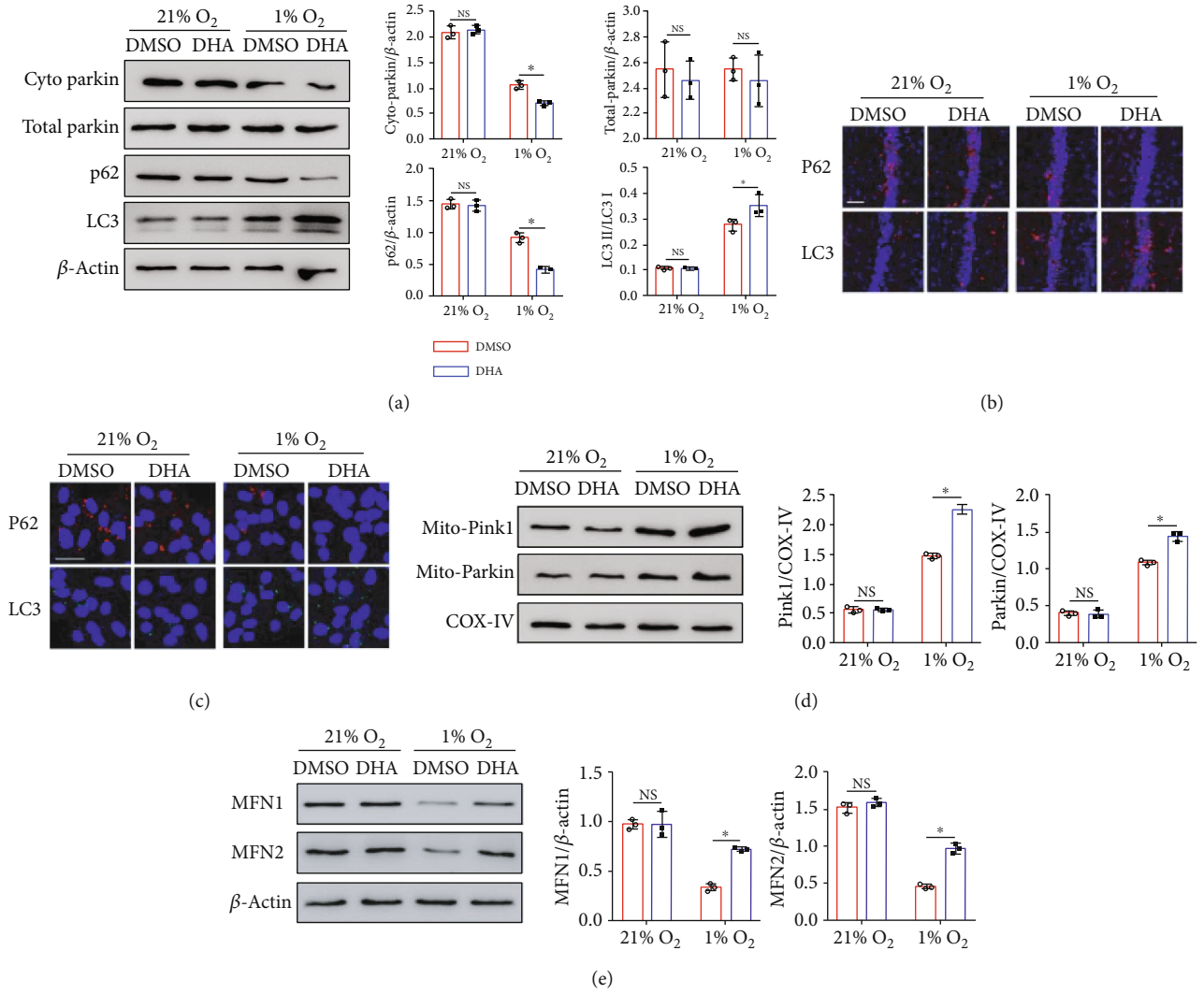

FIGURE 4: Effects of DHA on mitophagy in the astrocytes treated with hypoxia. Primary astrocytes were cultured at 21.0% or 1.0% oxygen in the presence or absence of DHA. (a) The expression of parkin, p62, and LC3 in the astrocytes was determined by Western blot analysis. The expressions of P62 and LC3 in brain tissue (b) and primary astrocytes (c) are shown by immunofluorescence staining. (d) The expression of mito-pink1 and mito-parkin in the mitochondrial fractions was determined by Western blot analysis. (e) The expression of mfn1 and mfn2 was detected by immunoblotting. Quantification was performed in images using the Image J software. $^{*}p < 0.05$. Data from one representative experiment of three independent experiments are presented. Scale bar 100 μm in (b), scale bar 20 μm in (c).

synapse formation, maturation, and maintenance [30]. It seems that the effects of n-3PUFAs on astrocytes are more direct. Considering that DHA has effects on both astrocyte and microglia, it is temporarily impossible to determine which cell plays a more critical role in ischemic brain injury based on the current experimental data. Thus, further investigations utilizing condition transgene mice aiming to astrocytes are warranted.

Astrocytes possess almost as many mitochondria as neurons to meet energy demands [31]. Of note, changes in astrocytic mitochondrial function are associated with the astrocyte activation in many neurodegenerative diseases. It has been reported that hypoxia and posthypoxia reoxygenation of primary astrocytes led to a drastic mitochondrial network change, followed by mitochondrial degradation and retraction of astrocytic extensions [32, 33]. Besides, mitophagy is essential for the quality control and homeostasis of mitochondria by eliminating dysfunctional mitochondria that produce reactive oxygen species (ROS) and result in cell death [34]. Mitophagy has fundamental connections with the mitochondria dynamic and is account for the various pathological stresses including stroke [12]. A previous study showed that supplementation with n-3 PUFAs exhibited mitochondrial phospholipid remodelling by increasing cardiolipin, a tetra-acyl phospholipid that is unique to mitochondrial and essential for optimal mitochondrial function [35]. DHA treatment after acute brain haemorrhage significantly attenuated mitochondrial disorder in neurons both in vivo and in vitro through preserving the mitochondrial morphology [36]. Similarly, our current research identified that DHA restored the mitochondrial junction disruption of astrocytes. Many studies reported that the damaged mitochondria accumulate under ischemic/reperfusion stress [37],

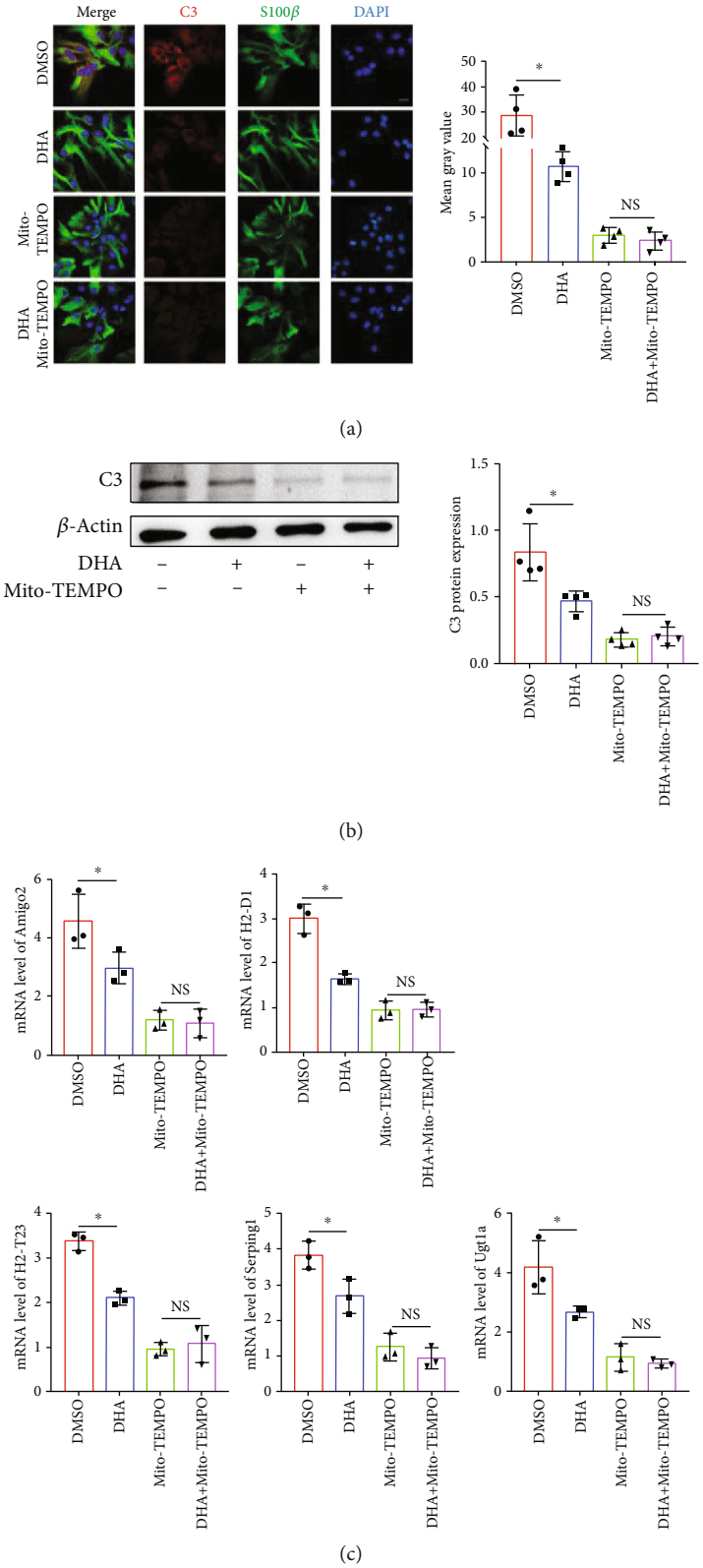

FIGURE 5: Mitochondria-targeted antioxidant abrogates the n-3 PUFA-mediated modulation of astrocyte polarization under hypoxia condition. Primary astrocytes were treated with DHA for indicated time periods under hypoxia condition. The mitochondria-targeted antioxidant and Mito-tempo were added 24 hours before the treatment. (a) The expression of C3 and S100β in primary cultural astrocytes was determined by immunofluorescence staining, and the integrated density was analyzed. (b) The protein level of C3 in astrocyte was evaluated by Western blotting. (c) The mRNA levels of the A1-specific markers were evaluated by quantitative RT-PCR. $^*p < 0.05$; NS: not significant. One of the three independent experiments is shown. Scale bar in (a) is 20 μm.

suggesting that maintaining a pool of healthy mitochondria is crucial for protecting against tissue injury [33]. To ensure mitochondrial quality, mitophagy activated in the early stage of ischemic plays a significant role in the removal of damaged mitochondria [38], subsequently reducing the mitochondrial-associated neuron apoptosis or inflammation [39]. Our present data showed DHA pretreatment upregulated the protein levels of mitophagy-specific molecules in astrocytes at 12 hours after hypoxia, suggesting that the mitochondrial protection from ischemic/reperfusion stress by DHA is to some extent due to mitophagy enhancement. Another reactive mitochondrial quality control is reshaped by fusion and fission [34, 40]. The result demonstrated an upregulation of mfn1 and mfn2 (mitofusin-specific protein), which indicated that DHA promoted mitochondrial fusion in the hypoxia-treated astrocytes. It should be emphasized that mfn1 and mfn2 play a controversial part in the regulation of mitophagy [41]. Depletion of both mfn1 and mfn2 in murine cardiomyocytes caused the accumulation of defective mitochondria by inhibiting mitophagy [42]. In contrast, an active role of mfn2 in preventing mitophagy was also proposed, associating with the maintenance of ER-mitochondrial contacts [43]. Our current results were prone to support the opinion that DHA facilitated mitophagy through promoting mitofusin. Further, mitochondrial injury is known to contribute to oxidative stress in brain ischemic/reperfusion injury [44, 45]. DHA treatment also reduces oxidative stress by downregulating ROS and SOD in stroke [46]. Mitochondrial overproduction of ROS also initiates cell death and aberrant immune responses [47]. Among transcription factors, NF-κB is induced in response to oxidative stress stimuli and participates in complex inflammatory loops regulating production and release of proinflammatory cytokines, such as tumor necrosis factor α (TNF-α) [48]. This proinflammatory cytokine is demonstrated to induce A1 astrocytes in previous studies [8, 49]. Thus, it is possible that n-3 PUFA participates in the polarization of A1-specific astrocytes through mitochondrial-derived oxidative stress and the inflammatory pathways.

5. Conclusions

In summary, we demonstrated that exogenous n-3 PUFA supplementation prevents mitochondrial-derived oxidative stress, resulting in limited A1-specific astrocyte polarization both in vivo and in vitro. N-3 PUFA-mediated blockage of A1 astrocyte polarization might be associated with the attenuated neuroinflammation in the brain ischemic/reperfusion stroke. These findings substantiate the concept that n-3 PUFAs have a potential clinical application to ameliorate ischemic/reperfusion brain injury.

Data Availability

The raw data supporting the conclusions of this article will be made available by the authors, without undue reservation, to any qualified researcher.

Conflicts of Interest

The authors declare that they have no known competing financial interests or personal relationships that could have appeared to influence the work reported in this paper.

Authors' Contributions

Jun Cao and Lijun Dong contributed equally to this work.

Acknowledgments

This work was supported in part by the Discipline Construction Fund of Central People's Hospital of Zhanjiang (2020A01 and 2020A02) and Science and Technology Planning Project of Guangzhou (grant no.: 202002030160).

Supplementary Materials

The Supplementary Material for this article can be found online. See Supplementary Tables 1-2 in the Supplementary Material for comprehensive image analysis. *(Supplementary Materials)*

References

[1] V. L. Feigin, R. V. Krishnamurthi, P. Parmar et al., "Update on the global burden of ischemic and hemorrhagic stroke in 1990-2013: the GBD 2013 study," *Neuroepidemiology*, vol. 45, no. 3, pp. 161–176, 2015.

[2] J. Silver and J. H. Miller, "Regeneration beyond the glial scar," *Nature Reviews Neuroscience*, vol. 5, no. 2, pp. 146–156, 2004.

[3] S. A. Liddelow and B. A. Barres, "Reactive astrocytes: production, function, and therapeutic potential," *Immunity*, vol. 46, no. 6, pp. 957–967, 2017.

[4] M. Gliem, K. Krammes, L. Liaw, N. van Rooijen, H. P. Hartung, and S. Jander, "Macrophage-derived osteopontin induces reactive astrocyte polarization and promotes re-establishment of the blood brain barrier after ischemic stroke," *Glia*, vol. 63, no. 12, pp. 2198–2207, 2015.

[5] P. J. Magistretti and I. Allaman, "Lactate in the brain: from metabolic end-product to signalling molecule," *Nature Reviews Neuroscience*, vol. 19, no. 4, pp. 235–249, 2018.

[6] K. Hayakawa, E. Esposito, X. Wang et al., "Transfer of mitochondria from astrocytes to neurons after stroke," *Nature*, vol. 535, no. 7613, pp. 551–555, 2016.

[7] C. S. Wilson, M. D. Bach, Z. Ashkavand et al., "Metabolic constraints of swelling-activated glutamate release in astrocytes and their implication for ischemic tissue damage," *Journal of Neurochemistry*, vol. 151, no. 2, pp. 255–272, 2019.

[8] S. A. Liddelow, K. A. Guttenplan, L. E. Clarke et al., "Neurotoxic reactive astrocytes are induced by activated microglia," *Nature*, vol. 541, no. 7638, pp. 481–487, 2017.

[9] M. J. Zhang and M. Spite, "Resolvins: anti-inflammatory and proresolving mediators derived from omega-3 polyunsaturated fatty acids," *Annual Review of Nutrition*, vol. 32, no. 1, pp. 203–227, 2012.

[10] R. P. Bazinet and S. Laye, "Polyunsaturated fatty acids and their metabolites in brain function and disease," *Nature Reviews Neuroscience*, vol. 15, no. 12, pp. 771–785, 2014.

[11] C. Luo, H. Ren, X. Yao et al., "Enriched brain omega-3 polyunsaturated fatty acids confer neuroprotection against microinfarction," *EBioMedicine*, vol. 32, pp. 50–61, 2018.

[12] E. Kroger and R. Laforce Jr., "Fish consumption, brain mercury, and neuropathology in patients with Alzheimer disease and dementia," *JAMA*, vol. 315, no. 5, pp. 465-466, 2016.

[13] G. P. Amminger and P. D. McGorry, "Update on omega-3 polyunsaturated fatty acids in early-stage psychotic disorders," *Neuropsychopharmacology*, vol. 37, no. 1, pp. 309-310, 2012.

[14] X. Jiang, H. Pu, X. Hu et al., "A post-stroke therapeutic regimen with omega-3 polyunsaturated fatty acids that promotes white matter integrity and beneficial microglial responses after cerebral ischemia," *Translational Stroke Research*, vol. 7, no. 6, pp. 548–561, 2016.

[15] J. Bu, Y. Dou, X. Tian, Z. Wang, and G. Chen, "The role of omega-3 polyunsaturated fatty acids in stroke," *Oxidative Medicine and Cellular Longevity*, vol. 2016, Article ID 6906712, 8 pages, 2016.

[16] W. Cai, S. Liu, M. Hu et al., "Post-stroke DHA treatment protects against acute ischemic brain injury by skewing macrophage polarity toward the M2 phenotype," *Translational Stroke Research*, vol. 9, no. 6, pp. 669–680, 2018.

[17] G. Begum, D. Kintner, Y. Liu, S. W. Cramer, and D. Sun, "DHA inhibits ER Ca^{2+} release and ER stress in astrocytes following in vitro ischemia," *Journal of Neurochemistry*, vol. 120, no. 4, pp. 622–630, 2012.

[18] C. Luo, M.-W. Ouyang, Y.-Y. Fang et al., "Dexmedetomidine protects mouse brain from ischemia-reperfusion injury via inhibiting neuronal autophagy through up-regulating HIF-1α," *Frontiers in Cellular Neuroscience*, vol. 11, 2017.

[19] Z. Chen, Y. Zhang, C. Jia et al., "mTORC1/2 targeted by n-3 polyunsaturated fatty acids in the prevention of mammary tumorigenesis and tumor progression," *Oncogene*, vol. 33, no. 37, pp. 4548–4557, 2014.

[20] A. J. Valente, L. A. Maddalena, E. L. Robb, F. Moradi, and J. A. Stuart, "A simple ImageJ macro tool for analyzing mitochondrial network morphology in mammalian cell culture," *Acta Histochemica*, vol. 119, no. 3, pp. 315–326, 2017.

[21] S. M. Q. Hussaini and M. H. Jang, "New roles for old glue: astrocyte function in synaptic plasticity and neurological disorders," *International Neurourology Journal*, vol. 22, Supplement 3, pp. S106–S114, 2018.

[22] M. Pekny, U. Wilhelmsson, and M. Pekna, "The dual role of astrocyte activation and reactive gliosis," *Neuroscience Letters*, vol. 565, pp. 30–38, 2014.

[23] S. Xu, J. Lu, A. Shao, J. H. Zhang, and J. Zhang, "Glial cells: role of the immune response in ischemic stroke," *Frontiers in Immunology*, vol. 11, p. 294, 2020.

[24] V. Basic Kes, A. M. Simundic, N. Nikolac, E. Topic, and V. Demarin, "Pro-inflammatory and anti-inflammatory cytokines in acute ischemic stroke and their relation to early neurological deficit and stroke outcome," *Clinical Biochemistry*, vol. 41, no. 16-17, pp. 1330–1334, 2008.

[25] L. E. Clarke, S. A. Liddelow, C. Chakraborty, A. E. Munch, M. Heiman, and B. A. Barres, "Normal aging induces A1-like astrocyte reactivity," *Proceedings of the National Academy of Sciences of the United States of America*, vol. 115, no. 8, pp. E1896–E1905, 2018.

[26] C. Rakers, M. Schleif, N. Blank et al., "Stroke target identification guided by astrocyte transcriptome analysis," *Glia*, vol. 67, no. 4, pp. 619–633, 2019.

[27] T. Li, X. Chen, C. Zhang, Y. Zhang, and W. Yao, "An update on reactive astrocytes in chronic pain," *Journal of Neuroinflammation*, vol. 16, no. 1, p. 140, 2019.

[28] C. Joffre, C. Rey, and S. Layé, "N-3 polyunsaturated fatty acids and the resolution of neuroinflammation," *Frontiers in Pharmacology*, vol. 10, 2019.

[29] H. Y. Kim, B. X. Huang, and A. A. Spector, "Phosphatidylserine in the brain: metabolism and function," *Progress in Lipid Research*, vol. 56, pp. 1–18, 2014.

[30] D. H. Mauch, K. Nägler, S. Schumacher et al., "CNS synaptogenesis promoted by glia-derived cholesterol," *Science*, vol. 294, no. 5545, pp. 1354–1357, 2001.

[31] D. Lovatt, U. Sonnewald, H. S. Waagepetersen et al., "The transcriptome and metabolic gene signature of protoplasmic astrocytes in the adult murine cortex," *Journal of Neuroscience*, vol. 27, no. 45, pp. 12255–12266, 2007.

[32] D. D. Quintana, J. A. Garcia, S. N. Sarkar et al., "Hypoxia-reoxygenation of primary astrocytes results in a redistribution of mitochondrial size and mitophagy," *Mitochondrion*, vol. 47, pp. 244–255, 2019.

[33] R. Guan, W. Zou, X. Dai et al., "Mitophagy, a potential therapeutic target for stroke," *Journal of Biomedical Science*, vol. 25, no. 1, p. 87, 2018.

[34] G. Ashrafi and T. L. Schwarz, "The pathways of mitophagy for quality control and clearance of mitochondria," *Cell Death & Differentiation*, vol. 20, no. 1, pp. 31–42, 2013.

[35] E. M. Sullivan, E. R. Pennington, W. D. Green, M. A. Beck, D. A. Brown, and S. R. Shaikh, "Mechanisms by which dietary fatty acids regulate mitochondrial structure-function in health and disease," *Advances in Nutrition*, vol. 9, no. 3, pp. 247–262, 2018.

[36] T. Zhang, P. Wu, J. H. Zhang et al., "Docosahexaenoic acid alleviates oxidative stress-based apoptosis via improving mitochondrial dynamics in early brain injury after subarachnoid hemorrhage," *Cellular and Molecular Neurobiology*, vol. 38, no. 7, pp. 1413–1423, 2018.

[37] A. R. Anzell, R. Maizy, K. Przyklenk, and T. H. Sanderson, "Mitochondrial quality control and disease: insights into ischemia-reperfusion injury," *Molecular Neurobiology*, vol. 55, no. 3, pp. 2547–2564, 2018.

[38] H. M. Ni, J. A. Williams, and W. X. Ding, "Mitochondrial dynamics and mitochondrial quality control," *Redox Biology*, vol. 4, pp. 6–13, 2015.

[39] E. Motori, J. Puyal, N. Toni et al., "Inflammation-induced alteration of astrocyte mitochondrial dynamics requires autophagy for mitochondrial network maintenance," *Cell Metabolism*, vol. 18, no. 6, pp. 844–859, 2013.

[40] M. Joaquim and M. Escobar-Henriques, "Role of mitofusins and mitophagy in life or death decisions," *Frontiers in Cell and Developmental Biology*, vol. 8, article 572182, 2020.

[41] R. J. Youle and A. M. van der Bliek, "Mitochondrial fission, fusion, and stress," *Science*, vol. 337, no. 6098, pp. 1062–1065, 2012.

[42] M. Liu, X. Li, and D. Huang, "Mfn2 overexpression attenuates cardio-cerebrovascular ischemia-reperfusion injury through mitochondrial fusion and activation of the AMPK/Sirt3 signaling," *Frontiers in Cell and Developmental Biology*, vol. 8, article 598078, 2020.

[43] S. Han, P. Nandy, Q. Austria et al., "Mfn2 ablation in the adult mouse hippocampus and cortex causes neuronal death," *Cells*, vol. 9, no. 1, p. 116, 2020.

[44] S. S. Andrabi, S. Parvez, and H. Tabassum, "Ischemic stroke and mitochondria: mechanisms and targets," *Protoplasma*, vol. 257, no. 2, pp. 335–343, 2020.

[45] E. T. Chouchani, V. R. Pell, E. Gaude et al., "Ischaemic accumulation of succinate controls reperfusion injury through mitochondrial ROS," *Nature*, vol. 515, no. 7527, pp. 431–435, 2014.

[46] R. Gonzalo-Gobernado, M. I. Ayuso, L. Sansone et al., "Neuroprotective effects of diets containing olive oil and DHA/EPA in a mouse model of cerebral ischemia," *Nutrients*, vol. 11, no. 5, p. 1109, 2019.

[47] P. R. Angelova and A. Y. Abramov, "Role of mitochondrial ROS in the brain: from physiology to neurodegeneration," *FEBS Letters*, vol. 592, no. 5, pp. 692–702, 2018.

[48] J. Liu and L. Du, "PERK pathway is involved in oxygen-glucose-serum deprivation-induced NF-kB activation via ROS generation in spinal cord astrocytes," *Biochemical and Biophysical Research Communications*, vol. 467, no. 2, pp. 197–203, 2015.

[49] F. Martorana, M. Foti, A. Virtuoso et al., "Differential modulation of NF-κB in neurons and astrocytes underlies neuroprotection and antigliosis activity of natural antioxidant molecules," *Oxidative Medicine and Cellular Longevity*, vol. 2019, 16 pages, 2019.

Hindawi
Oxidative Medicine and Cellular Longevity
Volume 2021, Article ID 9985701, 9 pages
https://doi.org/10.1155/2021/9985701

Review Article

Cellular Signal Transduction Pathways Involved in Acute Lung Injury Induced by Intestinal Ischemia-Reperfusion

Guangyao Li, Yingyi Zhang, and Zhe Fan

Department of General Surgery, The Third People's Hospital of Dalian, Dalian Medical University, Dalian, China

Correspondence should be addressed to Yingyi Zhang; zhangyingyidl@outlook.com and Zhe Fan; fanzhe1982@hotmail.com

Received 22 March 2021; Accepted 14 May 2021; Published 4 June 2021

Academic Editor: Haobo Li

Intestinal ischemia-reperfusion (II/R) injury is a common type of tissue and organ injury, secondary to intestinal and mesenteric vascular diseases. II/R is characterized by a high incidence rate and mortality. In the II/R process, intestinal barrier function is impaired and bacterial translocation leads to excessive reactive oxygen species, inflammatory cytokine release, and even apoptosis. A large number of inflammatory mediators and oxidative factors are released into the circulation, leading to severe systemic inflammation and multiple organ failure of the lung, liver, and kidney. Acute lung injury (ALI) is the most common complication, which gradually develops into acute respiratory distress syndrome and is the main cause of its high mortality. This review summarizes the signal transduction pathways and key molecules in the pathophysiological process of ALI induced by II/R injury and provides a new therapeutic basis for further exploration of the molecular mechanisms of ALI induced by II/R injury. In particular, this article will focus on the biomarkers involved in II/R-induced ALI.

1. Introduction

Intestinal ischemia-reperfusion (II/R) injury can occur in a variety of pathophysiological conditions, including acute mesenteric ischemia, severe trauma, acute shock, small bowel transplantation, and sepsis [1]. II/R is a clinical state. During ischemia, the blood supply of the intestine is limited, and then, the tissues and organs are damaged due to reperfusion and oxygen recovery [2]. The recovery of blood flow and oxygen during reperfusion leads to bacterial translocation, tissue damage, inflammatory response, and oxidative stress. During ischemia, tissue hypoxia leads to endothelial cell barrier function damage and increases in vascular permeability, followed by cell death, tissue damage, and organ failure during reperfusion [3]. In addition to intestinal injury, II/R can also lead to distal tissue injury and distal organ failure. Distant organs, especially the lungs, are very sensitive to II/R injury. According to the literature, the mortality of II/R is as high as 60%–80% [4]. An increasing number of reports show that secondary distal organ injury (acute lung injury (ALI) and acute respiratory distress syndrome) is more serious than intestinal injury and has been shown to be the main cause of death in patients with II/R [5].

The pathophysiology and pathogenesis of ALI induced by II/R are complicated and poorly understood. Some researchers have hypothesized that damage to the intestinal mucosal barrier after II/R leads to the translocation of bacteria and endotoxins, which leads to a systemic inflammatory response. The release of a large number of inflammatory mediators (TNF-α, IL-1, IL-6, IL-8, IL-10, NO, etc.) into the systemic circulation can lead to cell necrosis, tissue damage, and organ failure. Neutrophils and their products are increased in lung tissue, leading to increased vascular permeability, vascular and pulmonary interstitial edema, and pulmonary edema [6]. However, the specific mechanism of ALI is very complex, involving bacterial translocation, inflammatory response, oxidative stress, and initiation of apoptosis and necrosis. In this review, we focused on the multiple signaling pathways involved in II/R-induced ALI. The search Medical Subject Headings (MeSH) terms and keywords were as follows: acute lung injury, ALI, intestinal ischemia reperfusion, intestinal ischemia-reperfusion, and

gut ischemia-reperfusion by using PubMed, Embase, and MEDLINE. Cellular signal transduction pathways such as the MAPK signaling pathway, NF-κB signaling pathway, TLR4 signal transduction pathway, PKC/p66Shc signaling pathway, NLRP3 inflammasome, Nrf2 signaling pathway, SIRT1 signaling pathway, and other signaling pathways were also summarized to explore the potential pathogenesis of II/R-induced ALI and examine new targeted therapies using biomarkers.

2. Biomarkers of ALI Induced by Aggravating II/R

2.1. MAPK Signaling Pathway. The mitogen activated protein kinase (MAPK) signaling pathway is activated by a variety of inflammatory signals, including inflammatory mediators and oxidative stress factors [7]. At present, four MAPK pathways have been identified in mammals, including extracellular signal-regulated kinase (ERK), c-Jun N-terminal kinase (JNK), p38 mitogen-activated protein kinase, and ERK5 [8]. Different extracellular stimuli can activate different MAPK signaling pathways and mediate different cellular biological responses through their mutual regulation. The ERK signaling pathway plays an important role in the process of cell proliferation mediated by growth factors. JNK and p38MAPK pathways activate downstream factors (AP-1 and Jun), which are related to a variety of pathophysiological processes during cell apoptosis and stress [9]. Together with endoplasmic reticulum stress, IL-1β increases apoptosis through the JNK signaling pathway [10]. Recently, the p38MAPK signaling pathway has been proposed to play a key role in the inflammatory response of ALI [11]. During ALI, inflammatory factors enter into the lung tissue and destroy lung endothelial cells, leading to an increase in pulmonary capillary permeability that results in pulmonary edema. Therefore, inflammation and pulmonary edema may be two important pathological features of ALI [12].

It has been reported that one of the most bioactive cytokines in the early stage of ALI is IL-1β, which is a powerful inducer of lung inflammation and can cause the release of various proinflammatory factors [13]. The increase in IL-1β may be the result of ALI induced by II/R, so reducing the expression of IL-1β may be conducive to the recovery from lung injury. Increased expression of p38MAPK can also be observed after II/R. In addition, there are also reports that p38MAPK can activate rat pulmonary interstitial macrophages to produce nuclear factor kappa B (NF-κB) [14]. Studies have shown that the p38MAPK inhibitor sb239063 can effectively reduce the expression level of IL-1β after II/R by inhibiting the p38MAPK pathway, significantly improving lung injury, and providing a new therapeutic approach for the clinical application of p38MAPK as an intervention against ALI after II/R [15].

Aquaporins (AQPs) are a small family of integral membrane proteins that regulate water transport and play an important role in water homeostasis. Aquaporin 4 (AQP4) is a recently found protein related to edema [16]. Pulmonary edema, as an important pathological feature of ALI caused by II/R, suggests a novel approach for the treatment of ALI. Studies have shown that the increased expression of AQP4 is related to the severity of lung injury induced by II/R, and AQP4 plays an important role in the pathogenesis of ALI induced by II/R. The p38MAPK inhibitor SB239063 reduced the expression of AQP4 and alleviated the extent of lung injury, suggesting that p38MAPK may be the main pathway mediating the expression of AQP4 in ALI induced by II/R. Inhibition of the p38MAPK pathway may thus become an effective target for the prevention and treatment of ALI induced by II/R [17] (Figure 1).

2.2. NF-κB Signaling Pathway. NF-κB plays an important role in transcriptional regulation of many inflammatory and apoptotic regulatory genes during II/R. NF-κB is a rapid nuclear transcription factor. At present, there are five members of the NF-κB family in mammalian cells: NF-κB1 (P50), NF-κB2 (p52), Rel A (p65), Rel B, and c-Rel. NF-κB must form as a homodimer or heterodimer to have biological activity. When cells are stimulated by internal and external factors, NF-κB is activated and enters the nucleus to regulate gene transcription, including the genes for TNF-α, IL-1, IL-6, IL-8, and ICAM-1. Inflammatory factors play an important role in II/R injury, and TNF-α, as the induction factor, induces the release of various inflammatory factors [18–20].

NF-κB enters the nucleus and mediates the transcription and release of a variety of inflammatory factors, which then spread the inflammatory response and are causative factors leading to ALI. Inhibition of the NF-κB pathway can reduce lung inflammation and ALI caused by II/R [21]. After II/R, the levels of visfatin in plasma and lung tissue are significantly increased, and visfatin exerts a proinflammatory effect by upregulating the production of the proinflammatory factors IL-1β, IL-6, and TNF-α in a dose-dependent manner [22]. The visfatin inhibitor FK866 inhibits the nuclear translocation of NF-κB p65 by inhibiting the degradation of cytoplasmic I-κBα. Whether FK866 has the effect of reducing apoptosis in the process of inflammation needs further study. However, it has been reported that TNF-α, one of the main mediators of ALI, starts the apoptosis cascade, and FK866 at least partially inhibits apoptosis in ALI through an indirect pathway [23]. FK866 can significantly reduce the inflammatory response and apoptosis after organ injury by inhibiting the NF-κB signaling pathway and ultimately improves the survival rate [22]. Curcumin can also effectively prevent II/R-induced ALI by inhibiting the NF-κB pathway. After curcumin treatment, myeloperoxidase levels in lung tissue (a marker of neutrophil recruitment and lung injury [24]) were significantly decreased, while superoxide dismutase (SOD) level (an indicator of antioxidant effect [25]) was significantly increased. The levels of IL-6 and ICAM-1 were parallel to the changes of NF-κB, suggesting that curcumin can reduce the recruitment/infiltration of neutrophils and play an anti-inflammatory and antioxidant role by inhibiting the NF-κB pathway [26] (Figure 2).

2.3. TLR4 Signal Transduction Pathway. Toll-like receptors (TLRs) are a class of important proteins involved in innate immunity and act as the first barrier against infectious diseases. TLR4, a member of the TLR family, is responsible for

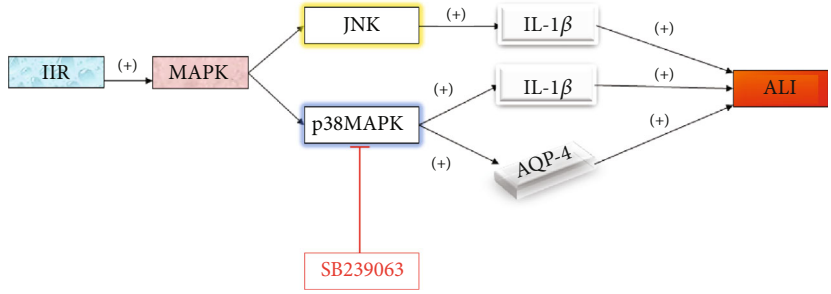

Figure 1: JNK and p38MAPK in the MAPK pathway aggravate ALI, while SB239063 inhibits the p38MAPK pathway to relieve ALI.

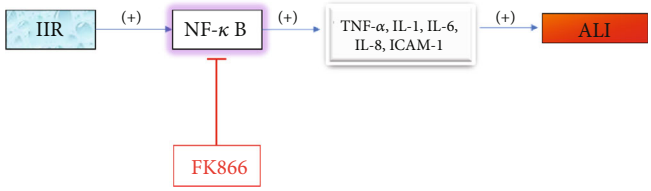

Figure 2: Nuclear translocation of p65 in NF-κB aggravates ALI, while FK866 inhibits p65 nuclear translocation to relieve ALI.

recognizing pathogens and activating the innate immune system. It can recognize a variety of ligands, such as endogenous ligands (low-density lipoprotein and heat shock protein) and exogenous ligands (lipopolysaccharide), so it plays a key role in the body's response to I/R injury [27]. TLR4 can activate multiple signaling pathways after specifically binding with ligands, including MAPK and NF-κB pathway proteins, which are key factors involved in the inflammatory immune response that regulate cell survival [8]. In the lung injury model induced by II/R in mice, TLR4 deletion can prevent the activation of p38MAPK and NF-κB signals, and the phosphorylation of p38MAPK and the activation of NK-κB in the lung tissue of TLR4-mutant mice are significantly inhibited, which indicates that these pathways are involved in ALI induced by II/R and are mediated by TLR4 [28]. The downstream effects regulated by TLRs vary with the type of receptors, and these mediators contribute to the production of local inflammation and the aggregation of neutrophils [29].

The signal transduction pathway mediated by TLRs depends on the interaction with cytoplasmic adaptor proteins and mainly myeloid differentiation factor 88 (MyD88). MyD88 is considered the central adaptor protein for signal transduction activated by MAPK and NF-κB in almost all TLRs (except TLR3) [30]. In fact, in the absence of MyD88, bacterial translocation is weakened and intestinal and lung injuries are alleviated, which is due to the reduction in neutrophil aggregation, lower levels of inflammatory mediators, alleviation of pulmonary vascular injury, and the improved survival rate [31]. Victoni et al. confirmed that blocking the TLR/MyD88 pathway reduced intestinal and lung injury after II/R, thus improving the survival rate [32].

TLRs play an important role in innate immunity by regulating the activity of different NF-κBs. It was reported that the TLR4/NF-κB signaling pathway is the key mechanism regulating proinflammatory factors in the II/R-induced lung injury model [28]. Activation of TLR4 can promote the activation of NF-κBp65 and lead to the release of proinflammatory factors TNF-α, IL-1, IL-6, and IL-8 from pulmonary macrophages, resulting in ALI. The α-7 nicotinic acetylcholine receptor agonist can inhibit the expression of TLR4, reduce the transport of p65, diminish the activation of NF-κB and production of proinflammatory factors, and also inhibit the inflammatory reaction, thus reducing ALI caused by II/R [33]. In addition, bone marrow mesenchymal stem cells can downregulate the expression of TLR4/NF-κB and reduce cell apoptosis and inflammatory responses, thereby alleviating ALI induced by II/R. The inactivation of TLR4/NF-κB signaling also leads to the downregulation of caspase-3, a key protease in the apoptotic response [34]. The results of this study suggested that using bone marrow mesenchymal stem cells to target TLR4 offers a therapeutic regimen for ALI induced by II/R. The same results were verified in an experiment by Soares et al. The lung inflammatory response and apoptosis in TLR4-deficient mice were significantly reduced, which confirms that the TLR4 receptor signaling pathway plays an important role in ALI. Consequently, interfering with the TLR signal may be a promising therapeutic strategy [35] (Figure 3).

2.4. PKC/p66Shc Signaling Pathway. SHC protein is widely expressed in mammals and is a proapoptotic factor and proinflammatory mediator. Adaptor protein p66Shc (a member of the SHCA protein family) is a proapoptotic protein, which is composed of p64shc and p52shc proteins. Its proapoptotic effect mainly depends on the binding of cytochrome-c in mitochondria and its oxidation function; in the oxidation process, cytochrome-c is released into the cytoplasm to activate caspase-3, thus inducing apoptosis [36]. The stress response phosphorylates serine 36 of p66Shc, which plays an important role in the oxidative stress response and apoptosis [37]. Manganese superoxide dismutase (MnSOD) and Bcl-2 play an important role in the pathophysiological process of II/R, and both of which can be regulated by p66Shc [38]. II/R activated changes in reactive oxygen species accumulation, in which p66Shc phosphorylation of antioxidant factors GSH and MnSOD decreased, while phosphorylation of apoptosis-related factors increased for caspase-3 and decreased for Bcl-2. The use of polyphenol protocatechuic acid (PCA) can significantly reduce II/R-induced ALI by inhibiting p66sshc, increasing lung antioxidant factors, and reducing proapoptotic factors and inflammatory mediators [39]. This is consistent with previous

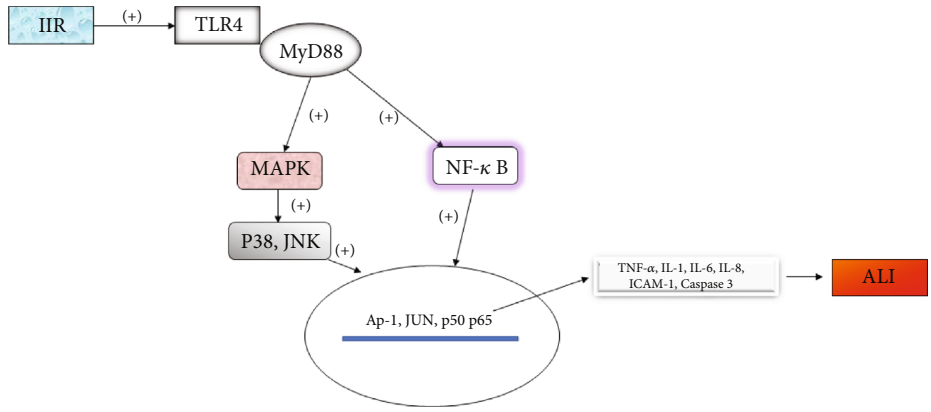

Figure 3: The TLR4 pathway regulates MAPK and NK-κB pathways to aggravate ALI.

studies in which the inhibition of p66Shc phosphorylation had a protective effect on lung epithelial cell apoptosis during ALI induced by II/R [38]. Inhibition of p66Shc phosphorylation may be a new treatment for ALI induced by II/R.

Protein kinase C (PKC) plays an important role in signal transduction by phosphorylating serine and threonine residues. Many conditions can cause PKC activation, including II/R [40]. Previous studies have shown that the activation of PKC βII specifically participates in the primary injury of II/R, and inhibiting the expression of PKC βII can prevent II/R injury [41]. However, PKC βII is selectively activated in the lung and liver after II/R. LY333531, a specific inhibitor of PKC βII, significantly reduced lung injury, inflammatory response, oxidative stress, and apoptosis after II/R. Meanwhile, it also significantly inhibited the activation of p66Shc and the binding of cytochrome-c, which resulted in a decrease of cytochrome-c release and caspase-3 cleavage, and reduced apoptosis. This study showed that the PKC βII/p66Shc pathway could be a specific therapeutic target, which can not only reduce II/R injury but also improve secondary lung injury, providing a new therapeutic strategy for the prevention of ALI caused by II/R [42] (Figure 4).

2.5. NLRP3 Inflammasome. An increasing number of studies have shown that nucleotide-binding oligomerization domain-like receptor (NLR) initiates an inflammatory response in a variety of diseases. When the body is injured, the NLRP3 inflammasome activates caspase-1 and IL-1β, leading to inflammation and tissue damage [43]. After II/R, the NLRP3 inflammasome plays an important role in early injury of the heart, liver, kidney, lung, intestine, and other organs [44]. Lipid mediators are effective regulators of innate and acquired immune responses and are associated with many inflammatory diseases [45]. II/R stimulates the release of lipid mediators, which can enhance the expression of NLRP3 inflammatory bodies and the production of IL-1β in pulmonary vascular endothelial cells, thereby increasing pulmonary vascular permeability and the inflammatory response and resulting in ALI. Thus, NLRP3 inflammation-driven IL-1β is a new potential target for the prevention and treatment of ALI induced by II/R [46] (Figure 5).

2.6. mTOR, VAP-1, NADPH Enzyme, IRHOM2, and CIRP. mTOR is a serine/threonine kinase, which plays a key role in cell proliferation and survival. A large number of studies have shown that mTOR plays an important role in the pathogenesis of ALI during II/R [47]. mTOR includes two different compounds, mTORC1 and mTORC2. mTORC1 promotes protein synthesis by phosphorylation of P70S6K and eIF4E binding protein (4EBP) [48]. FKBP25 is a member of the FKBP family of immunoavidin proteins, which can form a complex with mTOR and then plays a role by regulating mTOR [49]. Neurilifordin F (NF) may reduce lung injury by activating FKBP25 and inhibiting the mTOR/P70S6K pathway. On the other hand, NF can reduce the expression of p65 and the activation of IL-1β by inhibiting TLR4. The decrease in p65 expression also reduces the activation of NLRP3/caspase-1 and the expression of inflammatory mediators, with an overall anti-inflammatory effect that improves ALI induced by II/R [50]. Similarly, the mTOR inhibitor rapamycin can inhibit the activation of NF-κB and reduce distal lung injury after II/R. Inhibition of the mTOR pathway is now a targeted therapy for ALI after II/R [51].

Leukocyte extravasation is also involved in II/R injury and ALI. Excessive leukocyte extravasation is largely the result of the increased expression of adhesion molecules on the surface of endothelial cells and neutrophils [52]. Vascular adhesion protein-1 (VAP-1) is an extracellular enzyme expressed in endothelial cells, which can regulate leukocyte extravasation. In the II/R state, tissue damage is mainly caused by exudative leukocytes. Blocking adhesion molecules to inhibit the interaction between leukocytes and endothelial cells can reduce the degree of tissue damage in II/R [53]. Jan et al. used gene-targeted animals to show that VAP-1 is important in II/R and ALI. Anti-VAP-1 antibody or small molecule SSAO inhibitor reduced II/R injury and lung injury caused by neutrophil aggregation in the lungs [54].

Oxidative stress is the main underlying factor in ALI induced by II/R, and mast cell activation aggravates oxidative stress and ALI induced by II/R [5]. In the acute lung injury model induced by II/R, NADPH oxidase (p47phox and gp91phox) activity increased. Resveratrol inhibited the activation of mast cells and significantly reduced oxidative stress and inflammatory reactions in lung tissue after IIR [55].

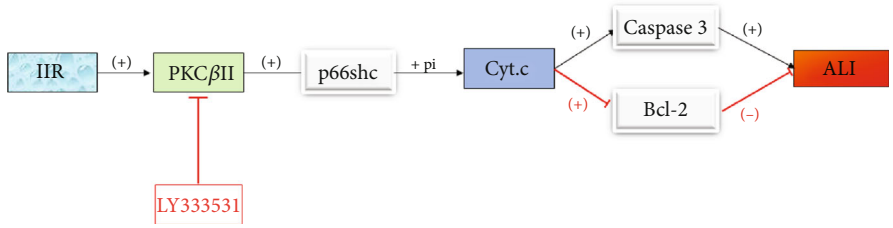

Figure 4: PKC βII promotes phosphorylation of p66shc, upregulates caspase-3, and downregulates Bcl-2, thereby aggravating ALI; LY333531 inhibits PKC βII and relieves ALI.

Figure 5: The NLRP3 inflammasome aggravates ALI.

Tryptase released by mast cells also plays a key role in II/R-induced ALI by activating protease-activated receptor-2 (PAR-2). Inhibition of tryptase release may be an effective scheme for the treatment of II/R-induced ALI [5].

TNF-alpha is involved in the pathogenesis of many inflammatory diseases. TNF-alpha converting enzyme (TACE) is necessary for the release of TNF-alpha. Inactivated rhomboid protein 2 (IRHOM2) has recently been identified as an important factor regulating TACE maturation in immune cells. In IRHOM2 gene knockout mice, inflammatory mediators, proapoptotic factors, and lung injury were significantly reduced. Therefore, IRHOM2 may play an important role in the pathogenesis of II/R-induced ALI and may be a new target for the treatment of II/R-induced ALI [56, 57].

The aseptic inflammation during II/R injury is triggered by endogenous injury-associated molecular pattern (DAMP) proteins. Cold-induced RNA-binding protein (CIRP) is a member of the DAMP family and constitutes a new inflammatory mediator, which can cause tissue damage during II/R [58]. DAMP binds to TLRs to enhance the activation of innate immune cells; furthermore, the immune system involves a wide range of inflammatory cascade reactions, which may be potential targets in the treatment of ALI caused by II/R [59]. In clinical trials, directly targeting TLR4 failed to show good efficacy, but targeting CIRP may be beneficial in the treatment of ALI and ARDS caused by II/R [60].

3. Biomarkers for Alleviating II/R-Induced ALI

3.1. Nrf2 Signaling Pathway. Nuclear factor erythroid 2-related factor (Nrf2) is a key regulator of intracellular oxidative homeostasis and plays an important role in inflammatory defense response [61]. Previous studies have shown that Nrf2 plays a protective role in ALI induced by II/R [62]. After II/R, the conformation of Nrf2 complex changes. Nrf2 dissociates from Keap1 and enters the nucleus through translocation, where it combines with antioxidant response elements to induce anti-inflammatory and antioxidative effects and promote cell survival [63].

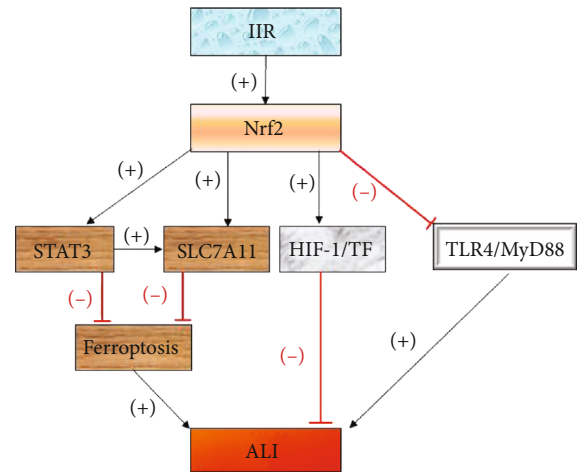

Figure 6: The Nrf2 pathway relieves ALI by regulating STAT3 and SLC7A11 to inhibit ferroptosis, by promoting HIF-1/TF and inhibiting TLR4.

Inflammation plays an important role in the pathogenesis of ALI induced by II/R. Blocking the TLR/MyD88 pathway has been shown to reduce lung injury in mice [32]. II/R can upregulate the expression of TLR4 and Nrf2 in the lung tissue of mice, while Nrf2 enters the nucleus to regulate the expression of TLR4, reduce the release of inflammatory mediators, and alleviate ALI. Nrf2 induces the expression of heme oxygenase-1 (HO-1), which is related to the PI3K/Akt pathway. The Nrf2/TLR4/Akt pathway, thus, plays an important role in II/R-induced ALI and provides a new therapeutic target for the treatment of ALI [64].

A number of studies have shown that II/R injury involves a nonapoptotic pathway, and ferroptosis is an iron-dependent and caspase-independent type of nonapoptotic cell death [65]. Ferroptosis is different from classical apoptosis in that iron catalyzes the formation of lipid-free radicals and the depletion of glutathione (GSH) [66]. Downstream factors of Nrf2 (HO-1, glutathione peroxidase, and SLC7A11) play a crucial role in cell defense [67]. Activated STAT3 reduces apoptosis under ferroptosis and plays an important role in the inflammatory response and development of tumors [68]. Nrf2 and STAT3 are both antioxidant

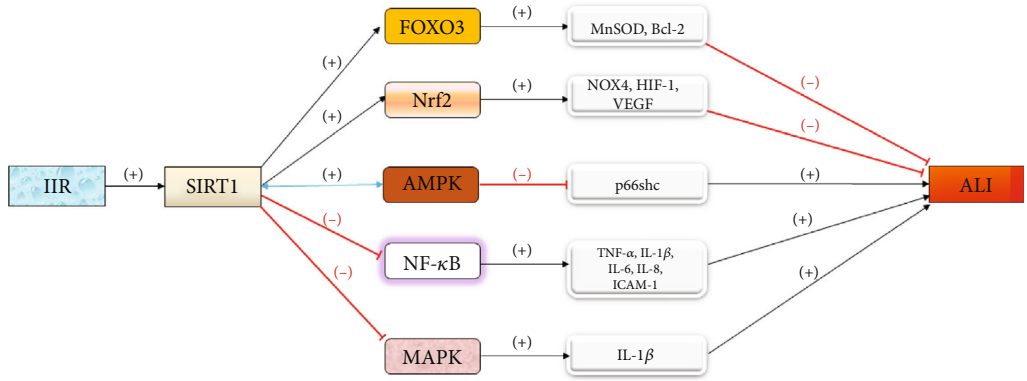

Figure 7: The SIRT1 pathway promotes FOXO3, Nrf2, and AMPK and inhibits NF-κB and MAPK to alleviate ALI.

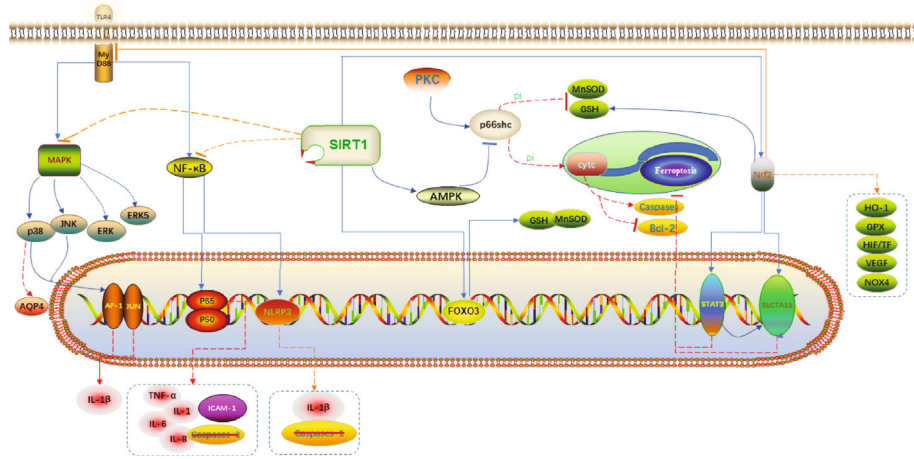

Figure 8: Cellular signal transduction pathways involved in ALI induced by II/R.

response elements. When cells are under oxidative stress, they can promote the expression of downstream target genes (such as SLC7A11) and reduce cell apoptosis and tissue damage. During II/R, Nrf2 and STAT3 jointly upregulate the expression of SLC7A11 and HO-1 and inhibit ferroptosis, thus reducing II/R-induced ALI and providing a new scheme for targeting the Nrf2 pathway in the treatment of II/R-induced ALI [69]. Similarly, p53 inhibitor IASPP inhibits ferroptosis through the Nrf2/HIF-1/TF signaling pathway [70]. Intestinal ischemic postconditioning promotes HO-1 expression through the Nrf2 pathway, inhibits oxidative stress and the inflammatory response, and reduces lung injury [71]. These studies all show that the Nrf2 pathway is an effective target for the treatment of ALI induced by II/R (Figure 6).

3.2. SIRT1 Signaling Pathway. SIRT1 is a nicotinamide adenine dinucleotide- (NAD-) dependent deacetylase. Through deacetylation of FOXO3, SIRT1 plays important antioxidative, anti-inflammatory, and antiapoptotic roles in ALI induced by II/R [72]. SIRT1 enhances cell viability under stress by regulating different downstream factors (p53, NF-κB, and FOXO); for example, SIRT1 deacetylates FOXO3 and enhances cell resistance to oxidative stress through an antioxidant molecule (MnSOD) [73]. It is well known that the weakening of antioxidant stress and the activation of apoptotic signals play an important role in the pathogenesis of ALI induced by II/R. The antioxidant molecule MnSOD and antiapoptotic molecule Bcl-2 are closely related to ALI induced by II/R [74]. II/R activates a cascading reaction, which leads to the accumulation of reactive oxygen species, a decrease in SIRT1 and FOXO3 deacetylation, and a decrease in MnSOD and Bcl-2. Icariin can upregulate the expression of SIRT1, promote FOXO3 deacetylation, enhance the release of antioxidant molecules and antiapoptotic factors, and reduce the release of inflammatory mediators, which can protect lung tissue from injury caused by II/R; in contrast, the SIRT1/FOXO3 signaling pathway has little effect on experimental lung injury. The protective effect against ALI induced by II/R may be achieved by upregulating MnSOD and enhancing the expression of Bcl-2 [75].

In addition, upregulation of SIRT1 level can increase the translocation of Nrf2, thereby inhibiting the activation of MAPK and protecting cells from damage [76]. Nrf2 is an important transcription factor, which not only protects cells from injury but also participates in ischemic angiogenesis [77]. Nrf2 regulates the expression of nonphagocytic oxidase 4 (NOX4), hypoxia-inducible factor 1A, and vascular endothelial growth factor and combines with them to resist oxidative stress [78]. In the model of II/R injury in mice, it was found that Nrf2 participates in the vascular remodeling

caused by ALI after II/R injury. The increase in SIRT1 level induces the upregulation of Nrf2 and then promotes the angiogenesis of human pulmonary microvascular endothelial cells through gene regulation mediated by NOX4 [79]. Adenosine 5′-monophosphate- (AMP-) activated protein kinase (AMPK) is a key enzyme in bioenergy metabolism, which can be activated by a variety of anti-inflammatory drugs, and when coupled with SIRTs increases the activity of SIRT1 [80]. U-3 polyunsaturated fatty acids inhibit the release of inflammatory mediators and reduce ALI by activating the AMPK/SIRT1 pathway; in addition, these polyunsaturated fatty acids can inhibit p66Shc, restore claudin5 expression, restore the alveolar-capillary barrier, and reduce apoptosis by activating the AMPK/SIRT1 pathway. Therefore, regulating the AMPK/SIRT1 pathway may become a new mechanism to protect against ALI induced by II/R [81] (Figure 7).

4. Conclusion

II/R injury is a common type of tissue and organ injury, secondary to intestinal and mesenteric vascular diseases. Ischemia leads to hypoxia, cell injury, and necrosis. However, the recovery of blood flow and oxygen during reperfusion results in bacterial translocation, tissue damage, inflammatory response, and oxidative stress. II/R can also lead to distal tissue damage and distal organ failure, of which lung injury is the most common, which is also the cause of the high mortality resulting from II/R injury. Previous studies have shown that II/R-induced ALI involves bacterial translocation, inflammatory response, oxidative stress, cell apoptosis, and necrosis; signaling pathways and markers are summarized in Figure 8. Further research has identified biomarkers that play an important role in the pathogenesis of II/R-induced ALI, which involves various targets and signaling pathways in the cascading reaction of II/R-induced ALI. By blocking pathways that can aggravate the disease and activating the pathways that can alleviate the disease, clinical trials have shown exciting results and suggest new approaches for better diagnosis and treatment of ALI caused by II/R. We believe that the continuing development of biomarkers will lead to novel therapeutic applications and cures for ALI caused by II/R.

Data Availability

No data were used to support this study.

Conflicts of Interest

The authors declare they have no competing interests.

Acknowledgments

For information retrieval, this study was supported by the National Natural Science Foundation of China (81701965 to ZF) and the Natural Science Foundation of Liaoning Province (20180550116 to ZF and 2019-MS-069 to ZF).

References

[1] A. PIERRO and S. EATON, "Intestinal ischemia reperfusion injury and multisystem organ failure," *Seminars in Pediatric Surgery*, vol. 13, no. 1, pp. 11–17, 2004.

[2] A. Stallion, T. D. Kou, S. Q. Latifi et al., "Ischemia/reperfusion: a clinically relevant model of intestinal injury yielding systemic inflammation," *Journal of Pediatric Surgery*, vol. 40, no. 3, pp. 470–477, 2005.

[3] J.-P. Idrovo, W.-L. Yang, A. Jacob et al., "AICAR attenuates organ injury and inflammatory response after intestinal ischemia and reperfusion," *Molecular Medicine*, vol. 20, no. 1, pp. 676–683, 2015.

[4] D. Tendler, "Acute intestinal ischemia and infarction," *Seminars in Gastrointestinal Disease*, vol. 14, no. 2, pp. 66–76, 2003.

[5] X. Gan, D. Liu, P. Huang, W. Gao, X. Chen, and Z. Hei, "Mast-cell-releasing tryptase triggers acute lung injury induced by small intestinal ischemia-reperfusion by activating PAR-2 in rats," *Inflammation*, vol. 35, no. 3, pp. 1144–1153, 2012.

[6] R. Ding, J. Han, Y. Tian, R. Guo, and X. Ma, "Sphingosine-1-phosphate attenuates lung injury induced by intestinal ischemia/reperfusion in mice: role of inducible nitric-oxide synthase," *Inflammation*, vol. 35, no. 1, pp. 158–166, 2012.

[7] T. ZARUBIN and J. HAN, "Activation and signaling of the p38 MAP kinase pathway," *Cell Research*, vol. 15, no. 1, pp. 11–18, 2005.

[8] T. V. Arumugam, E. Okun, S.-C. Tang, J. Thundyil, S. M. Taylor, and T. M. Woodruff, "Toll-like receptors in ischemia-reperfusion injury," *Shock*, vol. 32, no. 1, pp. 4–16, 2009.

[9] J. Fang, "The MAPK signalling pathways and colorectal cancer," *The Lancet Oncology*, vol. 6, no. 5, pp. 322–327, 2005.

[10] S. Salim, "VSL#3 probiotics provide protection against acute intestinal ischaemia/reperfusion injury," *Benef Microbes*, vol. 4, no. 4, pp. 357–365, 2013.

[11] Y.-h. Pei, X.-m. Cai, J. Chen et al., "The role of p38 MAPK in acute paraquat-induced lung injury in rats," *Inhalation Toxicology*, vol. 26, no. 14, pp. 880–884, 2014.

[12] R. L. Zemans and M. A. Matthay, "Bench-to-bedside review: the role of the alveolar epithelium in the resolution of pulmonary edema in acute lung injury," *Critical care*, vol. 8, no. 6, pp. 469–477, 2004.

[13] R. Goodman, "Cytokine-mediated inflammation in acute lung injury," *Cytokine & Growth Factor Reviews*, vol. 14, no. 6, pp. 523–535, 2003.

[14] S. Li, Z. Ni, B. Cong et al., "CCK-8 inhibits LPS-induced IL-1beta production in pulmonary interstitial macrophages by modulating PKA, p38, and NF-kappaB pathway," *Shock*, vol. 27, no. 6, pp. 678–686, 2007.

[15] D.-Y. Zheng, M. Zhou, J. Jin et al., "Inhibition of P38 MAPK downregulates the expression of IL-1beta to protect lung from acute injury in intestinal ischemia reperfusion rats," *Mediators Inflamm*, vol. 2016, article 9348037, 2016.

[16] A. S. Verkman, "Aquaporins in clinical medicine," *Annual review of medicine*, vol. 63, pp. 303–316, 2012.

[17] L.-L. Xiong, Y. Tan, H.-Y. Ma et al., "Administration of SB239063, a potent p38 MAPK inhibitor, alleviates acute lung injury induced by intestinal ischemia reperfusion in rats associated with AQP4 downregulation," *International Immunopharmacology*, vol. 38, pp. 54–60, 2016.

[18] A. S. Baldwin Jr., "The NF-kappa B and I kappa B proteins: new discoveries and insights," *Annual review of immunology*, vol. 14, pp. 649–683, 1996.

[19] J. H. Yao, X. S. Zhang, S. S. Zheng et al., "Prophylaxis with carnosol attenuates liver injury induced by intestinal ischemia/reperfusion," *World Journal of Gastroenterology*, vol. 15, no. 26, pp. 3240–3245, 2009.

[20] Z. Yang, X.-. R. Zhang, Q. Zhao et al., "Knockdown of TNF-α alleviates acute lung injury in rats with intestinal ischemia and reperfusion injury by upregulating IL-10 expression," *International Journal of Molecular Medicine*, vol. 42, no. 2, pp. 926–934, 2018.

[21] J. Fan, R. D. Ye, and A. B. Malik, "Transcriptional mechanisms of acute lung injury," *American journal of physiology Lung cellular and molecular physiology*, vol. 281, no. 5, pp. L1037–L1050, 2001.

[22] A. R. Moschen, A. Kaser, B. Enrich et al., "Visfatin, an adipocytokine with proinflammatory and immunomodulating properties," *Journal of immunology*, vol. 178, no. 3, pp. 1748–1758, 2007.

[23] H. MALHI and G. J. GORES, "Cellular and molecular mechanisms of liver injury," *Gastroenterology*, vol. 134, no. 6, pp. 1641–1654, 2008.

[24] M. HASMANN and I. SCHEMAINDA, "FK866, a highly specific noncompetitive inhibitor of nicotinamide phosphoribosyltransferase, represents a novel mechanism for induction of tumor cell apoptosis," *Cancer Research*, vol. 63, no. 21, pp. 7436–7442, 2003.

[25] I. Mallick, "Review: ischemia-reperfusion injury of the intestine and protective strategies against injury," *Digestive Diseases and Sciences*, vol. 49, no. 9, pp. 1359–1377, 2004.

[26] Z. Fan, J. Yao, Y. Li, X. Hu, H. Shao, and X. Tian, "Anti-inflammatory and antioxidant effects of curcumin on acute lung injury in a rodent model of intestinal ischemia reperfusion by inhibiting the pathway of NF-kb," *International Journal of Clinical and Experimental Pathology*, vol. 8, no. 4, pp. 3451–3459, 2015.

[27] J. A. Hagar, D. A. Powell, Y. Aachoui, R. K. Ernst, and E. A. Miao, "Cytoplasmic LPS activates caspase-11: implications in TLR4-independent endotoxic shock," *Science*, vol. 341, no. 6151, pp. 1250–1253, 2013.

[28] D. Ben, "TLR4 mediates lung injury and inflammation in intestinal ischemia-reperfusion," *The Journal of Surgical Research*, vol. 174, no. 2, pp. 326–333, 2012.

[29] M. Yamamoto, K. Takeda, and S. Akira, "TIR domain-containing adaptors define the specificity of TLR signaling," *Molecular Immunology*, vol. 40, no. 12, pp. 861–868, 2004.

[30] D. Jiang, J. Liang, Y. Li, and P. W. Noble, "The role of toll-like receptors in non-infectious lung injury," *Cell Research*, vol. 16, no. 8, pp. 693–701, 2006.

[31] J. L. Carvalho, A. Britto, A. L. de Oliveira et al., "Beneficial effect of low-level laser therapy in acute lung injury after i-I/R is dependent on the secretion of IL-10 and independent of the TLR/MyD88 signaling," *Lasers in Medical Science*, vol. 32, no. 2, pp. 305–315, 2017.

[32] T. Victoni, F. R. Coelho, A. L. Soares et al., "Local and remote tissue injury upon intestinal ischemia and reperfusion depends on the TLR/MyD88 signaling pathway," *Medical Microbiology and Immunology*, vol. 199, no. 1, pp. 35–42, 2010.

[33] Y. He, Z. Q. Ye, X. Li et al., "Alpha7 nicotinic acetylcholine receptor activation attenuated intestine-derived acute lung injury," *The Journal of Surgical Research*, vol. 201, no. 2, pp. 258–265, 2016.

[34] J. Liu, T. Chen, P. Lei, X. Tang, and P. Huang, "Exosomes released by bone marrow mesenchymal stem cells attenuate lung injury induced by intestinal ischemia reperfusion via the TLR4/NF-κB pathway," *International Journal of Medical Sciences*, vol. 16, no. 9, pp. 1238–1244, 2019.

[35] A. L. Soares, F. R. Coelho, R. Guabiraba et al., "Tumor necrosis factor is not associated with intestinal ischemia/reperfusion-induced lung inflammation," *Shock*, vol. 34, no. 3, pp. 306–313, 2010.

[36] M. Giorgio, E. Migliaccio, F. Orsini et al., "Electron transfer between cytochrome c and $p66^{Shc}$ generates reactive oxygen species that trigger mitochondrial apoptosis," *Cell*, vol. 122, no. 2, pp. 221–233, 2005.

[37] E. MIGLIACCIO, M. GIORGIO, and P. G. PELICCI, "Apoptosis and aging: role of p66Shc redox protein," *Antioxidants & Redox Signaling*, vol. 8, no. 3-4, pp. 600–608, 2006.

[38] S. Haga, K. Terui, M. Fukai et al., "Preventing hypoxia/reoxygenation damage to hepatocytes by $p66^{shc}$ ablation: up-regulation of anti-oxidant and anti- apoptotic proteins," *Journal of Hepatology*, vol. 48, no. 3, pp. 422–432, 2008.

[39] G. Z. Wang, J. H. Yao, H. R. Jing et al., "Suppression of the p66shc adapter protein by protocatechuic acid prevents the development of lung injury induced by intestinal ischemia reperfusion in mice," *The journal of trauma and acute care surgery*, vol. 73, no. 5, pp. 1130–1137, 2012.

[40] T. Fujita, T. Asai, M. Andrassy et al., "PKCbeta regulates ischemia/reperfusion injury in the lung," *The Journal of Clinical Investigation*, vol. 113, no. 11, pp. 1615–1623, 2004.

[41] Z. Chen, G. Wang, X. Zhai et al., "Selective inhibition of protein kinase C $\_\beta\__2$ attenuates the adaptor $P66^{Shc}$-mediated intestinal ischemia-reperfusion injury," *Cell Death & Disease*, vol. 5, no. 4, article e1164, 2014.

[42] G. Wang, Z. Chen, F. Zhang et al., "Blockade of PKCβ protects against remote organ injury induced by intestinal ischemia and reperfusion via a p66shc-mediated mitochondrial apoptotic pathway," *Apoptosis*, vol. 19, no. 9, pp. 1342–1353, 2014.

[43] Y. He, H. Hara, and G. Núñez, "Mechanism and regulation of NLRP3 inflammasome activation," *Trends in Biochemical Sciences*, vol. 41, no. 12, pp. 1012–1021, 2016.

[44] Y. Jia, R. Cui, C. Wang et al., "Metformin protects against intestinal ischemia-reperfusion injury and cell pyroptosis via TXNIP-NLRP3-GSDMD pathway," *Redox biology*, vol. 32, article 101534, 2020.

[45] J. Rossaint, J. L. Nadler, K. Ley, and A. Zarbock, "Eliminating or blocking 12/15-lipoxygenase reduces neutrophil recruitment in mouse models of acute lung injury," *Critical care*, vol. 16, no. 5, p. R166, 2012.

[46] H. Ito, H. Kimura, T. Karasawa et al., "NLRP3 inflammasome activation in lung vascular endothelial cells contributes to intestinal ischemia/reperfusion-induced acute lung injury," *Journal of immunology*, vol. 205, no. 5, pp. 1393–1405, 2020.

[47] Y. Hu, J. Liu, Y. F. Wu et al., "mTOR and autophagy in regulation of acute lung injury: a review and perspective," *Microbes and Infection*, vol. 16, no. 9, pp. 727–734, 2014.

[48] J. Jin, K. Hu, M. Ye, D. Wu, and Q. He, "Rapamycin reduces podocyte apoptosis and is involved in autophagy and mTOR/P70S6K/4EBP1 signaling," *Cellular Physiology and Biochemistry*, vol. 48, no. 2, pp. 765–772, 2018.

[49] C. Kang, "FKBP family proteins: immunophilins with versatile biological functions," *Neuro-Signals*, vol. 16, no. 4, pp. 318–325, 2008.

[50] Y. Tan, W. Zuo, L. Huang et al., "Nervilifordin F alleviates intestinal ischemia/reperfusion-induced acute lung injury via inhibiting inflammasome and mTOR pathway," *International Immunopharmacology*, vol. 89, article 107014, Partt A, 2020.

[51] T. Iida, T. Takagi, K. Katada et al., "Rapamycin improves mortality following intestinal ischemia-reperfusion via the inhibition of remote lung inflammation in mice," *Digestion*, vol. 92, no. 4, pp. 211–219, 2015.

[52] K. Ley, C. Laudanna, M. I. Cybulsky, and S. Nourshargh, "Getting to the site of inflammation: the leukocyte adhesion cascade updated," *Nature Reviews Immunology*, vol. 7, no. 9, pp. 678–689, 2007.

[53] A. Kakkar, "Leukocyte and endothelial adhesion molecule studies in knockout mice," *Current Opinion in Pharmacology*, vol. 4, no. 2, pp. 154–158, 2004.

[54] J. Kiss, S. Jalkanen, F. Fülöp, T. Savunen, and M. Salmi, "Ischemia-reperfusion injury is attenuated in VAP-1-deficient mice and by VAP-1 inhibitors," *European Journal of Immunology*, vol. 38, no. 11, pp. 3041–3049, 2008.

[55] X. Huang, W. Zhao, D. Hu et al., "Resveratrol efficiently improves pulmonary function via stabilizing mast cells in a rat intestinal injury model," *Life Sciences*, vol. 185, pp. 30–37, 2017.

[56] P. Issuree, T. Maretzky, D. R. McIlwain et al., "iRHOM2 is a critical pathogenic mediator of inflammatory arthritis," *The Journal of Clinical Investigation*, vol. 123, no. 2, pp. 928–932, 2013.

[57] J. H. Kim, J. Kim, J. Chun, C. Lee, J. P. Im, and J. S. Kim, "Role of iRhom2 in intestinal ischemia-reperfusion-mediated acute lung injury," *Scientific reports*, vol. 8, no. 1, p. 3797, 2018.

[58] X. Qiang, W. L. Yang, R. Wu et al., "Cold-inducible RNA-binding protein (CIRP) triggers inflammatory responses in hemorrhagic shock and sepsis," *Nature Medicine*, vol. 19, no. 11, pp. 1489–1495, 2013.

[59] H. Eltzschig, "Ischemia and reperfusion–from mechanism to translation," *Nature Medicine*, vol. 17, no. 11, pp. 1391–1401, 2011.

[60] C. Cen, J. McGinn, M. Aziz et al., "Deficiency in cold-inducible RNA-binding protein attenuates acute respiratory distress syndrome induced by intestinal ischemia-reperfusion," *Surgery*, vol. 162, no. 4, pp. 917–927, 2017.

[61] A. T. Dinkova-Kostova, R. V. Kostov, and A. G. Kazantsev, "The role of Nrf2 signaling in counteracting neurodegenerative diseases," *The FEBS Journal*, vol. 285, no. 19, pp. 3576–3590, 2018.

[62] B. M. Hybertson and B. Gao, "Role of the Nrf2 signaling system in health and disease," *Clinical Genetics*, vol. 86, no. 5, pp. 447–452, 2014.

[63] T. W. Kensler, N. Wakabayashi, and S. Biswal, "Cell survival responses to environmental stresses via the Keap1-Nrf2-ARE pathway," *Annual review of pharmacology and toxicology*, vol. 47, pp. 89–116, 2007.

[64] J. Yan, J. Li, L. Zhang et al., "Nrf2 protects against acute lung injury and inflammation by modulating TLR4 and Akt signaling," *Free Radical Biology and Medicine*, vol. 121, pp. 78–85, 2018.

[65] S. Dixon, "Ferroptosis: an iron-dependent form of nonapoptotic cell death," *Cell*, vol. 149, no. 5, pp. 1060–1072, 2012.

[66] J. Y. Cao and S. J. Dixon, "Mechanisms of ferroptosis," *Cellular and molecular life sciences : CMLS*, vol. 73, no. 11-12, pp. 2195–2209, 2016.

[67] Z. Fan, A. K. Wirth, D. Chen et al., "Nrf2-Keap1 pathway promotes cell proliferation and diminishes ferroptosis," *Oncogene*, vol. 6, no. 8, article ???, 2017.

[68] E. J. Hillmer, H. Zhang, H. S. Li, and S. S. Watowich, "STAT3 signaling in immunity. Cytokine & growth factor reviews," vol. 31, pp. 1–15, 2016.

[69] Z. Qiang, H. Dong, Y. Xia, D. Chai, R. Hu, and H. Jiang, "Nrf2 and STAT3 alleviates ferroptosis-mediated IIR-ALI by regulating SLC7A11," *Oxidative Medicine and Cellular Longevity*, vol. 2020, Article ID 5146982, 2020.

[70] Y. Li, Y. Cao, J. Xiao et al., "Inhibitor of apoptosis-stimulating protein of p53 inhibits ferroptosis and alleviates intestinal ischemia/reperfusion-induced acute lung injury," *Cell Death and Differentiation*, vol. 27, no. 9, pp. 2635–2650, 2020.

[71] Q. Meng, "Ischemic post-conditioning attenuates acute lung injury induced by intestinal ischemia-reperfusion in mice: role of Nrf2," *Laboratory Investigation*, vol. 96, no. 10, pp. 1087–1104, 2016.

[72] L. Lai, L. Yan, S. Gao et al., "Type 5 adenylyl cyclase increases oxidative stress by transcriptional regulation of manganese superoxide dismutase via the SIRT1/FoxO3a pathway," *Circulation*, vol. 127, no. 16, pp. 1692–1701, 2013.

[73] M. Motta, "Mammalian SIRT1 represses forkhead transcription factors," *Cell*, vol. 116, no. 4, pp. 551–563, 2004.

[74] G. Kostopanagiotou, E. Avgerinos, C. Costopanagiotou et al., "Acute lung injury in a rat model of intestinal ischemia-reperfusion: the potential time depended role of phospholipases A_2," *The Journal of Surgical Research*, vol. 147, no. 1, pp. 108–116, 2008.

[75] F. Zhang, Z. L. Li, X. M. Xu et al., "Protective effects of icariin-mediated SIRT1/FOXO3 signaling pathway on intestinal ischemia/reperfusion-induced acute lung injury," *Molecular Medicine Reports*, vol. 11, no. 1, pp. 269–276, 2015.

[76] L. Gu, X. Tao, Y. Xu et al., "Dioscin alleviates BDL- and DMN-induced hepatic fibrosis via Sirt1/Nrf2-mediated inhibition of p38 MAPK pathway," *Toxicology and applied pharmacology*, vol. 292, pp. 19–29, 2016.

[77] Y. Wei, J. Gong, Z. Xu et al., "Nrf2 in ischemic neurons promotes retinal vascular regeneration through regulation of semaphorin 6A," *Proceedings of the National Academy of Sciences of the United States of America*, vol. 112, no. 50, pp. E6927–E6936, 2015.

[78] S. Pendyala, J. Moitra, S. Kalari et al., "Nrf2 regulates hyperoxia-induced Nox4 expression in human lung endothelium: Identification of functional antioxidant response elements on the _Nox4_ promoter," *Free Radical Biology & Medicine*, vol. 50, no. 12, pp. 1749–1759, 2011.

[79] D. Chai, L. Zhang, S. Xi, Y. Cheng, H. Jiang, and R. Hu, "Nrf2 activation induced by Sirt1 ameliorates acute lung injury after intestinal ischemia/reperfusion through NOX4-mediated gene regulation," *Cellular Physiology and Biochemistry: International Journal of Experimental Cellular Physiology, Biochemistry, and Pharmacology*, vol. 46, no. 2, pp. 781–792, 2018.

[80] C. Cantó, Z. Gerhart-Hines, J. N. Feige et al., "AMPK regulates energy expenditure by modulating NAD+ metabolism and SIRT1 activity," *Nature*, vol. 458, no. 7241, pp. 1056–1060, 2009.

[81] H. Jing, J. Yao, X. Liu et al., "Fish-oil emulsion (omega-3 polyunsaturated fatty acids) attenuates acute lung injury induced by intestinal ischemia-reperfusion through adenosine 5′-monophosphate-activated protein kinase-sirtuin1 pathway," *The Journal of Surgical Research*, vol. 187, no. 1, pp. 252–261, 2014.

Hindawi
Oxidative Medicine and Cellular Longevity
Volume 2021, Article ID 6657529, 18 pages
https://doi.org/10.1155/2021/6657529

Research Article

Inactivation of TOPK Caused by Hyperglycemia Blocks Diabetic Heart Sensitivity to Sevoflurane Postconditioning by Impairing the PTEN/PI3K/Akt Signaling

Sumin Gao,[1,2] **Rong Wang**,[1] **Siwei Dong**,[1] **Jing Wu**,[1] **Bartłomiej Perek**,[3] **Zhengyuan Xia**,[4,5] **Shanglong Yao**,[1] **and Tingting Wang**[1]

[1]*Department of Anesthesiology, Union Hospital, Tongji Medical College, Huazhong University of Science and Technology, 1277 Jiefang Avenue, Wuhan 430022, China*
[2]*Department of Emergency Medicine, The Affiliated Huaian No.1 People's Hospital of Nanjing Medical University, Huai'an, Jiangsu 223001, China*
[3]*Department of Cardiac Surgery and Transplantology, Poznan University of Medical Sciences, Poznań, Poland*
[4]*State Key Laboratory of Pharmaceutical Biotechnology, The University of Hong Kong, Hong Kong, China*
[5]*Department of Anesthesiology, Affiliated Hospital of Guangdong Medical University, Zhanjiang, Guangdong, China*

Correspondence should be addressed to Shanglong Yao; ysltian@163.com and Tingting Wang; wangtt201307@163.com

Received 31 December 2020; Revised 26 March 2021; Accepted 7 April 2021; Published 26 April 2021

Academic Editor: Daniele Vergara

The cardioprotective effect of sevoflurane postconditioning (SPostC) is lost in diabetes that is associated with cardiac phosphatase and tensin homologue on chromosome 10 (PTEN) activation and phosphoinositide 3-kinase (PI3K)/Akt inactivation. T-LAK cell-originated protein kinase (TOPK), a mitogen-activated protein kinase- (MAPKK-) like serine/threonine kinase, has been shown to inactivate PTEN (phosphorylated status), which in turn activates the PI3K/Akt signaling (phosphorylated status). However, the functions of TOPK and molecular mechanism underlying SPostC cardioprotection in nondiabetes but not in diabetes remain unknown. We presumed that SPostC exerts cardioprotective effects by activating PTEN/PI3K/Akt through TOPK in nondiabetes and that impairment of TOPK/PTEN/Akt blocks diabetic heart sensitivity to SPostC. We found that in the nondiabetic C57BL/6 mice, SPostC significantly attenuated postischemic infarct size, oxidative stress, and myocardial apoptosis that was accompanied with enhanced p-TOPK, p-PTEN, and p-Akt. These beneficial effects of SPostC were abolished by either TOPK kinase inhibitor HI-TOPK-032 or PI3K/Akt inhibitor LY294002. Similarly, SPostC remarkably attenuated hypoxia/reoxygenation-induced cardiomyocyte damage and oxidative stress accompanied with increased p-TOPK, p-PTEN, and p-Akt in H9c2 cells exposed to normal glucose, which were canceled by either TOPK inhibition or Akt inhibition. However, either in streptozotocin-induced diabetic mice or in H9c2 cells exposed to high glucose, the cardioprotective effect of SPostC was canceled, accompanied by increased oxidative stress, decreased TOPK phosphorylation, and impaired PTEN/PI3K/Akt signaling. In addition, TOPK overexpression restored posthypoxic p-PTEN and p-Akt and decreased cell death and oxidative stress in H9c2 cells exposed to high glucose, which was blocked by PI3K/Akt inhibition. In summary, SPostC prevented myocardial ischemia/reperfusion injury possibly through TOPK-mediated PTEN/PI3K/Akt activation and impaired activation of this signaling pathway may be responsible for the loss of SPostC cardioprotection by SPostC in diabetes.

1. Introduction

Ischemic heart disease is one of the leading causes of death worldwide, particularly in patients with diabetes [1]. Restoration of blood flow to an ischemic heart is necessary to salvage the ischemic myocardium, but reperfusion of an ischemic region can result in myocardial ischemia/reperfusion (IR) injury due to oxidative stress [2]. Studies have shown that

sevoflurane postconditioning (SPostC) could protect the myocardium against reperfusion-induced injury and reduce myocardial infarct size [3, 4]. However, patients with diabetes have a remarkably higher mortality rate owing to increased IR injury and the beneficial effects of SPostC almost completely disappeared [5–7]. Therefore, elucidating the underlying mechanisms to prevent the myocardial IR injury in diabetes is a significant challenge faced by modern anesthetic practices.

Phosphatase and tensin homolog deleted on chromosome ten (PTEN) is a dual lipid and protein phosphatase that antagonizes the phosphatidylinositol 3-kinase/Akt (PI3K/Akt) signaling pathway and regulates cellular survival and growth. Studies have shown that cardiac-specific PTEN inactivation protects myocardial IR injury by activating the PI3K/Akt signaling in mice [8]. However, cardiac PTEN is increased in streptozotocin- (STZ-) induced diabetic rats, which is responsible for the loss of diabetic heart sensitivity to ischemic postconditioning through PI3K/Akt inactivation [9]. In addition, accumulating evidence has demonstrated that SPostC protects the rat hearts against IR injury via the activation of the PI3K/Akt signaling, which is one of the important signaling pathways involved in IR injury [10]. These investigations collectively suggest that the PTEN/PI3K/Akt signaling plays an important role in SPostC-induced cardioprotection and impairment of this signaling may be responsible for the loss of SPostC cardioprotection in diabetes. Thus, interventions that can enhance PTEN/PI3K/Akt activation may serve as a promising therapy against hyperglycemia-induced myocardial IR injury.

T-LAK cell-originated protein kinase (TOPK) is a mitogen-activated protein kinase- (MAPKK-) like serine/-threonine kinase, which plays a critical role in tumorigenesis and cell cycle regulation [11–13]. TOPK promotes cell proliferation and migration by modulating the PTEN/PI3K/Akt pathway and is associated with poor prognosis in lung cancer [14]. Interestingly, studies have shown that activation of TOPK-mediated antioxidation protects against focal cerebral IR injury [15]. Our previous study has demonstrated that remote ischemic postconditioning protects against renal IR injury that was associated with activation of TOPK and concomitant reduction in oxidative stress and inflammation [16]. However, whether TOPK plays significant roles in myocardial IR remains unclear. Of note, studies have shown that ischemic preconditioning alleviated myocardial IR injury and induced TOPK activation in rats, while TOPK inhibition aggravated the H_2O_2-induced oxidative stress in H9c2 cardiomyocytes [17]. These results suggest that TOPK may mediate a novel survival signal in myocardial IR through inhibiting oxidative stress. However, whether TOPK plays roles in SPostC cardioprotection through PTEN/PI3K/Akt and whether the impairment of this signaling is attributable to the loss of SPostC protection on the diabetic myocardium remain unclear.

Therefore, in the present study, TOPK or PI3K/Akt inhibitor and TOPK adenovirus were used both in *in vivo* models of myocardial IR in diabetic mice and *in vitro* models of hypoxia/reoxygenation (H/R) in the embryonic rat cardiomyocytes H9c2 cells, to test the hypotheses that SPostC protected against myocardial IR injury by activation of PTEN/PI3K/Akt through TOPK and that impairment of the TOPK/PTEN/Akt signaling blocked diabetic heart sensitivity to SPostC.

2. Materials and Methods

2.1. Experimental Animals and the Induction of Diabetes. Male C57BL/6 mice (7-8 weeks old) purchased from Wuhan University Animal Experiment Center (Wuhan, China) were used in this study. All animal studies were approved by the Institutional Animal Care and Use Committee of Tongji Medical College of Huazhong University of Science and Technology, China.

Mice were rendered diabetic by continuous intraperitoneal injection of streptozotocin (STZ) (40 mg/kg; Sigma-Aldrich, Merck Millipore, Darmstadt, Germany) diluted in citrate buffer (pH 4.2-4.5) for 5 days, whereas age- and sex-matched mice were injected with an equivalent volume of vehicle only (citrate buffer, pH 4.2-4.5). Three days after the last injection of STZ, the blood glucose concentrations of all mice were measured twice a week and mice with glucose levels higher than 300 mg/dl were considered as diabetic. All mice were housed in a temperature-controlled room and maintained on standard chow with free access to water. At termination (8 weeks after STZ treatment), mice were weighed and then subjected to myocardial IR as previously described [3].

2.2. Animal Experimental Protocol. The mice were randomly divided into seven groups as follows: (1) Sham: nondiabetic C57BL/6 mice received the surgery and were threaded the ligature underneath the left anterior descending coronary artery (LAD); however, there is no actual ligation in LAD; (2) IR: nondiabetic C57BL/6 mice underwent 45 min ischemia, followed by 120 min reperfusion; (3) IR+SPostC: nondiabetic C57BL/6 mice received IR and SPostC treatments. SPostC was achieved via continuous inhalation of 2% sevoflurane during the first 15 minutes of the reperfusion period; (4) IR+SPostC+LY: nondiabetic mice were pretreated with LY294002 (Sigma-Aldrich, Germany), a PI3K inhibitor, and then subjected to IR and SPostC. LY294002 was injected intraperitoneally at a single dose of 40 mg/kg 15 minutes before inducing coronary ischemia [16]; (5) IR+SPostC+HI: nondiabetic mice were pretreated with HI-TOPK-032 (Tocris Bioscience, UK), a TOPK-specific inhibitor which is reported to inhibit TOPK kinase activity [12, 16], and then subjected to IR and SPostC. HI-TOPK-032 was injected intraperitoneally at a single dose of 10 mg/kg for two consecutive days before inducing ischemia [16]; (6) DM+IR: diabetic mice underwent IR as previously described; (7) DM+IR+SPostC: diabetic mice underwent IR and SpostC as previously described. All groups except the IR+SPostC+HI and IR+SPostC+LY group received the same volume of vehicle intraperitoneally. The treatment protocol is outlined in Figure 1(a).

2.3. Cell Protocol. Embryonic rat cardiomyocytes H9c2 cells were obtained from the China Center for Type Culture

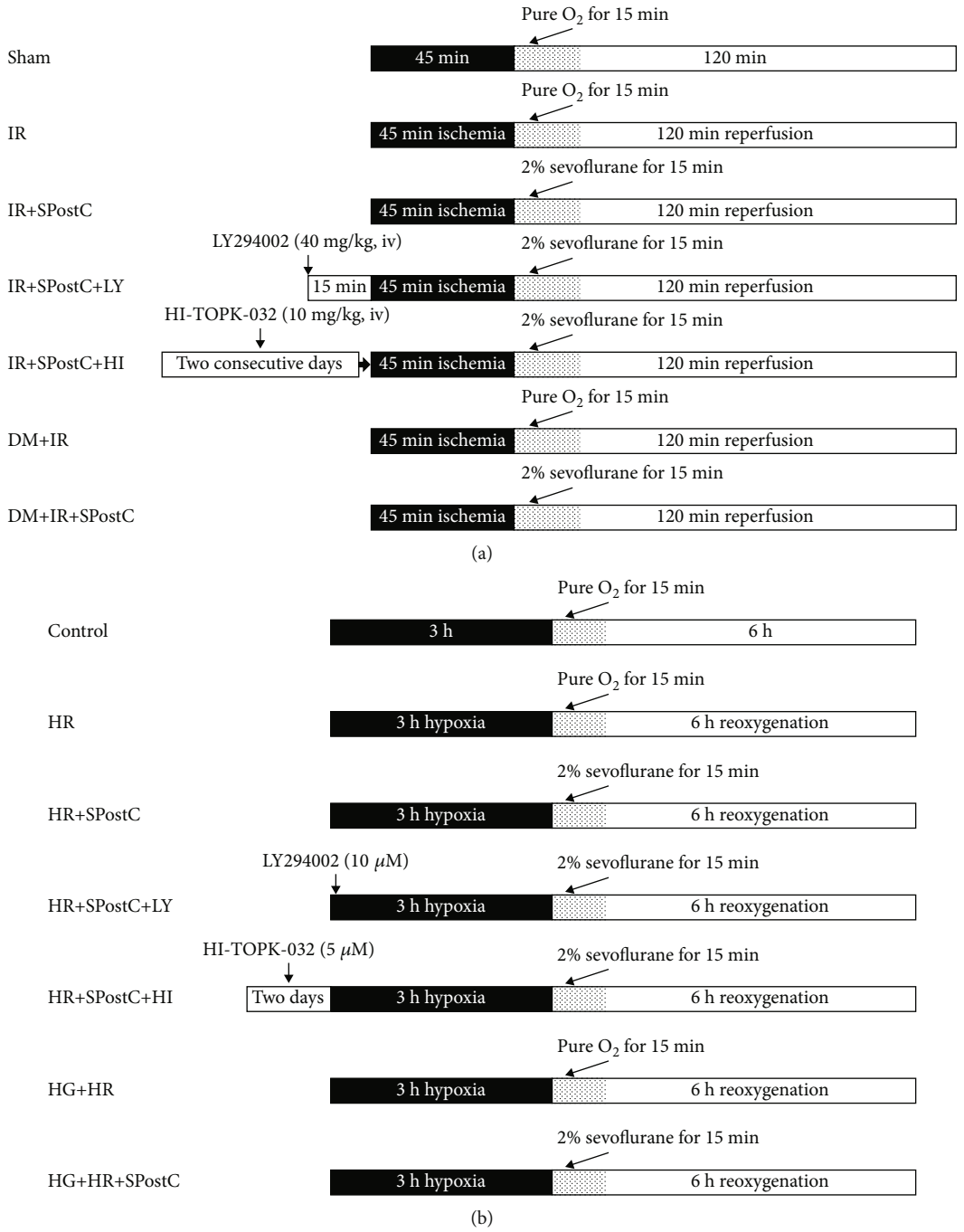

Figure 1: Model flow diagram of sevoflurane postconditioning (SPostC) protective effects against myocardial ischemia/reperfusion (IR) injury. (a) Experimental animal models. (b) Schematic presentation of the cell models.

Collection (Wuhan, China). Cells were cultured in Dulbecco's modified Eagle's medium with 5.5 mM (normal glucose) or 25 mM glucose (high glucose) containing 10% (*v*/*v*) fetal bovine serum (FBS, Gibco) and grown at 37°C in a humidified atmosphere of 5% CO_2 and 95% air. Cells reached 80% to 90% confluence were subjected to experimental procedures.

The H9c2 cells were subjected to hypoxia/reoxygenation (3 h of hypoxia followed by 6 h of reoxygenation) to achieve hypoxia/reoxygenation (HR) model as previously described [3]. The cells were divided into seven groups: (1) control: the H9c2 cells were incubated with 5.5 mM (normal glucose) glucose without performing HR; (2) HR: the H9c2 cells were incubated with normal glucose and subjected to HR; (3) HR+SPostC: H9c2 cells in the SpostC group were placed in a closed container at a temperature of 37°C; sevoflurane evaporation tank was then opened to allow 2% sevoflurane to flow through the closed container with O2 for 15 minutes at the onset of reoxygenation. Sevoflurane and oxygen concentrations were monitored using a multifunctional detector (PM8050; Drägerwerk, Germany) for the same duration of

time; (4) HR+SPostC+LY: the H9c2 cells exposed to a normal glucose concentration in the presence of 10 μM LY294002 were subjected to HR and SpostC [18]; (5) HR+SPostC+HI: the H9c2 cells exposed to a normal glucose concentration in the presence of HI-TOPK-032 were subjected to HR and SPostC. HI-TOPK-032 was given at 5 μM for two days before inducing HR [19]; (6) high glucose (HG)+HR: the H9c2 cells were incubated with a high-glucose concentration and subjected to HR; (7) HG+HR+SPostC: the H9c2 cells incubated with a high-glucose concentration were subjected to HR and SPostC. The model is illustrated in Figure 1(b).

The subgroups of H9c2 cells under high glucose were infected with adenoviral vectors encoding for full-length rat TOPK (Ad-TOPK) or adenoviral vectors (Ad-vector) provided by Vigene Bioscience (Jinan, China) for three days (MOI, 50). The generation of full-length rat TOPK was in term of NM_001079937.1 gene from NCBI. Recombinant adenovirus was constructed with a virus titer of 1×10^{11} vp/ml. After transfection with Ad-TOPK or Ad-vector, cells were subjected to HR with or without SPostC as described above. An additional group of H9c2 cells transfected with Ad-TOPK was treated with LY294002 before hypoxia stimulation. Following termination of the experiment, the cells and medium were collected and stored at -80°C until analysis.

2.4. Determination of Risk and Infarct Sizes. Myocardial infarct size was assessed by the Evans blue/TTC staining after 2 h reperfusion. The unstained region by Evans blue dye was considered as the area at risk (AAR), and the white color area was considered as the infarct size (IS). The area at risk was calculated as a percentage of the total ventricular area, while the infarct size was measured by macroscopic method and the infarcted area reported as the percentage of the area at risk. The extent of the area of necrosis was determined by computerized planimetry (ImageJ 1.4).

2.5. Measurement of Creatinine Kinase-MB (CK-MB). After reperfusion for 2 h, blood samples were collected and the release of CK-MB was measured by enzyme-linked immunoassay using a commercial kit (Uscn Life Science Inc., China) as previously described [2].

2.6. Detection of Myocardial Apoptosis and Immunofluorescence. Myocardial apoptosis was determined by TUNEL staining using an in situ cell detection kit (TUNEL assay, Roche Diagnostics GmbH, Mannheim, Germany). Tissues were extracted from infarcted regions of the myocardium. After fixation and permeabilization, TUNEL assays were performed. Tri-formol-fixed myocardial tissue samples embedded in paraffin were detected to identify the apoptotic cells via a fluorescence microscope. The TUNEL-positive cells were counted under a high-power microscopic field at a magnification of 400x, and at least three randomly selected fields per heart were analyzed.

The myocardial sections were incubated overnight with rabbit anti-TOPK (Phospho Thr9) antibody (Abcam, UK) at 4°C. After being washed, the sections were further incubated with CY3 goat anti-rabbit IgG at room temperature for 2 h followed by DAPI staining at room temperature for 10 min. All the stained sections were photographed by using an inverted microscope (Olympus Life Science, Tokyo, Japan) with a color CCD camera.

2.7. Measurement of Oxidative Stress. After 2 h reperfusion, blood samples were collected for the measurement of malondialdehyde (MDA) concentration. MDA was determined by using a thiobarbituric acid (TBA) method using a trace assay kit (Nanjing Jiancheng Bioengineering Institute, Nanjing, China) as reported [20]. Superoxide dismutase (SOD) level was measured by hydroxylamine method using an assay kit (Nanjing Jiancheng Bioengineering Institute, Nanjing, China).

Myocardial superoxide anion production was measured by fluorescent-labeled dihydroethidium (DHE) staining (Keygen Biotech Co., Ltd., Nanjing, China) according to the assay kit protocol.

2.8. Measurement of Cell Viability and Lactate Dehydrogenase (LDH). After 6 h reoxygenation, cell viability was determined by the MTT assay (Sigma-Aldrich, Germany) as described, and the supernatant of cell culture was collected for the measurement of LDH through a commercially available detection kit (Nanjing Jiancheng Bioengineering Institute, Nanjing, China) via the colorimetric method according to the manufacturer's instructions.

2.9. Western Blot Analysis. Protein extracts were prepared according to the manufacturer's protocol as described in the protein extract kit (Keygen Biotech Co., China). Peri-infarct region of the left ventricular myocardium was harvested after 2 h of reperfusion in order to extract total protein samples for immunoblotting analysis. Total protein was determined using the BCA Protein assay kit (Sigma-Aldrich, Germany), and size was separated by sodium dodecyl sulfate-polyacrylamide gel electrophoresis (SDS-PAGE). Proteins were transferred to PVDF membrane. Primary antibodies were then incubated with the membrane strips at 4°C overnight at the following dilutions: Akt, phospho-Akt (Ser473), PTEN, and phospho-PTEN (Ser380/Thr382/383) (Cell Signaling Technology, USA) 1 : 1000 and TOPK and phospho-TOPK (Thr9) (Abcam, UK) 1 : 1000. Then, protein bands were incubated with a secondary antibody and detected by the ECL chemiluminescence method. Densitometric analyses of western blot images were performed using ImageJ software (ImageJ 1.4).

2.10. Statistical Analysis. All the values were expressed as the mean ± SD unless otherwise stated. GraphPad Prism software package (San Diego, CA) was used for data statistical analysis. One-way analysis of variance (ANOVA) was performed to detect significant differences between the experimental groups, followed by a t-test corrected for multiple comparisons (Student-Newman-Keuls). The P values < 0.05 were considered statistically significant.

3. Results

3.1. Physiological Parameters. As presented in Table 1, the water intake, food consumption, and blood glucose levels in the mice with STZ-induced diabetes were higher than those in the normal control mice ($P < 0.001$), while body weight

Table 1: General characteristics.

Parameters	Sham ($n = 7$)	IR ($n = 16$)	IR+SPostC ($n = 15$)	IR+SPostC+LY ($n = 15$)	IR+SPostC+HI ($n = 15$)	DM+IR ($n = 17$)	DM+IR+SPostC ($n = 18$)
Water intake (ml/kg/day)	6.2 ± 0.8	7.2 ± 1.0	5.7 ± 1.0	7.3 ± 1.2	6.7 ± 1.4	28.4 ± 7.9***	27.1 ± 4.7***
Food consumption (g/kg/day)	4.6 ± 0.5	4.9 ± 0.5	4.3 ± 0.6	4.7 ± 0.7	5.0 ± 0.5	6.6 ± 1.0***	6.4 ± 0.7***
Body weight (g)	27.6 ± 0.9	25.9 ± 1.6	26.6 ± 1.8	26.3 ± 1.3	26.3 ± 1.4	23.2 ± 1.0***	23.3 ± 1.0***
Plasma glucose (mM)	5.7 ± 0.7	6.1 ± 0.6	6.4 ± 0.6	5.9 ± 0.5	6.0 ± 0.5	26.0 ± 4.0***	24.9 ± 4.6***

Nondiabetic and diabetic mice (DM) were subjected to myocardial ischemia/reperfusion (IR) with or without sevoflurane postconditioning (SPostC) in the presence or absence of the PI3K inhibitor LY294002 (LY) or the TOPK kinase inhibitor HI-TOPK-032 (HI). All values are expressed as the mean ± SD. Water intake and food consumption were the average value of 8 weeks. Body weight and plasma glucose were measured among groups before inducing myocardial IR. ***$P < 0.001$ vs. their corresponding IR groups.

Table 2: Hemodynamic measurements at baseline, at 15 min of ischemia, and at 2 h of reperfusion in nondiabetic and diabetic rats with or without treatments.

Parameters	Sham	IR	IR+SPostC	IR+SPostC+LY	IR+SPostC+HI	DM+IR	DM+IR+SPostC
Heart rate (beats/min)							
Baseline	368 ± 9	370 ± 12	378 ± 14	371 ± 12	378 ± 14	384 ± 15	383 ± 16
Ischemia 15 min	375 ± 9	372 ± 14	369 ± 8	370 ± 12	366 ± 12	370 ± 15	370 ± 12
Reperfusion 2 h	373 ± 8	368 ± 11	368 ± 8	366 ± 17	370 ± 11	368 ± 16	365 ± 17
Mean arterial blood pressure (mmHg)							
Baseline	82.9 ± 5.1	79.8 ± 5.6	81.9 ± 4.5	79.3 ± 5.5	78.3 ± 4.5	79.7 ± 5.7	81.2 ± 4.7
Ischemia 15 min	81.3 ± 6.2	62.1 ± 4.7**	62.7 ± 5.3**	63.4 ± 5.9**	62.1 ± 4.8**	55.1 ± 4.3**#	53.9 ± 5.1**#
Reperfusion 2 h	83.0 ± 5.8	59.3 ± 2.3**	66 ± 5.4**#	60.6 ± 3.4**	60 ± 3.7**	53.0 ± 5.3**#	50.9 ± 5.1**##

Nondiabetic and diabetic mice (DM) were subjected to myocardial ischemia/reperfusion (IR) with or without sevoflurane postconditioning (SPostC) in the presence or absence of the PI3K inhibitor LY294002 (LY) or the TOPK kinase inhibitor HI-TOPK-032 (HI). All values are expressed as the mean ± SD. $n = 7$ per group. Heart rate and mean arterial pressure were measured at baseline and during myocardial IR. **$P < 0.01$ vs. their corresponding baseline; #$P < 0.05$ and ##$P < 0.01$ vs. their corresponding IR groups.

was significantly lower in diabetic mice than that in nondiabetic control ($P < 0.001$).

As shown in Table 2, the heart rate and mean arterial pressure were recorded throughout the experimental period. No significant difference was observed in average heart rate among the seven groups at baseline and throughout the experiments. There was no significant difference in the baseline mean arterial pressure among all groups. The mean arterial pressure during ischemia and reperfusion was lower than the baseline in all groups ($P < 0.01$) except the sham group. During myocardial IR, the mean arterial pressure of all diabetic groups was remarkably lower than that of the nondiabetic IR group ($P < 0.05$, Table 2). After 2 h reperfusion, the mean arterial pressure in the IR+SPostC group was increased compared with that in the IR group ($P < 0.05$).

3.2. Myocardial Ischemia/Reperfusion Injury In Vivo. The area at risk and the infarct size in the sham group were zero in nondiabetic mice (Figure S1(a)), which was consistent with our previous study in rat [21]. As shown in Figures 2(a) and 2(b), the area at risk did not differ significantly among the other IR groups, which meant that our myocardial IR model was reliable and reproducible. As shown in Figure 2(c), SPostC greatly attenuated the infarct size in C57BL/6 nondiabetic mice ($P < 0.01$). However, LY294002 and HI-TOPK-032, respectively, abolished the protective effect of SPostC in increasing infarct size in nondiabetic mice ($P < 0.01$). Diabetes significantly increased the myocardial infarct size in the DM+IR and DM+IR+SPostC group compared with the IR group ($P < 0.001$). However, the anti-infarct effect of SPostC was abolished completely in the diabetic mice (DM+IR+SPostC group vs. DM+IR group, $P > 0.05$).

CK-MB is one of the major biomarkers of myocardial cellular injury and can reflect the damage degree of heart. As shown in Figure 2(f), the release of plasma CK-MB was significantly increased after myocardial IR in nondiabetic mice ($P < 0.001$). SPostC significantly decreased the release of plasma CK-MB when compared with the IR group ($P < 0.01$). The effect of SPostC in decreasing CK-MB secretion was abolished by LY294002 and HI-TOPK-032 ($P > 0.01$). When compared with the nondiabetic groups, diabetes displayed elevated post-ischemic CK-MB release (DM+IR and DM+IR+SPostC groups vs. IR group, $P < 0.05$). Nevertheless, SPostC exerted no significant effect on the serum level of CK-MB in diabetic mice (DM+IR group vs. DM+IR+SPostC group, $P > 0.05$).

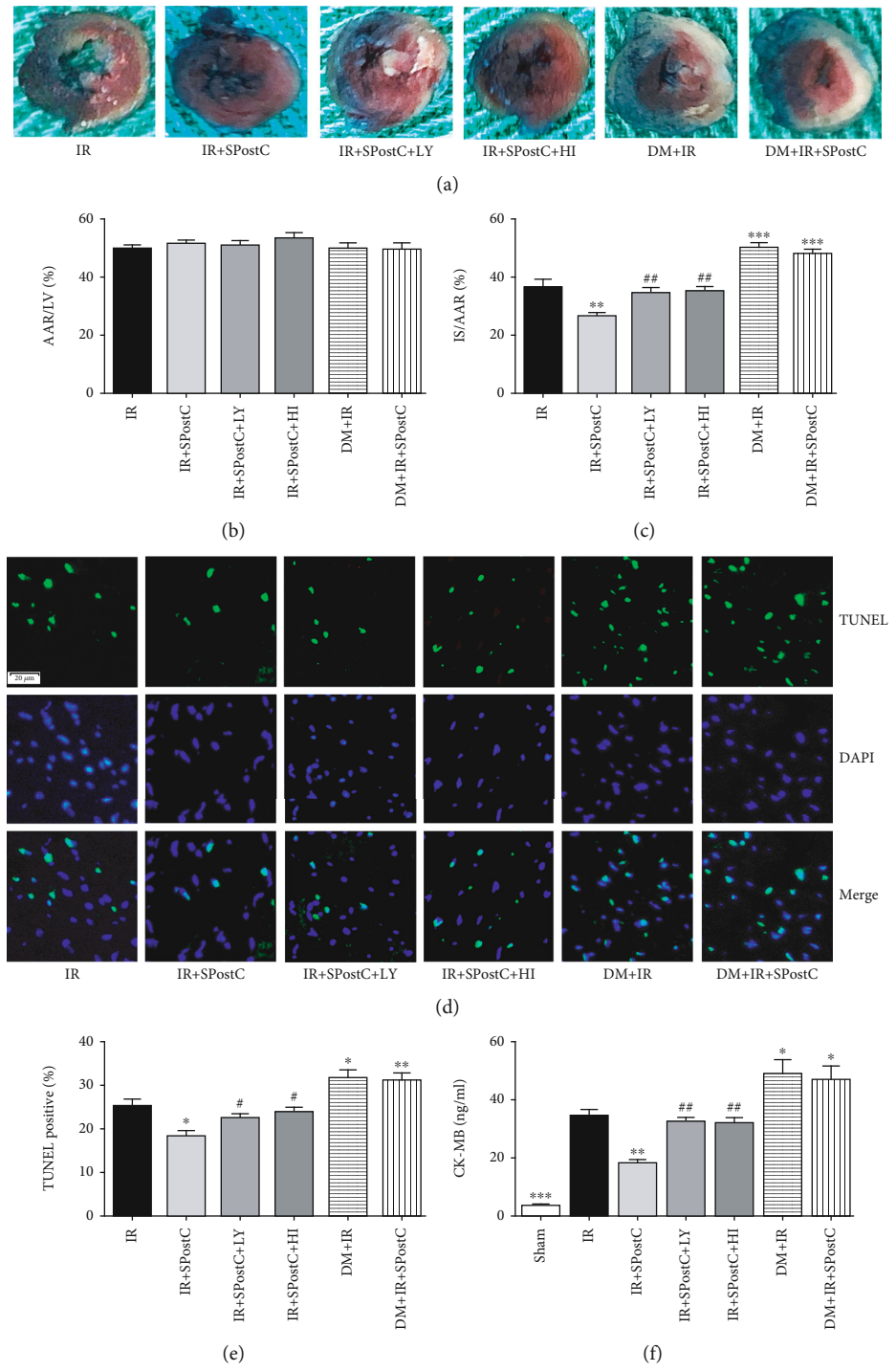

Figure 2: Myocardial IR injury and myocardial apoptosis after 45 min coronary occlusion followed by 120 min reperfusion with or without SPostC in nondiabetic and diabetic mice. IR and SPostC indicated nondiabetic mice received IR or IR+SPostC, respectively; IR+SPostC+LY and IR+SPostC+HI indicated nondiabetic mice pretreated with LY294002 (LY, a PI3K inhibitor) or HI-TOPK-032 (HI, a TOPK kinase inhibitor), respectively, and then subjected to IR and SPostC. DM+IR and DM+IR+SPostC indicated diabetic mice received IR or IR+SPostC, respectively. (a) Representative images of Evans blue and TTC staining in heart cross sections from each experimental group. Infarct area (INF: white); area at risk (AAR: red and white); perfused area (blue). (b) Comparison of area at risk per left ventricle (area at risk/left ventricle). (c) Comparison of area of infarct size normalized to the area at risk (infarct size/area at risk). (d) Myocardial apoptosis was assessed by the TUNEL assay in the heart sections (DAPI: nuclei, blue; TUNEL: apoptosis nuclei, green; magnification, ×400). (e) Quantification of TUNEL-positive cardiomyocytes (% of total). (f) Plasma CK-MB secretion detected using a commercial ELISA kit. All values are presented as the mean ± SD ($n = 7$ per group). $^{*}P < 0.05$, $^{**}P < 0.01$, and $^{***}P < 0.001$ compared with the IR group; $^{\#}P < 0.05$ and $^{\#\#}P < 0.01$ compared with the SPostC group.

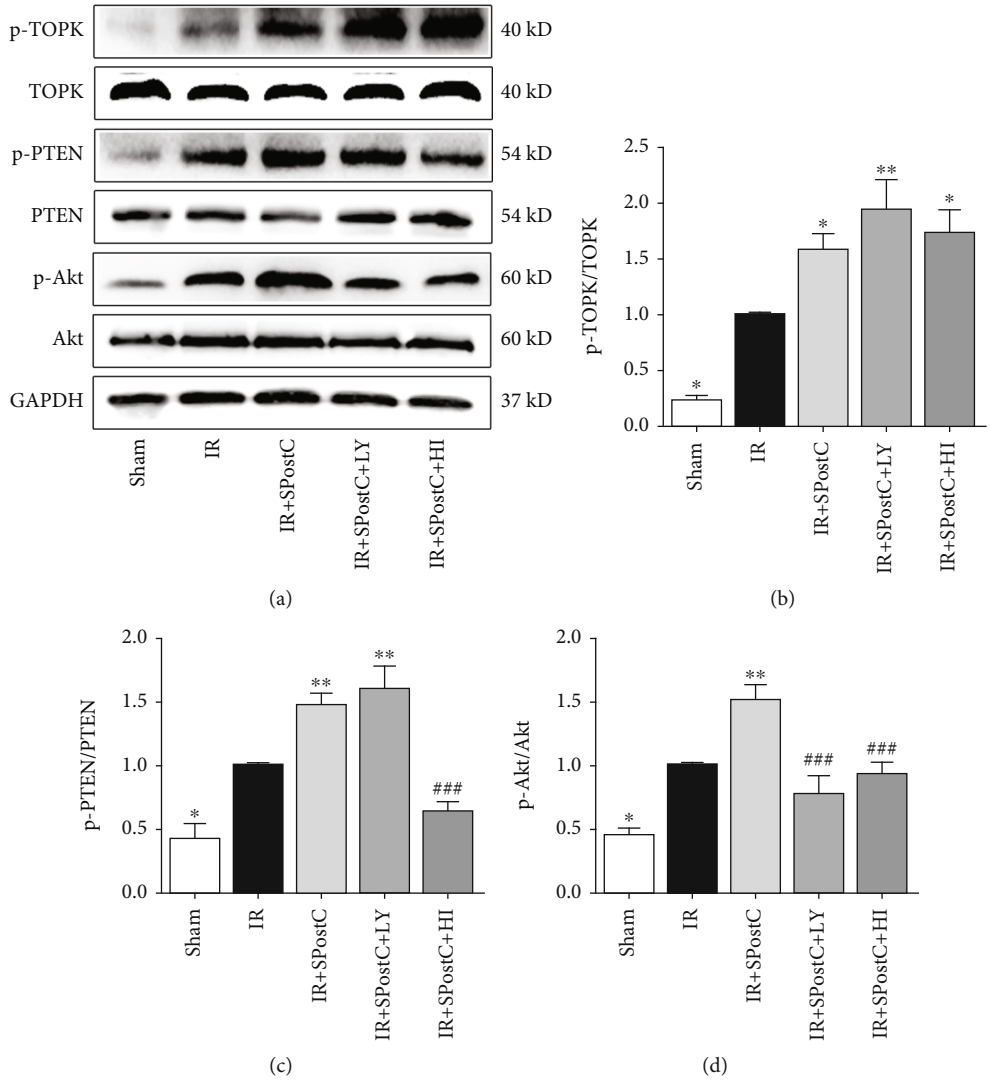

Figure 3: Myocardial TOPK (b), PTEN (c), and Akt (d) protein expression and their phosphorylation status after myocardial IR with or without SPostC in nondiabetic mice. IR+SPostC+LY and IR+SPostC+HI indicated mice pretreated with LY or HI, respectively, and then subjected to IR and SPostC. (a) Representation of western blots. Mean band density was normalized relative to GAPDH. The IR group was used as control and normalized to unity, and the protein expression of other groups was displayed as changes over this baseline. All values are presented as the mean ± SD ($n = 7$ per group). $^{*}P < 0.05$ and $^{**}P < 0.01$ compared with the IR group; $^{\#\#\#}P < 0.001$ compared with the SPostC group.

As shown in Figures 2(d) and 2(e), SPostC significantly reduced cardiomyocyte apoptosis, as evidenced by the decreased number of TUNEL-positive myocyte nuclei when compared with the IR group in nondiabetic mice ($P < 0.05$). However, the antiapoptotic effect of SPostC was canceled by LY294002 and HI-TOPK-032 ($P < 0.05$). Diabetic mice displayed increased cardiomyocyte apoptosis, as evidenced by the increased number of TUNEL-positive myocyte nuclei when compared with the nondiabetic groups (DM+IR and DM+IR+SPostC groups vs. IR group, $P < 0.05$). However, SPostC did not exert an antiapoptotic effect in the hearts of diabetic mice (DM+IR group vs. DM+IR+SPostC group, $P > 0.05$).

3.3. Levels of TOPK, PTEN, and Akt in the Hearts of Nondiabetic Mice. As shown in Figure 3, IR significantly induced the phosphorylation of cardiac TOPK, PTEN (inactivation), and Akt, which was further significantly increased by SPostC treatment (Figure 3, $P < 0.05$). LY294002, a PI3K inhibitor, decreased the Akt phosphorylation induced by SPostC ($P < 0.05$), but had no effect on TOPK or PTEN phosphorylation. Studies have shown that HI-TOPK-032 was docked to the active site of TOPK and directly suppressed TOPK kinase activity, which can inhibit the activation of its downstream target molecules but has no effect on the expression of total and phosphorylated TOPK [12]. As shown in Figure 3, HI-TOPK-032 remarkably blocked the increase of PTEN and Akt phosphorylation induced by SPostC ($P < 0.05$). However, the protein level of total and phosphorylated TOPK did not significantly change in the IR+SPostC+HI group when compared with the IR+SPostC group.

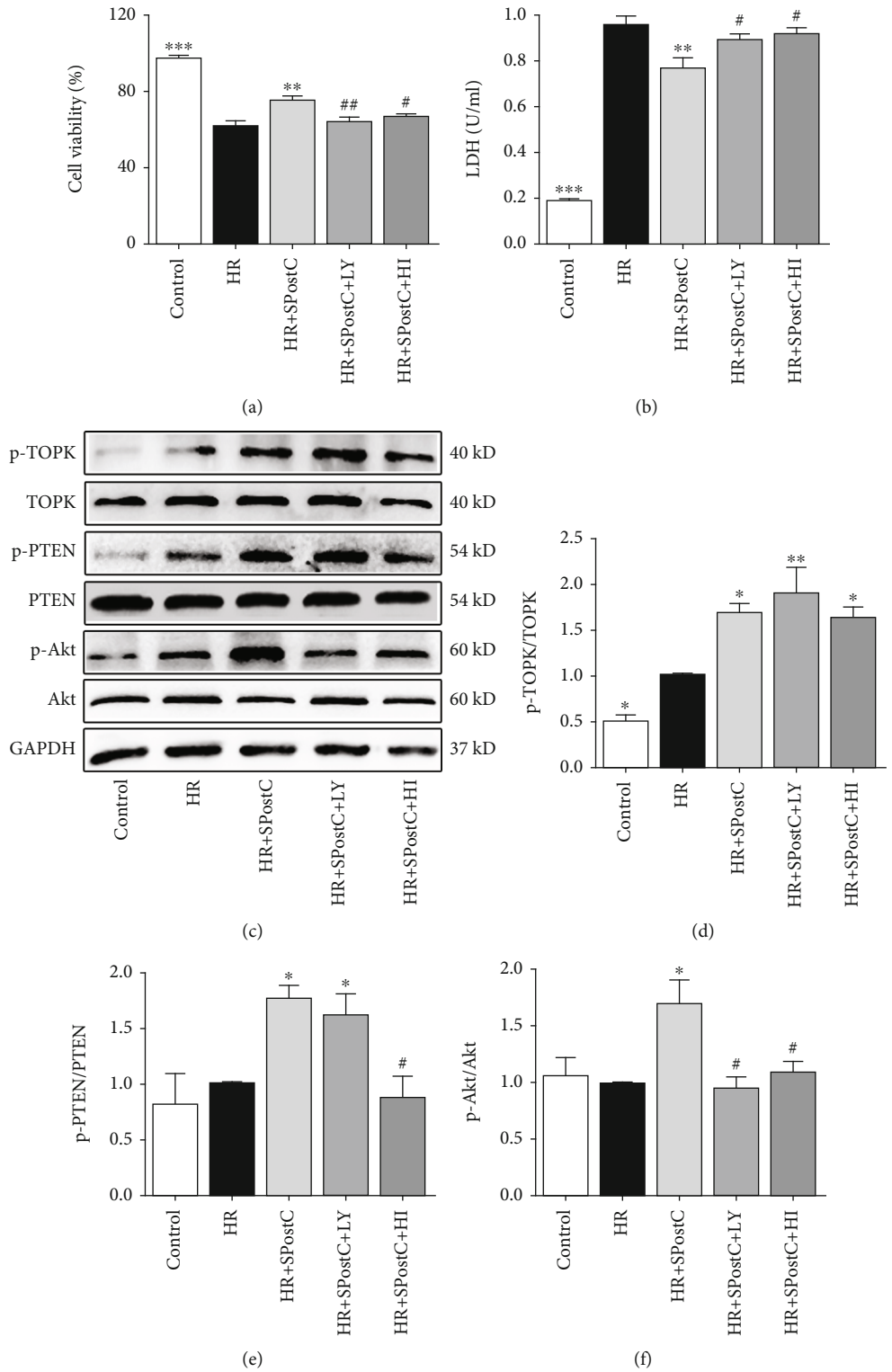

Figure 4: Cardiomyocyte injury and myocardial TOPK, PTEN, and Akt protein expression and their phosphorylation status assessed after hypoxia-reoxygenation (HR) with or without SPostC in H9c2 cells under normal glucose. LY or HI were applied, respectively, to block Akt and TOPK activation in H9c2 cells. (a) Cell viability assessed by MTT assay. (b) Lactate dehydrogenase (LDH) release. (c) Representative western blots. (d–f) Expression of TOPK (d), PTEN (e), and Akt (f) and their phosphorylation status. Mean band density was normalized relative to GAPDH. The IR group was used as control and normalized to unity, and the protein expression of other groups was displayed as changes over this baseline. All values are presented as the mean ± SD of three independent experiments each performed in triplicate. $^{*}P < 0.05$, $^{**}P < 0.01$, and $^{***}P < 0.001$ compared with the HR group; $^{\#}P < 0.05$ and $^{\#\#}P < 0.01$ compared with the SPostC group.

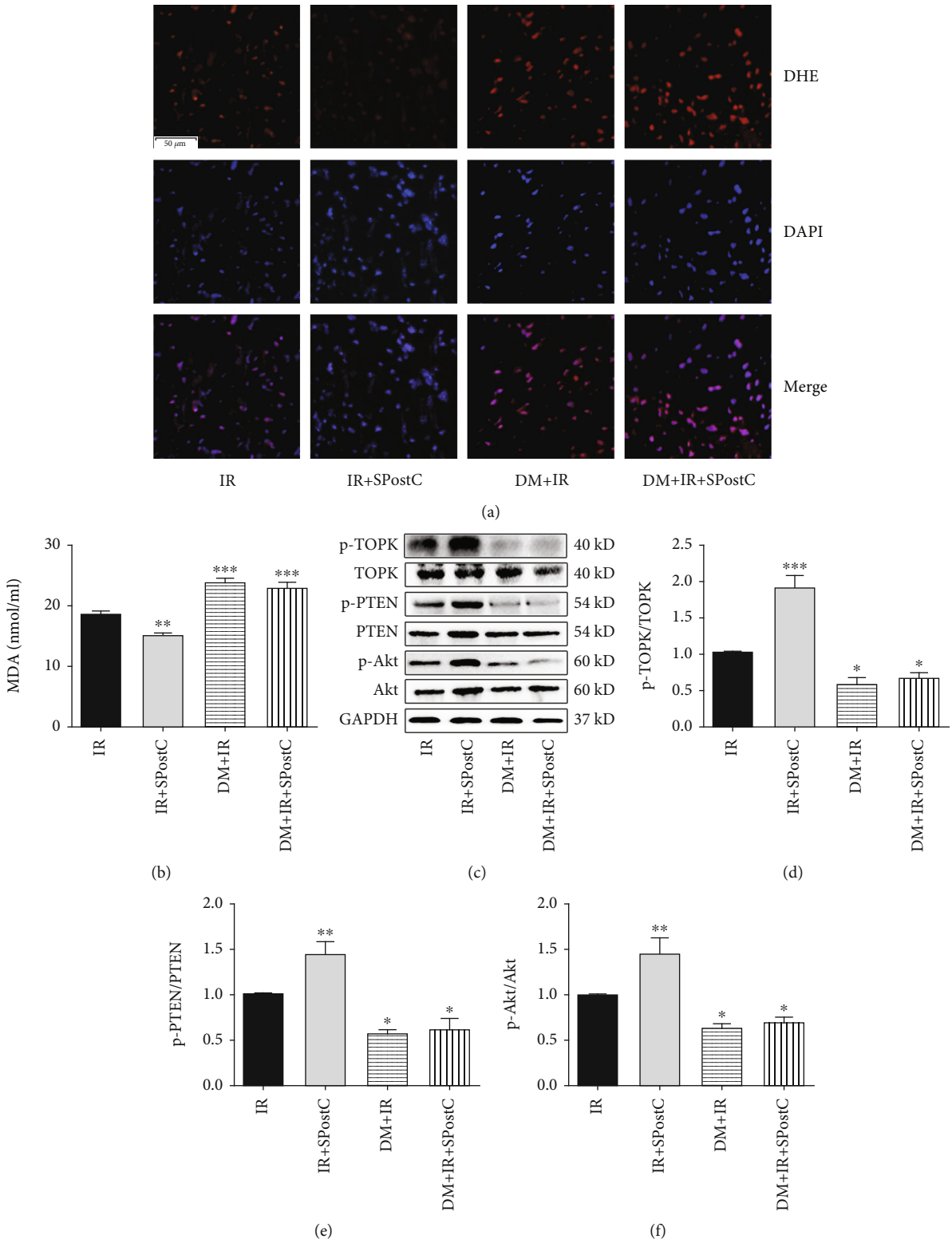

Figure 5: Continued.

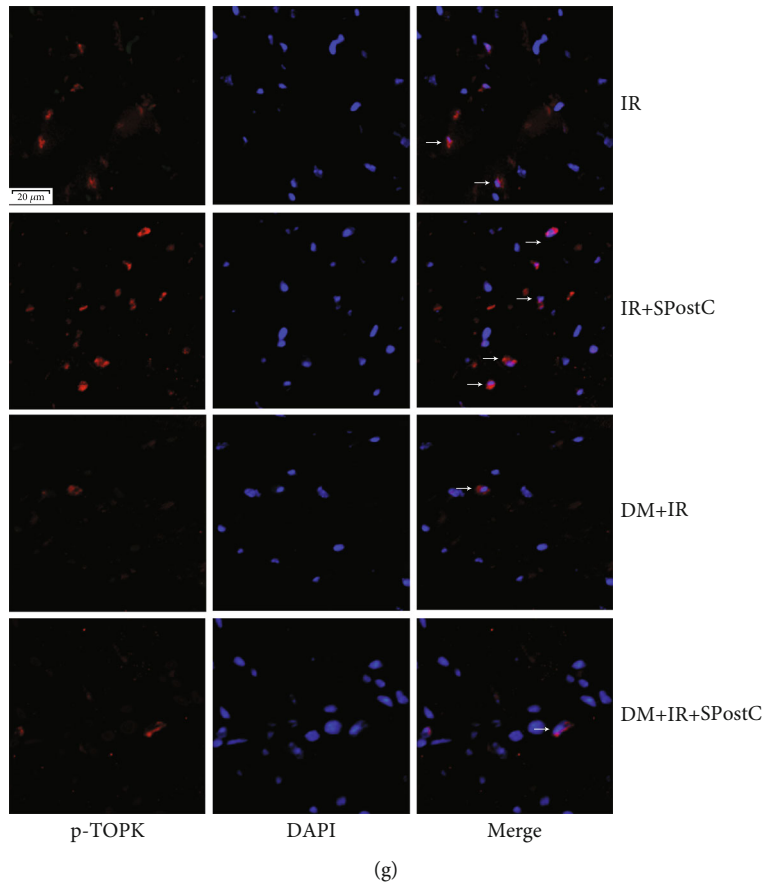

Figure 5: Oxidative stress and myocardial TOPK, PTEN, and Akt protein expression and their phosphorylation status assessed after myocardial IR with or without SPostC in nondiabetic and diabetic mice. (a) Representative photographs of dihydroethidium (DHE) staining detected by immunofluorescence in the mouse hearts. (DAPI: nuclei, blue; DHE fluorescence: red; magnification, ×400). (b) Serum levels of malondialdehyde (MDA) assessed by a kit. (c) Representative western blots. (d–f) Expression of TOPK (d), PTEN (e), and Akt (f) and their phosphorylation status. Mean band density was normalized relative to GAPDH. The IR group was used as control and normalized to unity, and the protein expression of other groups was displayed as changes over this baseline. (g) Myocardial phosphorylated TOPK level detected by immunofluorescence. All values are presented as the mean ± SD ($n = 7$ per group). $^{**}P < 0.01$ and $^{***}P < 0.001$ compared with the IR group.

3.4. Posthypoxic Cellular Injury and Levels of TOPK, PTEN, and Akt in H9c2 Cardiomyocytes Exposed to Normal Glucose. Posthypoxic cell death reflected as a decrease in cardiomyocyte viability and an increase in LDH activity in the medium after HR injury (Figures 4(a) and 4(b), $P < 0.05$). SPostC markedly increased cell viability and decreased LDH leakage in normal glucose condition ($P < 0.05$), which was canceled by LY294002 and HI-TOPK-032 in H9c2 cells.

In normal glucose condition, the phosphorylated levels of TOPK, PTEN, and Akt were elevated in the HR+SPostC group compared with the HR group (Figures 4(c)–4(f), $P < 0.05$). HI-TOPK-032 likewise inhibited the phosphorylation of PTEN and Akt induced by SPostC in H9c2 cells ($P < 0.05$). However, LY294002 blocked the phosphorylation of Akt induced by SPostC ($P < 0.05$), but had no effect on TOPK or PTEN phosphorylation in H9c2 cells.

3.5. Oxidative Stress Indicators and Levels of TOPK, PTEN, and Akt in the Hearts of Diabetic Mice. The immunofluorescence images showed that SPostC significantly reduced myocardial superoxide anion generation, as evidenced by the decreased number of dihydroethidium labeled nuclei in the IR+SPostC group when compared with the IR group in C57BL/6 mice (Figure 5(a), $P < 0.05$). Superoxide anion accumulation was increased in the hearts of diabetic mice when compared with that in nondiabetic mice ($P < 0.05$). However, the effect of SPostC in reducing superoxide anion generation was diminished in the hearts of diabetic mice.

The level of lipid peroxidation marker MDA in the IR+SPostC group was lower than that in the IR group (Figure 5(b), $P < 0.01$). Diabetes greatly augmented serum MDA level and canceled the antilipid oxidation effect of SPostC seen in the hearts of nondiabetic mice.

The phosphorylated level of TOPK in the peri-infarct tissue was detected by immunofluorescence (Figure 5(g)). SPostC increased the amount of p-TOPK-positive cells in the hearts of nondiabetic mice. In the diabetic heart, a significant decrease in TOPK activation was observed, and SPostC exerted no effect on the phosphorylation of TOPK in the hearts of diabetic mice.

Western blot analysis showed that the phosphorylation levels of TOPK, PTEN, and Akt were significantly increased

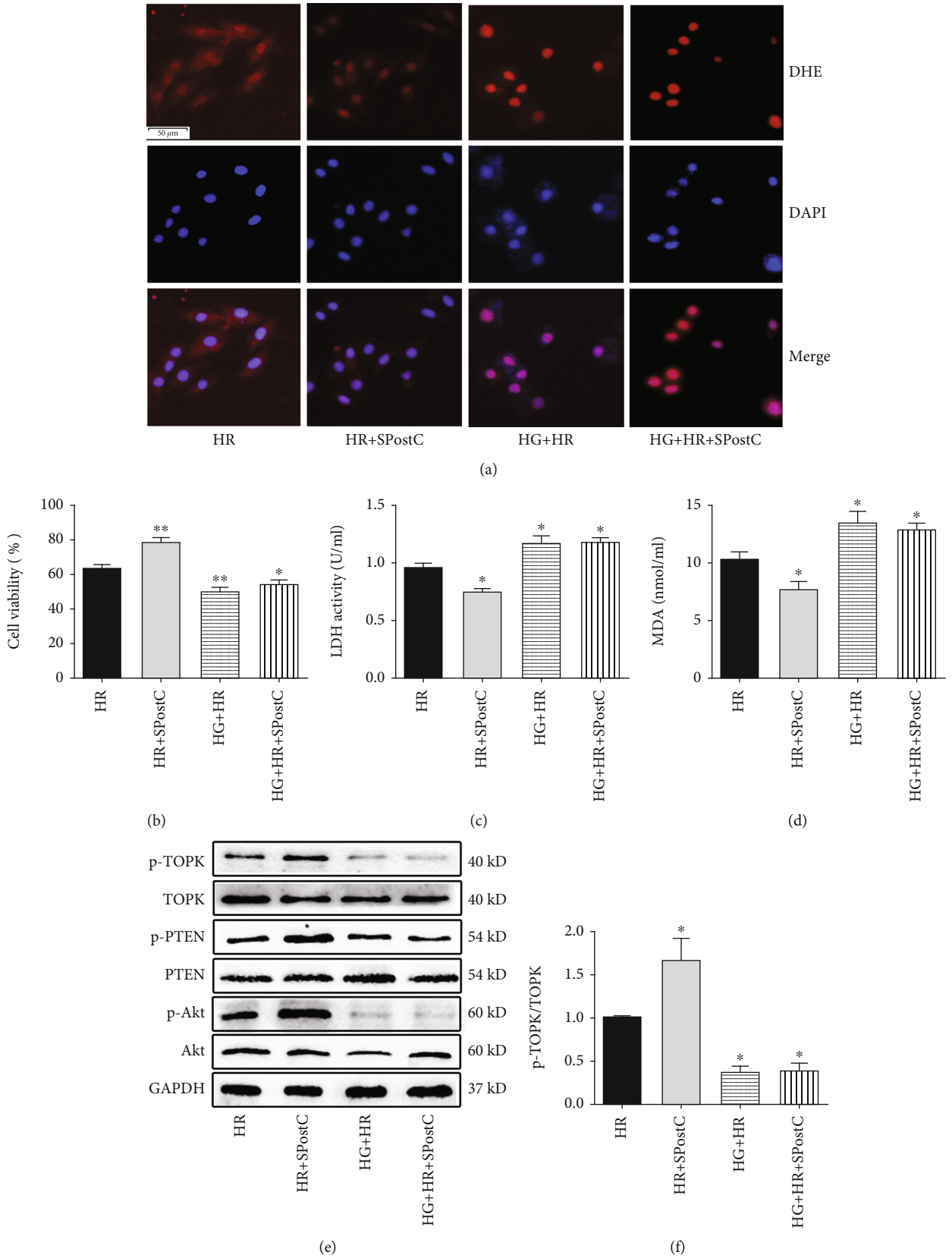

Figure 6: Continued.

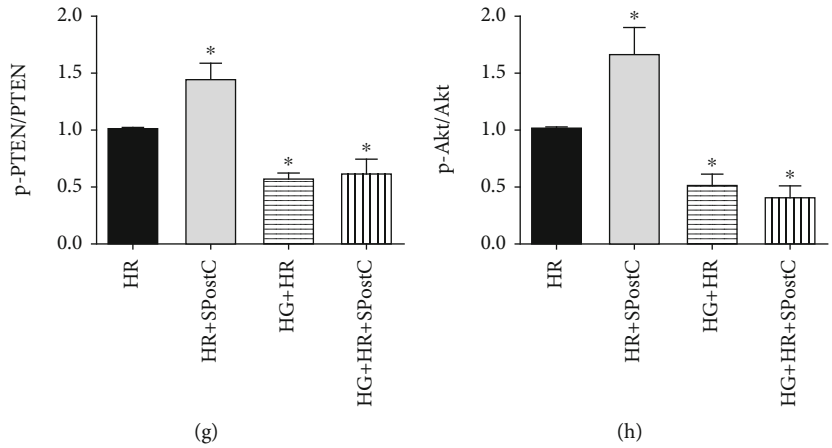

Figure 6: Cardiomyocyte injury and myocardial TOPK, PTEN, and Akt protein expression and their phosphorylation status as well as oxidative stress assessed after HR with or without SPostC in H9c2 cells under high glucose (HG) condition. (a) Representative photographs of dihydroethidium (DHE) staining detected by immunofluorescence in the mouse hearts. (DAPI: nuclei, blue; DHE fluorescence: red; magnification, ×400). (b) Cell viability assessed by MTT assay. (c) LDH release. (d) Serum levels of malondialdehyde (MDA) assessed by a kit. (e) Representation western blots. (f–h) Expression of TOPK (f), PTEN (g), and Akt (h) and their phosphorylation status. Mean band density was normalized relative to GAPDH. The IR group was used as control and normalized to unity, and the protein expression of other groups was displayed as changes over this baseline. All values are presented as the mean ± SD of three independent experiments each performed in triplicate. $^{*}P < 0.05$ and $^{**}P < 0.01$ compared with the HR group.

in the IR+SPostC group compared with the IR group (Figures 5(c)–5(f), $P < 0.05$). Importantly, diabetes remarkably reduced the phosphorylation levels of TOPK, PTEN, and Akt after myocardial IR (DM+IR and DM+IR+SPostC groups vs. IR group, $P < 0.05$). Nevertheless, the effect of SPostC in inducing the phosphorylation levels of TOPK, PTEN, and Akt was diminished in the hearts of diabetic mice ($P > 0.05$).

3.6. Posthypoxic Cellular Injury, Oxidative Stress, and Levels of TOPK, PTEN, and Akt in H9c2 Cardiomyocytes Exposed to High Glucose. After HR injury, H9c2 cardiomyocytes exposed to high glucose showed reduced cell viability and enlarged LDH leakage when compared with cells exposed to normal glucose (Figures 6(b) and 6(c), $P < 0.05$). Moreover, the effect of SPostC in reducing posthypoxic cellular injury was abolished in cells exposed to high glucose.

Superoxide anion and MDA accumulation were increased in H9c2 cardiomyocytes exposed to high glucose as compared to the HR group (Figures 6(a) and 6(d), $P < 0.05$). The posthypoxic elevations of superoxide anion and MDA generation in cardiomyocytes were attenuated by SPostC when cells were exposed to normal glucose but not to high glucose.

Posthypoxic phosphorylated levels of TOPK, PTEN, and Akt were remarkably reduced in H9c2 cardiomyocytes exposed to high glucose as compared to the HR group (Figures 6(e)–6(h), $P < 0.05$). SPostC exerted no significant effect on the phosphorylated levels of TOPK, PTEN, and Akt in cardiomyocytes exposed to high glucose.

3.7. Posthypoxic Cellular Injury and Oxidative Stress in Cardiomyocytes Exposed to High Glucose after TOPK Overexpression and Levels of TOPK, PTEN, and Akt. To determine whether or not cardiac TOPK overexpression can decrease the posthypoxic cellular injury in diabetes, TOPK was supplied using an adenoviral transfection system into H9c2 cells under high glucose. As shown in Figures 7(a) and 7(b), both the Ad-TOPK+HG+HR and Ad-TOPK+HG+HR+SPostC groups significantly increased cell viability and reduced LDH leakage when compared with the Ad-vector+HG+HR group ($P < 0.001$). However, when the PI3K/Akt inhibitor LY294002 was added in the Ad-TOPK+HG+HR group, the cell viability was reduced and released LDH concentration was increased significantly ($P < 0.001$), suggesting that PI3K/Akt inhibition blocked the cardioprotective effect of TOPK in H9c2 cardiomyocytes exposed to high glucose.

In order to observe the effect of TOPK supplementation on postischemic oxidative stress in diabetes, the levels of MDA and SOD were measured. Cardiac TOPK overexpression significantly decreased the postischemic MDA level (Figure 7(c)) and increased the postischemic SOD level (Figure S1(b)) in H9c2 cardiomyocytes exposed to high glucose (Ad-TOPK+HG+HR or Ad-TOPK+HG+HR+SPostC group vs. Ad-vector+HG+HR, $P < 0.01$). However, the antioxidation effect of TOPK was blocked by LY294002 in the Ad-TOPK+HG+HR+LY group when compared with the Ad-TOPK+HG+HR group ($P < 0.05$).

The bands of proteins in each group on western blot are shown in Figure 7(d). In Figure 7(e), the expression of TOPK was markedly elevated in the Ad-TOPK+HG+HR and Ad-TOPK+HG+HR+SPostC groups after TOPK transfection. The phosphorylated level of TOPK was likewise increased in the Ad-TOPK+HG+HR and Ad-TOPK+HG+HR+SPostC groups when compared with the Ad-vector+HG+HR group (Figure 7(f), $P < 0.001$). Then, the expression of PTEN was significantly reduced in the Ad-TOPK+HG+HR and Ad-TOPK+HG+HR+SPostC groups when compared with the Ad-vector+HG+HR group (Figure 7(g), $P < 0.01$). The phosphorylated levels of PTEN and Akt were enhanced in the Ad-TOPK+HG+HR and Ad-TOPK+HG+HR+SPostC groups

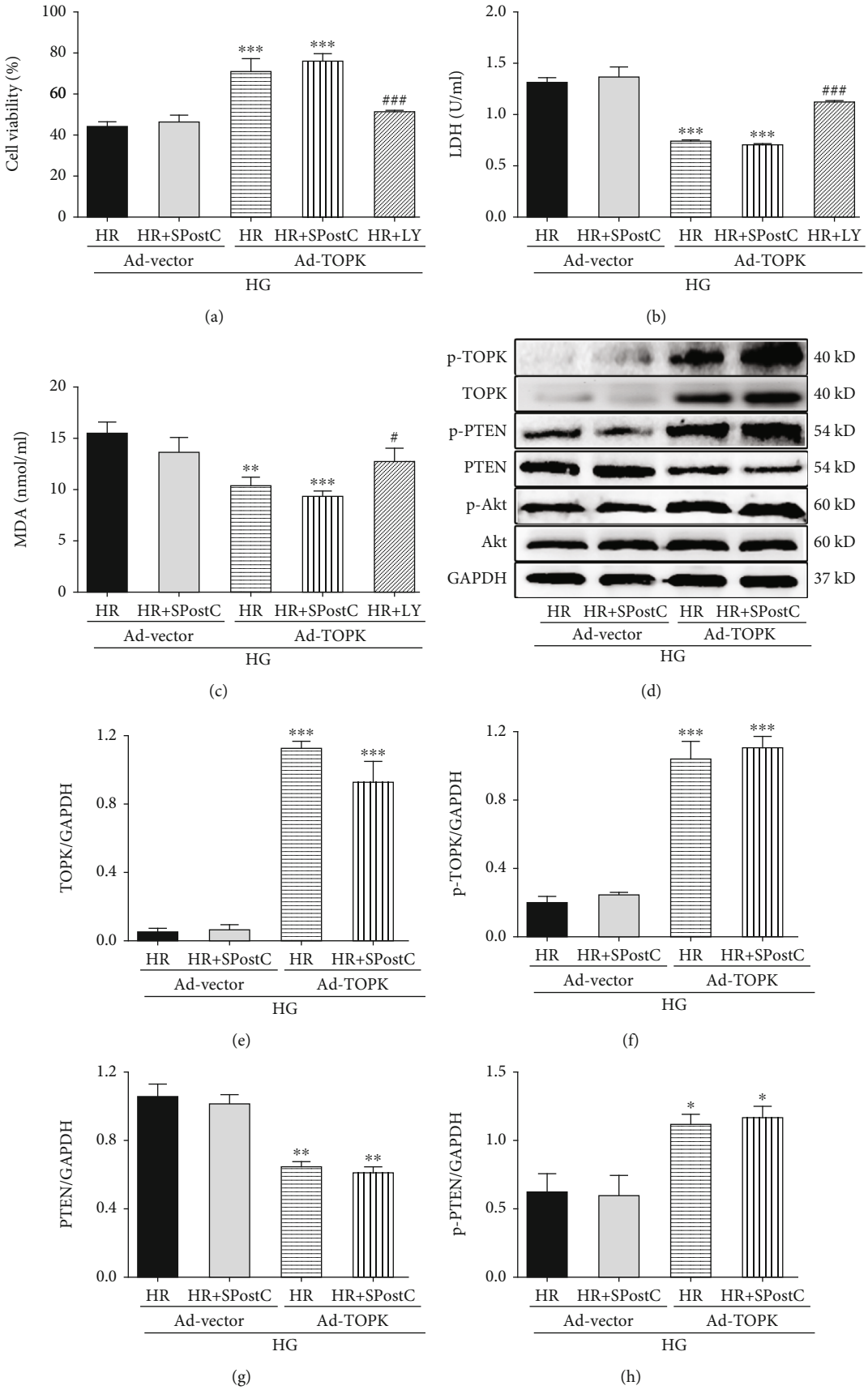

Figure 7: Continued.

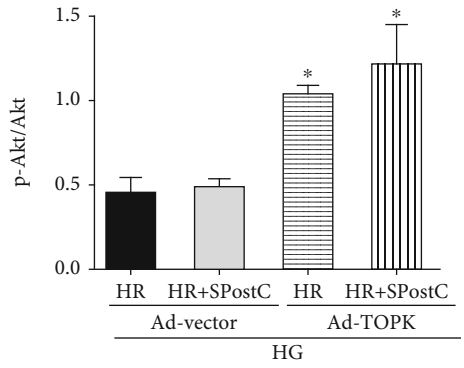

Figure 7: Cardiomyocyte injury, oxidative stress, and myocardial TOPK, PTEN, and Akt protein expression and their phosphorylation status assessed after HR with or without SPostC and LY in H9c2 cells under HG condition infected with adenovirus encoding rat TOPK (Ad-TOPK) or adenovirus vector (Ad-vector). (a) Cell viability was tested via MTT assay. (b) LDH release in the conditioned medium was analyzed by LDH assay. (c) MDA levels in different groups. (d) Representative western blots. Protein expression of TOPK (e, f), PTEN (g, h), and Akt (i) and their phosphorylation status in H9c2 cells detected by western blots. Mean band density was normalized relative to GAPDH. All values are presented as the mean ± SD of three independent experiments each performed in triplicate. $^{*}P < 0.05$, $^{**}P < 0.01$, and $^{***}P < 0.001$ compared with the Ad-vector+HG+HR group; $^{\#}P < 0.05$, $^{\#\#}P < 0.01$, and compared with the Ad-TOPK+HG+HR group.

when compared with the Ad-vector+HG+HR group (Figures 7(h) and 7(i), $P < 0.05$).

4. Discussion

Several major findings are presented in the current study. First, using *in vivo* mouse model of myocardial IR and *in vitro* HR model with of the H9c2 myocardial cell line, we showed that the cardioprotective effects mediated by SPostC were associated with activation of TOPK and PI3K/Akt (phosphorylated status), inactivation of PTEN (phosphorylated status), and a decrease in oxidative stress in response to myocardial IR insult. All these beneficial effects conferred by SPostC were attenuated by either the TOPK inhibitor HI-TOPK-032 or the PI3K/Akt inhibitor LY294002. The fact that TOPK inhibitor inhibited the phosphorylation of PTEN and Akt, whereas Akt inhibitor had no effect on the phosphorylation of TOPK and PTEN, it suggests that TOPK may have inactivated PTEN and in turn activated the PI3K/Akt signaling, which represents the major mechanism, whereby SPostC attenuates myocardial IR injury in nondiabetes. Second, we identified that the underlying molecular mechanism for the loss of cardioprotection of SPostC in diabetes or hyperglycemic condition is the impairment of the TOPK/PTEN/Akt signaling and the subsequently collapsed antioxidant system. In addition, TOPK supplementation protected against myocardial IR injury by activation of PTEN/Akt signaling pathway-mediated antioxidation.

SPostC has been proposed as a new strategy against myocardial IR injury, and it is more controllable, more convenient, and more conducive to clinical applications compared to ischemic postconditioning [10, 22–24]. However, the exact molecular mechanisms involved in SPostC-induced cardioprotection have not been fully clarified. TOPK, an innovative regulator of downstream PTEN/Akt pathway activity [14, 25], played a crucial role in the protection of renal or cerebral IR injury owing to its properties of antioxidation and anti-inflammation [16, 26]. PTEN, as a tumor suppressor gene, could encode a major lipid phosphatase which signals down the PI3K/Akt pathway by dephosphorylating PIP3 to PIP2, and is inactivated via phosphorylation or oxidation [27–29]. A number of studies have provided compelling evidence to confirm that the PI3K/Akt pathway was a classical signaling pathway in regulating cell proliferation, cell cycle progression, apoptosis, cell adhesion, migration, and invasion [30]. Recently, further evidence implicated that the PI3K/Akt/GSK-3β pathway could modulate mitochondrial dysfunction and oxidative stress and then determine the extent of myocardial IR injury [31]. Despite extensive studies, the prior reports focused primarily on how the PI3K/Akt signaling pathway influenced the cardioprotection induced by SPostC [10, 32]. It was unclear whether TOPK played critical roles in the cardioprotection of SPostC via the PTEN/Akt signaling. Herein, we demonstrate *in vivo* that the expression of TOPK in mouse cardiomyocytes after myocardial IR injury was increased, and that was further induced by SPostC. These results described above may be explained in part by the reduction of postmyocardial oxidative stress and attenuation of myocardial IR injury. Moreover, available data in our work indicated that the area of myocardial pathological injury was enlarged, the degree of cardiomyocyte apoptosis was aggravated, and the extent of cardiac myocytes injury was increased when SPostC mice were given TOPK inhibitor HI-TOPK-032 or PI3K inhibitor LY294002 beforehand. These results displayed that SPostC has a potent protective effect against myocardial IR injury possibly through phosphorylating the PTEN/ATK signaling pathway by the activation of TOPK, providing new insight into the mechanism by which SPostC reduced the risk of IR injury.

Over the course of the past 30 years, cardiovascular reperfusion therapy is still a major method for improving survival in patients suffered from acute myocardial infarction. Strikingly, several clinical studies indicated that infarct

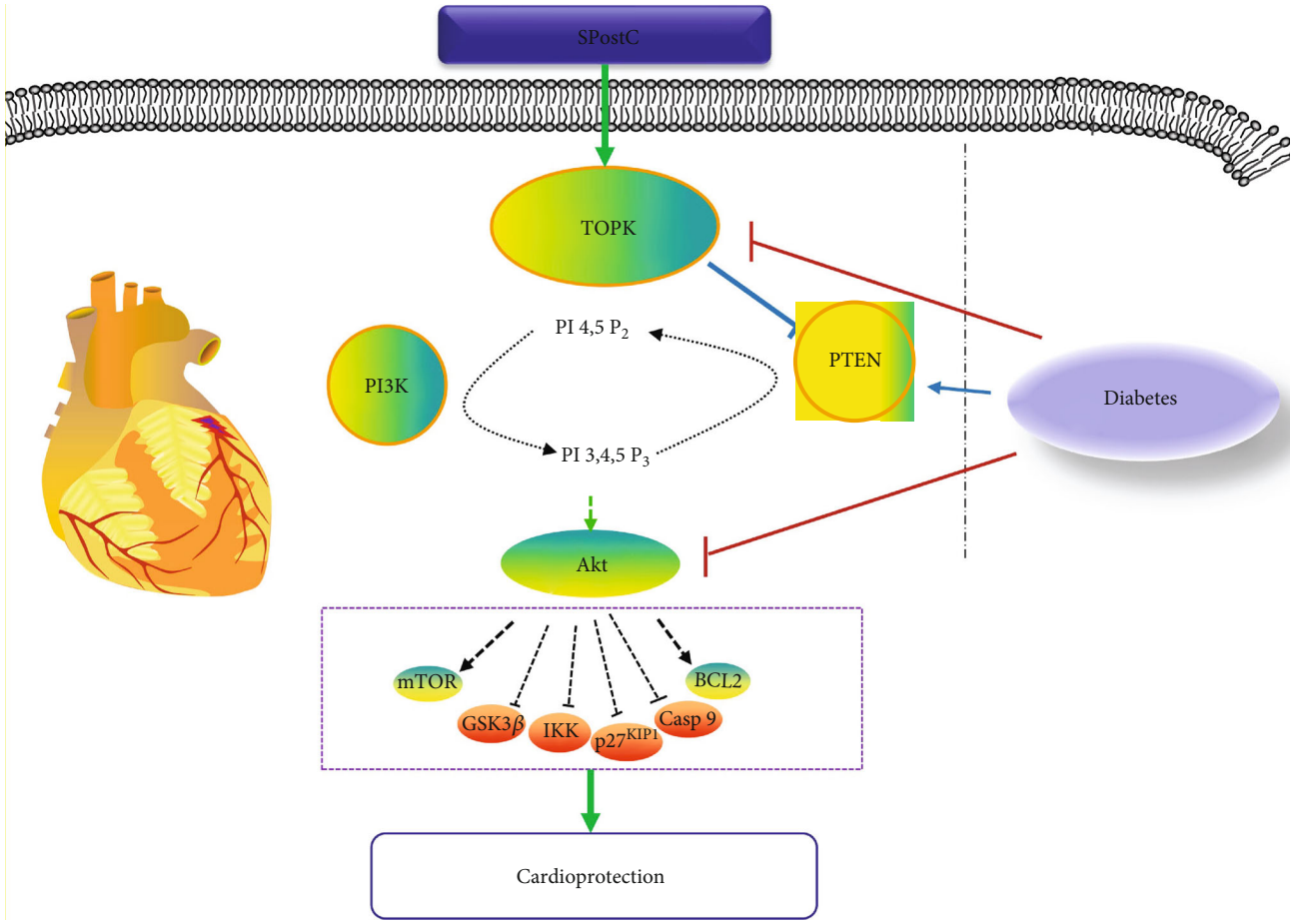

Figure 8: Schematic of proposed mechanism involved in the impairment of the TOPK/PTEN/Akt signaling that has rendered the diabetic hearts to loss responsiveness to sevoflurane postconditioning (SPostC) cardioprotection.

size was increased by 30–70% in diabetic patients after reperfusion therapy compared with nondiabetic patients treated in the same way, suggesting that diabetes mellitus sensitized the heart to IR injury [6, 33, 34]. As well, we found that the myocardial postischemic infarct size and apoptosis were significantly increased in diabetic mice under the treatment of 45 min ischemia followed by 2 h reperfusion, and that H9c2 cells exposed to high glucose markedly lowered its cell viability after HR as compared to H9c2 cells cultured under normal glucose. In addition, we observed that diabetes abolished the cardioprotective effect of SPostC, which fits well with previous studies which reported that diabetes may abolish the benefits of anesthetic pre/postconditioning [3, 35, 36]. Furthermore, the oxidative stress was significantly increased in both diabetic mice and H9c2 cells under high glucose, but SPostC exerted no effect on oxidative stress in diabetes [3]. Although a lot of effort has been spent on improving these weaknesses in diabetes, the efficient and effective method has yet to be developed. For example, a previous study indicated that the use of insulin for downregulating blood glucose failed to recover the advantages of SPostC, and it may be due to the diabetes-induced inhibition of the PI3K signaling [37]. Although previous studies have shown that increased cardiac PTEN is responsible for the loss of diabetic heart sensitivity to ischemic postconditioning through PI3K/Akt inactivation [9], the underlying molecular mechanism remains unknown. In our study, we found that either in streptozotocin-induced diabetic mice or in H9c2 cells exposed to high glucose, the cardioprotective effect of SPostC was canceled, accompanied by increased oxidative stress, decreased TOPK phosphorylation, decreased PTEN phosphorylation (inactivated status), and decreased Akt phosphorylation. Studies have shown that the adverse effects of hyperglycemia on grave myocardial IR injury were attributed to the oxidative stress properties [38, 39]. Therefore, these results suggested that the underlying mechanism attributable to the abolished cardioprotection induced by SPostC in diabetes or high glucose conditions is likely the impairment of the TOPK/PTEN/Akt signaling, and the subsequently collapsed antioxidant system. Then, we have extended these observations by employing gain-of-function approaches in cultured H9c2 cells to investigate the functional roles of TOPK, and initial results seem promising. Our study showed that TOPK overexpression restored posthypoxic p-PTEN and p-Akt and decreased cell death and oxidative stress in H9c2 cells exposed to high glucose, which was blocked by PI3K/Akt inhibition. Collectively, these findings indicated that TOPK supplementation prevented diabetic myocardial

IR injury through PTEN/PI3K/Akt activation-mediated antioxidation.

Finally, several limitations to the present study should be considered. First, the effective activator of TOPK was not invented in practice which may limit the application of TOPK in patients with diabetic ischemic cardiomyopathy. Second, given that HI-TOPK-032 is known to be docked to the active site of TOPK to directly and specifically suppress TOPK kinase activity [12], the TOPK kinase activity was not measured after the use of HI-TOPK-032 in our current study. However, the knockdown effect of TOPK small interfering RNAs on myocardial IR injury should be studied in the nondiabetic and diabetic myocardium in the future study to further confirm the role of TOPK in the context of diabetic myocardial IR and its impact on SPostC. Third, we only discussed the benefits of SPostC conducted on acute myocardial IR injury; however, several reports demonstrated that isoflurane played a pivotal role in delayed cardioprotection [40, 41]. More considerable works on delayed cardioprotection provided by SPostC will be done in our next research work. At last, while the advantages we observed in H9c2 cells transfected with TOPK phenotype suggest that TOPK has a potential cardioprotective function in diabetes, this needs to be directly tested by measuring myocardial infarct sizes in diabetic mice, which we are currently planning.

5. Conclusions

In summary, we demonstrated that SPostC protected against myocardial IR injury possibly through the activation of the TOPK/PTEN/Akt signaling pathway, while the impairment of the TOPK/PTEN/Akt signaling in cardiac might be the major mechanism that has rendered diabetic hearts less or not responsive to SPostC cardioprotection (Figure 8). In addition, TOPK supplementation protected against myocardial IR injury by activation of PTEN/Akt signaling pathway-mediated antioxidation. Our results provided new insight into the activation mechanisms of TOPK which may lead to the development of effective therapeutic targets to combat the myocardial complications of diabetes.

Abbreviations

TOPK: T-LAK cell-originated protein kinase
SPostC: Sevoflurane postconditioning
PTEN: Phosphatase and tensin homolog deleted on chromosome ten
PI3K: Phosphatidylinositol 3-kinase
Akt: Protein kinase B
IR: Ischemia/reperfusion
MAPKK: Mitogen-activated protein kinase
CK-MB: Creatine kinase-MB
TUNEL: Terminal deoxynucleotidyl transferase-mediated nick end labeling
MDA: Malondialdehyde
LDH: Lactate dehydrogenase
PIP3: Phosphatidylinositol 3,4,5-triphosphate
PIP2: Phosphatidylinositol 4,5-biphosphate
GSK-3β: Glycogen synthase kinase-3β.

Data Availability

The data used to support the findings of this study are available from the corresponding authors upon request.

Additional Points

(i) Sevoflurane postconditioning protected the heart from ischemia/reperfusion injury possibly through TOPK-mediated PTEN/PI3K/Akt activation in nondiabetic but not in diabetic rodents. (ii) Diabetes blocked the cardioprotection of sevoflurane postconditioning by impairing TOPK bioavailability. (iii) TOPK supplementation prevented diabetic myocardial ischemia/reperfusion injury through PTEN/PI3K/Akt activation

Ethical Approval

All animal experiments were approved by the Institutional Animal Use and Care Committee at Tongji Medical College, Huazhong University of Science and Technology.

Conflicts of Interest

The authors declare no conflict of interest.

Authors' Contributions

TW, SY, SG, and RW conceived and designed the experiments. SG, RW, SD, and JW performed the experiments. SG, RW, SD, JW, ZX, SY, and TW analyzed the data. SG, RW, BP, ZX, SY, and TW contributed to discussion and wrote the paper. All authors read and approved the final paper. Sumin Gao and Rong Wang contributed equally to this work.

Acknowledgments

This work was supported by grants from the National Natural Science Foundation of China (No. 81770824 and No. 81772131).

Supplementary Materials

Figure S1: (a) representative images of Evans blue and TTC staining in heart cross sections from the sham group. (b) SOD level assessed after HR with or without SPostC and LY294002 (LY) in H9c2 cells under HG condition infected with adenovirus encoding rat TOPK (Ad-TOPK) or adenovirus vector (Ad-vector). $^{***}P < 0.001$ compared with the Ad-vector+HG+HR group; $^{\#\#\#}P < 0.001$ compared with the Ad-TOPK+HG+HR group. *(Supplementary Materials)*

References

[1] E. J. Benjamin, S. S. Virani, C. W. Callaway et al., "Heart disease and stroke statistics -2018 update: a report from the American Heart Association," *Circulation*, vol. 137, no. 12, pp. E67–E492, 2018.

[2] T. Wang, X. Mao, H. Li et al., "N-Acetylcysteine and allopurinol up-regulated the Jak/STAT3 and PI3K/Akt pathways via adiponectin and attenuated myocardial postischemic injury

in diabetes," *Free Radical Biology and Medicine*, vol. 63, pp. 291–303, 2013.

[3] S. Gao, Z. Yang, R. Shi et al., "Diabetes blocks the cardioprotective effects of sevoflurane postconditioning by impairing Nrf2/Brg1/HO-1 signaling," *European Journal of Pharmacology*, vol. 779, pp. 111–121, 2016.

[4] R. C. Pasqualin, C. T. Mostarda, L. E. de Souza et al., "Sevoflurane preconditioning during myocardial ischemia-reperfusion reduces infarct size and preserves autonomic control of circulation in rats," *Acta Cirurgica Brasileira*, vol. 31, no. 5, pp. 338–345, 2016.

[5] S. Wild, G. Roglic, A. Green, R. Sicree, and H. King, "Global prevalence of diabetes: estimates for the year 2000 and projections for 2030," *Diabetes Care*, vol. 27, no. 5, pp. 1047–1053, 2004.

[6] S. M. Haffner, S. Lehto, T. Rönnemaa, K. Pyörälä, and M. Laakso, "Mortality from coronary heart disease in subjects with type 2 diabetes and in nondiabetic subjects with and without prior myocardial infarction," *New England Journal of Medicine*, vol. 339, no. 4, pp. 229–234, 1998.

[7] U. Benedetto, M. Caputo, H. Vohra et al., "Off-pump versus on-pump coronary artery bypass surgery in patients with actively treated diabetes and multivessel coronary disease," *The Journal of Thoracic and Cardiovascular Surgery*, vol. 152, no. 5, pp. 1321–1330.e12, 2016.

[8] H. Ruan, J. Li, S. Ren et al., "Inducible and cardiac specific PTEN inactivation protects ischemia/reperfusion injury," *Journal of Molecular and Cellular Cardiology*, vol. 46, no. 2, pp. 193–200, 2009.

[9] R. Xue, S. Lei, Z. Y. Xia et al., "Selective inhibition of PTEN preserves ischaemic post-conditioning cardioprotection in STZ-induced type 1 diabetic rats: role of the PI3K/Akt and JAK2/STAT3 pathways," *Clinical Science*, vol. 130, no. 5, pp. 377–392, 2016.

[10] J. Zhang, C. Wang, S. Yu et al., "Sevoflurane Postconditioning Protects Rat Hearts against Ischemia- Reperfusion Injury via the Activation of PI3K/AKT/mTOR Signaling," *Scientific Reports*, vol. 4, no. 1, p. 7317, 2015.

[11] J. H. Park, T. Nishidate, Y. Nakamura, and T. Katagiri, "Critical roles of T-LAK cell-originated protein kinase in cytokinesis," *Cancer Science*, vol. 101, no. 2, pp. 403–411, 2010.

[12] D. J. Kim, Y. Li, K. Reddy et al., "Novel TOPK inhibitor HI-TOPK-032 effectively suppresses colon cancer growth," *Cancer Research*, vol. 72, no. 12, pp. 3060–3068, 2012.

[13] K. J. Herbert, T. M. Ashton, R. Prevo, G. Pirovano, and G. S. Higgins, "T-LAK cell-originated protein kinase (TOPK): an emerging target for cancer- specific therapeutics," *Cell Death and Disease*, vol. 9, no. 11, p. 1089, 2018.

[14] M. C. Shih, J. Y. Chen, Y. C. Wu et al., "TOPK/PBK promotes cell migration via modulation of the PI3K/PTEN/AKT pathway and is associated with poor prognosis in lung cancer," *Oncogene*, vol. 31, no. 19, pp. 2389–2400, 2012.

[15] H. Zhao, R. Wang, Z. Tao et al., "Activation of T-LAK-cell-originated protein kinase-mediated antioxidation protects against focal cerebral ischemia-reperfusion injury," *FEBS Journal*, vol. 281, no. 19, pp. 4411–4420, 2014.

[16] S. Gao, Y. Zhu, H. Li et al., "Remote ischemic postconditioning protects against renal ischemia/reperfusion injury by activation of T-LAK-cell-originated protein kinase (TOPK)/PTEN/Akt signaling pathway mediated anti-oxidation and anti-inflammation," *International Immunopharmacology*, vol. 38, pp. 395–401, 2016.

[17] G. Sun, N. Ye, D. Dai, Y. Chen, C. Li, and Y. Sun, "The protective role of the TOPK/PBK pathway in myocardial ischemia/reperfusion and H_2O_2-induced injury in H9C2 cardiomyocytes," *International Journal of Molecular Sciences*, vol. 17, no. 3, p. 267, 2016.

[18] S. Wu, G. Chang, L. Gao et al., "Trimetazidine protects against myocardial ischemia/reperfusion injury by inhibiting excessive autophagy," *Journal of Molecular Medicine*, vol. 96, no. 8, pp. 791–806, 2018.

[19] M. Joel, A. A. Mughal, Z. Grieg et al., "Targeting PBK/TOPK decreases growth and survival of glioma initiating cells in vitro and attenuates tumor growth in vivo," *Molecular Cancer*, vol. 14, no. 1, p. 121, 2015.

[20] S. Lei, W. Su, H. Liu et al., "Nitroglycerine-induced nitrate tolerance compromises propofol protection of the endothelial cells against TNF-α: the role of PKC-β2 and NADPH oxidase," *Oxidative Medicine and Cellular Longevity*, vol. 2013, 9 pages, 2013.

[21] X. Mao, T. Wang, Y. Liu et al., "N-acetylcysteine and allopurinol confer synergy in attenuating myocardial ischemia injury via restoring HIF-1α/HO-1 signaling in diabetic rats," *PloS One*, vol. 8, no. 7, article e68949, 2013.

[22] D. Obal, S. Dettwiler, C. Favoccia, H. Scharbatke, B. Preckel, and W. Schlack, "The influence of mitochondrial KATP-channels in the cardioprotection of preconditioning and postconditioning by sevoflurane in the rat in vivo," *Anesthesia and Analgesia*, vol. 101, no. 5, pp. 1252–1260, 2005.

[23] J. Yu, J. Wu, P. Xie et al., "Sevoflurane postconditioning attenuates cardiomyocyte hypoxia/reoxygenation injury via restoring mitochondrial morphology," *Peer J*, vol. 4, article e2659, 2016.

[24] S. Qiao, Y. Sun, B. Sun et al., "Sevoflurane postconditioning protects against myocardial ischemia/reperfusion injury by restoring autophagic flux via an NO-dependent mechanism," *Acta Pharmacologica Sinica*, vol. 40, no. 1, pp. 35–45, 2019.

[25] S. R. Shinde, N. R. Gangula, S. Kavela, V. Pandey, and S. Maddika, "TOPK and PTEN participate in CHFR mediated mitotic checkpoint," *Cellular Signalling*, vol. 25, no. 12, pp. 2511–2517, 2013.

[26] H. Zhao, R. Wang, Z. Tao et al., "Ischemic postconditioning relieves cerebral ischemia and reperfusion injury through activating T-LAK cell–originated protein kinase/protein kinase B pathway in rats," *Stroke*, vol. 45, no. 8, pp. 2417–2424, 2014.

[27] C. Eng, "PTEN: one gene, many syndromes," *Human Mutation*, vol. 22, no. 3, pp. 183–198, 2003.

[28] T. Liu, Y. Wang, Y. Wang, and A. M. Chan, "Multifaceted regulation of PTEN subcellular distributions and biological functions," *Cancers*, vol. 11, no. 9, p. 1247, 2019.

[29] L. Bao, X. Li, and Z. Lin, "PTEN overexpression promotes glioblastoma death through triggering mitochondrial division and inactivating the Akt pathway," *Journal of Receptors and Signal Transduction*, vol. 39, no. 3, pp. 215–225, 2019.

[30] I. Hers, E. E. Vincent, and J. M. Tavaré, "Akt signalling in health and disease," *Cellular Signalling*, vol. 23, no. 10, pp. 1515–1527, 2011.

[31] D. Sulaiman, J. Li, A. Devarajan et al., "Paraoxonase 2 protects against acute myocardial ischemia-reperfusion injury by modulating mitochondrial function and oxidative stress via the PI3K/Akt/GSK-3β RISK pathway," *Journal of Molecular and Cellular Cardiology*, vol. 129, pp. 154–164, 2019.

[32] Y. Hao, H. Fang, H. Zhao et al., "The role of microRNA-1 targeting of MAPK3 in myocardial ischemia-reperfusion injury

in rats undergoing sevoflurane preconditioning via the PI3K/Akt pathway," *American Journal of Physiology-Cell Physiology*, vol. 315, no. 3, pp. C380–C388, 2018.

[33] S. P. Marso, T. Miller, B. D. Rutherford et al., "Comparison of myocardial reperfusion in patients undergoing percutaneous coronary intervention in ST-segment elevation acute myocardial infarction with versus without diabetes mellitus (from the EMERALD Trial)," *The American Journal of Cardiology*, vol. 100, no. 2, pp. 206–210, 2007.

[34] J. R. Alegria, T. D. Miller, R. J. Gibbons, Q. L. Yi, S. Yusuf, and Collaborative Organization of RheothRx Evaluation (CORE) Trial Investigators, "Infarct size, ejection fraction, and mortality in diabetic patients with acute myocardial infarction treated with thrombolytic therapy," *American Heart Journal*, vol. 154, no. 4, pp. 743–750, 2007.

[35] H. Grievink, N. Kuzmina, M. Chevion, and B. Drenger, "Sevoflurane postconditioning is not mediated by ferritin accumulation and cannot be rescued by simvastatin in isolated streptozotocin-induced diabetic rat hearts," *PLOS ONE*, vol. 14, no. 1, article e0211238, 2019.

[36] S. G. Canfield, A. Sepac, F. Sedlic, M. Y. Muravyeva, X. Bai, and Z. J. Bosnjak, "Marked hyperglycemia attenuates anesthetic preconditioning in human-induced pluripotent stem cell-derived cardiomyocytes," *Anesthesiology*, vol. 117, no. 4, pp. 735–744, 2012.

[37] B. Drenger, I. A. Ostrovsky, M. Barak, Y. Nechemia-Arbely, E. Ziv, and J. H. Axelrod, "Diabetes blockade of sevoflurane postconditioning is not restored by insulin in the rat heart," *Anesthesiology*, vol. 114, no. 6, pp. 1364–1372, 2011.

[38] H. Su, L. Ji, W. Xing et al., "Acute hyperglycaemia enhances oxidative stress and aggravates myocardial ischaemia/reperfusion injury: role of thioredoxin-interacting protein," *Journal of Cellular and Molecular Medicine*, vol. 17, no. 1, pp. 181–191, 2013.

[39] N. Fourny, C. Lan, E. Sérée, M. Bernard, and M. Desrois, "Protective effect of resveratrol against ischemia-reperfusion injury via enhanced high energy compounds and eNOS-SIRT1 expression in type 2 diabetic female rat heart," *Nutrients*, vol. 11, no. 1, p. 105, 2019.

[40] Y. Shi, W. C. Hutchins, J. Su et al., "Delayed cardioprotection with isoflurane: role of reactive oxygen and nitrogen," *American Journal of Physiology-Heart and Circulatory Physiology*, vol. 288, no. 1, pp. H175–H184, 2005.

[41] C. H. Chen, J. H. Chuang, K. Liu, and J. Y. H. Chan, "Nitric oxide triggers delayed anesthetic preconditioning-induced cardiac protection via activation of nuclear factor-κB and upregulation of inducible nitric oxide synthase," *Shock (Augusta, Ga.)*, vol. 30, no. 3, pp. 241–249, 2008.